

AD 708625



CONTRACT REPORT NO. 3-26

THE RESPONSE OF SOILS TO DYNAMIC LOADINGS

Report 26

FINAL REPORT

by

R. V. Whitman



May 1970

Sponsored by Defense Atomic Support Agency

Conducted for U. S. Army Engineer Waterways Experiment Station, Vicksburg, Mississippi

Under Contract No. DA-22-079-eng-224

By Massachusetts Institute of Technology, Cambridge, Massachusetts

ARMY-MRC VICKSBURG, MISS

This document has been approved for public release and sale; its distribution is unlimited

FOREWORD

Most of this report, especially Chapter 2, was written during 1967, and represents the writer's view of the state-of-the-art as the writer saw it at that time.

In 1967, the writer was very concerned about an apparent trend toward developing ever more complex computer codes while failing to use existing computer codes to understand important cause and effect relations and to ascertain the effect of uncertainties in the input on the nature of the computed results. The emphasis of Chapter 2, and many of the specific comments, reflected this concern. The writer quite frankly felt that the computer code development, as it was apparently being followed, was largely an academic exercise, that quite likely it would be impossible to rely on the codes for design predictions, and that designs would still have to be based on very simple prediction equations together with a large dose of judgment.

The writer has been "out of the business" since 1967, but from various conversations it appears that he may have been wrong in his assessment of the trends in computer code development and utilization. Apparently there has developed a close cooperation between experienced soil engineers and the developers and users of complex computer codes. Apparently there is also now a recognition of the need to make, in connection with specific design projects and field experiments, a series of computer runs so as to bracket the effect of uncertainties in the input and assumptions. If these statements do reflect the current situation, then some of the statements in this report may happily be out-of-date.

However, the writer still does believe in the necessity of developing improved but simple and approximate prediction techniques which do not require use of a computer for each application. Such techniques (or

equations or rules) are needed for small design projects where complex expensive analysis is not justified and for preliminary analysis of large design projects. One of the main objectives of calculations using complex computer codes must be to provide the insights and understandings upon which such simple rules (and statements regarding the limitations of these rules) can be based. Section 2.4.2 is an attempt to use theoretical results available as of 1967 to identify and understand the key features of airblast-induced ground motion and to assess the accuracy and limitations of the simple prediction methods described in Section 2.4.4. The writer urges those now active in generating new theoretical results to extend and complete the synthesis started in Sections 2.4.2 and 2.4.3.

This report is the 26th in a series of reports prepared by Massachusetts Institute of Technology (MIT) under contract with the U. S. Army Engineer Waterways Experiment Station (WES). The report was prepared by Dr. Robert V. Whitman, Professor of Civil Engineering, MIT. Helpful comments and guidance were provided by Messrs. R. W. Cunney, J. G. Jackson, Jr., R. C. Sloan, P. F. Hadala, and Dr. J. S. Zelasko, Soils Division, WES.

At the time of publication of this report, COL Levi A. Brown, CE, was Director of WES, and M. F. R. Brown was Technical Director.

ABSTRACT

This report, the 26th in a series of reports prepared under contract by MIT, deals with the role of soil mechanics with regard to weapons effects prediction and protective construction design. It assesses the state-of-the-art as of 1967, and summarizes all the research performed under the contract as well as contributions by other investigators. Results from field experiments and theoretical analyses are interpreted so as to show the relation between soil properties and such phenomena as crater size and shape, ground motions, and response of buried structures. Chapters deal specifically with the evaluation of dynamic uniaxial strain and dynamic shear strength, and with the relation between seismic wave velocity and soil properties. Appendix A contains abstracts of the 25 earlier reports issued under the contract. Appendix B gives a brief history of the MIT soil dynamics contract.

CONTENTS

	<u>Page</u>
FOREWORD-----	iii
ABSTRACT-----	v
NOTATION-----	xvii
CONVERSION FACTORS BRITISH TO METRIC UNITS OF MEASUREMENT-----	xxiii
CHAPTER 1 INTRODUCTION-----	1
1.1 Purpose and Scope of This Report-----	1
1.2 What Is Soil Dynamics-----	2
1.3 General Look at the Stress-Strain Behavior of Soil-----	3
1.3.1 Behavior During Compression and Shear-----	3
1.3.2 Hydrodynamic Time Lag-----	4
1.3.3 Use of Approximate Stress-Strain Rules-----	5
1.4 Heritage of Soil Mechanics-----	6
1.4.1 Value of Experience-----	6
1.4.2 Role of Theory-----	6
1.4.3 Application of Experience and Theory-----	7
CHAPTER 2 SOIL DYNAMICS AS PERTAINING TO NUCLEAR WEAPONS EFFECTS AND PROTECTIVE CONSTRUCTION DESIGN-----	8
2.1 Mechanical Effects of Nuclear Explosions-----	8
2.2 Cratering-----	11
2.2.1 General Features of a Crater-----	11
2.2.2 Sizes of Craters-----	14
2.2.3 Processes of Crater Formation-----	18
2.2.4 Requirements for Data Regarding Soil-----	24
2.3 Motions of Surface Structures-----	24
2.4 Airblast-Induced Stress Waves-----	26
2.4.1 Description of Airblast-----	28
2.4.2 General Features of Ground Motions-----	31
2.4.3 Effect of Nonelastic Behavior of Ground-----	52
2.4.4 Prediction of Ground Motions for Engineering Studies-----	57
2.4.5 Requirements for Data Regarding Soil-----	63
2.5 Soil-Structure Interaction with Airblast-Induced Stress Waves-----	65
2.5.1 Buried Horizontal Cylinders-----	65
2.5.2 Buried Closed Rectangular Structures-----	69
2.5.3 Buried Arches or Rectangular Structures Supported on Footings-----	71

	<u>Page</u>
2.5.4 Vertical Cylinder (Silo)-----	72
2.5.5 Motions of Buried Structures-----	72
2.5.6 Requirements for Data Regarding Soil-----	74
2.6 Directly Induced Stress Waves-----	76
2.6.1 Basic Phenomena-----	76
2.6.2 Prediction Methods-----	79
2.6.3 Requirements for Data Regarding Soil-----	82
2.7 Soil-Structure Interaction with Directly Induced Stress Waves--	82
2.8 Summary of Soil Data Requirements-----	83
2.8.1 Stress-Strain Relations in General Terms-----	84
2.8.2 Specific Values of Certain Soil Parameters-----	90
CHAPTER 3 SHEAR STRENGTH DURING RAPID LOADINGS-----	92
3.1 Introduction-----	92
3.1.1 Definitions-----	92
3.1.2 Single Versus Repeated Loadings-----	96
3.2 Factors Affecting the Relation Between Strength and Rate of Loading-----	97
3.2.1 Intrinsic Properties of Soil-----	97
3.2.2 Overall Action of Mass of Soil-----	98
3.2.3 Relative Importance of Factors-----	100
3.3 Testing Equipment and Procedures-----	101
3.3.1 Loading Systems-----	101
3.3.2 Triaxial Cells-----	103
3.3.3 Force Measurement-----	103
3.3.4 Pore Pressure Measurements-----	103
3.3.5 Permissible Loading Rates-----	104
3.4 Behavior of Dry Sands-----	105
3.5 Behavior of Saturated Sands-----	107
3.6 Behavior of Cohesive Soils-----	109
3.6.1 Situations in Which Pore Pressures Are Positive-----	110
3.6.2 Situations in Which Pore Pressures Are Negative-----	112
3.6.3 Other Effects-----	114
3.7 Summary and Recommendations-----	115
3.7.1 Summary of Results-----	115
3.7.2 Present Status of Work-----	116
3.7.3 Suggestions for Future Research-----	116
CHAPTER 4 ONE-DIMENSIONAL COMPRESSIBILITY-----	117
4.1 Introduction-----	117
4.2 Test Equipment and Procedures-----	119
4.2.1 The MIT Tester-----	119
4.2.2 Later Versions of the MIT Tester-----	125
4.2.3 Other Test Devices-----	126
4.3 General Aspects of Behavior-----	128
4.3.1 Ideal Packings of Perfect Spheres-----	128
4.3.2 Dry Granular Soils-----	130
4.3.3 Other Soils-----	136
4.4 Evaluation of Constrained Modulus-----	143
4.4.1 Recommended Procedures in Case of Compressible Soils-----	144

	<u>Page</u>
4.4.2 Experimental Verification of Procedure for Selecting Modulus-----	145
4.4.3 Recommended Procedures in Case of Stiff Soils-----	149
4.5 Evaluation of Other Parameters-----	153
4.6 Summary and Recommendations-----	154
4.6.1 Summary of Results-----	154
4.6.2 Present Status of Work-----	154
4.6.3 Suggestions for Future Research-----	155
CHAPTER 5 PROPAGATION VELOCITY FOR STRESS WAVES OF LOW INTENSITY-----	156
5.1 Introduction-----	156
5.1.1 Relation Between Wave Velocity and Modulus-----	157
5.1.2 Types of Waves-----	157
5.2 Tests for Measuring Wave Velocities in the Laboratory-----	159
5.2.1 Resonant Column Test-----	159
5.2.2 Pulse Technique-----	160
5.2.3 Other Tests-----	165
5.3 Wave Velocities Through Dry Granular Soils-----	166
5.3.1 Effect of Confining Stress-----	166
5.3.2 Effect of Amplitude of Dynamic Stress-----	170
5.3.3 Effect of Frequency-----	170
5.3.4 Effect of Void Ratio-----	170
5.3.5 Effect of Particle Size, Shape, and Gradation-----	171
5.3.6 Poisson's Ratio-----	172
5.3.7 Behavior with Small Porosity-----	172
5.4 Shear and Rod Velocities Through Soils with Water-----	173
5.4.1 Role of Total and Effective Stress-----	174
5.4.2 Effective Mass of Pore Fluid-----	174
5.4.3 Effects of Confining Stress and Void Ratio-----	178
5.4.4 Effect of Amplitude of Dynamic Stress-----	179
5.4.5 Effect of Frequency-----	179
5.4.6 Poisson's Ratio-----	179
5.4.7 Velocity and Strength-----	180
5.5 Dilatational Velocity Through Saturated Soils-----	180
5.5.1 Suspension of Soil in Water-----	181
5.5.2 Effect of Mineral Skeleton-----	182
5.5.3 Effect of Various Parameters-----	183
5.6 Dilatational Velocity Through Partially Saturated Soils-----	184
5.6.1 A Possible Mathematical Model-----	184
5.6.2 Data-----	186
5.7 Summary and Recommendations-----	188
5.7.1 Summary of Results-----	188
5.7.2 Present Status of Work-----	188
5.7.3 Suggestions for Future Research-----	189
LITERATURE CITED-----	190
APPENDIX A ABSTRACTS OF SOIL DYNAMICS REPORTS-----	A1
APPENDIX B HISTORY OF THE MIT SOIL DYNAMICS CONTRACT-----	B1

LIST OF TABLES

Table No.	Title	Page
2.1	Four Aspects of Explosion-Induced Stress Waves-----	10
2.2	Crater Dimensions According to Various Scaling Laws-----	16
2.3	Requirements for Data on Soil Properties in Connection with Cratering-----	25
2.4	Airblast Parameters for 1-Mt Surface Burst-----	29
2.5	Requirements for Data on Soil Properties in Connection with Airblast-Induced Ground Motions-----	64
2.6	Critical Buckling Condition of Underground Cylinders; Intersection of Elastic Buckling Curve with Yield Stress Line-----	68
2.7	Requirements for Data on Soil Properties in Connection with Soil-Structure Interaction-----	75
2.8	Equation and Factors for Predicting Peak Radial Particle Velocity in a Directly Induced Stress Wave-----	80
3.1	Summary of Transient-Loading Triaxial Tests on Cohesive Soils-----	111
4.1	Comparison of Predicted and Observed Particle Velocities in Laboratory Tests-----	147
4.2	Constrained Modulus for Frenchman Flat Silt-----	148
4.3	Results from One-Dimensional Compression Tests on Partially Saturated Soils-----	151
5.1	Rod and Shear Modulus Data for Saturated Clays-----	179

LIST OF FIGURES

Figure No.	Title	Page
1.1	Stress versus strain for a particulate system-----	1
1.2	Hydrodynamic time lag in compressibility of soil-----	4
2.1	Mechanical effects of near-surface nuclear explosion-----	8
2.2	Cross section through crater of Teapot-ESS-----	12
2.3	Typical crater profiles versus depth of burst for alluvium---	13
2.4	Crater dimensions versus depth of burst for 256-lb HE shots in NTS alluvium-----	14
2.5	Apparent craters from 256-lb TNT charges-----	16
2.6	Crater radii and depth versus depth of burst relation for various earth materials-----	17
2.7	Phases of crater formation-----	18
2.8	Relative contributions of various mechanisms to apparent crater depth for explosion crater-----	19
2.9	Computed pressures caused by 1-Mt surface explosion-----	19
2.10	Computed particle velocities caused by 1-Mt surface explosion-----	20

Figure No.	Title	Page
2.11	Sequence views of ground rise at ground zero in Scooter event-----	21
2.12	Distance to various peak overpressure levels in relation to crater size; 1-Mt surface burst-----	29
2.13	Overpressure versus time; 1-Mt surface burst-----	30
2.14	Overpressure versus radius; 1-Mt surface burst-----	31
2.15	Waves resulting from instantaneously applied point load-----	32
2.16	Time history of vertical displacement along ray beneath concentrated load-----	32
2.17	Time history of vertical displacement at shallow depth near concentrated load-----	33
2.18	Sequence of loadings applied by airblast-----	33
2.19	Superseismic and subseismic regions-----	34
2.20	Typical time histories of vertical acceleration at depths of 1 and 10 ft below ground surface-----	35
2.21	Wave fronts beneath superseismic strip load-----	35
2.22	Vertical and horizontal stresses versus time at two depths below superseismic strip load-----	36
2.23	Displacements at several depths below superseismic strip load-----	36
2.24	Comparison of one-dimensional and superseismic cases-----	38
2.25	Vertical stress versus time at various depths beneath linearly decaying superseismic strip load-----	39
2.26	Attenuation of peak vertical stress from airblast-----	39
2.27	Location of airblast shock front and P- and S-fronts at two different times giving superseismic conditions for $\mu = 1/3$ --	40
2.28	Theoretical results showing peak vertical stress at several deep points-----	41
2.29	Distribution of stresses and displacements along line A-A" as result of airblast loading-----	42
2.30	Stresses near surface toward end of superseismic region-----	43
2.31	Motions at surface from combined airblast-induced and directly induced stress waves-----	44
2.32	Wave fronts in subseismic region-----	45
2.33	Typical records of actual vertical motions at several distances from ground zero in subseismic region, Tumbler Shot 1-----	45
2.34	Stresses and displacements near ground surface in subseismic region, from approximate theoretical calculation-----	47
2.35	Wave fronts at a time when initial disturbance front is superseismic on $Z = 0$ and transseismic on $Z = H$ -----	48
2.36	Effect of layering upon near-surface motions-----	49
2.37	Ray path diagram for determination of critical ray path for two-layer medium-----	51
2.38	Summary of general features of ground motion-----	51
2.39	Typical and idealized stress-strain curves for studying effect of shear strength-----	52
2.40	Stress-strain curve exhibiting hysteresis-----	54

Figure No.	Title	Page
2.41	Three-element linear viscoelastic model and stress-strain curve during one-half of cycle of loading-----	55
2.42	Relation between type of stress-strain curve and nature of wave front-----	56
2.43	S-shaped stress-strain curve for confined compression-----	56
2.44	Typical changes in wave front with depth, as observed in soil shock tube-----	57
2.45	Distribution of stress at time t after airblast passes point on ground surface-----	62
2.46	Typical configurations of buried structures-----	65
2.47	Collapse of poorly backfilled, horizontal, buried flexible cylinders-----	66
2.48	Distribution of stresses against horizontal buried cylinder--	66
2.49	Trapdoor experiment-----	69
2.50	Results of trapdoor experiment-----	69
2.51	Marston-Spangler theory for arching-----	70
2.52	Arching at closed rectangular structure-----	71
2.53	Arching at structure supported on footings-----	71
2.54	Shock response spectrum chart-----	74
2.55	Movement and deformation of an element of soil behind spherical wave front-----	76
2.56	Stresses caused by pressure in spherical cavity within an elastic body-----	77
2.57	Effect of yield strength on stresses caused by pressure within a spherical cavity-----	78
2.58	Chart for prediction of peak radial acceleration-----	79
2.59	Chart for prediction of peak radial displacement-----	80
2.60	Structural concept for regions of extremely large stress-----	83
2.61	Typical stress-strain curves in hydrostatic or confined compression-----	85
2.62	Typical stress-strain and volume change curves in shear-----	86
2.63	Stress-strain relations for dynamic stability problems-----	89
2.64	Simplified stress-strain relations for wave propagation problems involving stresses, displacements, and velocities---	89
2.65	Stress-strain relations for wave propagation problems involving development of wave front-----	90
3.1	Stress-strain curves from controlled-strain tests-----	92
3.2	Strain-rate effect for saturated, normally consolidated fat clay-----	93
3.3	Results from controlled-stress tests with pulse loading-----	94
3.4	Results from controlled-stress tests with step loading-----	94
3.5	Relation between strain rate and time to failure-----	95
3.6	Rules for estimating strength to be used for practical problems-----	96
3.7	Factors affecting relation between strength and rate of loading-----	98
3.8	Effect of inertia during direct shear test-----	98

Figure No.	Title	Page
3.9	Lateral inertia during triaxial test-----	99
3.10	Effect of drainage on strength of saturated sand-----	99
3.11	MIT apparatus for rapidly loaded triaxial tests-----	102
3.12	Force transducer for recent tests at MIT-----	103
3.13	Pore pressure measuring system-----	104
3.14	Composite average result for three dry sands; early tests at MIT-----	105
3.15	Strain-rate effect for dry Ottawa sand-----	106
3.16	Comparison of strength during slow loading with and without vibrations-----	107
3.17	Stress-strain curves for a loose, saturated fine sand-----	107
3.18	Stress-strain curves for loose, saturated Ottawa sand-----	108
3.19	Stress-strain curves for dense, saturated Ottawa sand-----	109
3.20	Effect of strain rate on behavior of a saturated clay with and without confining pressure-----	109
3.21	Hypothesis for difference in strain-rate effect in different soils-----	113
3.22	Typical consolidated-undrained failure envelopes for a partially saturated soil-----	114
3.23	Strain-rate effect upon apparent cohesion-----	114
4.1	MIT one-dimensional compression device-----	119
4.2	Effects of side friction-----	120
4.3	Influence of disk size on measured strain-----	121
4.4	Typical loading sequence-----	122
4.5	Sketch of layout for one-dimensional compression tests-----	123
4.6	Arrangement for testing undisturbed samples-----	124
4.7	SRI version of MIT tester-----	125
4.8	WES version of MIT tester-----	126
4.9	Apparatus for accurate measurement of lateral stress during one-dimensional compression-----	127
4.10	One-dimensional compression device with fluid boundary-----	127
4.11	Articulated lateral boundary for one-dimensional wave propagation tests-----	128
4.12	Stress-strain curves for hypothetical one-dimensional compression tests on planar array of spheres-----	129
4.13	Behavior of Ottawa sand during initial loading in one-dimensional compression-----	131
4.14	Behavior of several sands during one-dimensional compression-----	132
4.15	One-dimensional stress-strain curve for small stress increments-----	132
4.16	One-dimensional stress-strain behavior during unloading and reloading-----	133
4.17	One-dimensional stress-strain curves for very loose sand and gravel-----	133
4.18	Effect of unloading and reloading during repeated one-dimensional compression-----	134
4.19	Secant modulus versus number of repeated loadings-----	134
4.20	Hysteresis loops after about 500 cycles in one-dimensional compression-----	135

Figure No.	Title	Page
4.21	Creep during rapid one-dimensional compression tests-----	135
4.22	Loading rate versus one-dimensional stress-strain behavior---	135
4.23	Lateral stress during one-dimensional compression-----	136
4.24	Dynamic one-dimensional stress-strain curves for compacted silty clay-----	138
4.25	Pattern of behavior for undrained loading of partially saturated soil-----	139
4.26	Triaxial cell for bulk modulus measurements-----	139
4.27	Dynamic one-dimensional stress-strain curve for undisturbed sample of till-----	140
4.28	Dynamic stress-strain curves, one-dimensional compression, 100-psi surcharge-----	141
4.29	Secant modulus versus dynamic axial stress, 100-psi surcharge-----	141
4.30	Tangent modulus versus dynamic axial stress, 100-psi surcharge-----	142
4.31	Static and dynamic one-dimensional stress-strain curves for undisturbed sample of till-----	142
4.32	Creep during one-dimensional compression of natural soils----	142
4.33	Constrained moduli-peak attenuated vertical stress-depth relations, WES 250-ft station, Operation Snowball-----	146
5.1	One-dimensional waves-----	157
5.2	Equations for elastic wave velocities-----	159
5.3	Relation between elastic wave velocities-----	159
5.4	Soil container and crystals for pulse tests-----	160
5.5	Circuit diagram for pulse test apparatus-----	161
5.6	Photograph of oscilloscope screen showing arrival of dilatational wave-----	162
5.7	Triaxial cell for velocity measurements by pulse technique---	162
5.8	End cap with radial crystals for sending and receiving shear wave-----	163
5.9	Photograph of oscilloscope screen showing arrival of shear wave-----	163
5.10	Comparison of dilatational, rod, and shear wave velocities in a dry sand-----	166
5.11	Rod wave velocity through dry sand as a function of confining stress-----	166
5.12	Deformation of elastic spheres by contact forces-----	167
5.13	Predicted and actual rod velocities through dense array of steel balls-----	168
5.14	Influence of shear stress on shear wave velocity in Ottawa sand-----	169
5.15	Effect of amplitude of dynamic stress on velocity-----	170
5.16	Young's modulus versus confining stress for quartz sand by various methods-----	171
5.17	Shear wave velocity versus void ratio for Ottawa sand-----	171
5.18	Shear wave velocity versus void ratio for quartz sand-----	172
5.19	Factors which influence magnitude of effective mass-----	175

Figure No.	Title	Page
5.20	Effect of mass of pore water on shear wave velocity through sand-----	176
5.21	Shear wave velocity for different degrees of saturation-----	177
5.22	Shear wave velocities through saturated clays and sands-----	178
5.23	Relation of rod modulus to undrained compressive strength in clays-----	180
5.24	Wave velocity through soil assuming no stress is carried by mineral skeleton-----	181
5.25	Calculated dilatational wave velocity through saturated soil-----	183
5.26	Measured dilatational velocity through dry and saturated sands-----	183
5.27	Calculated relation between dilatational velocity and degree of saturation-----	185
5.28	Dilatational velocity for various degrees of saturation-----	186
5.29	Dilatational velocity through partially saturated undisturbed sample-----	187

NOTATION

a_r	Peak radial acceleration
B^w	Bulk modulus of water
B, C, β	Factors in equation for predicting peak radial particle velocity; $v_r = \frac{B}{C} \left(\frac{W^{1/3}}{R} \right)^\beta$
c	Cohesion
\bar{c}	Cohesion intercept
$(c)_d$	Apparent cohesion intercept for dynamic tests
$(c)_{rs}$	Apparent cohesion intercept for rapid static tests
C	Wave velocity
C^a	Dilatational wave velocity through air
C^v	Dilatational wave velocity through pore fluid (for air, $C^v = C^a$)
C^w	Dilatational wave velocity through water
C_D	Dilatational wave velocity in the ground (i.e. velocity of a P-wave)
C_{DO}	Dilatational wave velocity of a seismic level signal
C_D^m	Dilatational wave velocity through solid mineral
C_D^s	Dilatational wave velocity through dry mineral skeleton
C_L	Rod wave velocity
C_s	Shear wave velocity in the ground (i.e. velocity of an S-wave)

d_r	Peak radial displacement
dN	Increment of force
$d\alpha$	Increment of movement
D	Constrained modulus ($D = \rho C_D^2$); also, diameter
D^S	Constrained modulus of mineral skeleton
D_p^+	Duration of positive overpressure
D_r	Relative density = $\frac{e_{\max} - e}{e_{\max} - e_{\min}}$
e	Void ratio
e_f	Void ratio at failure
e_{\max}	Maximum void ratio
e_{\min}	Minimum void ratio
E	Tangent modulus; also, Young's modulus
E_d, G_d	Modulus from resonant vibration
E_s	Modulus from static repeated loading
EI	Flexural rigidity of cylinder
f	Coefficient of friction of sphere material
g	Gravitational acceleration
G	Shear modulus; also, specific gravity
G_d	Shear modulus from dynamic tests
G_s	Specific gravity
HE	High explosive
I	Applied impulse
K	Constant $\left(= 1 - \frac{C_D}{C_{D0}} \right)$; also, a factor in Equation 2.15
K_o	Dynamic coefficient of lateral stress; also, coefficient of earth pressure at rest

LVDT	Linear variable differential transformer
L_w	$230 \text{ ft} \left(\frac{100 \text{ psi}}{p_s} \right)^{1/2} \left(\frac{W}{1 \text{ Mt}} \right)^{1/3}$ (see Equation 2.3)
m	Exponent
M	Constrained modulus; also, ratio of stress to strain
n	Porosity
N	Normal contact force between spheres
O.C.R.	Overconsolidation ratio
p	Overpressure behind shock front at time of p_s
p_s	Peak overpressure in shock front; also, applied stress
p_l	Peak overpressure at $r = R_l$
P	Pressure or load
PI	Plasticity index
PL	Plastic limit
$P(t)$	Pressure or load at time t
PVC	Polyvinylchloride
P-wave	Compression wave
r	Radius
R	Range or distance; also, radius
R-wave	Rayleigh wave
R_l	Radius at which $U = C_D$
s	Maximum shear stress possible on a plane (i.e. shear strength)
S	Degree of saturation
S-wave	Shear wave
SP-wave	von Schmidt wave
t	Time; also, thickness
t_{cr}	Critical thickness

t_r	Rise time
t_s	Shock arrival time
T	Time; also, side friction
TNT	Trinitrotoluene
u	Pore pressure; also, horizontal displacement
\dot{u}	Horizontal velocity
u_i	Initial pore pressure
U	Velocity; also, shock velocity of the airblast
v_r	Peak radial particle velocity
w	Vertical displacement; also, water content
\dot{w}	Vertical velocity
\ddot{w}	Vertical acceleration
$(w)_{\max}$	Peak displacement
$(\dot{w})_{\max}$	Peak vertical particle velocity
$(\ddot{w})_{\max}$	Peak vertical acceleration
W	Equivalent charge weight
z	Depth
z_c	Depth at which unloading P-wave and loading S-wave intersect
z_i	Depth at which attenuation ceases beneath linearly decaying superseismic strip load
α	Attenuation factor, Equation 2.2 $\left(\frac{1}{1 + z/L_w} \right)$; also, relative normal displacement between centers of spheres
β	Factor in Equation 5.5; proportion of pore fluid which moves with mineral skeleton
γ_d	Dry density
Δ	Increment

Δu	Excess pore pressure; also, change in pressure; also, increment of pore pressure
Δu_{cw}	Excess pore pressure developed during shear at constant water content
Δu_{dis}	Excess pore water pressure dissipated by partial consolidation during loading
Δw	Peak transient relative displacement
$\Delta \epsilon$	Increment of strain
$\Delta \sigma$	Increment of total stress
$\Delta \bar{\sigma}$	Increment of effective stress
ϵ	Strain
ϵ_a	Axial strain
θ_D	Inclination of the dilatational superseismic wave front
θ_s	Inclination of the shear superseismic wave front
μ	Poisson's ratio
ν	Poisson's ratio of sphere material
ρ	Mass density of soil
ρ^s	Mass density of mineral skeleton
ρ^w	Mass density of water
σ	Stress; also, total stress normal to plane
σ_a	Axial stress
σ_c	Confining pressure
σ_D	Dynamic axial or shear stress
σ_h	Horizontal total stress
σ_o	Initial stress; also, all-around confining stress; also, average principal stress $\left(\frac{\sigma_1 + \sigma_2 + \sigma_3}{3} \right)$
$\bar{\sigma}_o$	Effective confining stress; $\frac{\bar{\sigma}_1 + \bar{\sigma}_2 + \bar{\sigma}_3}{3}$

σ_v	Vertical total stress
σ_y	Yield stress
σ'_2	Free-field vertical soil stress leading to buckling
$(\sigma'_2)_{cr}$	Critical vertical stress
$(\sigma_2)_{max}$	Peak vertical stress
σ_1	Major principal total stress
$\bar{\sigma}_1$	Major principal effective stress
σ_2	Intermediate principal total stress
$\bar{\sigma}_2$	Intermediate principal effective stress
σ_3	Lateral stress; also, minor principal total stress
$\bar{\sigma}_3$	Minor principal effective stress
τ	$C_D t / R_1$ = time at which dilatational wave from the origin reaches $r = R_1$
$\phi, \bar{\phi}$	Angle of internal friction
$(\phi)_d$	Apparent friction angle for dynamic tests
$(\phi)_{rs}$	Apparent friction angle for rapid static tests

CONVERSION FACTORS, BRITISH TO METRIC UNITS OF MEASUREMENT

British units of measurement used in this report can be converted to metric units as follows:

<u>Multiply</u>	<u>By</u>	<u>To Obtain</u>
inches	2.54	centimeters
feet	0.3048	meters
inches per second	2.54	centimeters per second
feet per second	0.3048	meters per second
pounds	0.45359237	kilograms
pounds per square inch	0.070307	kilograms per square centimeter
pounds per square foot	4.88243	kilograms per square meter
pounds per cubic foot	16.0185	kilograms per cubic meter
kip per square inch	70.307	kilograms per square centimeter
kilotons	907,185	kilograms
megatons	907,185,000	kilograms
tons per square foot	9,764.86	kilograms per square meter
slugs per cubic foot	515.379	kilograms per cubic meter

CHAPTER 1 INTRODUCTION

1.1 PURPOSE AND SCOPE OF THIS REPORT

This report deals with soil dynamics as it applies to the prediction of the effects of nuclear weapons and to the design of protective structures to resist these effects. In particular, this report strives to indicate which properties of soil are important to such tasks, just how these properties enter into the analyses which are commonly performed in connection with these tasks, and how numerical values of these properties may be determined for individual practical problems.

Although mention is made of all aspects of soil dynamics as it applies to nuclear weapons effects and protective construction, this report is primarily concerned with airblast-induced ground shock and with the effects of this ground shock upon shallow-buried structures. The content of the report is based principally upon the research performed under the existing contract, and serves as a final report for that contract.* The report has also been heavily influenced by the experiences of the writer in the setting of ground motion criteria for the design of protective structures for the Atlas, Titan, and Minuteman missile systems, and in the evaluation and selection of sites for those facilities. Research results obtained by other engineers and researchers are included in the discussions in this report, insofar as they bear upon topics which have been studied by the writer.

The writer already has undertaken one summary of soil dynamics in the context of nuclear weapons effects and protective structures: Part II (Soils) of NUCLEAR GEOPLOSICS. In that earlier summary, testing equipment available for the study of soil during dynamic loadings and measurements obtained using this equipment were described in great detail. This information was then used as a basis for indicating which properties of soil might be especially important in practical problems.

In this report, the approach is reversed. Chapter 2 discusses, in

* Reports issued under this contract are listed in Appendix A, which presents an abstract of each report. Appendix B contains a brief history of research in soil dynamics at MIT.

general terms, the ways in which soil properties enter into the prediction of nuclear weapons effects and protective construction design. The subsequent chapters then discuss three particular aspects of soil behavior which have been found to be of especially great importance in practical work: shear strength, compressibility as measured in the oedometer test, and the velocity of propagation of seismic waves. This report emphasizes the important general features of soil behavior and practical procedures for estimating numerical values of these properties for use in particular problems. The reader is referred to NUCLEAR GEOPLOSICS for more detailed information.

There is another difference between this report and NUCLEAR GEOPLOSICS: this report presumes familiarity with the subject matter of soil mechanics, whereas NUCLEAR GEOPLOSICS was written for a much broader audience.

1.2 WHAT IS SOIL DYNAMICS?

As a body of knowledge, soil mechanics involves: (a) a collection of facts and interpretations concerning the stress-strain behavior of soil, together with a set of practical procedures for evaluating the stress-strain properties to be used in any particular problem; and (b) theoretical methods for relating the movements within a mass of soil to the applied loadings and boundary conditions, taking into consideration the stress-strain properties of the soil. Both of these aspects of soil mechanics have their complications. The stress-strain behavior of soil is extremely complex. Evaluating stress and strain distributions within a continuum is also a complex problem--much more difficult than analyzing framed structures, especially when the continuum is not a linearly elastic material.

Soil dynamics, which is a branch of soil mechanics, is characterized by two additional complications: (a) it is necessary to know the stress-strain behavior of soil during loadings which are rapidly applied and of short duration, and which are often repeated several times in rapid succession; and (b) it is necessary to account for the inertia forces which are developed within a mass of soil.

The stress-strain behavior of soil during rapidly applied loadings is fundamentally the same as that during ordinary rates of loading, although

the numerical value of the ratio of stress to strain is generally increasing as the rate of loading increases. In other words, the effect of rapid loadings is to cause quantitative rather than qualitative differences. Certain aspects of stress-strain behavior often assume greater importance in dynamic problems than in static problems: for example, the energy lost per cycle of loading, and loss of strength with successive cycles of loading. These aspects can be observed in static stress-strain tests, but engineers seldom worry about these aspects when dealing with the effects of static loadings.

On the other hand, the need to account for the effects of inertia forces makes dynamic problems qualitatively very different from static problems. That is, the presence of inertia forces generally means that the whole way of looking at a problem must be changed. New concepts, such as those associated with wave propagation, must be utilized. It is this aspect of soil dynamics which tends to set it apart from the rest of soil mechanics.

1.3 GENERAL LOOK AT THE STRESS-STRAIN BEHAVIOR OF SOIL

Soil is particulate; i.e. it is composed of a system of discrete mineral particles which are more or less free to move relative to one another, subject to the forces of adhesion and friction between particles and to the geometric constraints imposed by the arrangement of the particles. Being particulate, soil is also inherently multiphase. Except when the soil is in a vacuum, the pore spaces between the mineral particles must be filled with some fluid, usually air or water or both, and the interaction between mineral skeleton and pore phase has great influence upon the stress-strain behavior of the soil.

Since soil is particulate and thus multiphase, it would be expected that soil would exhibit complex stress-strain properties: nonlinear, irreversible, and time-dependent effects, as well as sensitivity to stress level and stress history. Two general aspects of the stress-strain behavior of soil are especially important as discussed below.

1.3.1 Behavior During Compression and Shear. The first important general aspect is the difference in behavior during compression which

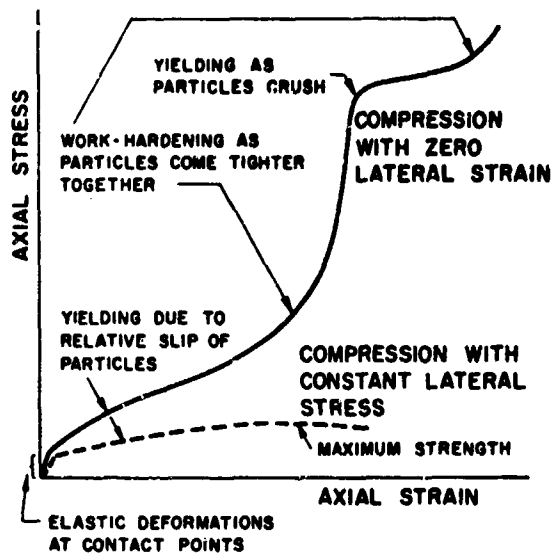


Fig. 1.1 Stress versus strain for a particulate system

produces little shearing action and compression which produces much shearing action (see fig. 1.1). In both cases the behavior results principally from relative motions between particles. In the case of a confined compression, the particles are pushed into progressively tighter packings with their neighbors, while during shear the particles are rolled and shoved past their neighbors. For small changes in stress, the behavior during the two forms of compression is similar. However, large changes in stress

cause quite different kinds of behavior during the two forms of compression.

The type of test chosen to evaluate stress-strain behavior in a given situation must reflect the type of confinement and magnitude of stress change expected in that problem.

1.3.2 Hydrodynamic Time Lag. The second important general aspect arises from the occurrence of relative movement between the mineral skeleton and the pore fluid. When a saturated soil is compressed, water tends to flow out of the soil. However, certain time is required for this movement of water. During a load of short duration, there may be no flow of water, and hence a soil will compress much less during a rapid loading than it will during a slow loading of the same magnitude (see fig. 1.2).

The movement of water out of or into soil as the result of some change in the applied load is referred to as consolidation or swell, respectively,

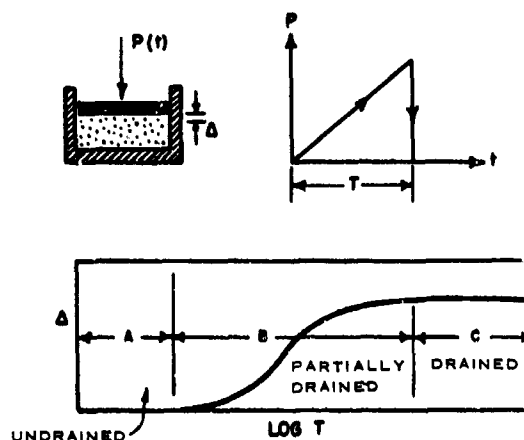


Fig. 1.2 Hydrodynamic time lag in compressibility of soil

and the time required to complete this movement is the hydrodynamic time lag or consolidation time. The hydrodynamic time lag of a mass of soil is a function of (a) type of pore fluid, (b) permeability and compressibility of the soil, (c) size of the soil mass, and (d) drainage provided along the boundaries of the soil mass. For a large soil mass typically involved in practical problems and composed of coarse, granular soil, the consolidation time will generally be on the order of a few minutes or less. For a fine-grained cohesive soil, the consolidation time may range from days to years to decades, depending upon the size of the soil mass.

The amount of consolidation of a given soil mass during a given loading is controlled by the ratio of the duration of the load to the consolidation time of the soil deposit. The following rules apply:

Ratio	<u>Consolidation Time</u> <u>Duration of Load</u>	Condition of Soil Mass	Time Period Shown in Fig. 1.2
	$\ll 1$	Drained	C
	$\gg 1$	Undrained	A
	≈ 1	Partially drained	B

With the rates of loading encountered in ordinary soil engineering work, deposits of coarse, granular soil usually are fully drained. However, such a deposit may be only partially drained or even undrained during a dynamic loading. Fine-grained cohesive soils may be either drained, partially drained, or undrained during the loadings encountered in ordinary practice. During dynamic loadings, such soils usually are undrained.

Other types of time-dependent effects are also present in soils, but the hydrodynamic time lag is by far the most important.

1.3.3 Use of Approximate Stress-Strain Rules. In view of the complexity of the stress-strain behavior of soils, it is not surprising that there is no one complete description of the stress-strain properties. Rather, engineers must adopt simplified "models" for the behavior of soils. The model adopted for any particular problem must emphasize the aspects of soil behavior which are most important to that particular problem. Chapter 2 will indicate some of the "models" for soil behavior which have been

found particularly useful for problems involving nuclear weapons effects in protective construction design.

1.4 HERITAGE OF SOIL MECHANICS

1.4.1 Value of Experience. The practice of foundation and earthwork engineering has acquired the reputation of being an art, in which experience and judgment are paramount and theory is relegated to a minor role. To a large extent, of course, the same statement can be made concerning any branch of engineering, but it is especially true of foundation and earthwork engineering.

There are indeed sound reasons why experience must play an important role in foundation and earthwork engineering. Two of these reasons have already been mentioned: (a) soil has a complex stress-strain behavior, and (b) soil occurs as a massive continuous body rather than as a simple, framed structure. Approximations are thus necessary if one wants to estimate the motions which will occur within soil masses, and experience and judgment are always necessary for the intelligent application of engineering approximations. Even more important, soil is a natural material susceptible of large variations from site to site and within a particular site. The nature of the soil at any site must be revealed by sampling, which actually "sees" only an infinitesimal portion of the soil at the site. Often a very thin layer of soil, easily missed by random sampling, will completely control the engineering behavior of the soil mass. Again, experience and judgment are necessary when estimating the response of natural soil deposits.

1.4.2 Role of Theory. On the other hand, theory clearly cannot be ignored. Only through use of theory can an engineer satisfactorily extrapolate his experience to new unprecedented situations (different forms of loading, different types of design criteria, etc.). New situations of this type have occurred frequently in the protective construction field within the past several decades, as well as in other fields in which soil dynamics plays an important role.

The past practice of soil engineering provides valuable insights into

the proper and improper use of theory. There are two general ways in which theory can properly be applied:

- (a) By fitting a theory (which may be either very simple or of any degree of sophistication) to experience through proper evaluation of the parameters. This approach does not eliminate uncertainty, since there is always the question of whether the experience can properly be extrapolated in this way to the next (and possibly quite different) situation. Nonetheless, when used with judgment this is a valid approach. For any new application of the theory, fairly precise quantitative data will be required regarding the properties of the soil.
- (b) Use of theory to help understand what might happen in a new situation; i.e., use of theory to investigate the consequences of the several assumptions which might reasonably be made to blanket the uncertainties concerning the nature of the soil at a site. This is generally the approach which must be taken whenever experience is limited. It is essential that calculations be made in such a way that there is a clear relation between each assumption and its effect. For this approach, knowledge of the general features of stress-strain behavior is essential, together with data to indicate the possible range of parameters. That is, the data must be qualitative rather than quantitative.

Experience has also shown that it is improper to make one very complex calculation using a single set of assumed soil properties. From the quantitative standpoint, the results of such a calculation may be vastly in error because of all the questionable assumptions which inevitably will have been made. From the qualitative standpoint, the results will not give clear cause-and-effect relations between each assumption and its consequence, and thus will fail to provide even a basis for engineering judgment.

1.4.3 Application of Experience and Theory. Thus value is derived from both experience and judgment and the intelligent use of theory. The challenge in every soil engineering problem is to satisfactorily blend both of these approaches to arrive at the best possible solution.

CHAPTER 2 SOIL DYNAMICS AS PERTAINING TO NUCLEAR WEAPONS EFFECTS AND PROTECTIVE CONSTRUCTION DESIGN

2.1 MECHANICAL EFFECTS OF NUCLEAR EXPLOSIONS

A large, near-surface nuclear explosion produces three general mechanical phenomena: (a) formation of a crater; (b) generation of an airblast wave which sweeps outward over the surface of the earth; and (c) generation of stress waves within the earth, as a result of energy entering the earth immediately at the point of the explosion (directly induced ground shock) and also as a result of the loadings of the ground surface by the airblast wave (airblast-induced ground shock). These three phenomena are depicted schematically in fig. 2.1. All three are of interest to civil engineers and are affected in some way by soil dynamics.

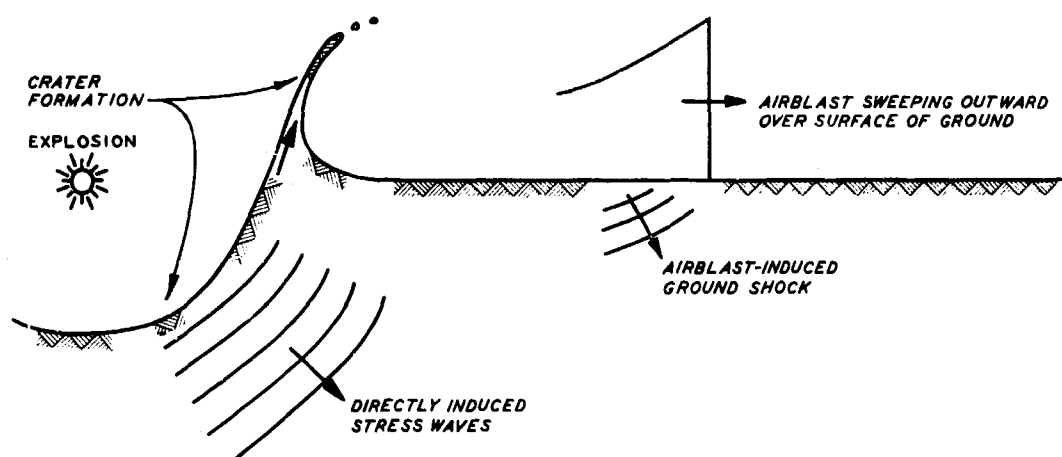


Fig. 2.1 Mechanical effects of near-surface nuclear explosion

The size of the crater formed by an explosion is itself of interest in protective construction design and in the military or civil use of nuclear explosions for demolition or excavation (Nordyke et al., 1963*; Graves, 1964; Vortman, 1964). The crater is of course a zone of total destruction. The earth thrown out of the crater (ejecta) and landing in the area immediately around the crater will bury and often render useless any facilities

* See Literature Cited at end of text.

located close to the crater. Obviously the response of soils to dynamic loadings must have some bearing on the size and shape of the crater formed by such an explosion.

The airblast sweeping outward from the point of the explosion will impose loadings upon surface and above-surface structures. Airblast will totally destroy almost all aboveground structures located near the point of the explosion. However, properly designed structures located at some distance from the explosion can survive, and the design of such structures is of prime interest in civil defense (Newmark, 1965). Moreover, very special structures of low profile, such as radar antennas, can survive severe airblast and are of interest in military applications. Since the foundation supporting a structure often has some influence upon the way in which a building will respond to this type of loading, soil dynamics is of importance to the problem of structures subjected to airblast loadings.

The stress waves generated within the earth are of interest because they cause the earth to deform and move, thus causing forces upon and movements of structures founded upon or located within the earth. Prime military targets which might be the subject of direct nuclear attack, such as missile emplacements and command centers, must be located underground and must be designed to withstand such stress waves (Newmark, 1965). The propagation of stress waves through earth and the interaction of these stress waves with structures are obviously problems in soil dynamics. For simplicity in dealing with the enormously complicated problem of these stress waves and their effects, it has been found convenient to break the problem into the four parts shown in table 2.1.

Thus we have six types of problems in which soil dynamics enters into protective construction and nuclear weapons effects: (a) cratering; (b) the effect of foundation conditions on the motion of surface structures; (c) free-field ground motions and stresses with airblast-induced stress waves; (d) soil-structure interaction with airblast-induced stress waves; (e) free-field motions and stresses with directly induced stress waves; and (f) soil-structure interaction with directly induced stress waves. The following sections will discuss the soil properties pertinent to each of these problem areas, both from a general standpoint and in

Table 2.1
Four Aspects of Explosion-Induced Stress Waves

According to the Source of the Stress Wave	According to the Effect of the Stress Wave
<p>1. <u>Directly induced stress waves:</u> The effects of these waves are important when designing buried structures which are to survive below or very close to the explosion crater. Such structures will be subject to very intense stresses: on the order of 10,000 psi or more.</p> <p>2. <u>Airblast-induced stress waves:</u> The effects of these waves are important when designing surface structures or structures which must, for operational or economic reasons, be buried at shallow depth. Inevitably, such structures can survive only at a considerable distance from the point of the explosion, and the stresses will be much less than for directly induced waves: on the order of 10,000 psi and less.</p>	<p>1. <u>Free-field ground motions and stresses:</u> These are the effects experienced by the ground when no structures are present. The motions of embedded structures are more or less the same as the free-field motions, and thus knowledge of free-field motions is important to evaluate damage to the contents of any structure.</p> <p>2. <u>Soil-structure interaction:</u> The stresses in the free field are modified by the presence of an embedded structure, and the stresses actually acting upon a structure are determined by the deformability of the structure and the strength and deformability of the surrounding soil.</p>

connection with specific problem analyses. Most of the emphasis will be on problems (a), (c), and (d), which are the problems with which the author is most familiar and toward which most of the work of the present contract has been oriented.

Although this chapter will provide some quantitative information regarding the size of craters and the magnitude of directly induced and airblast-induced ground shock, the reader who wishes more detailed information can consult the following basic references:

Effects of Nuclear Weapons, S. Glasstone, editor, Supt of Documents, U. S. Government Printing Office, Washington, D. C., 1962.

Nuclear Geoplosics, F. Sauer (Stanford Research Institute), editor-in-chief, Defense Atomic Support Agency, Washington, D. C., DASA 1285 in five volumes.

Design of Structures to Resist Nuclear Weapons Effects, Manual No. 42, American Society of Civil Engineers, New York, 1961.

"A Review of Nuclear Explosion Phenomena Pertinent to Protective Construction," H. L. Brode, Report R-425-PR, Rand Corporation, May 1964.

"Air Force Design Manual - Principles and Practices for Design of Hardened Structures," Air Force Special Weapons Center (now Air Force Weapons Laboratory), Kirtland AFB, New Mexico, AFSWC-TDR-62-138, AD 295408, 1962.

These references also provide information regarding other important effects of nuclear explosions: thermal, radiation, and electromagnetic.

2.2 CRATERING

2.2.1 General Features of a Crater. Fig. 2.2 shows the general features of a crater resulting from a large near-surface explosion.

The crater as viewed from above is called the apparent crater. The dimensions of the apparent crater are measured with respect to the original ground surface. Thus the apparent diameter is measured at the elevation of the original ground surface, and the apparent depth is measured from the original surface.

Such a crater is partially filled with earth which has been thrown

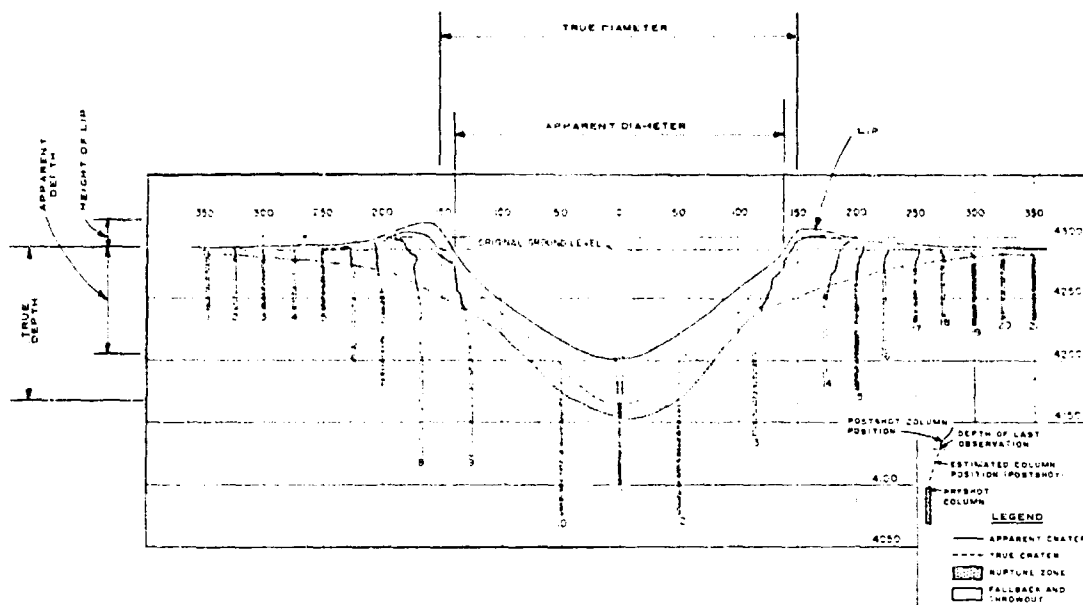


Fig. 2.2 Cross section through crater of Teapot-ESS

into the air by the explosion and then has fallen back into the crater. This material is called fallback. Similarly, the surface of the ground around the crater is covered in varying degrees by throwout. The true crater is defined as the boundary between the fallback or throwout and the underlying material which has been crushed and fractured but which has not been thrown into the air and experienced free fall.

Often it is difficult to distinguish precisely the boundaries of the true crater. The earth within the rupture zone is displaced, having been pushed down below the crater and pushed upward and outward at the sides of the crater. These motions are large, and there is not always a clear distinction between this sheared and compressed material and that which has been thrown from the crater and fallen back. Note that the crater lip is formed in part by upthrusting of the more or less intact material of the rupture zone.

It is even more difficult to differentiate the rupture zone from the surrounding plastic zone. Near the true crater interface there are large amounts of fracturing by shear failure and crushing by compressive stresses, and gross displacements by faulting and underthrusting are generally seen. The severity of these effects decreases with increasing distance into the

rupture zone, until near the interface between the rupture zone and the plastic zone only small-scale shear failures are found. In the plastic zone there are small, uniform, permanent displacements which gradually disappear with increasing distance into the elastic zone.

The various features of a crater are affected greatly by the location of the explosive charge relative to the ground surface as indicated in fig. 2.3. Fig. 2.4 gives apparent crater dimension data obtained from detonation of small (256-lb*) high-explosive (HE) charges; large

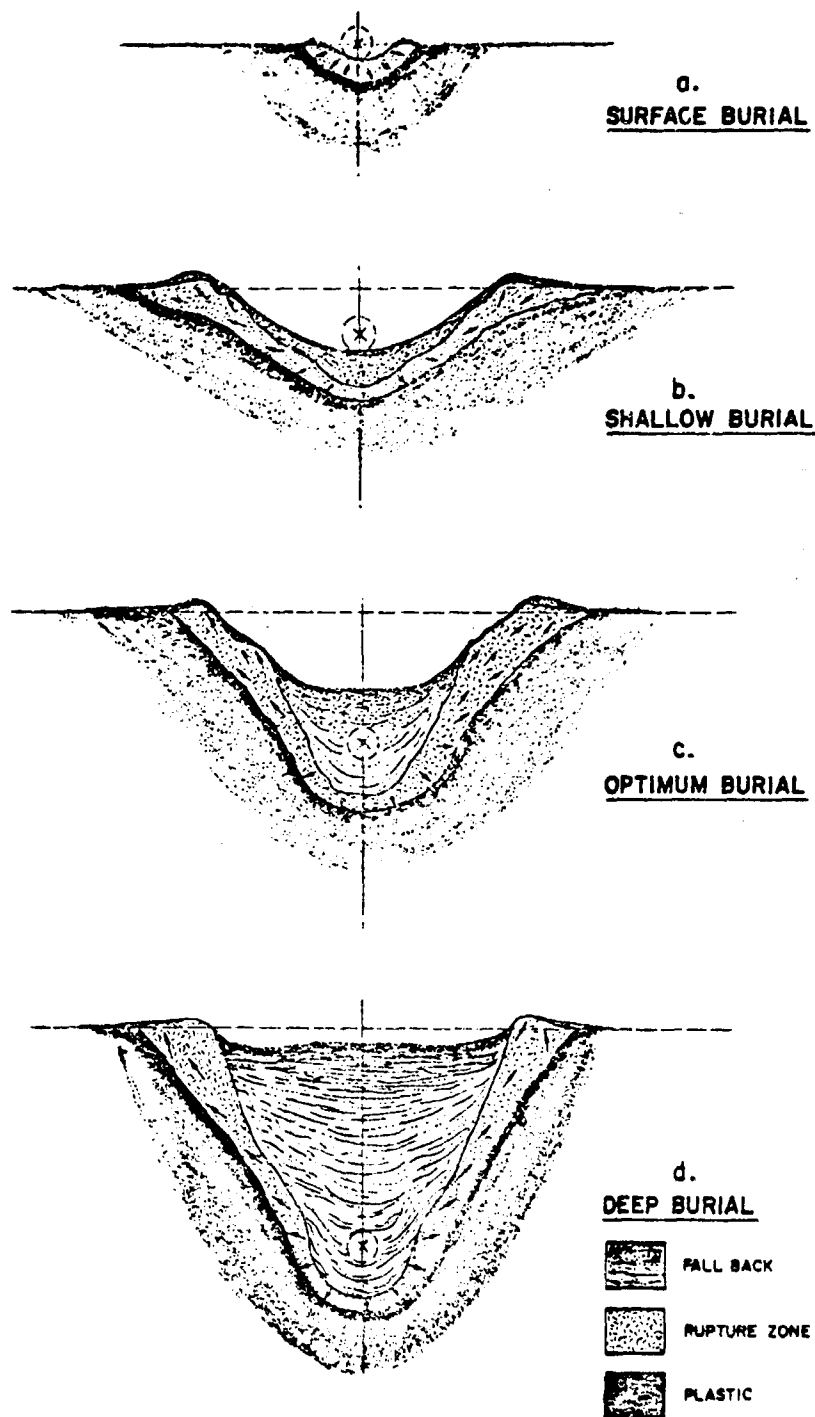


Fig. 2.3 Typical crater profiles versus depth of burst for alluvium (from Nordyke, 1961a)

* A table of factors for converting British units of measurement to metric units is presented on page xxiii.

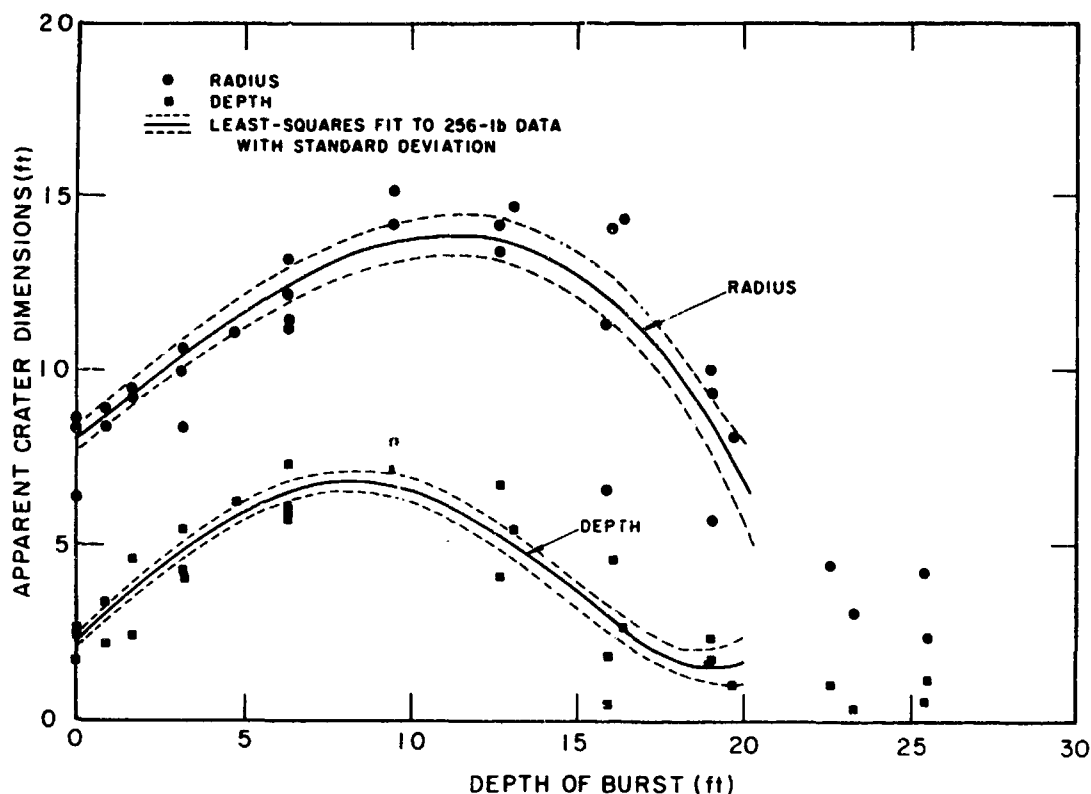


Fig. 2.4 Crater dimensions versus depth of burst for 256-lb HE shots in NTS alluvium (from Nordyke, 1961a)

explosions produce similar trends. Explosions above the ground surface tend to create a shallow depression with a barely distinguishable lip. The depth of the crater and the height of the lip increase when the explosion point is right at ground surface, and increase even more dramatically as the explosion point moves somewhat below ground surface. However, deeply buried explosions will produce only an underground cavity and perhaps some settling of the surface. The depth of burial which gives maximum crater dimensions is called the optimum depth.

This general concept has been developed from experiments in dry soils and rocks. If there is a high (i.e. near the surface) water table, the concept may change somewhat as will be discussed subsequently.

2.2.2 Sizes of Craters. The following references have compiled data from cratering experiments through 1960: Sager et al. (1960); Strange et al. (1961); and Nordyke (1961b). More recent references include Rooke

and Chew (1965) and Nordyke (1964). Although this section will consider only craters caused by a single charge, craters produced by multiple charges have also been studied. Row charges, which might be used to excavate a canal, are of special interest.

Effect of size of explosion: The parameter which has most effect upon the size of a crater is of course the energy released by the explosion. The standard unit for rating explosives is the equivalent weight of TNT. Thus a nuclear explosive may be rated as 200 kt, meaning that the energy release is the same as that for 400,000,000 lb of TNT. This method of rating leads to some problems, especially when comparing the results of craters produced by high explosives and nuclear devices, since the time history and general nature of the energy release are different for the two types of explosives.

For a surface explosion, it generally is assumed that crater dimensions scale as $W^{1/3}$, where W is the equivalent weight. A 1-kt nuclear surface burst in desert alluvium produces approximately the following crater dimensions:

Apparent diameter:	130 ft
Apparent depth:	32 ft
Height of lip:	8 ft

Following the usual scaling law, a 20-Mt surface burst in the same soil would produce these dimensions:

Apparent diameter:	3500 ft
Apparent depth:	850 ft
Height of lip:	210 ft

For belowground explosions, the situation is much more complicated. The available evidence indicates that dimensions scale more like $W^{0.295}$ or even $W^{0.25}$. The proper exponent for the scaling law has received considerable discussion: for example, see Nordyke (1961b) and Chabai and Hankins (1960). The largest crater actually measured (the SEDAN crater in desert alluvium, caused by a buried nuclear device rated at 100 kt) had dimensions as shown in table 2.2. The table also shows the difference in the predicted crater dimensions for a 10-Mt explosion using the several scaling laws.

Table 2.2
Crater Dimensions According to Various Scaling Laws

	SEDAN (100-kt) <u>Actual</u>	Scaled to 10 Mt		
		$W^{1/3}$	$W^{0.295}$	$W^{1/4}$
Apparent diameter, ft	604	2800	2340	1910
Apparent depth, ft	320	1490	1240	1010

Effect of type of soil: Clearly the type of soil or rock in which the explosion occurs must have some influence upon the dimensions of the resulting crater. Fig. 2.5 compares, for example, craters produced in dry alluvium and wet clay by 256-lb HE charges. However, the effect of soil type upon crater size is still largely undetermined, owing to the scarcity of large cratering explosions.

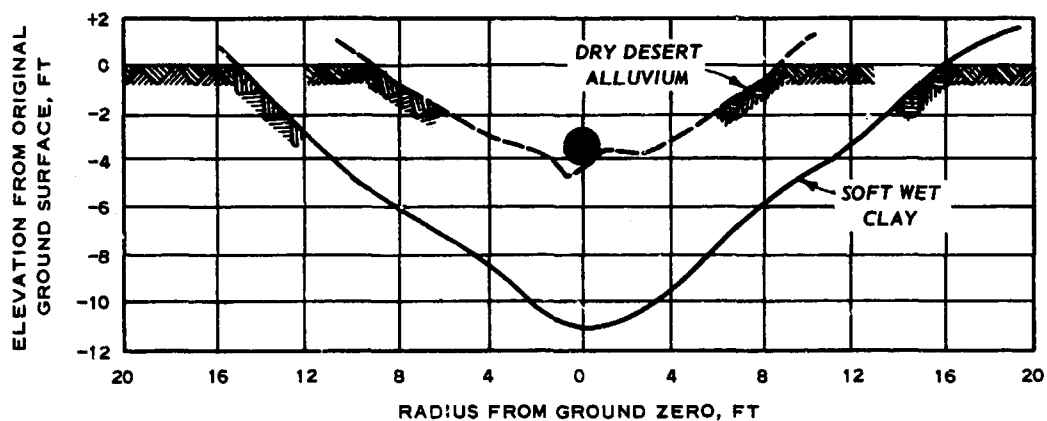


Fig. 2.5 Apparent craters from 256-lb HE charges
 (from Swift and Sachs, 1954)

Fig. 2.6 gives data showing the size of craters produced by rather small HE charges in various soils and rocks. Crater sizes in most soils and rocks are surprisingly similar. Larger explosions appear to give even less difference in crater size for various media. Craters in hard rock are usually taken to have dimensions 0.8 times those in dry soil. Craters in soft rock have generally run about the same as those in dry soil.

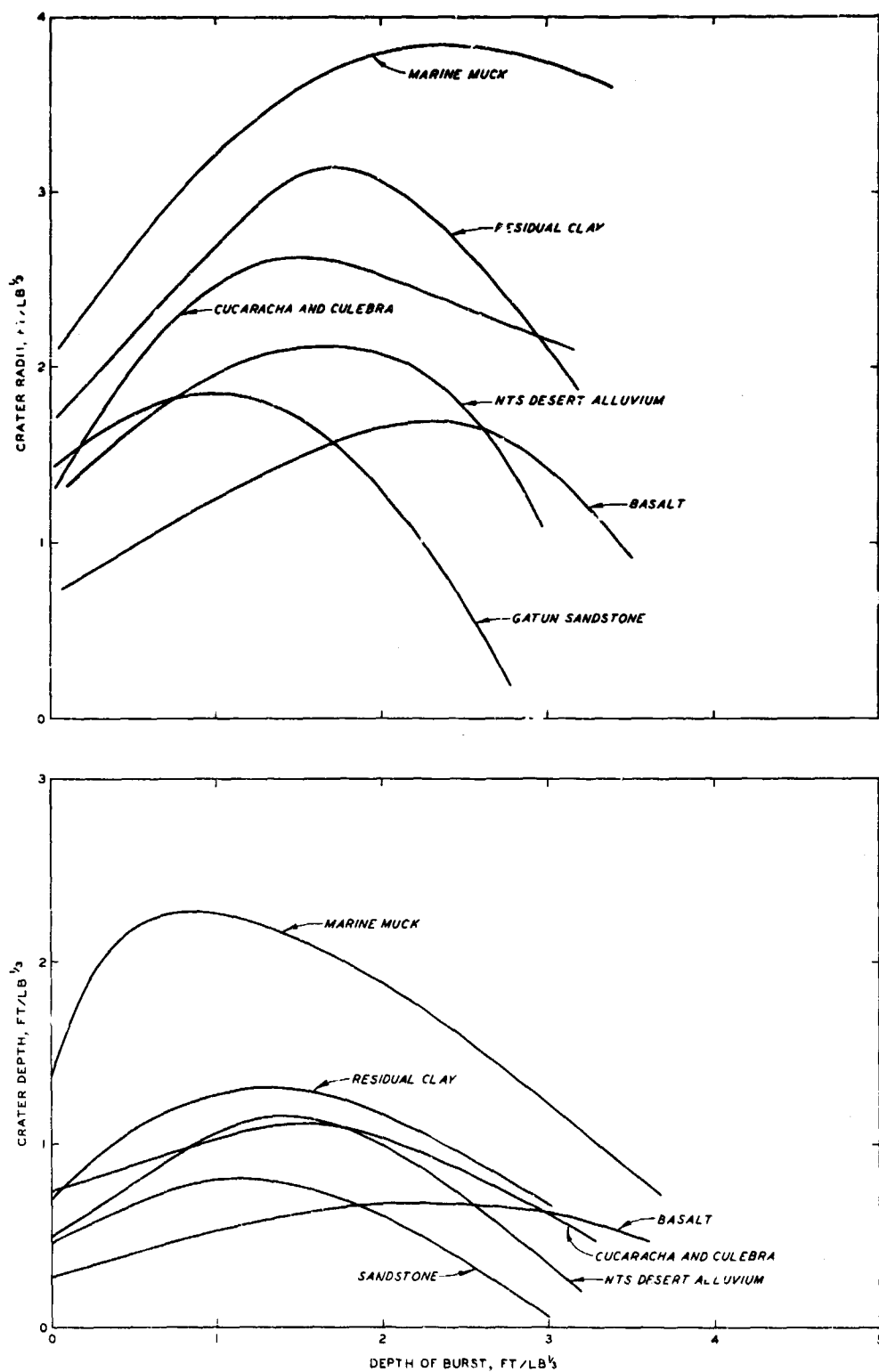
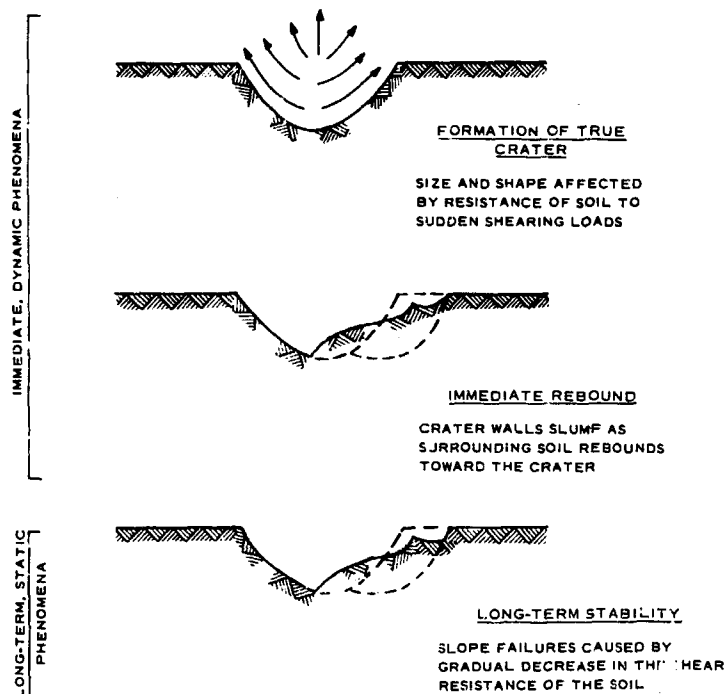


Fig. 2.6 Crater radii and depth versus depth of burst relation for various earth materials (from Nordyke, 1961a)

Craters in saturated clays and sands have shown dimensions averaging 1.7 times those in dry soils.

2.2.3 Processes of Crater Formation. Study of the craters formed by large explosions can conveniently be divided into three phases as follows (see fig. 2.7):



(a) Formation of true crater: During this phase, earth is moved outward from the point of the explosion, in part by throwing earth upward into the air and in part by distorting and compressing the earth.

(b) Immediate rebound: During this phase, earth which has been thrown into the air falls back into the crater and

Fig. 2.7 Phases of crater formation

onto the surface around the crater, and the compressed and distorted earth around the crater rebounds toward the crater.

(c) Long-term stability: During this phase, natural geological processes bring about the gradual reduction of the crater volume.

The first two phases involve dynamic processes, and are intimately coupled together. Practically speaking, it is impossible to say when the first phase ends and the second begins. For the typical explosion, some earth undoubtedly is moving outward while other earth has already started to rebound. Nonetheless, it is convenient to discuss the two phases separately since soil properties enter in a different way for each phase. The third phase involves essentially static phenomena; discussion of this phase is

included here only because it is of much interest in connection with a dynamic process.

Formation of the true crater: Three general processes are involved in causing the outward movement of earth during formation of the true crater:

(a) compaction of the earth beneath and to the sides of the explosion point;
 (b) spall of the ground surface above the explosion, as the initial stress wave from the explosion reaches the surface, and (c) acceleration, over a longer period of time, of the soil around the explosion. Fig. 2.8 suggests the relative contribution of these three processes.

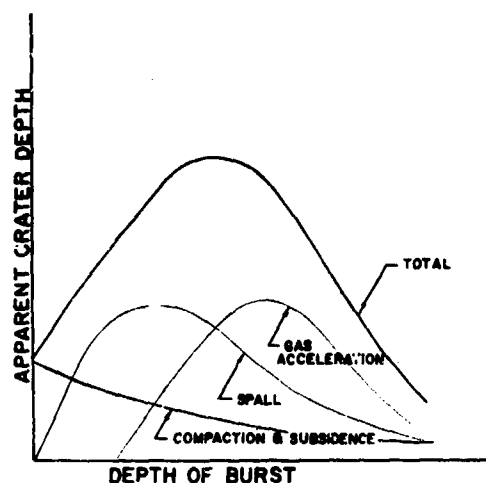


Fig. 2.8 Relative contributions of various mechanisms to apparent crater depth for explosion crater (from Nordyke, 1961b)

The first two of these processes have received considerable attention from physicists: see Brode and Bjork (1960), Knox and Terhune (1964). Detailed calculations have been made tracing the effect of the first wave coming outward from the explosion. Figs. 2.9 and 2.10 show, as an example,

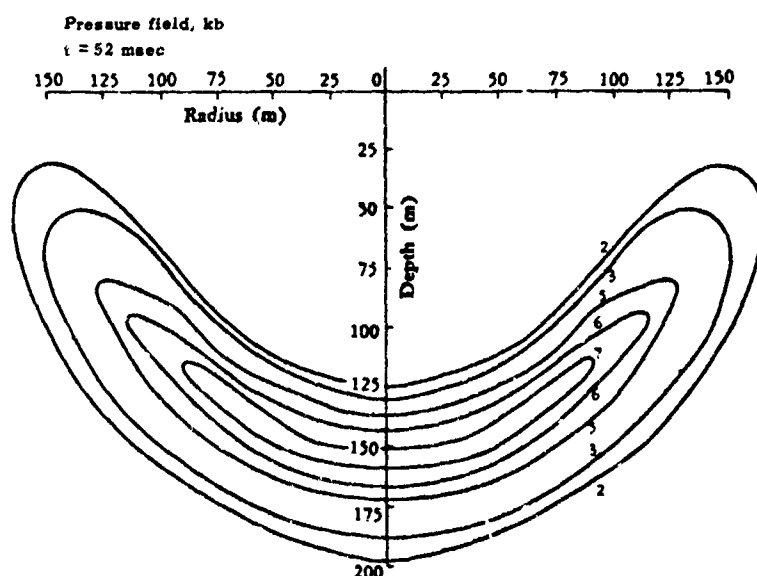


Fig. 2.9 Computed pressures caused by 1-Mt surface explosion (from Brode, 1964)

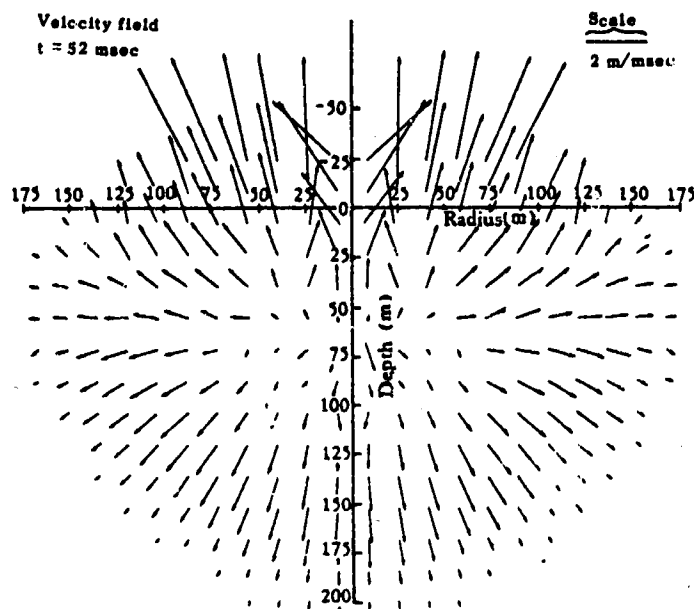


Fig. 2.10 Computed particle velocities caused by 1-Mt surface explosion
(from Brode, 1964)

the calculated pressures and particle velocities at a particular instant of time following a hypothetical 1-Mt nuclear surface burst. Note the magnitude of the pressures (1 kb \approx 14,500 psi). The throwout of soil from the ground surface is evident from the vectors in fig. 2.10. Calculations such as these assume that the shear resistance of the soil is negligible compared to the large stresses; i.e. that the soil behaves as a fluid. The region in which this condition is valid, the so-called hydrodynamic region, probably is contained within the true crater. A compressive stress-strain relation or equation-of-state which accounts for thermal effects and phase changes at the very high temperatures and pressures is required for the calculations. To date, results of these calculations provide the best basis for estimating the stresses existing in the soil immediately at the boundary of the crater, in spite of the possibility that the true hydrodynamic zone ends somewhere within the true crater. The calculations can also be used to predict patterns of throwout, and correlations have been made between the theoretical results and field observations (Hess and Nordyke, 1961). High-speed photographs of the ground rise above an explosion (fig. 2.11) have been invaluable in the study of throwout.



Fig. 2.11 Sequence views of ground rise at ground zero in Scooter event (from Violet, 1961)

Gas acceleration is the predominant effect during the final stages of crater formation, and thus greatly influences the size of the true crater. The calculation mentioned in the previous paragraph also accounts for the

effect of gas acceleration, at least out to the time at which the pressures decrease to the point where the shear strength of the earth is significant. Soil engineers have made several rather crude analyses which consider the effect of gas acceleration together with the strength of soil: Whitman and Taylor (1954), Whitman (1959), and Vesić and Barksdale (1963). Although these calculations are too naive to give good quantitative predictions of crater size, they have helped to explain certain facts:

- (a) Once rock has fractured (as by the first shock wave arrival, or before the explosion by geological processes) its resistance to shear will be similar to that of dry sand, and hence craters in rock (especially soft rock or closely jointed rock) are about the same size as those in dry soils for comparable explosions.
- (b) Because the strength of soft saturated soils is independent of normal stress changes (and hence there is no component of strength developed by the blast pressures), craters in such soils are larger than those in dry soils for comparable explosions.

In order to achieve a real understanding of the relation between soil strength and crater size, the more complex type of calculation, which accounts simultaneously for all three processes, must be extended to consider the shear resistance of the earth during the latter stages of crater formation. When this is done, it will be necessary to provide data regarding the shear resistance of soils during sudden loadings.

Immediate rebound: When the gas pressure against the crater walls drops to a negligible level, instability of the crater slope becomes a problem. For deep craters in weak materials, slides into the crater may develop at this stage (Whitman, 1959).

To date, there have been no detailed analyses of this immediate rebound situation. It seems likely that slides will develop in a crater slope if they would develop in a slope of the same geometry excavated "instantaneously" by conventional methods. Thus a lower limit to the maximum stable crater depth might be obtained by a conventional static slope stability analysis using static undrained strength.

There are several reasons why the actual transient situation may be more severe than the corresponding static situation:

- (a) The earth must resist not only the pull of gravity but also the deceleration of the slope at the end of rebound. This latter effect is similar to that produced by a single very strong earthquake pulse.
- (b) The strength of the earth may have been reduced by the passage of ground shock through it. This effect will be especially important in sensitive soils and in rocks.
- (c) The timing of the rebound and the fallback may be crucial. That is, the slope of the true crater may fail immediately even if the slope of the apparent crater would be stable.

Unfortunately, there are no means available for accounting for these effects in a quantitative way.

Significant sliding during immediate rebound has not been observed during explosions in dry soil and rock, although there have been detailed studies of the opening of joints and fissures around craters in rock (Sherman and Strohm, 1964). However, slides during immediate rebound did occur during the first large explosion test (Operation SNOWBALL) in a soil with a high water table (Rook and Chew, 1965). This aspect of cratering will assume major proportions if larger explosions are made in such soils.

Long-term stability: Generally speaking, the strength of the earth within a slope decreases with time following formation of the slope. This decrease results from various physical and chemical interactions between groundwater and the earth. Thus slides may develop at some time after cratering. The problem will be especially severe for craters in saturated soils of high permeability such as sand. Water flowing from a sand into the crater will give rise to a quick condition, causing heave of the bottom of the crater and slumping of the crater walls (Whitman, 1959). Severe problems can also be expected in soils which tend to lose strength when unloaded, such as stiff-fissured clay-shales (Whitman, 1959).

One important problem involved in nuclear excavation is the stability of a crater slope when another crater is formed nearby. The best guidance for this problem comes from studies of slope stability during earthquakes: Seed and Martin (1966) and Bustamante (1965). Trouble should be expected only when the slope is in a precarious state of stability or when the soil

is likely to lose strength if subjected to repeated loadings.

2.2.4 Requirements for Data Regarding Soil. A full analysis of cratering action would require the type of stress-strain information summarized in table 2.3. The first column states the requirement in general terms. The second column indicates the status of the theory in which the data are to be used. The final column indicates the realistic present requirement for data, considering the present status of the theory and its probable development in the immediate future.

In general, there are today no calculation procedures on which absolute reliance can be placed and there are no proven empirical relations. This situation seems unlikely to change in the immediate future. Hence the need is to establish the key features of the stress-strain behavior of soil and to give probable ranges for the values of the key parameters. Except for data applicable to the hydrodynamic region, there is no realistic requirement for data of a specific kind for any given site other than that which would normally be obtained during a thorough, modern soil mechanics investigation.

2.3 MOTIONS OF SURFACE STRUCTURES

Aboveground structures will be loaded by the airblast from an explosion; this loading will be transmitted to the structure foundation, causing the structure to displace into the supporting soil. In addition, the foundations of these structures will be moved by airblast-induced and directly induced stress waves, in much the same way as foundations will be moved by an earthquake. From the soil mechanics point of view, there are two problems: (a) how soil conditions affect the magnitude of the foundation motions, and (b) how to analyze the interaction between the soil and the structure.

If the explosion is aboveground or buried to less than the optimum depth of burial, the airblast effect on a nearby aboveground structure will be much more severe than the ground motion effect. Airblast pressures on the order of 5 to 10 psi will seriously damage or destroy conventional buildings, and 30 psi is usually considered to be the practical limit for design of aboveground protective structures. Hence the response of surface

Table 2.3

Requirements for Data on Soil Properties in Connection with Cratering

General Requirement	Status of Theory	Present Requirement
Compressive stress-strain relation for the hydrodynamic region.	Theory well developed, but little actual verification from field experiments.	Detailed data required; methods beyond scope of this report.
Stress-strain relation (including shear strength) sufficient to define wave propagation effects within plastic zone.	Theoretical development still in infancy.	Knowledge of key features of stress-strain behavior; probable range of values for key parameters.
Shear strength during immediate rebound.	None.	Probable range of values.
Shear strength for long-term stability.	Theory well developed, except for clay-shales, but almost no actual verification of applicability to craters.	Detailed strength data required.

structures to ground motions is of concern for deeply buried explosions or at very great distance from near-surface explosions. Hankins (1964) and Mickey (1964) give data concerning these ground motions. Very little is known concerning the effect of soil type upon these motions, although there is reason to believe that these motions and their effects may be greater if the soils are highly saturated than if they are dry.

Structural response to either airblast or ground motions is usually analyzed by adopting an equivalent lumped parameter system. The effect of the foundation upon the response can be considered by including a spring, dashpot, and mass to represent the foundation. The general approach for selecting the equivalent spring, dashpot, and mass is just the same as would be used for machine foundations or in earthquake studies (Whitman and Richart, 1967); of course, the spring constant applicable for the large dynamic foundation stresses caused by an explosion generally will be different from that applicable for small dynamic foundation stresses. Some measure of the stiffness of the soil is necessary for this purpose, either by means of dynamic laboratory tests on undisturbed samples or in situ plate bearing tests using repeated loadings. In analyzing the response of above-ground protective structure foundations to airblast loading, choice of lumped parameter foundation elements should be guided by the data summarized in Whitman and Luscher (1965).

It is possible that ground motions from an explosion may densify the soil below a building by vibratory action, and thus lead to differential settlements which will cause cracking of buildings, etc. Very little is known about this problem. Presumably the types of damage criteria discussed by Cauthen (1964) allow for this effect, at least in a general way.

2.4 AIRBLAST-INDUCED STRESS WAVES

This section is concerned with the stress waves within the ground caused by airblast moving outward from the explosion and thereby imposing stresses upon the surface of the ground. The pattern of these stress waves is very complex, and hence simplifications are necessary in order to permit engineering predictions concerning the motions. While there have been many measurements of the motions due to actual stress waves caused by nuclear

and large chemical explosions, these data actually are scant in view of the great complexity of the problem. Moreover, such tests have been conducted only for very restrictive soil conditions. Many theories, some involving very complex calculations, have been developed to aid in the understanding of the propagation and attenuation of these stress waves. There is increasing use of these theories to generate ground motions for use in design of protective structures, but theories should be so used only when they have been verified by checking against field experience and considerable effort is required when evaluating soil parameters to be used for a new site. Relatively simple prediction techniques have evolved from study of the field data and theoretical results, and are often used for actual engineering design of simple protective structures and for preliminary design of more complex facilities.

This section will not attempt to describe all of the field data, theories, and prediction techniques in detail.* Rather, the emphasis will be upon fundamental considerations: the influence of various factors upon stress waves, and the role of soil mechanics in stress wave predictions.

A study of stress waves cannot be completely divorced from the question of how stress waves affect protective construction design.

For convenience, the design of a buried structure can be thought of as involving two steps: (a) design of a protective structural shell which will withstand the stresses imposed by the stress wave, and (b) design of mountings and shock isolation systems which will make it possible for personnel and equipment to survive the ground motions, i.e. the accelerations, velocities, and displacements of the ground. Thus, prediction of stress waves is usually broken into two parts: prediction of stresses and prediction of ground motions. However, these two aspects of the design problem are really inseparable.

The stresses and motions experienced by a structure are generally determined in two steps: (a) an estimate is made for the stresses and

* The best single reference regarding field test data is Part IV of NUCLEAR GEOPLOSICS. The best single reference for prediction techniques is the Air Force Design Manual. Unfortunately, there is no one single good reference describing the many theories for stress waves. This section gives references to a number of these theories.

motions which would exist at a point if no structure were present--the so-called free-field stresses and ground motions; and (b) the modification caused by the presence of the structure is estimated. This section is concerned with free-field effects; section 2.5 will consider soil-structure interaction.

2.4.1 Description of Airblast. Fig. 2.1 shows the general features of the airblast wave which sweeps outward from a surface nuclear explosion.

As viewed at a fixed point, the airblast arrives as a sharply defined shock front traveling at a shock wave velocity which is a function of the peak overpressure in the shock front. After passage of the shock front, the overpressure decreases and eventually becomes negative. As the point of observation is moved away from the point of explosion, the peak overpressure and shock wave velocity decrease while the total duration of the airblast wave increases.

As viewed at an instant of time, the ground surface from the explosion point out to the shock front will be loaded by air pressure. With increasing time from explosion, a larger area of ground surface is loaded, but the magnitude of the stresses decreases.

The formation of airblast waves is controlled by the release of heat and radiation from the explosion. Brode (1964) gives a detailed discussion of these interrelated phenomena. Table 2.4 and figs. 2.12 through 2.14 give quantitative information of interest to soil engineers, using a 1-Mt surface explosion as an example.

Table 2.4 summarizes data regarding shock front overpressure, shock wave velocity, arrival time, duration, and impulse as a function of distance from the explosion. (Impulse is the integral of pressure versus time.) Shock front velocity is directly related to the peak overpressure. (Note that this velocity is larger than the velocity of acoustical waves through air--1100 fps at sea level.) All other factors scale as the cube root of the size of the explosion. For comparison, a 1-Mt surface explosion will give a crater with an apparent radius of 700 ft. Fig. 2.12 shows distances to various peak overpressures in relation to crater size.

Fig. 2.13 indicates how the overpressure decreases with time at several different distances away from the explosions (the duration of the

Table 2.4
Airblast Parameters for 1-Mt Surface Burst

Shock Over-pressure psi	Distance ft	Shock Front Velocity fps	Arrival Time of Shock Front, sec	Positive Phase Duration sec	Impulse lb/in. ² -sec
5000	850	18,000	~0.02	1.4	110
2000	1200	11,500	~0.04	1.3	77
1000	1500	8,200	0.08	1.2	55
500	1900	6,000	0.13	1.0	40
300	2300	4,600	0.20	0.95	30
100	3400	2,900	0.52	0.83	18
50	4500	2,200	0.97	0.92	13
25	6100	1,800	1.8	1.25	8.8
10	9500	1,400	4.2	1.9	5.5
Scales as $W^{1/3}$		Scales as $W^{1/3}$		Scales as $W^{1/3}$	Scales as $W^{1/3}$

Data from Brode (1964)

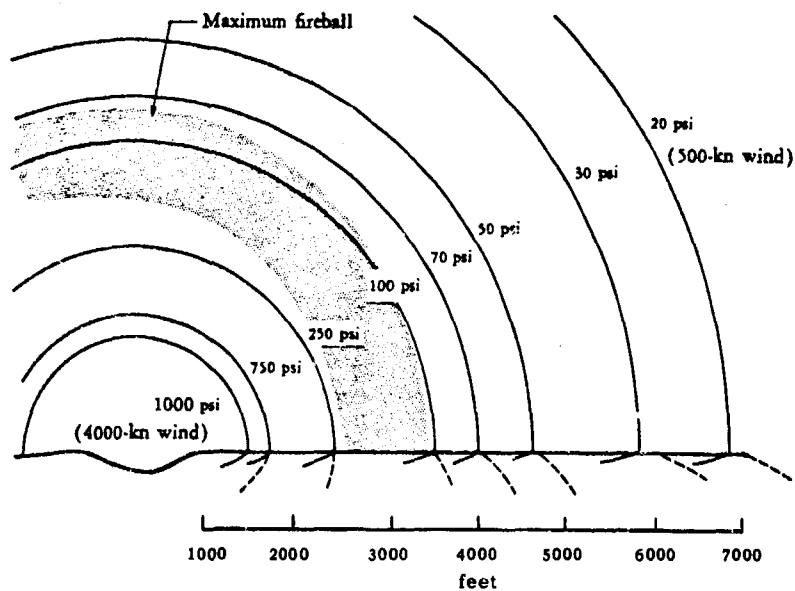


Fig. 2.12 Distance to various peak overpressure levels in relation to crater size; 1-Mt surface burst (from Brode, 1964)

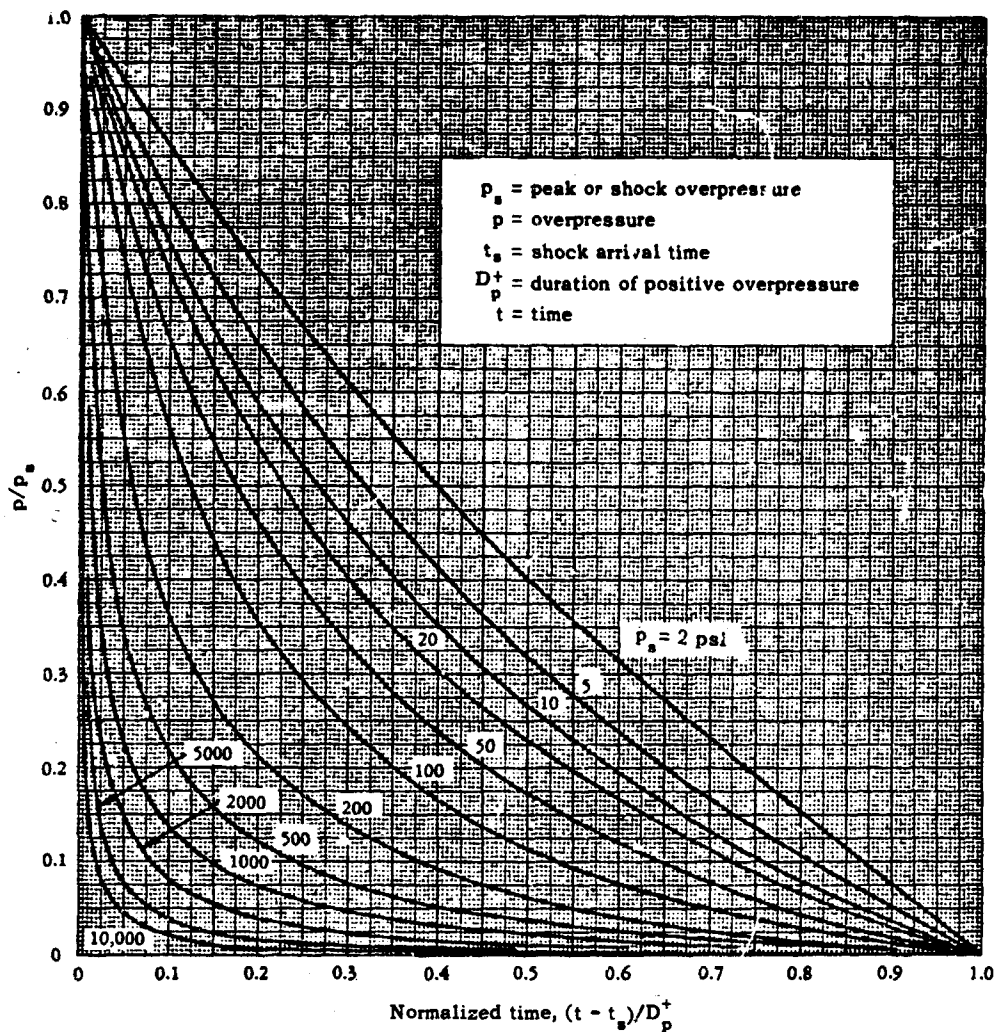


Fig. 2.13 Overpressure versus time; 1-Mt surface burst
(from Brode, 1964)

positive phase is on the order of 1 to 3 sec). The decay is not a simple exponential. For the higher overpressures, the rate of decay initially is very rapid and then slows, as illustrated by the following tabulation:

Peak Shock Overpressure psi	Fraction of Positive Phase Duration to Achiev		
	$p/p_s = 0.75$	$p/p_s = 0.50$	$p/p_s = 0.25$
1000	0.005	0.02	0.04
400	0.01	0.05	0.1
100	0.05	0.12	0.3
40	0.09	0.25	0.5

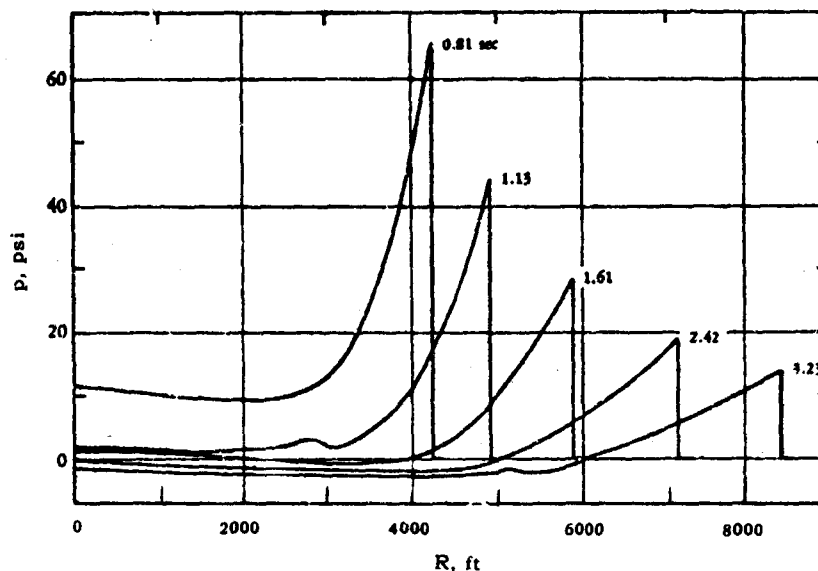


Fig. 2.14 Overpressure versus radius; 1-Mt surface burst (from Brode, 1964)

where p_s is the peak overpressure in the shock front and p is the overpressure at the same time behind the shock front. For $p_s = 1000$ psi, the overpressure drops to 250 psi within only 4% of the time required for the overpressure to drop to zero.

Fig. 2.14 shows overpressure versus distance for various times. After the positive phase there is a suction pressure: as much as 3 psi, or enough to lift a concrete lid 3 ft thick.

Relatively simple equations can be derived which describe the airblast approximately but adequately (for example, see Brode, 1964, and Neidhardt and Harkin, 1962). These equations are often used as a basis for ground motion calculations.

2.4.2 General Features of Ground Motions. As a first step toward predicting airblast-induced ground motions, it is necessary to understand the various factors which contribute to the pattern of ground motion that might be observed in any particular situation. In this section, this understanding will be developed by studying a series of highly idealized situations.

Concentrated transient point load: Fig. 2.15 shows the waves emanating from a concentrated load applied instantaneously at the surface of an

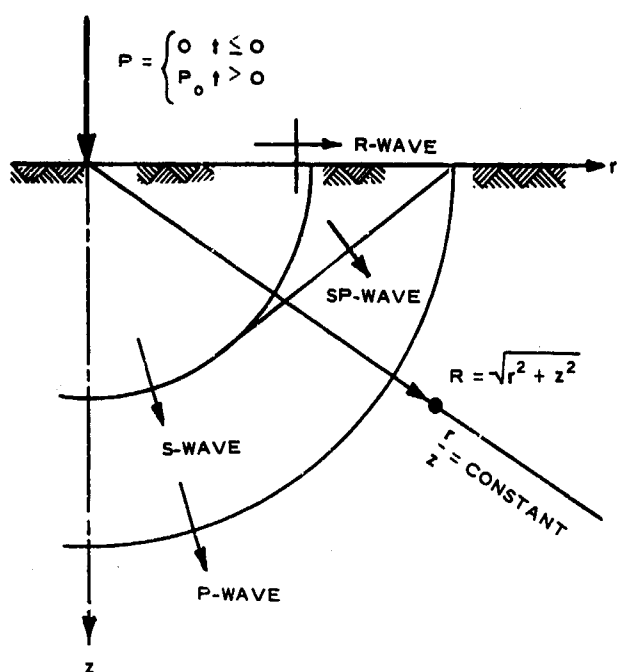


Fig. 2.15 Waves resulting from instantaneously applied point load

stress at a point as the wave fronts pass vary as $1/R^2$, while the peak displacement at a point varies as $1/R$. Passage of the waves causes downward and outward motion.

For points lying nearer the surface, the behavior is much more complicated. The boundary condition at the surface gives rise to a von Schmidt wave (SP-wave), which is the precursor of the Rayleigh wave (R-wave) running outward along the surface. Fig. 2.17 gives a typical time history of motion for a near-surface point. A point first moves upward and outward as the P- and SP-wave fronts pass. As the

elastic half-space. The nature of the motions and stresses caused by this loading is discussed by Baron et al. (1960). A general understanding of the response results from examining the distribution of motions along several rays emanating from the point of load applications.

A point located beneath the load experiences two wave front arrivals, corresponding to the compression (P-wave) and shear (S-wave) waves.* A typical time history of vertical displacement w is shown in fig. 2.16. The changes in particle velocity and

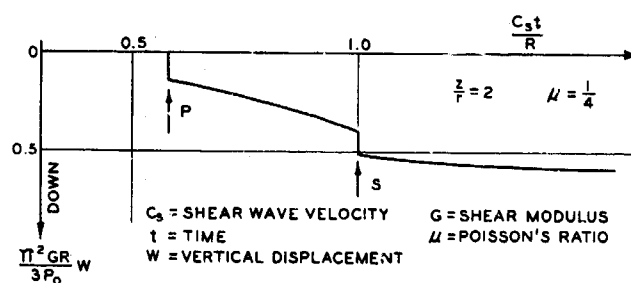


Fig. 2.16 Time history of vertical displacement along ray beneath concentrated load

* For detailed definitions of these waves and of the associated wave velocities, see Chapter 5.

R-wave approaches, the upward movement increases but is accompanied by inward motion.

After passage of the R-wave, there is a permanent downward and inward displacement. The effect of the Rayleigh wave, which is not a sharp-fronted wave, decreases rapidly with depth.

For points near the surface, the maximum stresses and displacements occur during passage of the Rayleigh wave. These maximum near-surface stresses and displacements vary as $1/\sqrt{R}$.

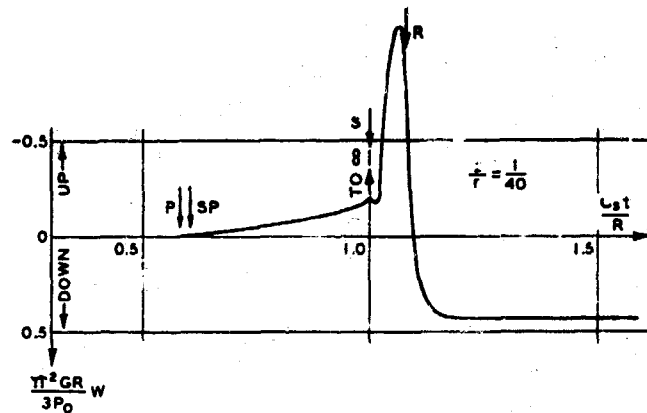


Fig. 2.17 Time history of vertical displacement at shallow depth near concentrated load

Sequence of events caused by blast wave: A blast wave sweeping outward over the surface of a half-space (figs. 2.12-2.14) in effect applies

instantaneous loads in succession at points spaced outward from ground zero. The effects of these loadings can be conveniently divided into two parts (see fig. 2.18):

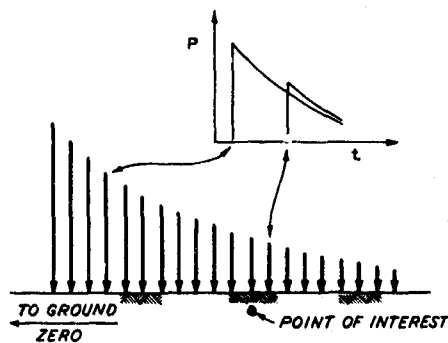


Fig. 2.18 Sequence of loadings applied by airblast

- (a) The effect of the loading immediately above the point. This loading produces the type of response shown in fig. 2.16.
- (b) The effect of the loadings not

immediately above the point. Each of these loadings produces the pattern of response shown in fig. 2.17. Because the loadings near ground zero are very large, these loadings may cause at a distant point a response which is as significant as the response caused by the loading directly over the point.

The loading directly over the point primarily causes downward motion. The more distant loadings cause both upward and downward motion as well as inward and outward motion.

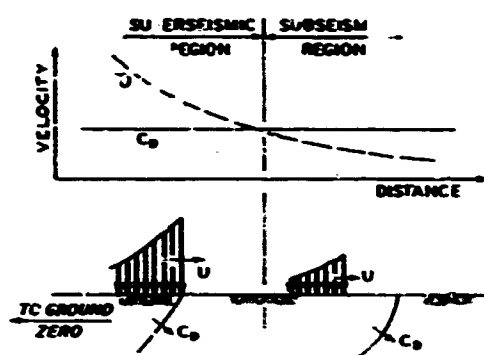


Fig. 2.19 Superseismic and subseismic regions

Depending upon the relative magnitude of the dilatational wave velocity C_D (the velocity of a P-wave) in the ground and the shock velocity U of the airblast, two general types of situations can occur (see fig. 2.19):

- (a) If $U > C_D$, the first motion at any point within the half-space is caused by the loading immediately above the point.

That is, a point within the body does not move until the shock front of the airblast sweeps over the point. This is called the superseismic case. This case occurs close to ground zero where the overpressures and the shock velocity are great. The smaller the value of C_D , the farther the superseismic region will extend from ground zero.

- (b) If $U < C_D$, motion at a point begins before the shock front of the airblast passes over the point. This is called the subseismic case or the outrunning case. The subseismic region begins at the end of the superseismic region. The larger the value of C_D , the closer to ground zero the transition point will lie. Sometimes reference is also made to a transseismic region, where $C_S < U < C_D$ (C_S is the shear wave velocity in the ground).

Within both regions, the response at a point is influenced both by the loading just above the point and by the loadings distant from the point. As shown in fig. 2.20, there is always a significant response when the front of the airblast passes over a point, regardless of whether the point is located in the superseismic, transseismic, or subseismic region, but this aspect of the loading tends to predominate within the superseismic region. The effect of loadings distant from a point becomes especially important within the subseismic region.

Since the region near ground zero is especially of interest with regard to protective construction, the superseismic region is of special

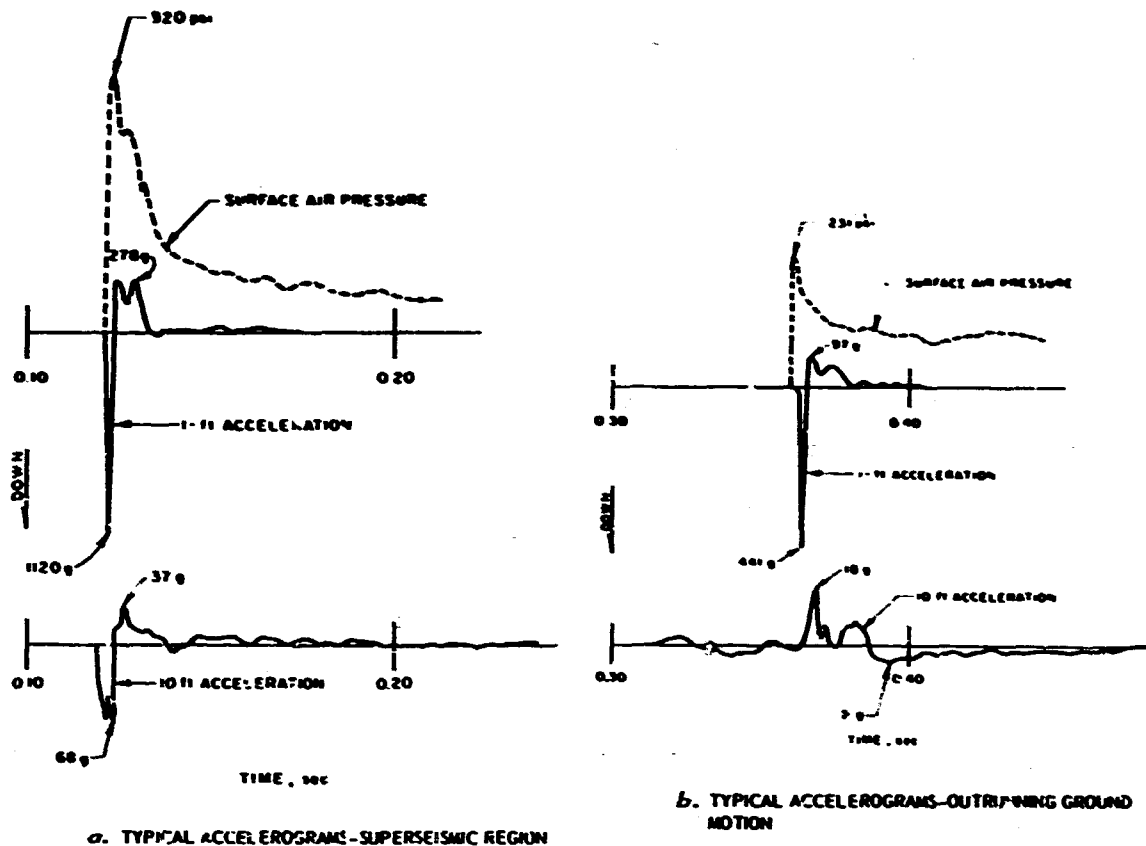


Fig. 2.20 Typical time histories of vertical acceleration at depths of 1 and 10 ft below ground surface (from Sauer et al., 1964)

concern. For further discussion of the superseismic case, it is convenient to discuss the response under three headings: (a) response at shallow depth as P- and S-waves pass; (b) response at greater depth as P- and S-waves pass; and (c) response after passage of wave fronts.

Superseismic case; initial response at shallow depth: Consider first the situation shown in fig. 2.21, where a uniformly distributed strip load is moving with constant velocity U over the surface of an elastic half-space. This loading causes four wave fronts, with regions of constant stress between the wave fronts.

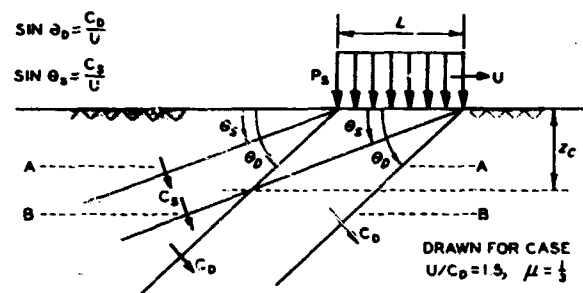


Fig. 2.21 Wave fronts beneath superseismic strip load

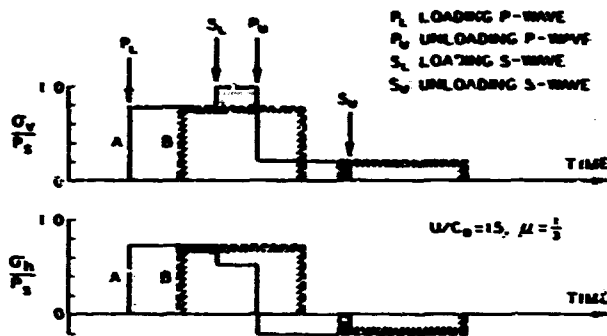


Fig. 2.22 Vertical and horizontal stresses versus time at two depths below superseismic strip load

Fig. 2.23 shows the patterns of motion at these same two depths. Initially the motion is normal to the P-wave front, i.e. downward and outward. Arrival of the S-wave causes additional downward movement but a reverse horizontal movement. After passage of the final wave front, there is a residual vertical displacement and a smaller residual

horizontal displacement. These residual displacements are caused by the continuing compression of points lying at greater depths than the depth considered. The motions at the surface are shown for comparison. The maximum vertical displacements are the same at each depth, but the maximum horizontal displacements are smaller near the surface.

The inclination of the wave fronts, the magnitude of the stress changes at the wave front, and the pattern of motions are functions of the velocity ratio U/C_D . For $U/C_D > 2$, the wave fronts are inclined only slightly from the horizontal and the motions are predominantly vertical. It is interesting to compare the stresses and motions for:

- The superseismic case of a transient wave sweeping over the surface.
- The one-dimensional problem of a pulse of stress applied over a

Fig. 2.22 shows the variation with time of horizontal and vertical stresses at two depths. Down to the depth z_c where the unloading P-wave and the loading S-wave intersect, the maximum vertical stress equals the applied stress p_s . Below this depth, the maximum vertical stress is less than p_s .

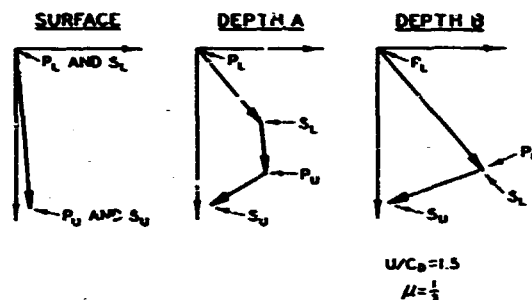


Fig. 2.23 Displacements at several depths below superseismic strip load

wide area of the surface, with a duration just equal to the duration of the stress applied at any point in the superseismic case. This comparison is presented in fig. 2.24 for $U/C_D = 2.25$.* The vertical stresses and motions are quite similar for the two cases, and the agreement becomes better as U/C_D increases. The same can be said for the horizontal stress. The wave shapes are somewhat different for the two cases, as there is a spreading out of the wave in the superseismic case. The two cases differ most with regard to horizontal motions. However, the horizontal motions in the superseismic case can be approximately related to the vertical motion in the one-dimensional case by considering the inclination θ_D of the superseismic wave front. For example, the maximum horizontal velocity and displacement can be estimated approximately by multiplying the vertical component by $\tan \theta_D$. These comparisons hence suggest that the simpler one-dimensional problem may be useful for estimating the behavior in the more complicated superseismic problem.

Fig. 2.25 shows stress versus time patterns at various depths beneath a superseismic loading consisting of a sudden stress jump followed by a linearly decaying stress. The P- and S-waves each cause a similar sudden jump followed by a decaying stress. At a depth z_i , the vertical stress at the instant of S-wave arrival just equals the vertical stress at the instant of P-wave arrival. For $z < z_i$, the maximum vertical stress occurs at the S-front, but for $z > z_i$ the vertical stress at the P-front is the maximum that occurs. Below z_i , the peak vertical stress is constant with depth. For $z < z_i$, there is a linear attenuation of peak vertical stress with depth. This attenuation is caused by the two-dimensional nature of the problem, and is called spatial attenuation.

The depth z_i depends upon the velocity ratio U/C_D , Poisson's

* The results in the left column of this figure come from the theory for phenomena during passage of a plane wave. The key principles are that particle velocity jump across a wave front (in this case the vertical velocity \dot{w}) is proportional to stress change across the front, while peak displacement (in this case the peak vertical displacement w_{\max}) is proportional to the impulse imparted by the surface loading. The actual relations appear as Equations 2.4 and 2.6 in section 2.4.4. The symbol D is the constrained modulus: $D = \rho C_D^2$, where ρ is the mass density.

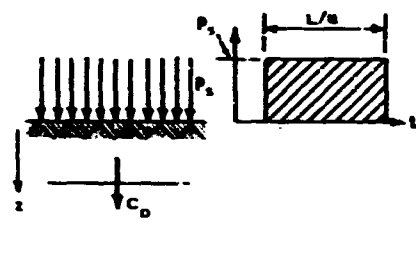
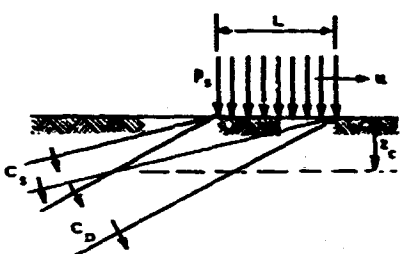
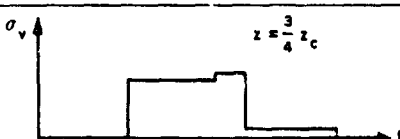
LOADING CONDITION	ONE-DIMENSIONAL		TWO-DIMENSIONAL SUPERSEISMIC WITH $\mu/C_D = 2.25$ AND $\mu = 1/3$	
				
DIMENSIONLESS RESPONSE	MAXIMUM VERTICAL STRESS $\frac{(\sigma_v)_{MAX}}{P_s}$		$z < z_c: 1.000$ $z > z_c: 0.903$	
	MAXIMUM HORIZONTAL STRESS $\frac{(\sigma_h)_{MAX}}{P_s}$		$0.504 = 1.21 \frac{\mu}{1-\mu}$	
	MAXIMUM VERTICAL VELOCITY $\frac{w_D}{C_D P_s}$ (D = CONSTRAINED MODULUS)		$z < z_c: 1.001$ $z > z_c: 0.303$	
	MAXIMUM HORIZONTAL VELOCITY $\frac{u_D}{C_D P_s}$		$0.446 = 0.90 \tan \theta_D$	
	MAXIMUM VERTICAL DISPLACEMENT $\frac{w_{MAX} \rho C_D}{P_s L/a}$		1.001	
	MAXIMUM HORIZONTAL DISPLACEMENT $\frac{u_{MAX} \rho C_D}{P_s L/a}$		$z = 0: 0.403$ $z > z_c: 0.446 = 0.90 \tan \theta_D$	
	FIRST ARRIVAL TIME z/C_D		$1.118 = \frac{1}{\cos \theta_D}$	
	WAVE SHAPE FOR VERTICAL STRESS			

Fig. 2.24 Comparison of one-dimensional and superseismic cases

Fig. 2.25 Vertical stress versus time at various depths beneath linearly decaying superseismic strip load

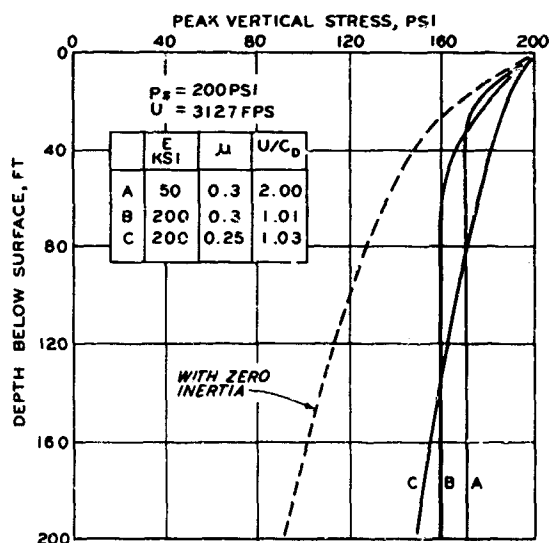
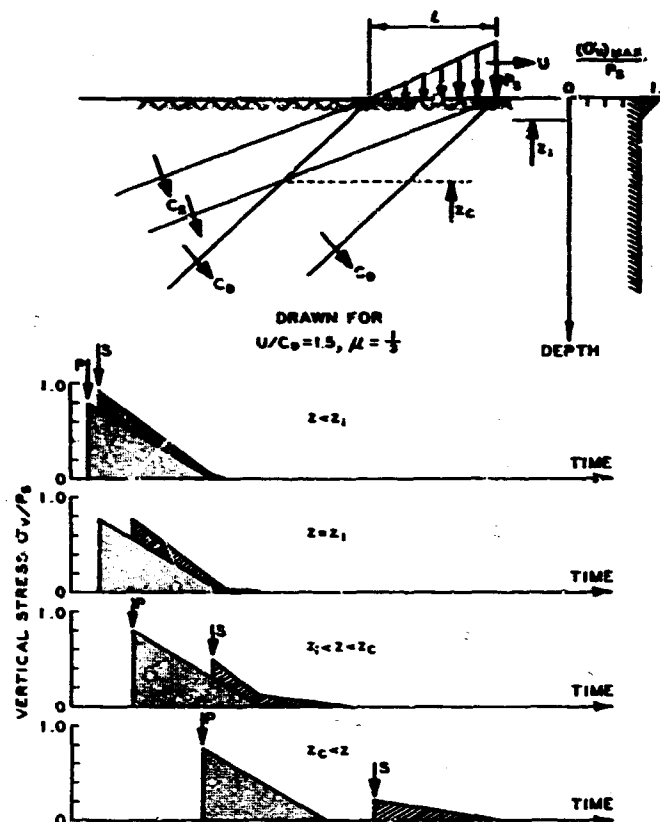


Fig. 2.26 Attenuation of peak vertical stress from airblast (from McCormick and Baron, 1966)

ratio μ , and the rate at which the loading decays behind the wave front. The amount of stress attenuation which occurs above $z = z_1$ depends upon U/C_D and μ . Fig. 2.26 shows some results which have been calculated for an airblast loading as described in section 2.4.1. For comparison is shown the attenuation which would result if this same loading were applied to a soil without inertia (i.e. with an infinite dilatational stress wave velocity): see Air Force, 1962.

Airblast from an explosion does not move with constant velocity U

nor with constant shock front stress p_s . However, over a small region of the surface, U and p_s will vary only slightly and may be treated as constants. Thus the foregoing solutions give a meaningful indication of the motions and stresses at shallow depth beneath a superseismic airblast loading.

Superseismic case; initial response at greater depth: Because the shock velocity U of the airblast decreases as the airblast front moves

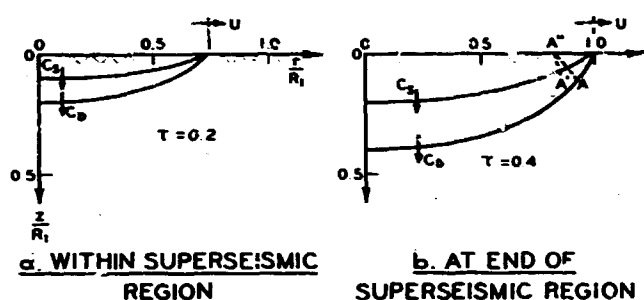


Fig. 2.27 Location of airblast shock front and P- and S-fronts at two different times giving superseismic conditions for $\mu = 1/3$

outward, the P- and S-fronts at any instant of time are curved rather than straight. Given the variation of U with radius r , expressions can be derived giving the locations of these wave fronts (Neidhardt and Harkin, 1962).

Fig. 2.27* shows the position of these fronts at two different times within the superseismic region, as calculated assuming an intense airblast which originates at ground zero without producing a crater.

The stress and particle velocity jumps which occur at points on these fronts can be related directly to the peak overpressure p_s applied at corresponding points on the surface of the ground. Thus the jump across the P-front at point A of fig. 2.27b results from the dilatational wave which originated when the front of the airblast passed over point A". Similarly, the jump across the S-front at point A' results from the shear wave which originated at A". Because of the curvature of the wave fronts, the stress jumps decrease along rays A"A and A"A'. Expressions giving the attenuation of the stress jumps with travel distance are given in Neidhardt

* Figs. 2.27 through 2.29 are normalized with respect to the end of the superseismic region. Thus:

R_1 = radius at which $U = C_D$

p_1 = peak overpressure at $r = R_1$

$\tau = C_D t / R_1$ = time at which a dilatational wave from the origin reaches $r = R_1$

and Harkin (1962). Fig. 2.28 shows a few computed results.

It is of interest to compare the peak vertical stress at various points with the peak overpressure at the surface directly above the points. The depths for which these stresses are shown in fig. 2.28 are much greater than those usually of practical interest. Considering that some attenuation of peak stress occurs at relatively shallow depths (owing to the spatial attenuation phenomenon described under the previous subheading), there appears to be remarkably little decrease of peak vertical stress with depth.

For example, the normalized peak vertical stress at point F in fig. 2.28 is 2.9, whereas the normalized peak overpressure on the ground surface directly above point F is 3.8. Ang and Ranier (1965) show similar results.

Superseismic case; behavior behind wave fronts: Though the locations of the wave fronts and the stress jumps at these fronts can be computed with only modest difficulty and can be understood in general terms as described above, the behavior behind the wave front is much more complicated. The stresses and motions at any point are influenced by the airblast pressures at many surface points. Several solutions which begin to show the behavior behind the wave front have been accomplished by means of computers. However, at the time of writing of this report, the writer still had not seen results from which the effects of the airblast can be satisfactorily isolated from other sources of loading such as directly induced effects. The following paragraphs indicate some of the interesting features which can be seen in available solutions.

Fig. 2.29 shows the distribution of stress and displacement along a

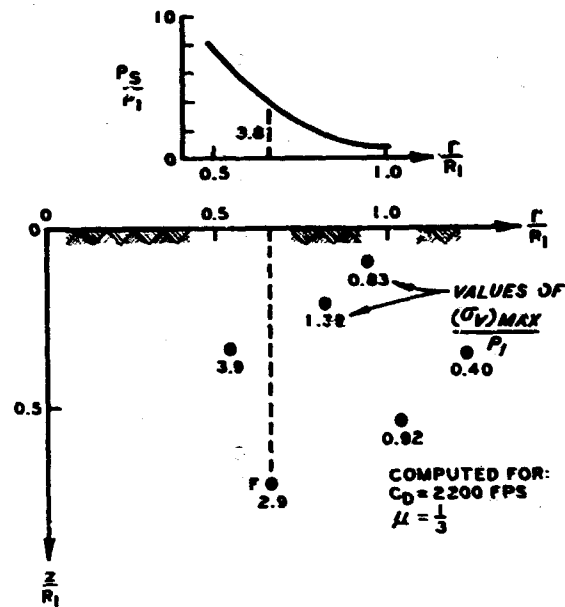


Fig. 2.28 Theoretical results showing peak vertical stress at several deep points (from Neidhardt and Harkin, 1962)

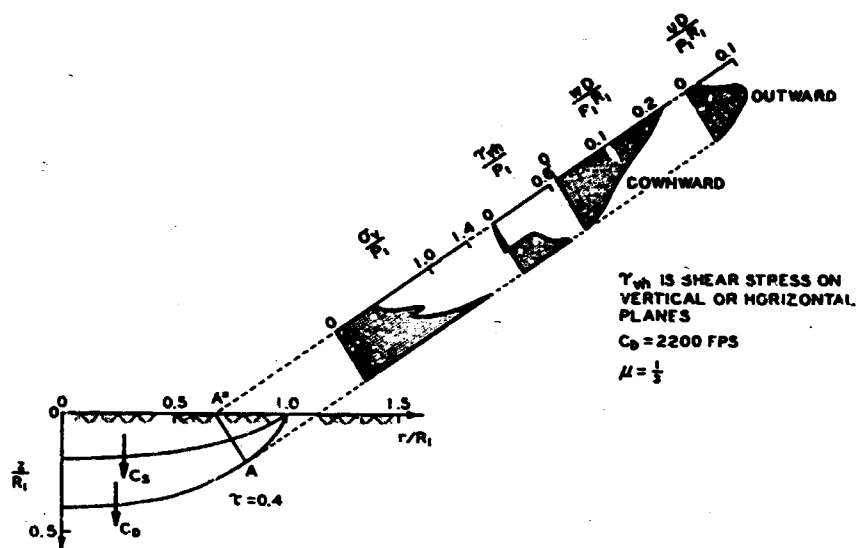


Fig. 2.29 Distribution of stresses and displacements along line A-A" as result of airblast loading (from Neidhardt and Harkin, 1962)

particular ray at a particular time. Note that the variation of stress behind the wave fronts is rather complicated. The calculations show that tensile stresses can develop at certain locations at certain times. The vertical displacement w increases from the P-front to ground surface, and the effect of the S-front can be discerned in the curve. The vertical displacement at any point is still increasing with time, inasmuch as the overpressure has not yet decreased to zero. Because it is difficult to carry the calculation out to such a time, and because the peak vertical displacement is affected by the response at very great depth where soil properties usually are poorly defined, it is difficult to estimate peak vertical displacement. The horizontal displacement u is at this time less at the surface than at some depth (compare fig. 2.29 with fig. 2.23). With time, the depth of maximum u increases, and the horizontal displacement at the surface becomes inward.

For points within the superseismic region very close to the surface, it can be reasoned that the stresses will result: (a) from passage of the airblast front, and (b) from a surface wave generated by the very large stresses applied near ground zero (see Baron et al., 1960). The first set

of stresses can be calculated from the solution for an airblast pressure traveling over the surface at constant velocity. The second set of stresses can be estimated by superimposing the Rayleigh wave terms from a succession of concentrated loadings (fig. 2.13). The two sets of stresses can then be superimposed to give an indication of the combined effects. Fig. 2.30 shows the result of one such calculation. The stresses associated with the Rayleigh wave, especially the horizontal stress, can be of considerable significance.

The importance of the Rayleigh wave of course decreases rapidly with depth. Unfortunately it is quite difficult to calculate the surface wave contribution since it originates at a shock front which is varying in intensity and velocity, and results have been computed for only a very few cases.

Fig. 2.31 shows displacement-time histories for a point at ground surface near the end of the superseismic region (Constantino, 1966). Here the loading involves airblast sweeping out over the ground surface plus a stress applied to the wall of a hemispherical cavity which simulates a crater. The passage of the airblast front causes a downward and outward displacement, but the horizontal displacement almost immediately switches and becomes inward. There is a pronounced surface wave, which results in part from the directly induced stress waves from the "crater" and in part from

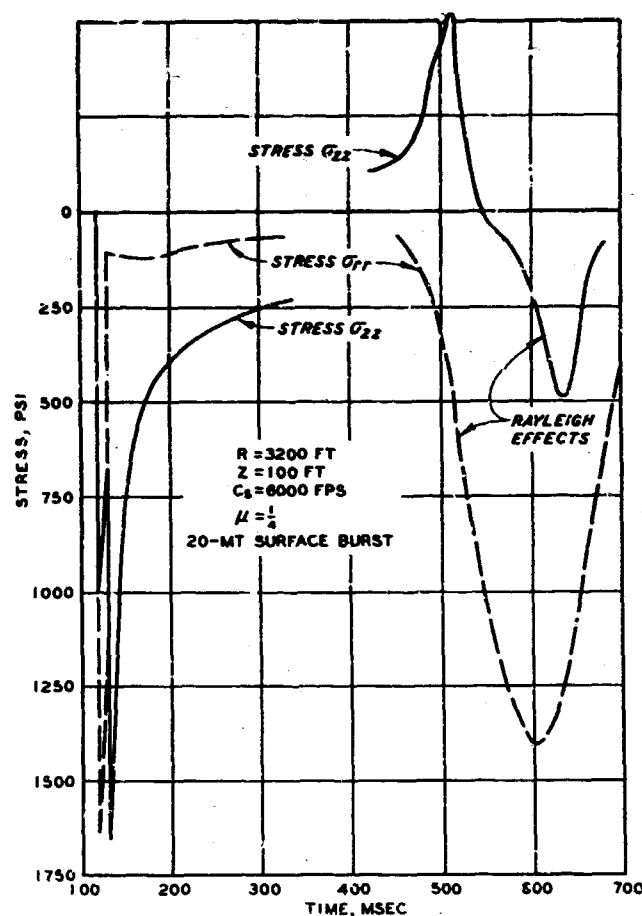
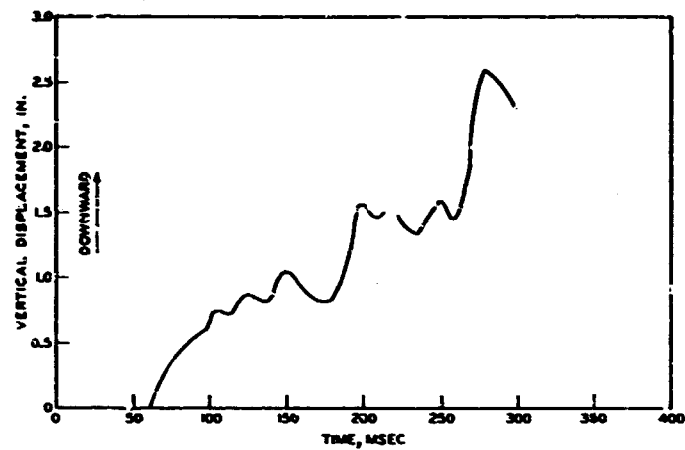
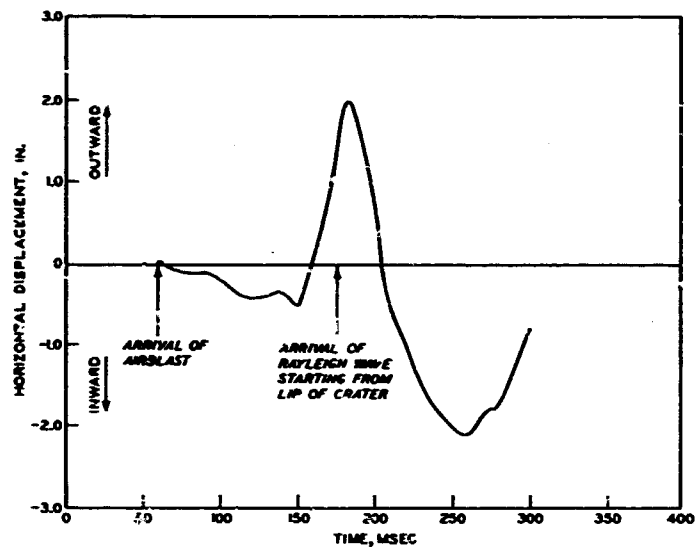


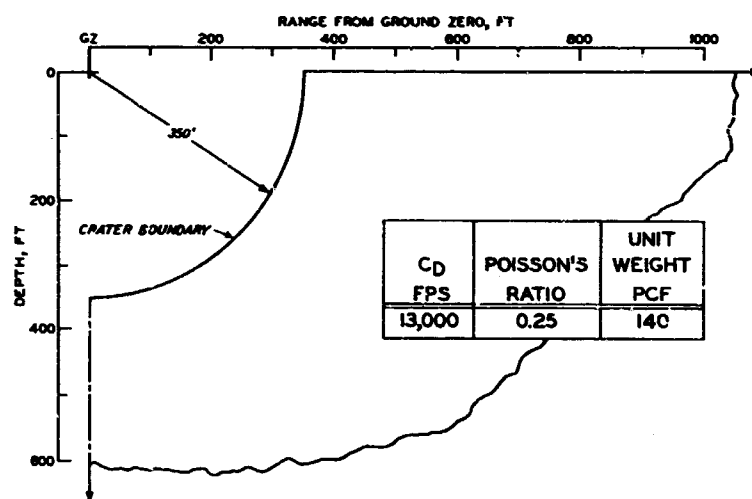
Fig. 2.30 Stresses near surface toward end of superseismic region (from Baron et al., 1960)



a. VERTICAL DISPLACEMENTS AT R=1550 FT



b. HORIZONTAL DISPLACEMENTS AT R=1550 FT



c. CONFIGURATION AND PROPERTIES OF SITE

Fig. 2.31 Motions at surface from combined airblast-induced and directly induced stress waves (from Constantino, 1966)

Rayleigh waves originated by the large peak stresses acting upon the ground surface near the crater. This surface wave causes a marked outward displacement followed by a large rebound toward the crater.

Much additional insight into the nature of ground motions will be gained as additional computations such as these are completed.

Subseismic case: Within the subseismic region, stress waves run ahead of the advancing airblast shock front (fig. 2.32) so that the ground begins to move before the airblast arrives. The sequence of motions is generally as described in connection with fig. 2.17. The first effect is a small outward motion as the P-wave arrives. Then the surface wave effects take over, causing

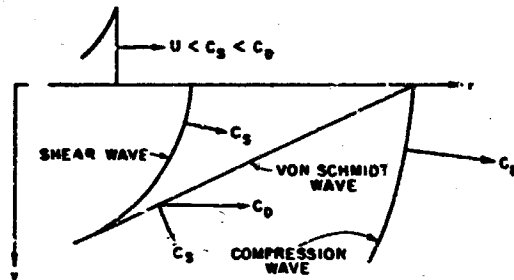


Fig. 2.32 Wave fronts in subseismic region.

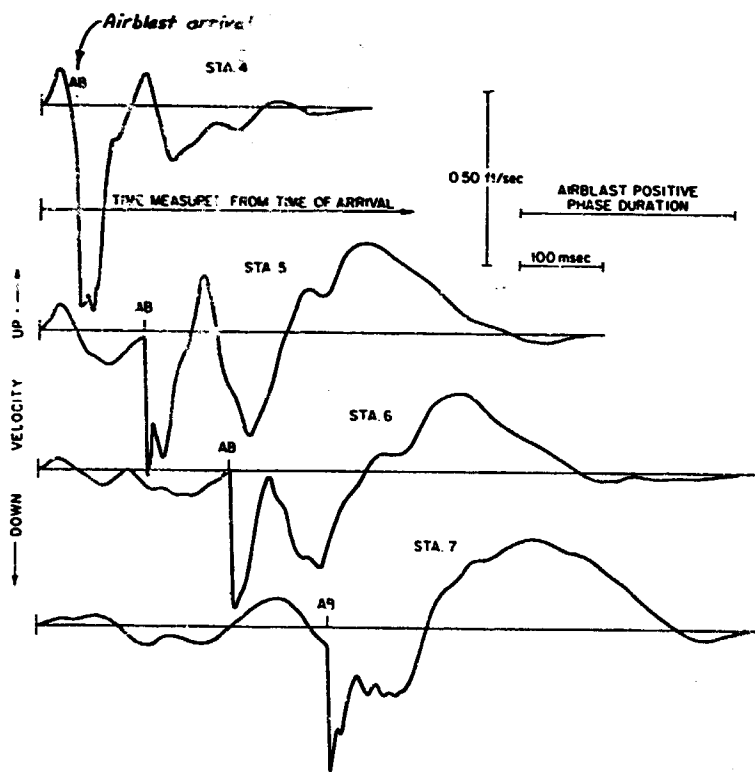


Fig. 2.33 Typical records of actual vertical motions at several distances from ground zero in subseismic region, Tumbler Shot 1 (from Sauer et al., 1964)

upward motion as well as additional horizontal motion. Then finally the airblast arrives, causing as in the superseismic range a predominantly downward movement. The net result of these effects is a complex pattern of motion. Fig. 2.33 shows a typical set of actual ground motion records for stations within the subseismic region at increasing distances from the ground zero. The effect of

the airblast is still clearly evident, but significant motion occurs before the airblast arrives.

At the time of this writing, theoretical calculations reproducing all of the important aspects of behavior in the subseismic region are still not available. Fig. 2.34 gives results from one calculation which illustrates some of the important features. In this calculation an airblast is assumed to spread outward from ground zero. However, the variation of overpressure and velocity at the shock front only approximates actual airblast behavior, and the overpressure is assumed constant behind the shock front instead of decreasing as with actual airblast. The figure shows stresses and motions at a given point for a limited range of times. The P-wave has already arrived some time ago, and thus relatively small motions are already in progress at the beginning of the plots. The major motions begin with the arrival of the Rayleigh wave which is being pushed ahead of the airblast. The horizontal stresses (tensile) are particularly large as the Rayleigh wave passes. Arrival of the airblast is marked by the sudden increase (compression) in vertical stress.

For shallow depths, the stresses and motions associated with passage of the airblast can be estimated with reasonable accuracy from the theory for a surface loading moving at constant velocity and intensity. Equations with some numerical results are given in Rogers and Palmer (1962). Once $U/C_s < 0.5$, the stresses and motions can be estimated with good accuracy by using a series of static distributions for each successive position of the surface loading. This is equivalent to neglecting the inertia of the soil, so as to have an infinite wave velocity. For this case, the stresses and motions attenuate steadily with depth (see fig. 2.26).

The stresses and motions associated with the outrunning are in effect governed by a surface wave, and hence also attenuate rapidly with depth. The attenuation of horizontal stress with depth stands out clearly in fig. 2.34b. The vertical stress associated with the Rayleigh wave first increases (it must be zero at the surface) and then decreases with depth. The effect of this surface wave is difficult to calculate, since this wave originates at a shock front which is changing in intensity and velocity, and only a few cases have been evaluated.

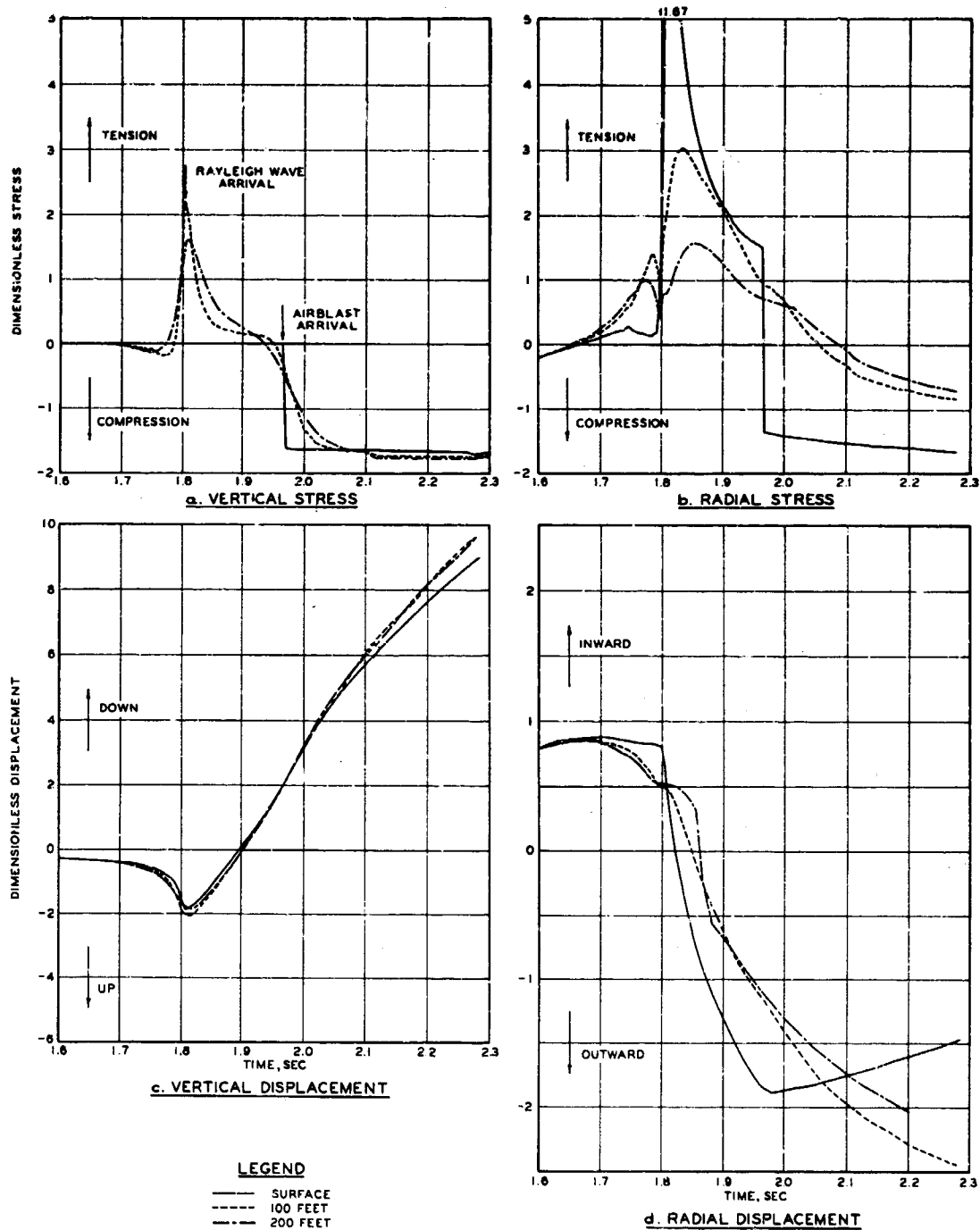


Fig. 2.34 Stresses and displacements near ground surface in subseismic region, from approximate theoretical calculation (from Gans and Brooks, 1965)

The attenuation of peak vertical stress with depth in the subseismic region is illustrated by calculations presented by Ang and Ranier (1965).

Effect of layering: When a plane-wave running through one material encounters a second material with different properties, four new wave fronts are generated at the boundary between the two materials: P- and S-waves reflected back into the first material and P- and S-waves refracted into the second material.

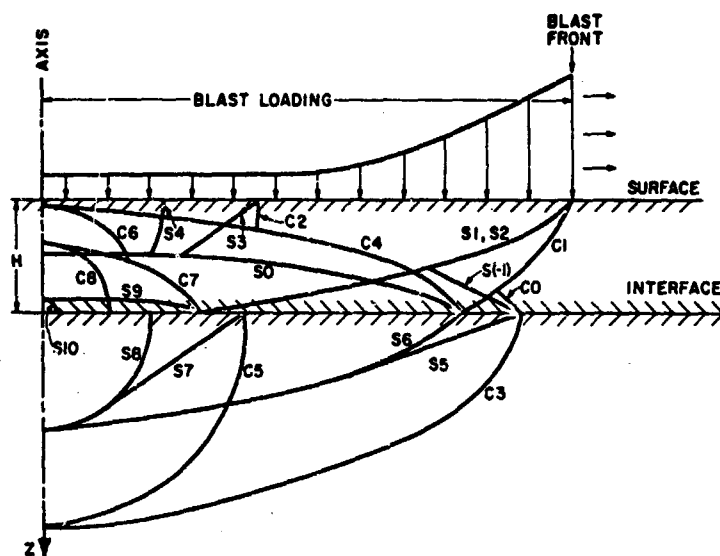


Fig. 2.35 Wave fronts at a time when initial disturbance front is superseismic on $Z = 0$ and transseismic on $Z = H$ (from Ablow and Sauer, 1967)

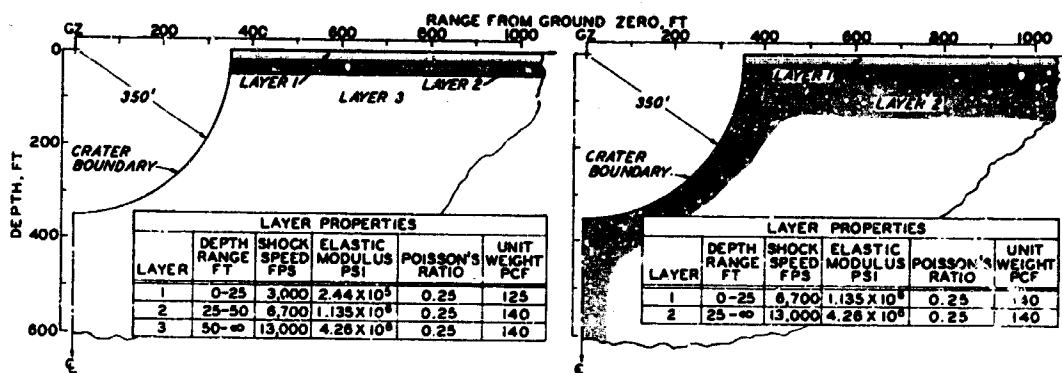
Thus in the typical situation where airblast sweeps over ground composed of a soft layer over one or more harder layers, a very complex pattern of wave fronts develops. Fig. 2.35 shows an example of these wave front patterns as revealed by theoretical calculations.

From the engineering viewpoint, the

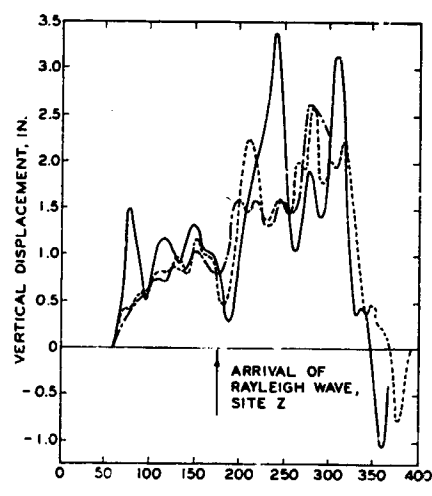
effects of these reflections and refractions may be considered under two headings: (a) the modification to the stresses and motions within the superseismic region, and (b) the change in the extent of the superseismic region.

Fig. 2.36 illustrates the effect of layering on the motions near the surface of the ground. By comparing the curves for sites X, Y, and Z (site Z is the homogeneous case shown in fig. 2.31), several important features may be noted:

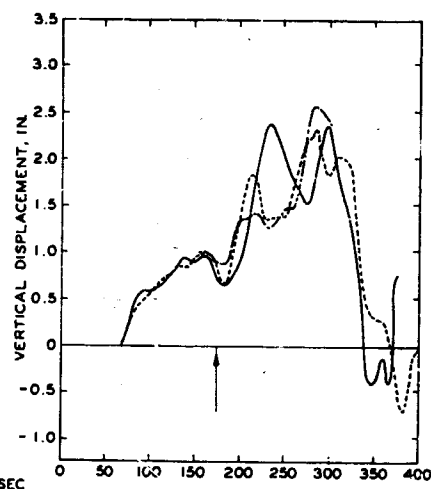
- (a) The initial vertical particle velocity (slope of displacement-time curve) at the surface caused by the airblast arrival is greater at site X because of the greater compressibility of the topmost layer.
- (b) The first reflection within the topmost layer soon causes a reverse particle velocity at ground surface, and this and



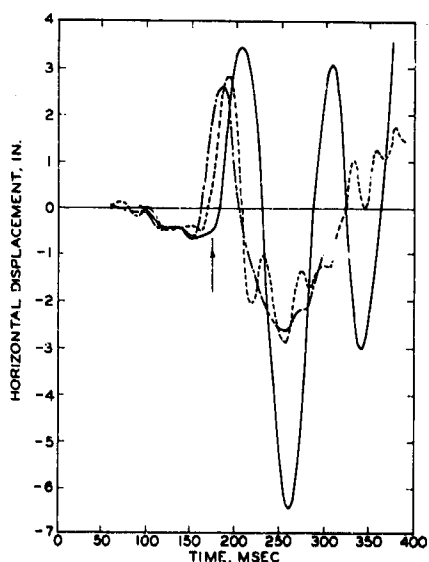
a. CONFIGURATION AND PROPERTIES OF SITE X - b. CONFIGURATION AND PROPERTIES OF SITE Y



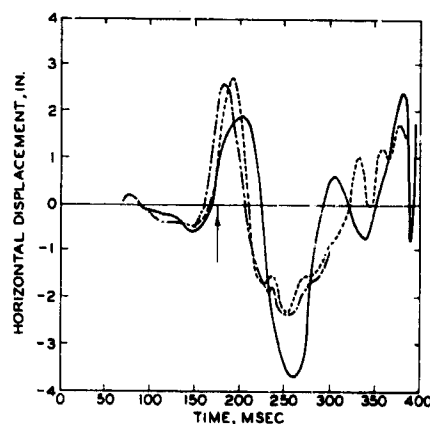
c. VERTICAL DISPLACEMENT HISTORIES AT SURFACE FOR R = 1550 FT, SITES X, Y, AND Z



d. VERTICAL DISPLACEMENT HISTORIES AT Z = 50 FT, FOR R = 1550 FT, SITES X, Y, AND Z



e. HORIZONTAL DISPLACEMENT HISTORIES AT SURFACE FOR R = 1550 FT, SITES X, Y, AND Z



f. HORIZONTAL DISPLACEMENT HISTORIES AT Z = 50 FT, FOR R = 1550 FT, SITES X, Y, AND Z

LEGEND

- SITE X
- - - SITE Y
- · · SITE Z

Fig. 2.36 Effect of layering upon near-surface motions (from Constantino, 1966)

subsequent reflections cause the displacement-time histories at site X to show oscillations which are not present at site Z.

- (c) Until the arrival of the surface wave, the average vertical displacement at 50-ft depth is the same for all three sites, but the surface vertical displacements at sites X and Y exceed that at site Z because of the greater compressibility of the topmost layers.
- (d) Prior to the arrival of the surface wave, the horizontal displacements (which are small anyway) are relatively unaffected by the layering.
- (e) The motions associated with the surface wave are increased by the layering, especially the horizontal motions. This effect is partly the result of the greater flexibility and stiffness of the topmost layer. This effect also comes about because layers can "channel" the energy in horizontally moving waves and thus can under certain conditions amplify the motions associated with surface waves.

Just as wave propagation down a vertical column can be used to explain quantitatively many of the features of superseismic ground motion in a homogeneous soil (fig. 2.23), the effects of layering on the initial ground motions can be explained simply in terms of reflections of P-waves within a vertical column. However, the effect of layering on surface waves is very complex.

The effect of layering upon the extent of the superseismic region is illustrated in fig. 2.37. In this figure, the solid lines show successive positions of the initial P-front. This front is complex because the P-front in the lower stratum runs ahead of the P-front in the upper stratum, and hence energy is fed back from the lower to the upper stratum. Energy which is put into the ground when the airblast front passes point D, and which follows the path DEFG, reaches point G at the same instant as the airblast. For points at greater range than G, ground motion will start prior to the airblast arrival even though the airblast is still superseismic with regard to the top stratum.

Summary: As stated at the outset of section 2.4.2, the aim has been

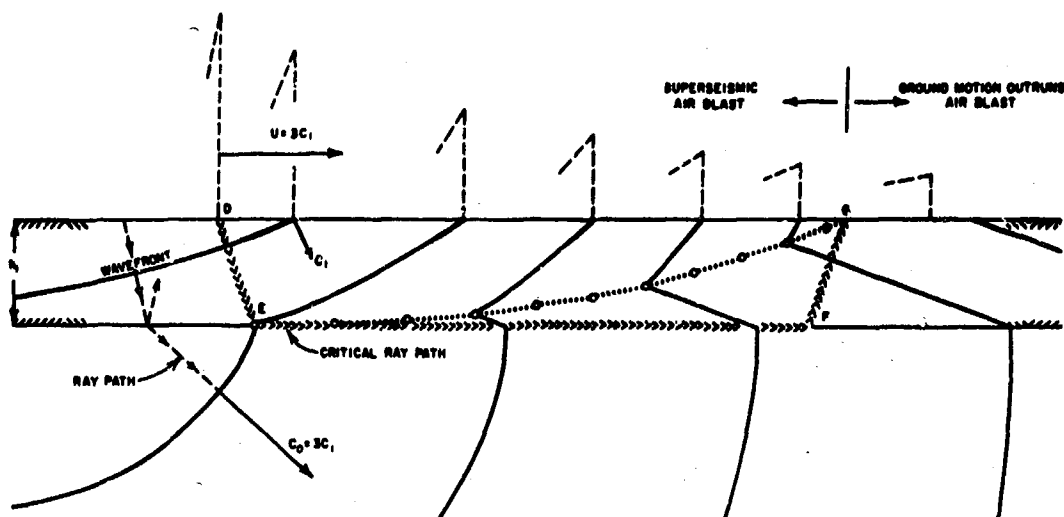


Fig. 2.37 Ray path diagram for determination of critical ray path for two-layer medium (from Sauer et al., 1964)

to develop a general understanding of the nature of airblast-induced ground motion by examining the response for a number of highly idealized situations. The key ideas and principles which have emerged from this study are summarized in fig. 2.38. This study has also given a general picture as to the status of the theories which may be used to calculate these various effects, and has indicated simplified theories which can be used to

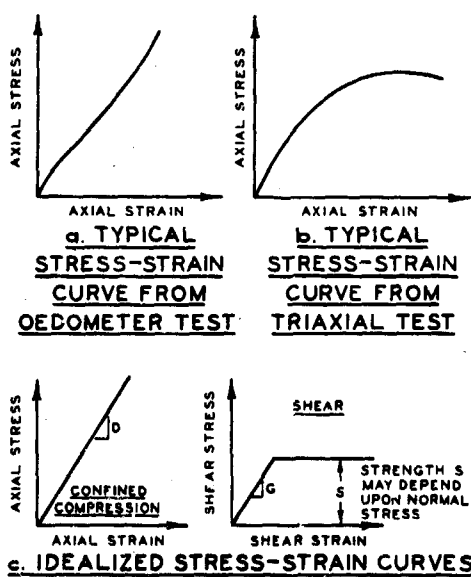
	EFFECT OF AIRBLAST FRONT PASSING OVER POINT		EFFECT OF OVERPRESSURE EARLIER AND NEARER GROUND ZERO	
	SUPERSEISMIC REGION	SUBSEISMIC REGION	SUPERSEISMIC REGION	SUBSEISMIC REGION
ROLE	FIRST AND USUALLY PREDOMINANT RESPONSE	IMPORTANT RESPONSE SUPERIMPOSED UPON MOTIONS ALREADY UNDERWAY		FIRST AND OFTEN PREDOMINANT RESPONSE
NATURE OF RESPONSE	SHARP DISCONTINUITIES AT WAVE FRONTS	SMOOTH BUT RAPID CHANGES		
STATUS OF THEORY	COMPLETE RESULTS AVAILABLE FOR INITIAL RESPONSE	COMPLETE RESULTS AVAILABLE	DIFFICULT TO EVALUATE AND RESULTS AVAILABLE ONLY FOR FEW CASES	
SIMPLIFIED THEORY	ONE-DIMENSIONAL PROPAGATION IN VERTICAL ROD	NEGLECT INERTIA	NONE	
VERTICAL STRESS	SOME SPATIAL ATTENUATION NEAR SURFACE, THEN NEARLY CONSTANT WITH DEPTH	STEADY ATTENUATION WITH DEPTH	INCREASES TO MAXIMUM SOMEWHAT BELOW SURFACE AND THEN ATTENUATES RAPIDLY WITH DEPTH	
VERTICAL VELOCITY			ATTENUATES RAPIDLY WITH DEPTH	
HORIZONTAL STRESS AND VELOCITY	LESS THAN VERTICAL		GENERALLY GREATER THAN VERTICAL	
VERTICAL DISPLACEMENT	AFFECTED BY RESPONSE TO GREAT DEPTH	AFFECTED BY RESPONSE TO MODERATE DEPTH	AFFECTED BY RESPONSE AT SHALLOW DEPTH	
HORIZONTAL DISPLACEMENT	AFFECTED BY RESPONSE AT SHALLOW DEPTH ONLY			
EFFECT OF LAYERING	VERTICAL RESPONSE CAN BE ESTIMATED BY SIMPLIFIED THEORY; HORIZONTAL RESPONSE INCREASED		ACCENTUATES IMPORTANCE; RESPONSE MAY BE AMPLIFIED BY CERTAIN LAYERING PATTERNS	

Fig. 2.38 Summary of general features of ground motion

approximate the response for certain cases. The ideas and principles developed here provide the basis for organizing the complex results of field measurements of ground motions and for developing engineering approaches to the prediction of ground motions in situations of practical interest.

2.4.3 Effect of Nonelastic Behavior of Ground. The solutions presented in section 2.4.2 assumed ground to be linearly elastic. Even though soil and rock actually exhibit nonelastic effects, these solutions still serve to illustrate and to permit understanding of most of the important features of airblast-induced ground motion. This section briefly considers the consequences of the actual nonelastic effects. This is accomplished by considering several simplified models of soil behavior, each of which incorporates a specific nonelastic feature.

Shear strength: When soil is compressed in one direction without permitting strains in the transverse directions (as in the standard oedometer



test), the stress-strain curve trends continuously upward (fig. 2.39a). However, if the soil is sheared (or compressed in one direction with complete freedom to strain laterally, as in the standard triaxial test), the stress-strain curve reveals a limited peak strength (fig. 2.39b). As a first approximation, the idealized stress-strain curves of fig. 2.39c can be used to investigate the consequences of this limited shear strength.

Fig. 2.39 Typical and idealized stress-strain curves for studying effect of shear strength

The behavior at the front of a P-wave is controlled by the behavior in confined compression; while shear stresses are present in such a loading,

there is no shear strength failure in the usual sense of the phrase. Because many of the important features of the ground motions within the superseismic region (peak vertical stress and particle velocity, peak horizontal stress and particle velocity) are determined mainly by the

response at the P-front, shear strength is of no direct interest with regard to these features.

The behavior right at the front of an S-wave is of course controlled by the behavior in shear, and under certain circumstances the jump in shear stress as predicted by elastic theory may exceed the shear strength of the ground. Some aspects of this situation have been explored by Bleich et al. (1965). The response of the S-front affects the rate of attenuation of peak vertical and horizontal stress and velocity within the top-most several hundred feet of the superseismic region. The influence of this shear stress upon attenuation has not been systematically examined as yet. However, since the total attenuation is relatively small (see fig. 2.26) the rate at which this attenuation occurs is of secondary importance.

The behavior behind the wave fronts within the superseismic region is affected by the entire stress-strain relation for ground, and limited shear strength must have some effect upon this behavior. A few calculations have recently been made, but the writer has not examined the results. However, since the main response within the superseismic region is a downward compression with relatively little horizontal straining, it might be expected that the consequences of limited shear strength are relatively minor.

The most important consequence of limited shear strength lies in the effect upon surface waves. As the analyses summarized in section 2.4.2 have shown, surface waves may involve large shear stresses and always involve tensile stresses (soil, of course, has a very low tensile strength). Some yielding thus must occur in an intense surface wave. Because some loss of energy occurs during a cycle of loading-yielding-unloading, the displacements resulting from surface waves will tend to attenuate more rapidly with distance than indicated by elastic theory. Thus shear strength may affect the magnitude of the ground motions within the out-running region, and will have a particularly great effect in reducing the intense, late arriving surface waves predicted for superseismic regions (fig. 2.30). Only now is this consequence being investigated systematically.

Thus, in summary, limited shear strength appears to have relatively little effect upon those aspects of ground motion which are associated

primarily with the passage of airblast directly over a point, but may have important effects upon surface waves originating nearer ground zero.

Hysteresis: As indicated in fig. 2.40, the stress-strain curve of soil and rock during unloading generally will not exactly follow the

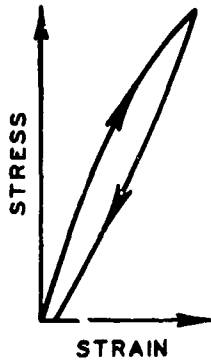


Fig. 2.40 Stress-strain curve exhibiting hysteresis

stress-strain curve during loading. This is true for shear even for stresses much less than the shear strength. It is also true for compression.

The energy loss associated with hysteresis will cause attenuation of the response at a superseismic wave front as well as attenuation of surface waves. Two-dimensional problems involving hysteresis have recently been investigated, but again the writer has not yet examined the results. However, section 2.4.2 has indicated that most of the main features of ground motion within the superseismic region can be

approximated by studying one-dimensional wave propagation within a vertical column of soil, and some approximate crude studies of the effect of hysteresis upon one-dimensional wave motions have been made (Whitman, 1963). By assuming reasonable values for the energy loss per cycle, it was found that hysteresis generally will cause less than 10% attenuation of peak stress and particle velocity within the uppermost 200 ft in the case of a large explosion such as 30 Mt, but might cause very considerable attenuation over such a depth in the case of a relatively small explosion such as 1 kt. Laboratory experiments on long soil columns have shown that the predictions of this crude theory are substantially correct for depths which are small compared to the wavelength of the airblast (Seaman, 1964 and 1966), which are the depths of greatest interest in most practical problems.

Viscosity: Soils generally exhibit time-dependent behavior, such as creep under constant load, for both shear and compression. As with hysteresis, viscosity must have some effect upon all aspects of airblast-induced ground motion. However, the only effect which has been studied in detail, and then but crudely, is the possible attenuation of peak vertical stress and particle velocity with depth (Whitman, 1963). The conclusion was generally the same as for hysteresis: that attenuation is relatively

unimportant in the case of large explosions but may be quite important for small explosions.

It is important to note that the stress-strain curve for a viscous material during a cycle of loading and unloading is very similar to that for a hysteretic material. This is illustrated in fig. 2.41, using the simplest viscoelastic model which exhibits the most important features of soil behavior. Thus, although most of the energy loss in soils actually results from hysteresis, the viscoelastic model can by

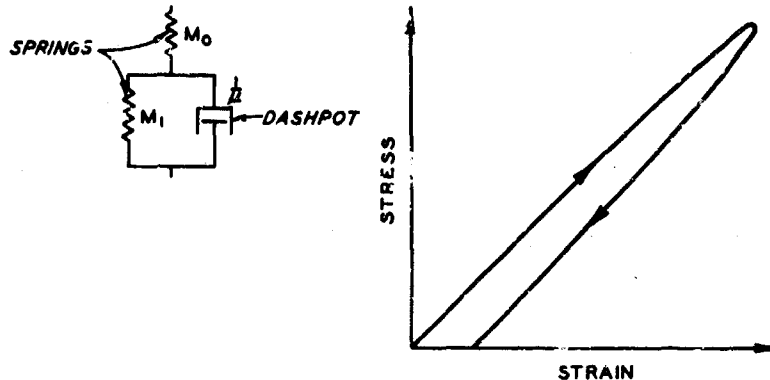


Fig. 2.41. Three-element linear viscoelastic model and stress-strain curve during one-half of cycle of loading

appropriate choice of constants be made to properly represent this energy loss (Seaman, 1966). Mathematical analysis of wave propagation, particularly in two or three dimensions, is much easier for a linear viscoelastic material than for a hysteretic material. The economic advantages of using viscoelastic theory for studying the consequences of energy losses within soil may have been greatly overlooked in weapons effects research. The steady-state problem of airblast moving over a viscoelastic material has been treated by Rajapaksee et al. (1960), but only limited numerical results are presented and no attempt has been made to compare these results with those of the one-dimensional case.

Nonlinearity: Stress-strain curves for soil and rock are usually far from being linear (figs. 2.39a and 2.39b). This nonlinearity affects primarily the rise times at wave fronts. As shown in fig. 2.42a, a yielding type of stress-strain curve means that rise time increases with distance, because increasing stress means decreasing modulus and thus decreasing velocity of propagation. On the other hand, a stiffening type of stress-strain curve (fig. 2.42b) implies that rise time decreases with distance

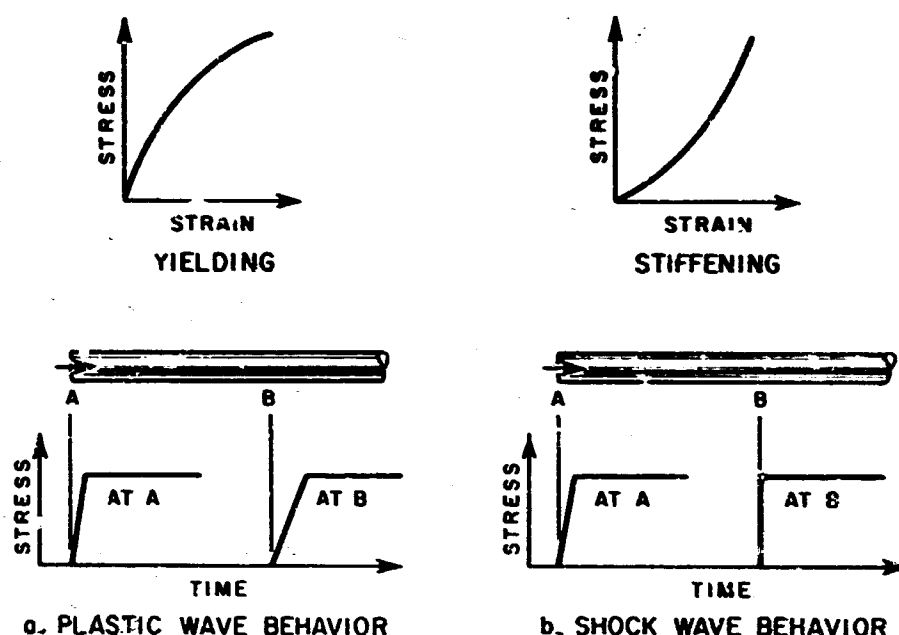


Fig. 2.42 Relation between type of stress-strain curve and nature of wave front

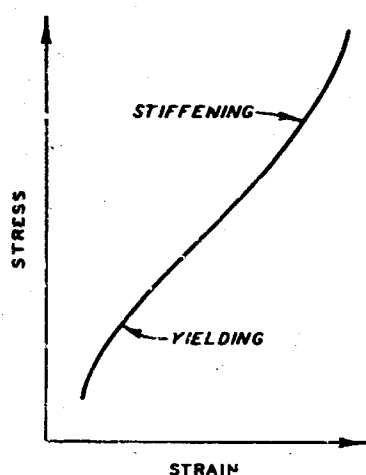


Fig. 2.43 S-shaped stress-strain curve for confined compression

until a shock wave of zero rise time develops.

Typically, actual stress-strain curves during loading in confined compression are S-shaped as shown in fig. 2.43, having both yielding and stiffening behavior (for example, see Whitman, Miller, and Moore, 1964). Hence P-waves in soil may be either shock waves or show increasing rise times, depending upon the conditions.

Fig. 2.44 gives results from a laboratory test which showed shock waves forming at shallow depths but then degenerating into plastic-type waves. Detailed study (Seaman and Whitman, 1964) indicates that shock waves can develop only at very shallow depths in soils of low modulus.

Otherwise, increasing rise times are to be expected.

Other factors also influence the rise times at wave fronts, and hence the accelerations at such fronts. Stoll and Ebeido (1965) have studied the role of viscosity. Reflections among the many small-scale stratifications

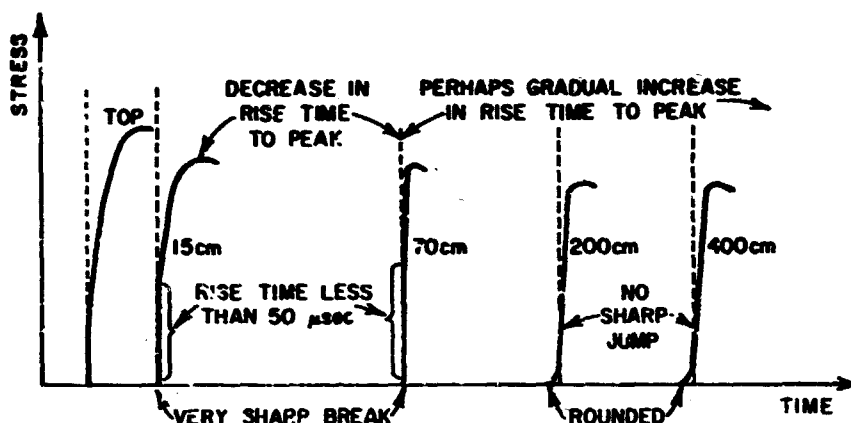


Fig. 2.44 Typical changes in wave front with depth, as observed in soil shock tube (from Searan and Whitman, 1964)

and lenses within actual soils also act to scatter the energy at the wave front and hence cause the peak accelerations to decrease with distance. It is extremely difficult to predict peak accelerations from theory alone, and heavy reliance must be placed upon actual field observations.

Other implications of nonlinearity, as it affects the wave propagation problem in soils, are treated by Zaccor (1967).

Summary: The consequences of the nonelastic effects discussed in this section are still poorly understood. Nonlinearity has an important qualitative consequence: rise times at wave fronts are actually finite and increase with distance rather than being zero as predicted by elastic theory. The consequences of shear strength, hysteresis, and viscosity are large quantitatively. These effects cause loss of energy and hence attenuation of waves with distance. This attenuation appears to be especially important for surface waves. For stresses and velocities at P-fronts, attenuation caused by nonelastic effects is similar in magnitude to the attenuation caused by the two-dimensional effects discussed in section 2.4.2 (fig. 2.26).

2.4.4 Prediction of Ground Motions for Engineering Studies. In principle, use of modern computational techniques together with high-speed digital computers makes it possible to compute the ground motion response for any soil profile with any desired stress-strain characteristics.

Within the past several years, since the bulk of this report was written, there have been opportunities to compare the results as predicted by lengthy calculations using realistic soil properties with actual field observations. Apparently the results have been encouraging, and it may well be that such calculations can now be used to generate input for design. Because of the cost of a single computer run, there naturally is a tendency to make a single run using "best estimate" soil properties. However, in view of the inevitable uncertainties which (in the writer's opinion) will always exist concerning in situ soil properties, it is essential that a series of computer runs be made for each problem, using a range of soil properties.

Because of these shortcomings of predictions based on lengthy computer runs, at the present time the engineer should still rely heavily upon simpler approaches which are based upon field observations organized in accordance with simple theoretical concepts. There are a variety of such methods: for example, those presented by ASCE (1961), Wilson and Sibley (1962), Air Force (1962), Sauer et al. (1964), and Agbabian-Jacobsen Associates (1966). Predictions are usually made in two steps. First, peak stresses and motions are estimated. These estimates can be made with a fair degree of confidence. Next the time history of the ground motion, or at least the phasing of the major events, is estimated. Estimates of the time history or wave form are much more difficult and much more uncertain.

A full discussion of these approximate engineering approaches is beyond the scope of this report. The general philosophy and approach will be illustrated by presenting prediction techniques for a specific case: stresses and ground motions within the superseismic region of homogeneous ground.

Prediction equations for superseismic region, homogeneous soil: The prediction methods for this case are based upon one-dimensional elastic wave propagation theory, with some simple but inexact modifications which make the predictions more in accord with reality. The extent to which one-dimensional theory can be used to approximate superseismic behavior has been illustrated in fig. 2.24.

The first step is to predict the attenuation of peak vertical stress

with depth. This is done using the equations

$$(\sigma_z)_{\max} = \alpha p_s \quad (2.1)$$

$$\alpha = \frac{1}{1 + z/L_w} \quad (2.2)$$

$$L_w = 230 \text{ ft} \left(\frac{100 \text{ psi}}{p_s} \right)^{\frac{1}{2}} \left(\frac{W}{1 \text{ Mt}} \right)^{\frac{1}{3}} \quad (2.3)$$

where p_s is the peak surface overpressure directly above the point in question, α is an attenuation factor, z is the depth in feet, and W is the equivalent weight of the explosive in megatons. Equations 2.2 and 2.3 were originally obtained using a quasi-static calculation which neglects the inertia of the soil. An example of the attenuation predicted by these equations appears in fig. 2.26. As discussed in section 2.4.2, this result overestimates the attenuation which occurs within an elastic medium. However, considering that attenuation introduced by hysteresis and viscosity cause additional attenuation (section 2.4.3), the predictions obtained by means of the above equations are, rather fortuitously, in agreement with the very few measurements of the actual attenuation of peak vertical stress.

Next the peak vertical particle velocity is estimated. According to one-dimensional elastic theory, this velocity is

$$(\dot{w})_{\max} = \frac{(\sigma_z)_{\max}}{D} C_D = \frac{(\sigma_z)_{\max}}{\rho C_D} \quad (2.4)$$

where D is the constrained modulus, C_D is the velocity of a P-wave, and ρ is the mass density. For a soil with a unit weight of 115 pcf, this equation becomes:

$$(\dot{w})_{\max} = 50 \text{ in./sec} \left(\frac{p_s}{100 \text{ psi}} \right) \left(\frac{1000 \text{ fps}}{C_D} \right) \alpha \quad (2.5)$$

It must be emphasized that C_D serves here as a measure of the resistance of the soil to compression. The evaluation of this compressive resistance for a given soil is discussed in section 2.4.5. Equation 2.4, though

approximate for two-dimensional superseismic motion, nonetheless is a sound and good approximation. For a given $(\sigma_z)_{\max}$, $(\dot{w})_{\max}$ depends primarily upon the properties of the soil at the point in question, and only to a lesser degree upon what happens above or below the point. Of all the various aspects of ground motion, peak vertical particle velocity can be estimated most accurately. For near-surface points where $\alpha \approx 1$, it generally is possible to estimate $(\dot{w})_{\max}$ to within a factor of 1.3 or at worst a factor of 2.

Peak vertical displacement is more difficult to predict, since this displacement depends upon the strains developed at great depth. In the one-dimensional case, the peak displacement is

$$(\dot{w})_{\max} = \frac{I}{\rho C_D} \quad (2.6)$$

where I is the applied impulse; that is, the integral of overpressure versus time at the surface. Some rationale can be found for applying this same expression to the two-dimensional airblast problem. For example, it can be argued that impulse will be approximately preserved with depth down a vertical column of soil cutting through the two-dimensional field. However, the best justification for the use of this equation is that it provides a simple method which contains the correct factors and which provides results that are in reasonable agreement with observations. Using an approximate expression for the impulse within the airblast and assuming a unit weight of 115 pcf, Equation 2.6 becomes

$$(\dot{w})_{\max} = 9 \text{ in.} \left(\frac{p_s}{100 \text{ psi}} \right)^{\frac{1}{2}} \left(\frac{1000 \text{ fps}}{C_D} \right) \left(\frac{W}{1 \text{ Mt}} \right)^{\frac{1}{3}} \quad (2.7)$$

Predictions based upon this equation probably are accurate to within a factor of 2 but may err by as much as a factor of 4 or 5.

According to this approach, the peak vertical displacement is the same at all depths, which is approximately true for shallow depth ($z < 0.3L_w$) in homogeneous soils. Clearly this cannot remain true for all depths, however. The peak transient relative displacement between the surface and depth z can be estimated from the fact that the maximum average strain

between the two points must be less than the maximum strain at the surface.

Hence:

$$\Delta w < \frac{p_s}{D} z = \frac{p_s}{\rho C_D^2} z \quad (2.8)$$

For a soil with a unit weight of 115 pcf, this becomes

$$\Delta w < 4.8 \text{ in.} \left(\frac{p_s}{100 \text{ psi}} \right) \left(\frac{1000 \text{ fps}}{C_D} \right)^2 \left(\frac{z}{100 \text{ ft}} \right) \quad (2.9)$$

Predictions using this equation are probably good to within a factor of 2 or at worst a factor of 3.

Predictions of peak vertical acceleration depend almost entirely upon empirical data regarding rise times. If the rise time t_r is known, and if the particle velocity is assumed to increase parabolically, then

$$(\dot{w})_{\max} = \frac{2(\dot{w})_{\max}}{t_r} \quad (2.10)$$

Near or at ground surface, t_r is typically observed to be about 2 msec. Using this result and increasing the predictions by 20% to give a better fit with observed accelerations, the peak surface downward acceleration becomes:

$$(\dot{w})_{\max} = 150 \text{ g's} \left(\frac{p_s}{100 \text{ psi}} \right) \left(\frac{1000 \text{ fps}}{C_D} \right) \quad (2.11)$$

The rise time increases with depth, and so the peak downward acceleration decreases with depth. As an approximation, t_r can be taken as equal to a constant K times the transit time of a seismic signal from the surface to the depth considered. Thus

$$t_r = K C_{DO} \quad (2.12)$$

where

$$K = 1 - \frac{C_D}{C_{DO}} \quad (2.13)$$

Here C_{DO} is the dilatational velocity of a seismic level signal. This leads to:

$$(\dot{w})_{\max} = 5 g's \left(\frac{P_s}{100 \text{ psi}} \right) \left(\frac{100 \text{ ft}}{z} \right) \left(\frac{0.5}{K} \right) \alpha \quad (2.14)$$

Equation 2.14 overestimates the peak acceleration at very shallow depth, and hence no value greater than that given by Equation 2.11 should be used. For depths greater than 10 ft, the predictions of Equation 2.14 agree with field observations to within a factor of 2 or 3.

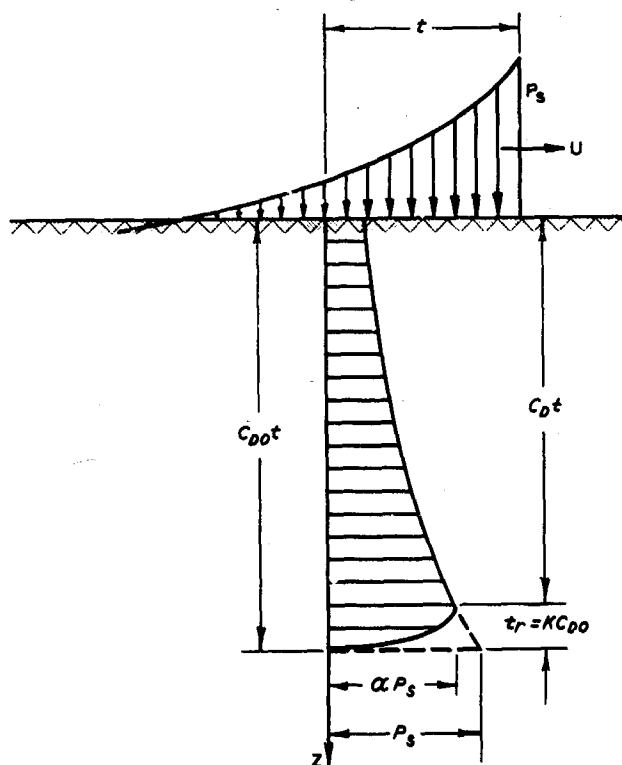
The foregoing prediction equations give the vertical components of motion for the superseismic range. Horizontal components can be estimated from the following rules which are based upon scattered field observations plus the insight provided by theoretical calculations.

Peak horizontal stress = $2/3$ peak vertical stress

Peak horizontal velocity = $2/3$ peak vertical velocity

Peak horizontal displacement = $1/3$ peak vertical displacement

Peak horizontal acceleration = peak vertical acceleration



The wave form for vertical stress (the wave form for particle velocity would be similar) is shown in fig. 2.45. Basically the wave form is that of the airblast overpressure, with the peak attenuated according to Equation 2.1 and the rise time increased according to Equation 2.12. If impulse is to be preserved with depth, there

Fig. 2.45 Distribution of stress at time t after airblast passes point on ground surface

must be some lengthening of the tail of the wave form. Wave forms of acceleration and displacement can be derived from the time history for particle velocity.

Needed research: The foregoing prediction equations for ground motions within the superseismic region of homogeneous ground illustrate the blending of simple theoretical concepts and field observations in order to arrive at a self-consistent and simple set of prediction equations. There is a need to develop more complete prediction techniques which will take into account such complexities as layering of the ground. The development of such advanced procedures must be based upon two principles:

- (a) The procedure must permit the user to understand clearly the link between assumption and result, so that he can use his judgment and experience in assessing the probable accuracy of the result.
- (b) The procedure should be adequately based upon actual field observations. Limited confidence can be placed in any prediction unless it represents only a modest extrapolation of that which is already known through experience.

Engineers and scientists should avoid lengthy computer runs in which many new complexities are considered at the same time. However, it is essential to have computer studies in which the effect of each variable, or groups of variables, is examined singly and the results are compared with field experience. In this way it will be possible to build confidence in the use of complex computer programs and at the same time to form a basis for developing more versatile and yet simple and reliable prediction techniques.

2.4.5 Requirements for Data Regarding Soil. Table 2.5 summarizes the requirements for soil data in connection with predictions of airblast-induced ground motions.

When the simple prediction techniques discussed in section 2.4.4 are used, there is only a limited requirement for specific values of certain soil parameters. By far the most important parameter is the secant modulus of soil in confined compression (constrained modulus) for the stress increment of concern. A value of this modulus is needed for every prediction. It can well be said that no prediction can be more accurate than the estimate of the constrained modulus. This modulus is related to the velocity

Table 2.5
Requirements for Data on Soil Properties in Connection
with Airblast-Induced Ground Motions

1. Data for Studies to Ascertain Importance and Effect of Various Features of Soil Behavior

Need to identify key features of behavior and to establish general range of values for key parameters such as:

- compressibility
- shear strength
- energy loss per cycle of loading
- time-dependent effects

2. Data for Use in Simple Prediction Procedures

a. Modulus in confined compression

- Needed for every prediction
- Alternatively can use C_D = dilatational velocity of peak stress

b. Seismic dilatational velocity

- Useful for judging variation of rise time with distance
- Useful as indirect measure of modulus during confined compression

c. Energy loss per cycle

- Of some use in judging relative attenuation at various sites
-

of propagation for the peak level of stress, and is generally less than the seismic wave velocity as conventionally measured in the field. While the seismic dilatational velocity is useful as a crude estimate for the modulus in confined compression, reliable estimates of ground motions can be expected only when a direct determination is made of either the modulus or the propagation velocity C_D for peak stress. Some direct use can be made today of the energy loss per cycle for a soil; however, the computational techniques needed for a full use of this quantity are still under development.

There is a growing requirement for detailed soil data regarding various sites to be used in complex computer codes. The most important parameters appear to be compressibility, shear strength, and energy loss per cycle of loading. Evaluation of such parameters will require considerable effort and expense in field exploration, sampling, and testing, and it is essential that there be close liaison between those providing the soil data and those who write and use the computer codes.

2.5 SOIL-STRUCTURE INTERACTION WITH AIRBLAST-INDUCED STRESS WAVES

As noted earlier, soil-structure interaction concepts are used (a) to design the structural shell to carry the applied stresses, and (b) to determine the motions of the structure as an input to the design of any shock isolation systems necessary to allow the personnel and equipment to survive the motions. The inputs for these considerations are the free-field stresses and ground motions as discussed in section 2.4.

The design of buried protective structures is even more complicated than the evaluation of free-field ground motions and stresses. Detailed discussions are provided by Merritt and Newmark (1964), Agbabian-Jacobsen Associates (1966), and Newmark and Halmiwanger (1962). This section will be restricted to the most essential soil mechanics considerations. Sections 2.5.1 through 2.5.4 will discuss methods for estimating the stresses reaching buried structures of different geometries (fig. 2.46). Section 2.5.5 will discuss the motions experienced by such buried structures. The emphasis will be on the relation between soil properties and response.

2.5.1 Buried Horizontal Cylinders. Horizontal cylinders buried at shallow depth can, with proper backfilling, sustain

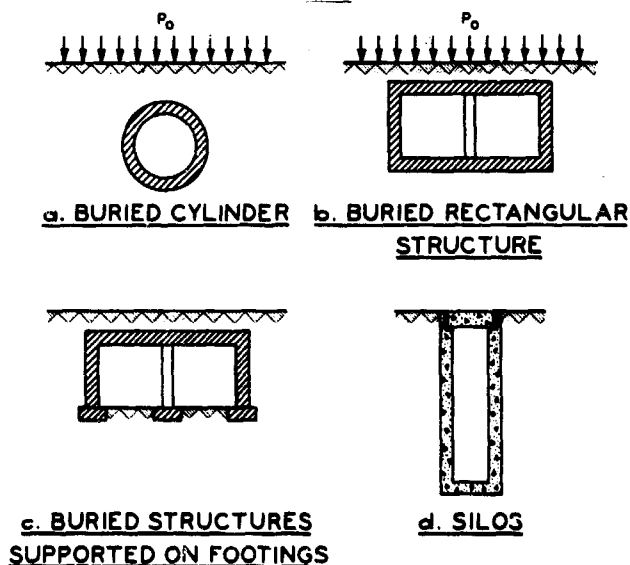


Fig. 2.46 Typical configurations of buried structures

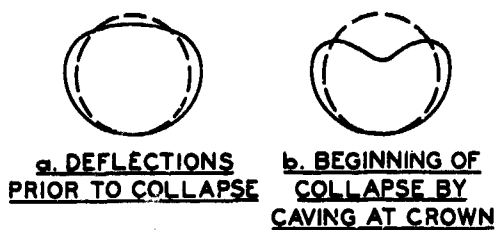


Fig. 2.47 Collapse of poorly backfilled, horizontal, buried flexible cylinder

large applied stresses owing to their favorable structural configuration. Proper backfilling prevents excessive lateral deformation followed by a caving in of the cylinder crown (see fig. 2.47). Careful backfilling is always justified economically in protective construction. It also is often justified in conventional engineering, especially where

circular conduits are in use under dams and embankments up to several hundred feet in height.

It has been shown (Luscher, 1963; Dorris, 1965) that for shallow burial the dynamic response is similar to the static response under an applied surface loading equal to the peak dynamic pressure. This similarity has been used extensively in the past to learn from much simpler static tests a great deal about prototype dynamic behavior. Most of the following rules were, in fact, developed on the basis of small-scale static tests.

Provided that careful backfilling keeps the lateral deformations small, elastic theory provides reasonably accurate estimates for the stresses between the soil and the cylinder. That is, the shear stresses within the soil (except perhaps in a very small zone right next to the structure) remain less than the shear strength of the soil until structural failure develops. The validity and usefulness of elastic theory have been demonstrated by small-scale tests by Höeg (1966), for a wide range of cylinder stiffness. Fig. 2.48a shows a typical pattern of contact stress. Depending upon the relative stiffness of the structure and the soil, the peak contact stress may be either somewhat greater or somewhat less than the surface overpressure. Suitable values for

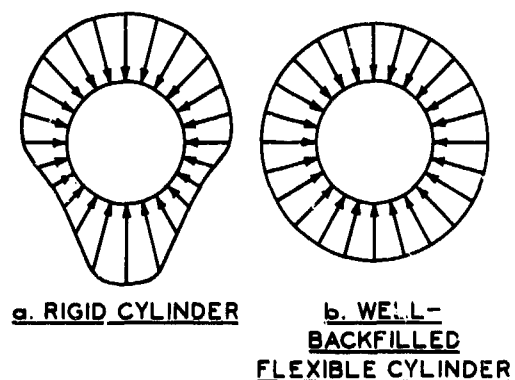


Fig. 2.48 Distribution of stresses against horizontal buried cylinder

the modulus of the soil may be determined from confined compression tests. The proper value for this modulus will vary depending upon the magnitude of the applied overpressure.

For the special case of a flexible buried cylinder, after a small amount of deformation the stresses between the cylinder and the soil become uniform (fig. 2.48b). The amount of deformation required to reach this condition can be estimated using the theory proposed by Spangler (1960), but using values of lateral resistance coefficient much larger than those suggested by Spangler (see Lambe, 1963). For such a situation, the critical design force is the ring compression, which may cause failure by either buckling or compressive failure. (If buckling in the inelastic range is also considered, compressive failure actually corresponds to inelastic buckling.) The compressibility of the soil backfill is an important factor with regard to the susceptibility of the cylinder to buckling. The buckling equation is (Luscher, 1965):

$$\sigma'_z = K \sqrt{\frac{EI}{R^3}} \sqrt{M} \quad (2.15)$$

where

σ'_z = free-field vertical soil stress leading to buckling; for shallow burial, σ'_z is equal to the pressure applied at the surface

K = a factor which takes into account the depth of burial and other geometrical aspects of the problem

EI = flexural rigidity of cylinder; if E is defined as the tangent modulus of the cylinder material at any stress level, the equation is valid for inelastic as well as elastic buckling

R = radius of cylinder

M = constrained modulus* of the soil backfill; may be a function of σ'_z

Table 2.6 gives results computed by means of this equation. With a diameter/thickness ratio $D/t = D/t_{cr}$, elastic buckling occurs at a ring stress just equal to the yield hoop stress. If the design stress σ'_z is

* The modulus M is the same as the modulus D in section 2.4. The symbol M is used here to avoid confusion with the diameter D.

Table 2.6

Critical Buckling Condition of Underground Cylinders; Intersection of
Elastic Buckling Curve with Yield Stress Line

Material	E ksi	σ_y ksi	Upper Limit of M $M = 1000(\sigma'_z)^{0.8}$			Lower Limit of M $M = 62(\sigma'_z)^{0.9}$		
			D/t _{cr}	t _{cr} for D = 10 ft in.	$(\sigma'_z)_{cr}$ psi	D/t _{cr}	t _{cr} for D = 10 ft in.	$(\sigma'_z)_{cr}$ psi
High-strength steel	30,000	70	300	0.46	470	65	1.85	2150
Mild steel	30,000	30	530	0.23	110	114	1.05	530
High-strength aluminum	10,000	30	290	0.41	210	62	1.94	970
Mild aluminum	10,000	10	600	0.20	33	130	0.92	150

Note: For a depth $d \geq D$.

less than the tabulated values of $(\sigma'_z)_{cr}$, the load can be carried most efficiently by choosing $D/t > D/t_{cr}$, and failure would then be by elastic buckling. If the design stress is greater than $(\sigma'_z)_{cr}$, the load can be most efficiently carried by choosing $D/t < D/t_{cr}$ and failure would then be by compressive yielding (inelastic buckling).

Thus, modulus as measured in confined compression is the key soil property governing the interaction between soil and well-backfilled horizontal cylinders. This is true whether the cylinder has some rigidity and fails by yielding in bending or is extremely flexible and fails by elastic or inelastic buckling.

2.5.2 Buried Closed Rectangular Structures. Structures of this geometry are used when moderate stresses, say up to 100 psi or maybe 200 psi, are to be sustained. The loadings sustained by the relatively flexible and ductile roof (fig. 2.46b) have often been observed to be considerably reduced compared to the pressures applied at the surface (Bultmann et al., 1959).

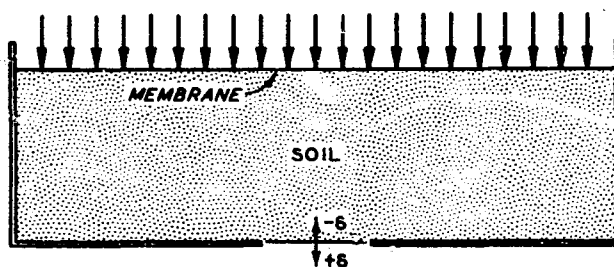


Fig. 2.49 Trapdoor experiment

The fundamentals of this situation have been studied by means of so-called "trapdoor" experiments (fig. 2.49). Here a movable plate in the bottom of a bin of soil is moved away from the soil, simulating a flexible

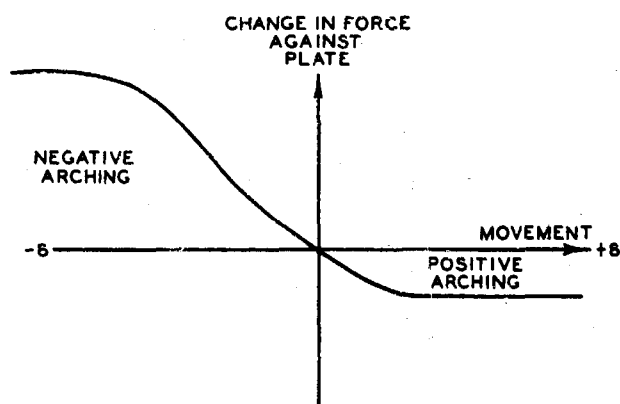


Fig. 2.50 Results of trapdoor experiment

roof of a buried structure, and the force against the plate is observed as a function of the movement. Experiments have also been made in which the plate is pushed into the soil, simulating the behavior of a very rigid buried structure. Fig. 2.50 shows a typical set of results.

For small movements, the behavior of the soil is

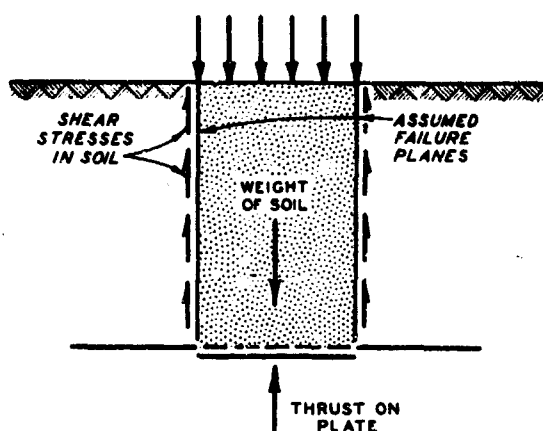


Fig. 2.51 Marston-Spangler theory for arching

essentially elastic, and the force-deflection relation can be estimated from elastic theory (Finn, 1963; Chelapati, 1964).

With larger movement of the plate away from the soil, a limiting force is reached. This limiting condition is called positive arching, since the shear resistance of the soil acts to decrease the force against the plate. Fig. 2.51 shows a hypothetical model, originally pro-

posed by Marston (Spangler, 1960), which has often been used to estimate the load reaching the plate. This classical method has been extended (Newmark and Haltiwanger, 1962) to take into account the compressibility of the soil and only partial mobilization of shear stresses along the hypothesized vertical failure surfaces. Other theories for estimating the reduction in stress have also been advanced, based upon the concept of formation of arches over the structure (Mason et al., 1963; Luscher and Höeg, 1965; Nielsen, 1967).

While there is considerable doubt as to the exact mechanism of arching, the procedures outlined by Newmark and Haltiwanger give reasonably good agreement with the available data regarding buried structures.

With large movement of the plate into the soil, there is also limiting force corresponding to negative arching. The Newmark-Haltiwanger theory, with shear stress acting in the opposite direction, can also be used to estimate this limiting force.

The application of these principles to buried rectangular structures indicates a distribution of stress against the top of the structure as shown in fig. 2.52. Because of the flexibility of the roof and base in bending, the vertical compressibility along B-B is greater than the vertical compressibility of the soil (A-A). Hence the stress over the major portion of the roof is less than the average stress at this elevation. However, the walls (C-C) are generally stiffer than the soil, so that

negative arching occurs over the walls.

The stresses on the vertical sides of the rectangular structure are computed as percentages K_0 of the dynamic vertical stress. Proposed values of K_0 , the dynamic coefficient of lateral stress,

range from 0.25 to 1.0 depending upon the type of soil and the degree of saturation with water (Newmark and Halmiwanger, 1962).

2.5.3 Buried Arches or Rectangular Structures Supported on Footings.

Structures supported on footings (fig. 2.46c) can generally be used for relatively small pressures only (up to 50 or maybe 100 psi). As the footings punch into the supporting soil, the structure can move downward with respect to the soil at the side of the structure, thus permitting considerable positive arching to develop above the structure (fig. 2.53). Thus,

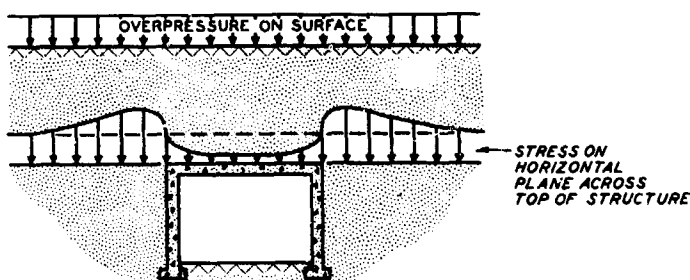


Fig. 2.53 Arching at structure supported on footings

because of the flexibility introduced by the footings, even rather rigid structures such as well-backfilled arches will experience vertical loads much less than the overpressures applied at ground surface (Allgood et al., 1963; Gill and Allgood, 1964).

Design of the footings is a key step in the design of this type of buried structure. Use of narrow footings means more effective flexibility, hence more arching and smaller loads reaching the structure, and thus a more economical structure. On the other hand, too narrow a footing may lead to intolerably large movements of the structure. The design of footings hence must strike an optimum balance (Whitman and Luscher, 1965).

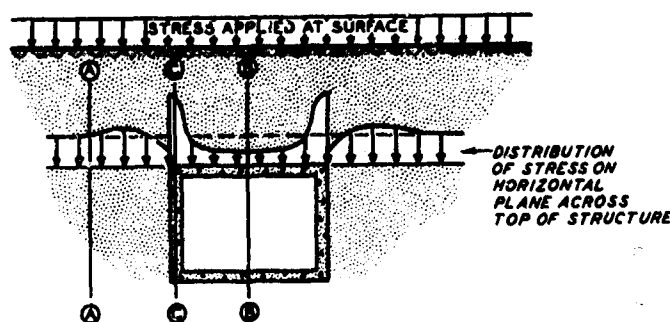


Fig. 2.52 Arching at closed rectangular structure

Numerous small-scale tests have been made to study the behavior of footings subjected to transient loads (for a summary, see Whitman and Luscher, 1965). Since the idea is to permit relatively large settlements (perhaps as much as 6 in.), complete or partial shear failures develop beneath the footings and hence shear strength is the most important parameter governing response.

2.5.4 Vertical Cylinder (Silo). This type of structure (fig. 2.46d) has received wide usage as a protective housing for missiles. Approaches used in designing silos are discussed by Newmark and Halmiwanger (1962). There are three major concerns with regard to design.

First, the radially applied stresses, both static and those resulting from surface overpressure, must be considered. Since silos are quite thick-walled, little if any positive arching occurs. These stresses are hence based on K_0 values as discussed in section 2.5.2.

Second, since the surrounding soil generally is more compressible in the vertical direction than the silo, downward drag forces upon the silo will develop. These drag forces increase the vertical stresses for which the silo walls must be designed. Evaluation of these forces is similar to the evaluation of possible wall shear forces at retaining walls.

Third, because the dynamic motions of the surrounding soil vary with depth, silos tend to bend as cantilever beams. The result is a very complicated problem in soil-structure interaction, in which the deformation modulus of the soil plays a key role. Numerous complicated computer programs, usually based upon elastic theory, have been written to permit analysis of this interaction, but practical work still relies heavily upon rather simple and intuitive design rules to guard against possible adverse effects of this interaction.

2.5.5 Motions of Buried Structures. As discussed in sections 2.5.1 through 2.5.4, relative motions between structure and soil have important influences upon the loads for which the structures must be designed. The absolute motions of buried structures are also important, since these motions can cause damage to equipment mounted within the structure or injury to personnel. In assessing possible damage to contents, and in designing shock mountings to minimize this damage, the peak acceleration and

peak particle velocity of the structure are most important. Peak displacement is important in providing adequate "rattle space" around very soft shock mountings.

In most analyses of the effects of structural motions, the absolute motions of the structure are assumed to be equal to the free-field motions of the surrounding soil. That is, the relative motions are neglected.

In part this assumption stems from lack of knowledge as to the actual effect. Differential motion of the structure with respect to the surrounding soil was studied by Heller (1965). His pilot study indicated that "rigid" inclusions, regardless of their density, displaced into the soil in the direction of the propagating soil stress wave. More rigid structures (which were also denser) experienced greater differential motions than less rigid ones. The maximum differential displacement between a stiff inclusion and the surrounding soil was of the order of one-third of the maximum absolute displacement of the inclusion. While tests of this type and computerized theoretical studies can give some indication of the difference between free-field and structural displacement, it is much more difficult to establish differences in free-field particle velocity and acceleration, especially for nonrigid structures. Except possibly for displacement, the rule that structural motion equals free-field motion generally leads to reasonable and satisfactory designs.

Design of shock mountings is usually based upon a response spectrum approach. As shown in fig. 2.54, a spectrum is usually constructed by drawing three lines at:

- (a) A spectral displacement equal to the maximum free-field displacement.
- (b) A spectral velocity 1.5 times the maximum free-field particle velocity.
- (c) A spectral acceleration 2 times the maximum free-field acceleration.

The factors of 1.5 and 2 take into consideration the amplification of transient base motion by a single-degree-of-freedom spring-mass system. For the spectrum shown in fig. 2.54, a component with a natural frequency of 30 cps would experience an absolute acceleration of 21 g's and a

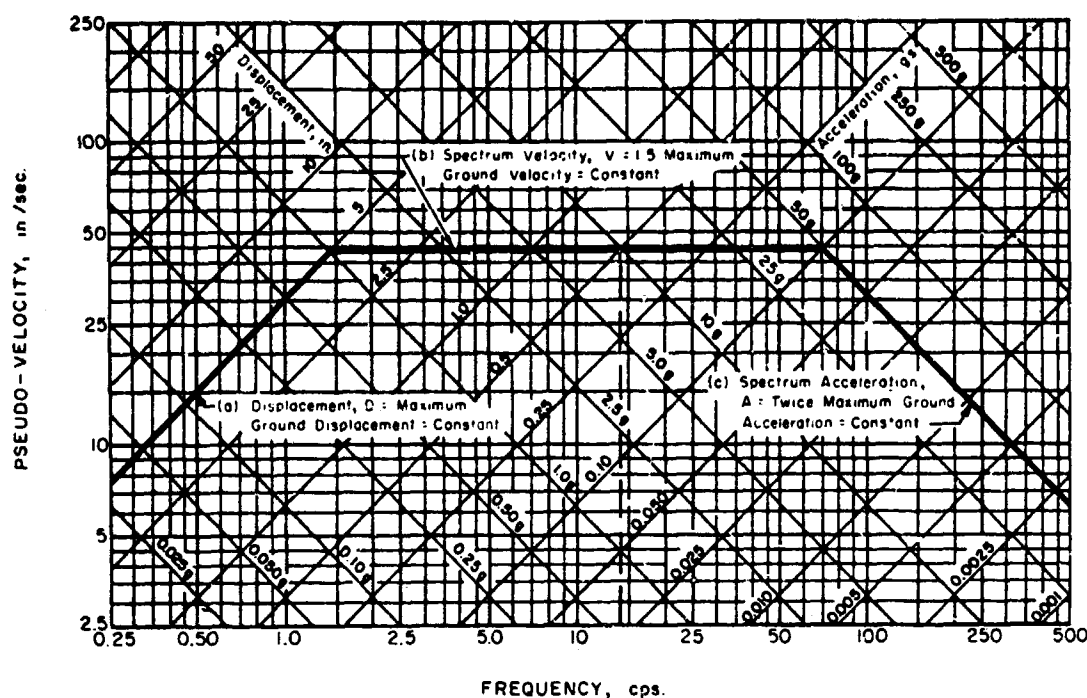


Fig. 2.54 Shock response spectrum chart

displacement of 0.23 in. relative to its mounting point. The above rules for determining the design response spectrum were specifically developed for superseismic conditions.

2.5.6 Requirements for Data Regarding Soil. As for the topics considered in sections 2.3 and 2.4, there is a great need to study the important features of soil-structure interaction using computerized theories which can handle complex geometries. This is especially true for complicated soil-structure systems such as footing-supported structures and silos. Much can be done using linear stress-strain relations, but nonlinear behavior must soon be considered for situations such as footing response. As in the case of free-field ground motions, very general information concerning the qualitative and quantitative behavior of soil is required for these studies. The most important parameters are shear strength and compressibility.

The requirements for specific values of certain soil parameters for use in engineering design are summarized in table 2.7. The most generally required parameter is K_0 , the coefficient of lateral stress at rest.

Table 2.7
Requirements for Data on Soil Properties in Connection
with Soil-Structure Interaction

<u>Type of Structure</u>	<u>Soil Property Required</u>
Horizontal cylinder	Compressibility, for evaluation of arching K_o , for estimating horizontal stress against rigid structures
Closed rectangular box	Compressibility, for evaluation of arching Shear strength for evaluation of arching K_o , for estimating horizontal stress
Footing-supported structure	Compressibility, for evaluation of arching and footing response Shear strength, for evaluation of arching and footing response K_o , for estimating horizontal stress
Vertical cylinder	K_o , for estimating horizontal stress Shear strength, for estimating vertical drag forces Compressibility, for estimating vertical drag forces

Values of this parameter can be estimated using ordinary soil mechanics considerations, keeping in mind that K_o approaches unity for fully or nearly saturated soils loaded rapidly enough to have undrained conditions. Compressibility (or modulus of deformation) is of prime importance for evaluating arching. Shear strength is used extensively in the evaluation of arching, although the writer suspects that the use of arching theories is overdone since large zones of shear failure probably develop only in extreme cases such as footing-supported structures. If structures are to be supported on footings, static plate bearing tests should be conducted at the site at the founding depth as the resulting load-displacement curves can sometimes be related to the dynamic load-displacement curve of interest

by using the ratio of dynamic to static shear strengths of the soil to adjust the plate bearing results.

2.6 DIRECTLY INDUCED STRESS WAVES

This section is concerned with the stress waves which move directly outward along radial lines from the point of the explosion. Stress waves of this type are encountered (a) near a deeply buried explosion which produces a cavity but does not vent to the surface, (b) immediately below a near-surface explosion which produces a crater, and (c) at near-surface points very close to the edge of the crater. This section is concerned with the free-field stresses and ground motions associated with such stress waves. Section 2.7 discusses briefly the problem of soil-structure interaction involving such waves.

When considered in more general terms, the problem of directly induced waves becomes quite complicated. If the properties of the earth vary with depth, these waves no longer move simply along radial lines. Near ground surface, directly induced waves and surface waves originated by airblast become almost indistinguishable, as in fig. 2.36. Various intuitive techniques have been evolved to estimate the effects of these complexities, but there is little basis for faith in the results.

2.6.1 Basic Phenomena. Spherical wave propagation from a cavity is a one-dimensional problem, in that only one coordinate (the radius) and one displacement (radial motion) are needed to describe the problem. However, spherical wave propagation differs significantly from the true one-dimensional form of wave propagation discussed in section 2.4. These dif-

ferences arise from two considerations indicated in fig. 2.55.

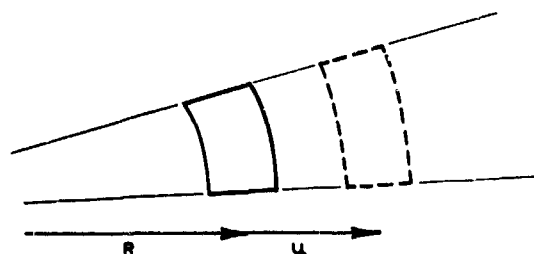


Fig. 2.55 Movement and deformation of an element of soil behind spherical wave front

- (a) The surface area encompassed by a spherical wave front increases with the distance traveled.
- (b) Outward motions give rise to circumferential strains. If a point at radius R

moves outward by an amount u ; the circumferential strain will be tensile and equal to u/R . Right at the wave front where the motion is still zero, the circumferential stress will be equal to the coefficient of lateral stress at rest, K_0 , times the radial stress. However, as soon as the point begins to move, the circumferential stress will decrease and will even become tensile (see fig. 2.56).

Even for an elastic material, these two effects combine to cause attenuation of peak stress with distance and smoothing out of an initially sharp wave front together with broadening of the stress pulse. Because the difference between the radial and circumferential stresses may become quite large, the material may fail in shear and either crack or flow plastically. Such a failure will cause increased attenuation of stress and smoothing of the stress wave, as illustrated in fig. 2.57.

Despite the apparent simplicity of the pattern of spherical waves emerging from a cavity, the situation

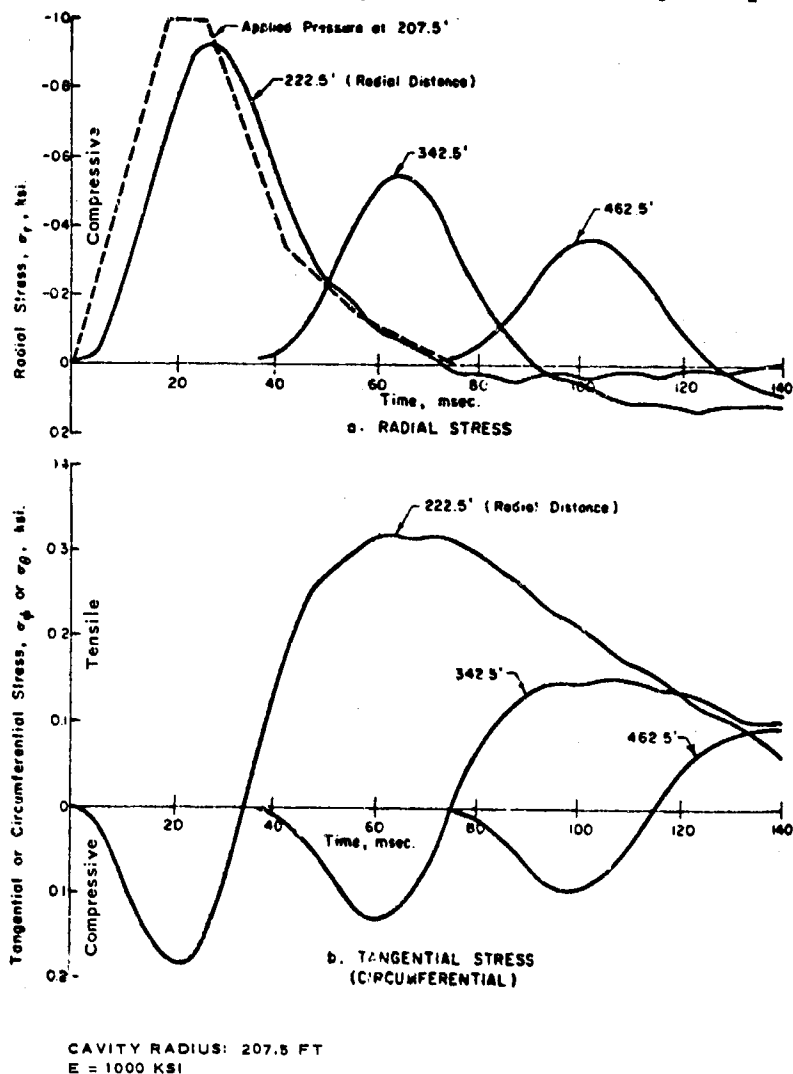


Fig. 2.56 Stresses caused by pressure in spherical cavity within an elastic body (from Ang and Ranier, 1964)

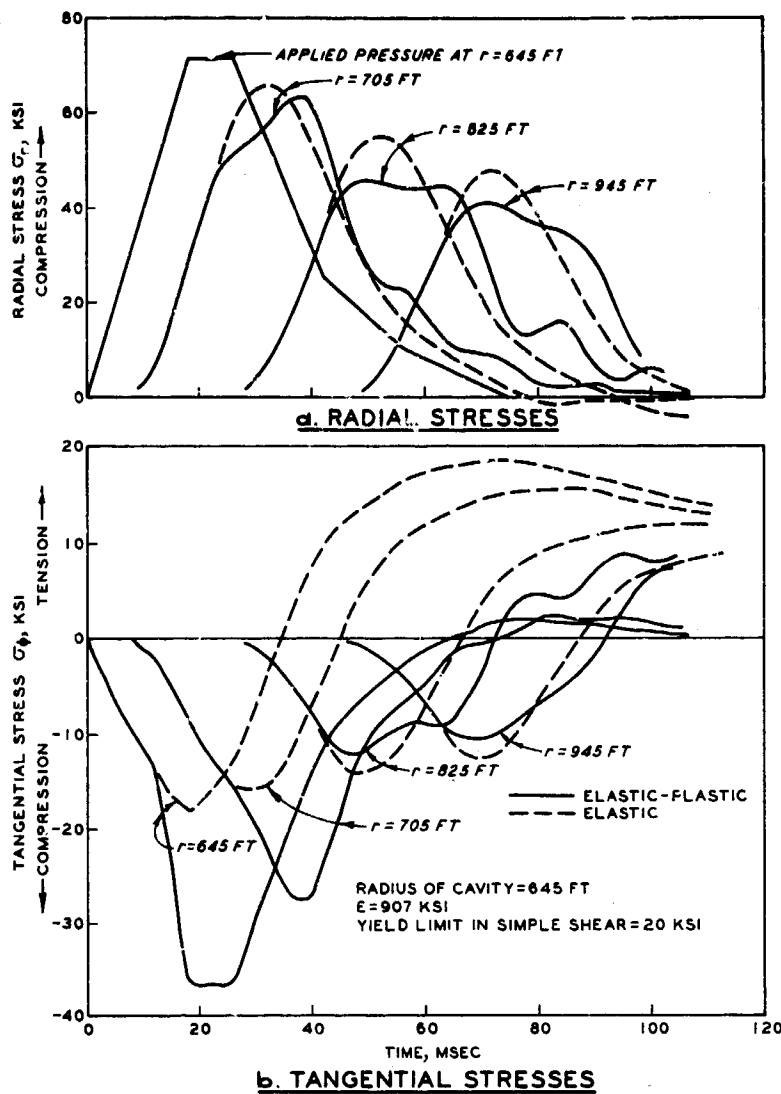


Fig. 2.57 Effect of yield strength on stresses caused by pressure within a spherical cavity (from Ang and Ranier, 1965)

still is complex mathematically. Even for an elastic material, the rate of attenuation of motion is not constant with distance. For example, peak radial particle velocity varies as $1/R^2$ near the cavity but as $1/R$ at great distances from the cavity. Attempts to incorporate limited shear strength, or other realistic soil or rock properties, into calculations immediately add greater complexities. Any completely satisfactory calculation must start with the hydrodynamic range and work outward into the region where the

shear strength of the soil is of significance. The assumed stress-strain and failure relations will have a considerable influence on the predicted results.

More calculations, using a variety of reasonable assumptions as to stress-strain behavior and with a range of values for the key parameters, should be carried out to increase our knowledge as to the possible and probable behavior of directly induced stress waves. An example of

calculations which have already provided useful insights is given by Ang and Ranier (1965), using an elastoplastic model with a fixed yield point. Other studies, which the writer has not examined, have very recently been completed.

2.6.2 Prediction

Methods. The various theories mentioned above generally are too complex for practical predictions of ground motions and stresses. Hence, simple prediction methods have been developed, using the results of theories to guide the form of equations and field results to give numerical coefficients.

A comprehensive survey of data, including relatively recent data, is given by Sauer (1964) in Part IV of NUCLEAR GEOPLOSICS. Fig. 2.58 gives a chart for peak radial acceleration. Table 2.8 gives an equation and coefficients for peak radial velocity.

Fig. 2.59 gives curves, based on elastic theory, for predicting peak displacement. The predictions obtained using this latter figure are described as upper bounds. The user of these curves and equations must judge for himself how the soil or rock with which he is dealing compares with the four materials for which results are given.

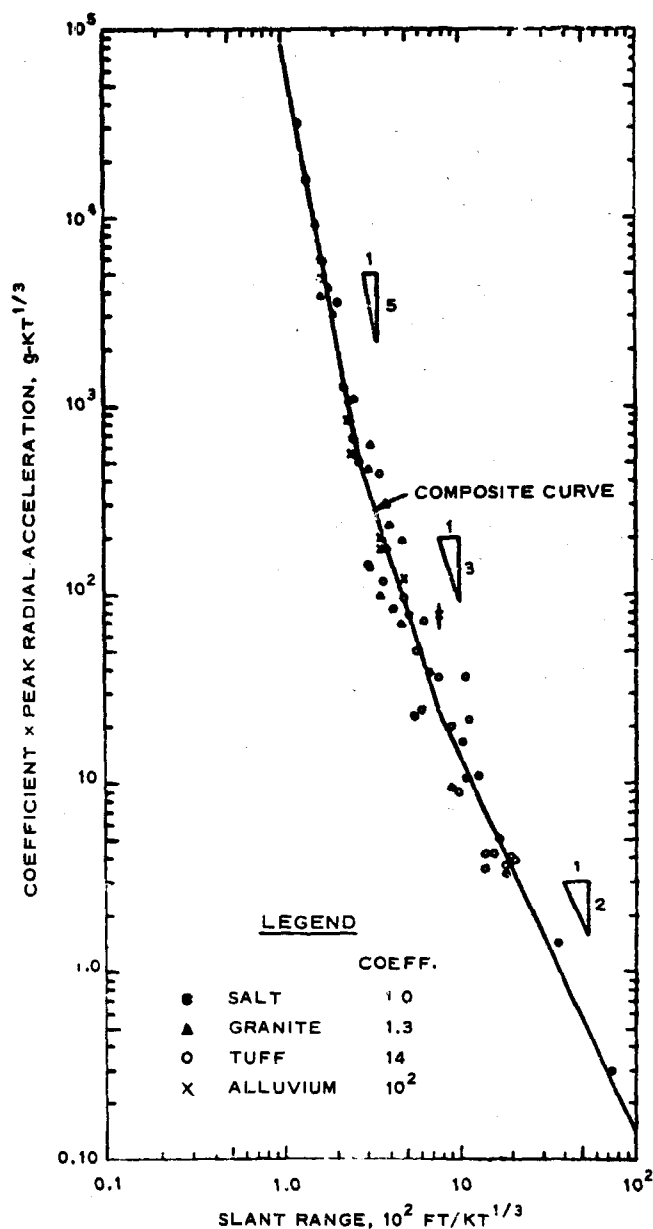


Fig. 2.58 Chart for prediction of peak radial acceleration (from NUCLEAR GEOPLOSICS, Part IV)

Table 2.58
Equation and Factors for Predicting Peak Radial Part 1b
Velocity in a Pipe (in) Inland Stress Wave

$$v = \frac{1}{2} \left(\frac{E}{\rho} \right)^{1/2}$$

Range, 10^{12}	$\frac{1}{2}$	$\frac{1}{2}$
100-500	0.5	1.5×10^{-1} CM
1,000-5,000	1.0	1.5×10^{-1} CM

Medium	$\frac{1}{2}$
Salt	1.0
Tuff	1.0
Granite	1.0
Alluvium	1.0-50

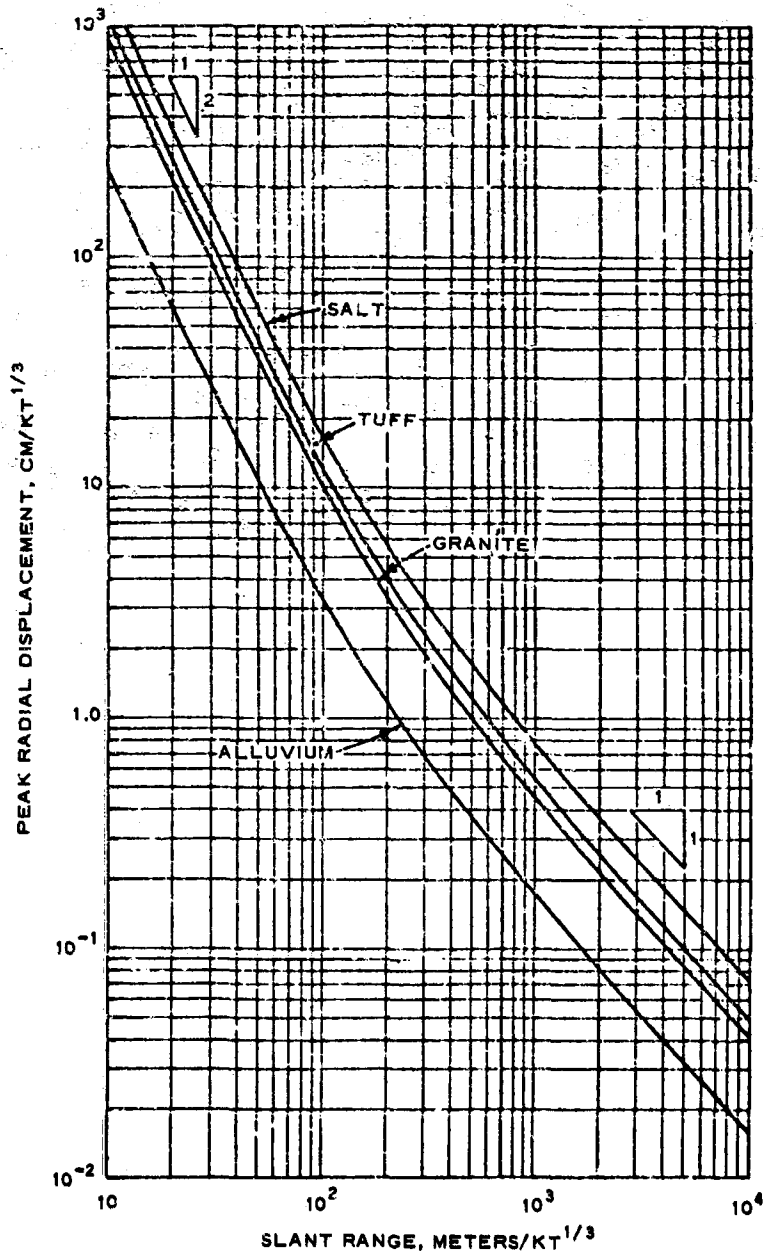


Fig. 2.59 Chart for prediction of peak radial displacement (from NUCLEAR GEOPLOSICS, Part IV)

Newmark and Haultiwanger (1962) give the following equations for predicting direct-induced ground motions:

$$a_r = 0.36 g \left(\frac{W}{1 \text{ Mt}} \right)^{5/6} \left(\frac{1000 \text{ ft}}{R} \right)^{3.5} \left(\frac{C_D}{1000 \text{ fps}} \right)^2 \quad (2.16)$$

$$v_r = 0.95 \text{ fps} \left(\frac{W}{1 \text{ Mt}} \right)^{5/6} \left(\frac{1000 \text{ ft}}{R} \right)^{2.5} \left(\frac{C_D}{1000 \text{ fps}} \right) \quad (2.17)$$

$$d_r = 3.8 \text{ in.} \left(\frac{W}{1 \text{ Mt}} \right)^{5/6} \left(\frac{1000}{R} \right)^{1.5} \quad (2.18)$$

where

a_r = peak radial acceleration, g's

W = weapon yield, Mt

R = radius to point, ft

C_D = seismic dilatational velocity, fps

v_r = peak radial particle velocity, fps

d_r = peak radial displacement, in.

These equations contain a numerical factor, the seismic velocity, which accounts for the type of soil or rock. The trends which result from varying this factor are similar but not identical to those indicated by Sauer's factors. Note that the motions are smallest in the more compressible materials; i.e. the greater attenuation more than offsets the greater compressibility. The use of seismic velocity does not imply that the soil or rock is elastic under the large stresses involved in such waves. However, at the time of this writing, use of seismic velocity plus the numerical coefficients in the equations provides the best method for accounting for the combined elastic and plastic action of various soils.

Theoretically, directly induced waves should not cause tangential motions. In actuality, such motions occur because of the heterogeneous nature of actual earth.

No simple, proven prediction methods are available for radial stress, primarily because there have been essentially no satisfactory measurements of actual stresses. Peak radial stress may be estimated as $\rho C_D v_r$, where ρ is the mass density.

As an example of the prediction techniques, let us estimate the motions at a depth of 1200 ft below a 20-Mt surface burst in a rock with a seismic velocity of 10,000 fps. Referring to section 2.2, we see that this depth is somewhat over twice the depth of the apparent crater. The mass density may be taken as 4.7 slugs/ft³. The predicted peak radial motions and stresses are:

$$a_r = 0.36(20)^{5/6}(0.83)^{3.5}(10)^2 = 2300 \text{ g's}$$

$$v_r = 0.95(12.2)(0.635)(10) = 73.5 \text{ fps}$$

$$d_r = 3.8(12.2)(0.76) = 35 \text{ in.}$$

$$\text{Radial stress} = (4.7)(10,000)(73.5) = 3,500,000 \text{ psf}$$

$$\text{Radial strain} = 73.5/10,000 = 0.7\%$$

If the seismic velocity were 2000 fps, the acceleration, particle velocity, and stress would be reduced, while the displacement and strain would remain unchanged.

2.6.3 Requirements for Data Regarding Soil. As with all of the other aspects of nuclear weapons effects which have already been discussed, there is need for mathematical models for stress-strain behavior and for ranges of values of the parameters involved in these models. These models and parameters should first be used in calculations aimed at elucidating the general features of directly induced stress waves, and then, after verification by field experience, they may become useful for actual predictions. Shear strength is of particular importance for study of this type of stress wave, in addition, of course, to compressibility. Shear failure during passage of the wave may well account for most of the apparent damping at close-in points. At greater distance, it will be necessary to consider hysteretic damping.

The one type of data which is useful for the simple prediction techniques is the dilatational seismic wave velocity.

2.7 SOIL-STRUCTURE INTERACTION WITH DIRECTLY INDUCED STRESS WAVES

As the numerical example in section 2.6 shows, any structure which is to survive and function near a crater must withstand a very severe

environment. Fig. 2.60 shows a suggested design concept for such structures. The soft backpacking, which might be a plastic foam or foamed, lightweight concrete, reduces the acceleration, particle velocity, and stress reaching the structure and absorbs any relative displacement between the earth and the structure.* The earth around the cavity containing the structure must be able to sustain the

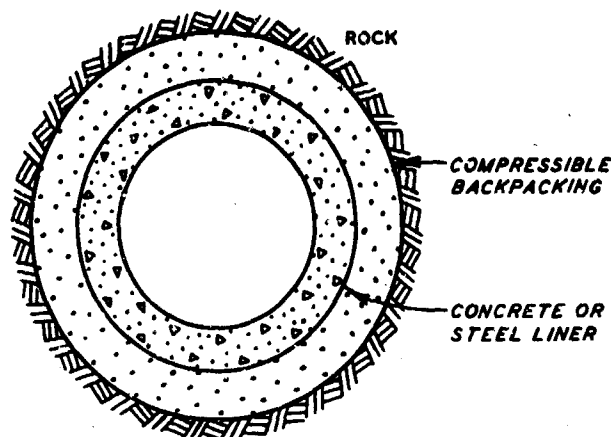


Fig. 2.60 Structural concept for regions of extremely large stress

large free-field stresses without crushing the cavity. Hence structures must be located in rock, and the major problems are ones of rock mechanics rather than soil mechanics. The concentration of stress at the boundary of the cavity and the compressive strength of the rock become crucial factors. The backpacking also serves to absorb the kinetic energy of pieces of rock which spall or are squeezed from the cavity wall.

The degree of stress concentration at the cavity walls has been investigated extensively (Baron et al., 1960; Baron and Parnes, 1961). Fortunately, the stress concentration during passage of a stress wave is only about 10% greater than the stress concentration in a static stress field.

2.8 SUMMARY OF SOIL DATA REQUIREMENTS

As has repeatedly been suggested in this chapter, requirements for soil data in connection with weapons effects studies and protective construction design should be divided into two categories.

On the one hand, models for stress-strain behavior and numerical values for the pertinent parameters of these models are required for theoretical analyses which study the effects of boundary conditions and soil

* Large attenuation will occur provided practical means are employed to keep soft backpacking material from becoming saturated with groundwater after installation.

properties upon the magnitude and time history of free-field ground motion and structural response. Because of uncertainties regarding the assumptions and soil properties, the results of any single theoretical analysis should not, at least at the present, be relied upon for design purposes. Rather, there should always be a series of computer runs using input which brackets the range of uncertainty regarding the assumptions and soil properties. Reasonable stress-strain models are discussed in section 2.8.1. Evaluation of parameters for use in design studies should be attempted only by experienced soil engineers working in close collaboration with the developers of the computer codes.

On the other hand, specific values of certain soil parameters are required for the simple rules of analysis which are currently in use and which, with suitable updating and improvement, should continue to be used at least for preliminary analysis and design. Such rules must permit the user to understand clearly the link between assumption and result, so that he can use his judgment and experience in assessing the probable accuracy of the result. The procedures should also be adequately based upon actual field observations, and should represent only a modest extrapolation of that which is already known through experience. Examples of such procedures have been provided in the several sections of this chapter. The requirements concerning specific values of parameters are summarized in section 2.8.2.

Finally, it must be mentioned that the routine soil investigations required for any construction upon or in soil must also be made in connection with protective construction. Such investigations include standard penetration tests and determinations of grain size characteristics, water content, and Atterberg limits. At a minimum, such information is required to permit economical design against the purely static aspects of construction.

2.8.1 Stress-Strain Relations in General Terms.

Behavior in compression: The compression curves in fig. 2.61 represent the writer's ideas of the important general features of the stress-strain behavior in undrained compression. These features are: (a) initially the curve is concave to the strain axis; (b) finally the curve is

concave to the stress axis; (c) one cycle of loading and unloading leads to a residual strain and is accompanied by an energy loss; (d) subsequent cycles of loading and unloading produce similar curves, although the additional residual strain and energy loss associated with each cycle gradually decrease with successive cycles; and (e) after many cycles of loading and unloading, an essentially stable hysteresis loop is developed.

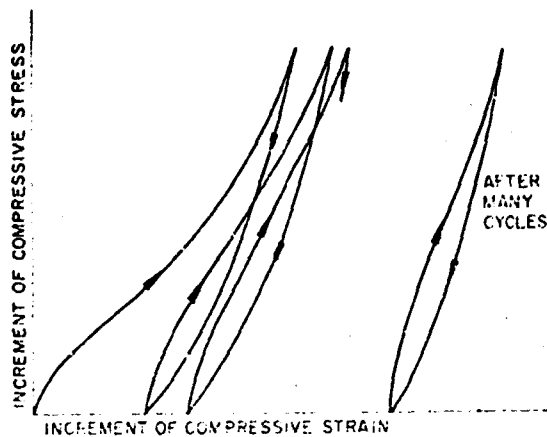


Fig. 2.61 Typical stress-strain curves in hydrostatic or confined compression

These concepts concerning compression behavior have come primarily from one-dimensional compression tests but are equally applicable to a state of hydrostatic compression. Even when no shear stresses are present, soil will generally be anisotropic; that is, application of hydrostatic stress will not cause equal strains in all directions. The presence of initial shear stresses will lead to additional anisotropic behavior. The possible importance of this anisotropic behavior in stress analysis problems has received little study. Although there is little quantitative data on the possible and probable amounts of anisotropy, this effect should be included in some analyses for comparative purposes. For most theoretical analyses, at the present time at least, it should suffice to assume that soil is isotropic in pure compression. If isotropy is assumed, the curves in fig. 2.61 relate any normal stress change to the corresponding linear strain change or the average normal stress change to the volume change.

Behavior in shear: The two diagrams in fig. 2.62 show the essential general features of the undrained response of soil to the application of shear stresses.

The essential features of the behavior in shear are: (a) the curves for loading are concave to the strain axis almost from the very beginning of loading; (b) there is a limit beyond which the shear stress cannot increase; (c) the limiting shear stress is reached at a strain much larger

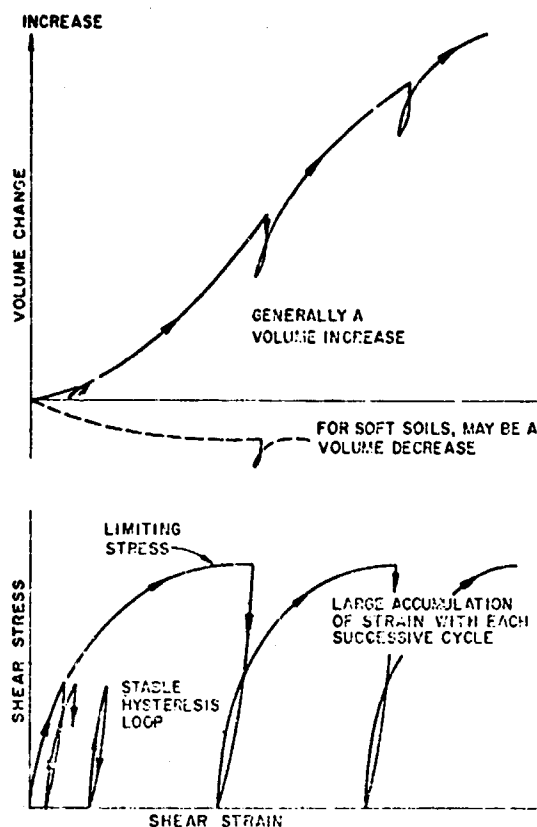


Fig. 2.62 Typical stress-strain and volume change curves in shear

than the strain obtained by projecting the initial tangent up to the level of the limiting shear stress; (d) a change in volume, generally a volume increase, occurs as the shear stress is increased; (e) one cycle of loading and unloading leads to a residual strain and is accompanied by an energy loss; (f) subsequent cycles of loading and unloading produce similar curves, but the additional residual strain and energy loss associated with each cycle decrease during the first several cycles following the first cycle; (g) for shear stress levels less than about one-half of the limiting stress, an essentially stable hysteresis loop is developed after many cycles of loading; (h) for greater

shear stress levels, a considerable residual strain occurs for each cycle of loading, regardless of how many cycles are applied; and (i) the volume of the soil generally increases as shear stresses are increased and decreases as shear stresses are decreased.

The foregoing concepts concerning shear behavior have come mainly from triaxial compression tests involving a change in average normal stress as well as a change in shear stress. However, these concepts are applicable to a stress state involving change only in the shear stress.

The proper way to formulate the stress-strain behavior of soil for three-dimensional shear is not at all clear. In the first place, there is no general agreement on whether the state of limiting shear is controlled by a Mises, Tresca, or some other failure criterion. If the magnitude of the shear stress in the x-y plane affects the maximum shear stress that can be applied in the y-z plane, it is reasonable to expect that the shear

strain in the y-z plane prior to failure will be influenced by the shear stress present in the x-y plane. However, there appears to be almost no information which can be used to formulate an appropriate stress-strain rule for three dimensions. Fortunately, there are a host of two-dimensional problems that need solving before it really becomes essential to consider three-dimensional effects. While it is essential to formulate problems in three dimensions, it is appropriate at this time to adopt a simple form of stress-strain rule.

Time effects: Since the stress-strain behavior of soil is definitely time-dependent, it is somewhat meaningless to indicate a typical shape for a stress-strain curve. However, the available evidence suggests that time effects are "relatively unimportant" in dynamic problems as long as the rise time and duration of the applied stress are between 5 msec and about 5 sec. To illustrate what is meant by "relatively unimportant," imagine a stress pulse with a duration of 1 sec. The stress-strain curve for soil in response to this stress pulse would be substantially the same whether the rise time to peak stress is 5 or 20 msec.

There is evidence to indicate that time effects become very important when the duration of the stress pulse drops to about 1 msec or less. It is also true that stress-strain curves will often be quantitatively quite different for 5-msec rise times than those for 5-min rise times. In some problems time effects can be ignored, but in others they must be considered. The possible importance of time effects needs more study for specific situations.

Need for simplification: The stress-strain patterns in figs. 2.61 and 2.62 are enormously complicated. The problem becomes even worse when one attempts to express the curves in quantitative form, since for example the magnitude of the tangent shear modulus depends upon the magnitude of the average normal stress. Simplifications of these relations are necessary for any theoretical calculation. The type of simplification that is acceptable depends upon the particular problem at hand. Possible simplifications are discussed in the following sections.

This discussion will for convenience be divided into three rather arbitrary subsections: (a) simple dynamic problems in which wave

propagation effects are neglected; (b) wave propagation problems involving consideration of stresses, particle displacements, and particle velocities; and (c) wave propagation problems involving consideration of particle accelerations.

Simple dynamic problems: A problem falls into this category when the mass of the soil is considered to be concentrated at a point rather than to be distributed. Foundation vibration problems are often treated this way, although it is now known that it is important to consider wave propagation effects in analyses of such problems. Examples of problems which may profitably be studied as simple dynamic problems are: (a) magnitude of punching motion by a footing during transient loading; and (b) magnitude of slope movement during transient or repeated loading. The key question involved in these examples is: how far can the soil move as the result of plastic deformation during a limited interval of time? Generally, it suffices to know whether this motion is very small or very large.

For such problems, it is generally appropriate to consider the soil as being rigid in compression and rigid-plastic in shear. If the problem involves a saturated clay or a loose saturated sand, the yield shear stress will be a fixed quantity. For dense sands and for all partly saturated or dry soils, it will be necessary to allow the yield stress to vary with time as the normal stress varies. The relation between normal stress and shear stress can be represented by

$$\tau_{\max} = c + \sigma \tan \phi$$

where c and ϕ are evaluated for undrained shear conditions. Volume changes caused by shear can with reason be neglected in such relatively crude analyses.

In some problems, it may be necessary to consider the strains which occur before peak shear resistance is developed. Such problems arise when the allowable limit on motions is rather small, and when the stress-strain curve for shear shows a pronounced peak. In these special cases, it will generally be necessary to preserve the essential features of the stress-strain curves, as indicated in fig. 2.63. However, it is likely that wave

propagation effects will also be important in such problems.

Although the ultimate shear resistance of a soil is certainly dependent upon strain rate, it is doubtful that it is important to consider the rate effect when analyzing simple dynamic problems. A yield strength (or stress-strain curve) appropriate for the typical rate of shearing involved in the problem should be selected, but otherwise the time effects may be ignored.

Wave propagation; stresses, displacements, and velocities: This section considers a group of problems for which it is not essential to describe the change of the wave front with distance; i.e., where emphasis is upon attenuation of peak stresses, lengthening of the duration of the stress pulse, etc. In such problems it

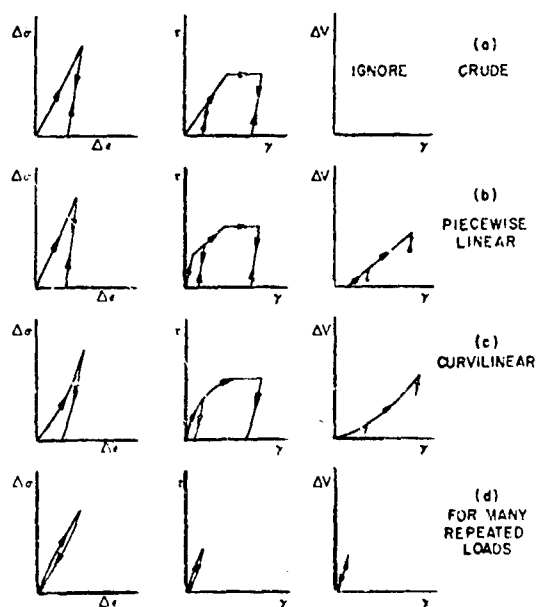


Fig. 2.64 Simplified stress-strain relations for wave propagation problems involving stresses, displacements, and velocities

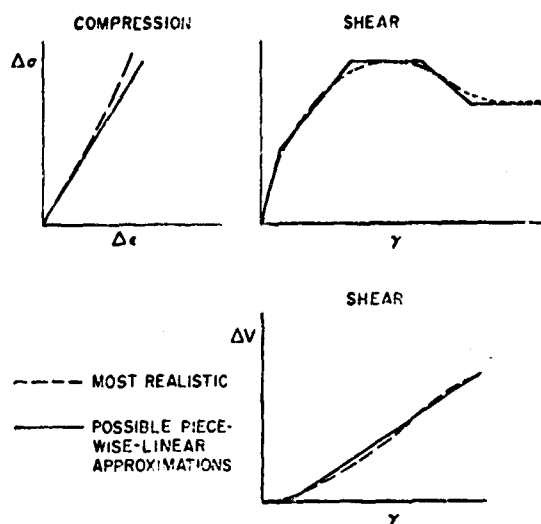


Fig. 2.63 Stress-strain relations for dynamic stability problems

is essential to consider the energy loss which occurs during a cycle of loading and unloading.

For many dynamic problems, this energy loss can best be taken into account by using time-independent, irreversible stress-strain curves (see fig. 2.64). If the loading involves a significant component having a period of less than a millisecond, it may well be necessary to include time-dependency.

As usual, the complexity of the stress-strain curve will depend upon the level of sophistication involved in the problem. The various parts of

fig. 2.64 illustrate the evolution of increasingly complex relations. The simple relations shown in part (a) may be useful for first analyses, but the degree of complexity illustrated in part (b) will probably be necessary wherever large shearing stresses are possible. If the loading is repeated many times (as in foundation vibration problems), a stable hysteresis loop must be used (see part (d)).

Wave propagation; accelerations: Change of peak particle acceleration with distance is determined largely by changes in the form and sharpness of

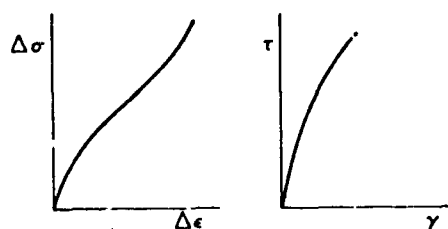


Fig. 2.65 Stress-strain relations for wave propagation problems involving development of wave front

the wave front. Not much is really known concerning the factors which influence the evolution of the wave front, but certainly the exact form of the stress-strain curve is important. Fig. 2.65 illustrates the stress-strain features that need to be considered. The initial downward concavity of the stress-strain curve in compression is important with regard to the question as to

whether true shock waves occur in soil. If time-dependent effects are thought to be important, a nonlinear stress-strain relation should be used for the "spring" portion of any rheological model.

2.8.2 Specific Values of Certain Soil Parameters. The single most important soil parameter controlling protective construction design is dynamic compressibility, i.e., the ratio of strain to stress during confined compression. Compressibility determines the magnitude of the ground motions at a given distance from the explosion, and its magnitude in relation to structural flexibility determines the degree of arching around a structure and whether this arching is beneficial or unfavorable. Procedures for evaluation of dynamic compressibility are presented in Chapter 4.

The next most important parameter is dynamic shear strength. Shear strength is used to evaluate the arching which can occur over very flexible buried structures, box structures with flexible, ductile roofs, and structures supported on footings. Dynamic shear strength is also invaluable in the evaluation of footing behavior at a given site, although this evaluation should be based primarily upon load bearing tests made at the site.

Procedures for evaluation of dynamic shear strength are presented in Chapter 3.

The seismic dilatational wave velocity C_D appears in many of the simple prediction procedures presented in this chapter. This is primarily because C_D is the easiest to measure of all soil parameters. Moreover, for some materials (including some earth materials), C_D is a useful measure of dynamic compressibility which, as noted above, is really the key parameter. Hence it becomes very important to understand the relation between wave velocity and stress-strain behavior. This relation is discussed in Chapter 5.

CHAPTER 3 SHEAR STRENGTH DURING RAPID LOADINGS

3.1 INTRODUCTION

This chapter deals with the strength of soils during a single rapid loading. Techniques used to measure this strength are described, and relations are presented which may be used to estimate the strength available during a rapid loading from the strength at ordinary rates of loading.

3.1.1 Definitions. There are two general types of tests which are used in the laboratory to study the strength characteristics of soils: tests with controlled strain and tests with controlled stress.

Tests with controlled strain:

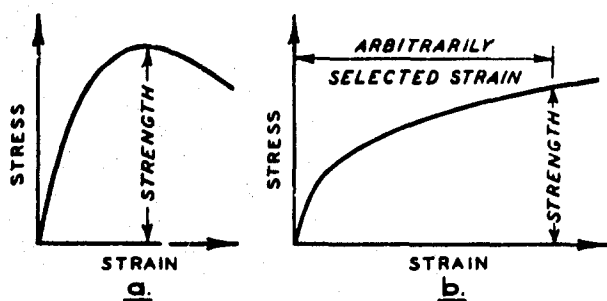


Fig. 3.1 Stress-strain curves from controlled-strain tests

In this type of test, a specimen is subjected to a preestablished pattern of deformation. For example, a cylindrical specimen may be compressed axially with a preestablished rate of axial strain. This strain causes resisting stresses to develop, and by measuring these stresses a stress-strain curve, such

as those shown in fig. 3.1, can be determined.

The peak ordinate of such a stress-strain curve is usually defined as the strength of the specimen. If the curve has no peak but continues to rise slowly as the strain increases (fig. 3.1b), the stress at some arbitrarily selected strain, such as 20% strain, is taken as a measure of the strength.

By running tests using several rates of axial deformation, the effect of strain rate on strength can be established. Fig. 3.2 shows values of strength measured at several different rates of strain. The phrase strain-rate effect is used either in a quantitative or in a qualitative sense. Qualitatively, the phrase denotes any tendency for the strength of a soil to change as the strain rate changes. By relating the strength at one strain rate to the strength at some other strain rate, strain-rate effect can be expressed quantitatively.

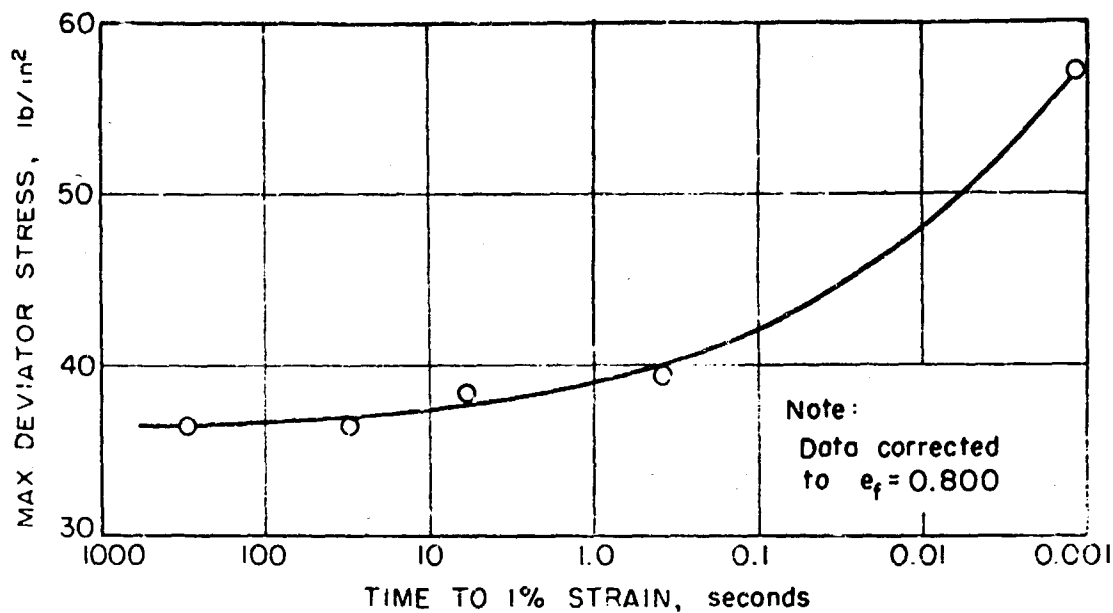


Fig. 3.2 Strain-rate effect for saturated, normally consolidated fat clay

Tests with controlled stress: In this type of test, a specimen is subjected to a preestablished time history of stress. For example, a cylindrical specimen may be stressed axially with the stress-time patterns shown in figs. 3.3a and 3.3b.* This stress causes strains to develop as a function of time. The figures show two typical resulting strain-time patterns. It is also possible to plot the stress at any time versus the resultant strain at that time, so as to give a form of stress-strain curve (see fig. 3.3c). Another way to form a stress-strain relation is to plot the peak stress applied during a particular test versus the peak strain occurring in that test, as in fig. 3.3d. This latter form of plot leads to the definition of strength shown in the plot.

The value of strength obtained in this way, of course, applies only for the particular stress-time history used for the tests. More typically,

* The results shown in this figure are hypothetical and are based on the behavior observed during plate bearing tests using pulse loadings. The U. S. Navy Civil Engineering Laboratory has conducted a few triaxial tests on sand using controlled stress loadings, and found that specimens either failed immediately or did not fail at all, depending upon the ratio of the peak applied stress to the static strength.

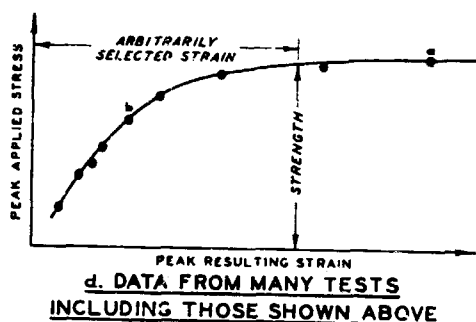
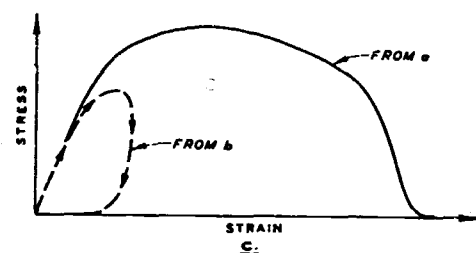
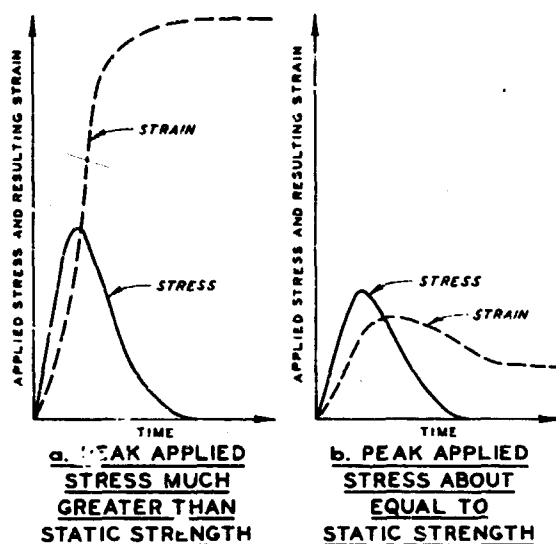


Fig. 3.3 Results from controlled-stress tests with pulse loading

we wish to know how strength will vary with the duration of the load. One convenient way to establish this relation is to use a step loading in which the applied stress is rapidly increased to a prestablished value and then held at this value until either the specimen fails or until it is apparent that the specimen is not going to fail. Fig. 3.4 gives the typical results obtained from a series of experiments of this type.

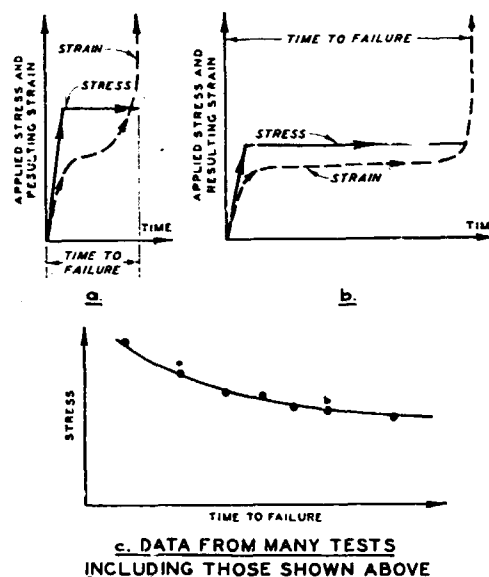


Fig. 3.4 Results from controlled-stress tests with step loading

The time interval from the onset of loading until the specimen collapses is called the time to failure. If a collapse does occur under a given applied stress, this stress becomes the strength for the observed time to failure.

Using controlled-stress tests to establish a strength-time relation

* While the results shown in fig. 3.4 are hypothetical, this type of result has been obtained when studying time effects during tests lasting many days; for example, see Casagrande and Wilson (1951).

is a rather uncertain procedure. If the applied load is too small, no failure results. If the applied load is too large, failure develops so quickly that the results have little meaning. Generally, many tests are necessary in order to define the desired relation.

Relation between results from controlled-strain and controlled-stress tests: The quantity time to failure is the basis for relating the results

from the two types of tests, although this relation can only be approximate. For the controlled-strain test, time to failure is taken as the time interval from the onset of loading until the peak resistance is reached. This time to failure will be related to the

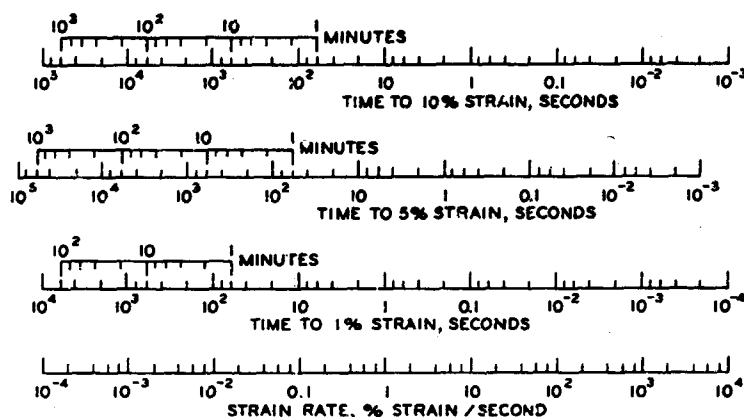


Fig. 3.5 Relation between strain rate and time to failure

rate of strain and to the strain required to reach peak resistance, as indicated by the nomograph in fig. 3.5.

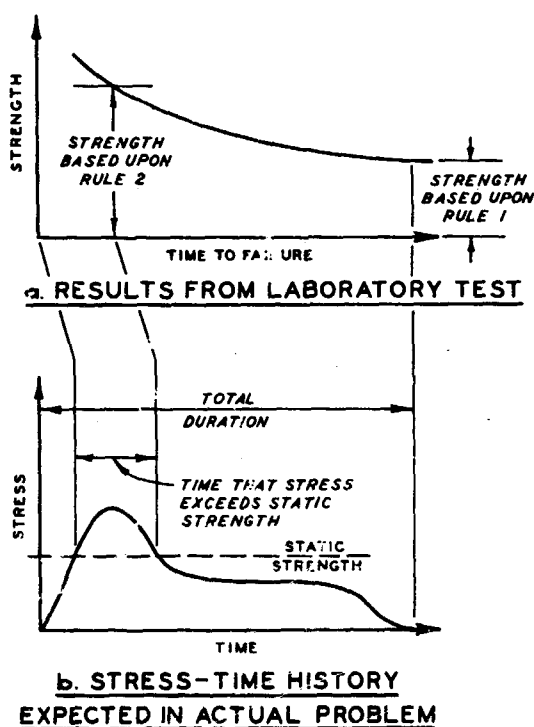
Relation between laboratory tests and behavior in situ: In most practical problems, the mass of soil as a whole is subjected to a controlled-stress type of loading. However, the conditions at any particular point within the mass are neither truly controlled stress nor controlled strain. Rather, the stress-time and strain-time patterns at each point are influenced by the stress-strain behavior at that point and at all surrounding points.

There are two general ways in which data regarding the strain-rate effect upon strength can be used in practical problems.

In some problems, it may be possible to perform an accurate analysis of the response of a soil mass to a given applied loading; i.e. to solve a two- or three-dimensional boundary value problem taking into account the actual stress-strain-time properties of the soil. In such cases, it is desirable to have strength expressed in terms of the strain rate.

In most problems, it will be more appropriate to perform an approximate analysis in which strength is mathematically treated as being independent of time, but the strength is assigned a value appropriate for the duration of the loads being applied. There is no fixed rule for relating the expected duration of the actual loading to the time to failure in a laboratory test. The most conservative rule (Rule 1) would be to use the strength achieved in a laboratory test having a time to failure equal to the total duration of the stresses in the actual problem. This rule will always underestimate the strength actually available. A more appropriate (but still conservative) rule would be: use the strength achieved in a laboratory test having a time to failure equal to the interval of time that the stresses in the actual problem will exceed the ordinary static strength

(Rule 2). These rules are illustrated in fig. 3.6.



On the basis of these considerations, there is little reason to argue that either a controlled-stress or a controlled-strain test is fundamentally superior. The choice between them can be made solely on the basis of convenience. Usually it is more convenient to use controlled-strain tests, since fewer tests will be necessary to define the strain-rate effect relation.

3.1.2 Single Versus Repeated Loadings. The strength during a single rapid loading, such as generally occurs in nuclear weapons effects problems, must be distinguished from the strength available during a suc-

cession of rapid loadings such as those which occur during earthquakes. The problem of strength during repeated loadings has been discussed in detail by Seed and Chan (1966) and by Seed and Lee (1965). The strength

available during repeated dynamic loadings may in some cases be less than the ordinary static strength. However, the strength during any cycle of a repeated loading will be greater if the loading is applied rapidly than if it is applied slowly, provided that the same conditions exist at the beginning of the cycle and if the same drainage conditions exist during the cycle.

3.2 FACTORS AFFECTING THE RELATION BETWEEN STRENGTH AND RATE OF LOADING

The Mohr-Coulomb hypothesis regarding the strength of soils, as modified by Terzaghi to include the effects of pore pressure, can be stated as:

$$s = \bar{c} + (\sigma - u) \tan \bar{\phi} \quad (3.1)$$

where s is the maximum shear stress possible on a plane (shear strength), \bar{c} is the cohesion intercept, σ is the total stress normal to the plane, u is the pore pressure, and $\bar{\phi}$ is the friction angle. The pore pressure u is the sum of any initial pore pressure u_i plus any excess pore pressure Δu generated during the shear process. In turn, Δu can be expressed as Δu_{cw} , the excess pore pressure developed during shear at constant water content, minus Δu_{dis} , the excess pore water pressure dissipated by consolidation which takes place during the loading. Thus Equation 3.1 can be rewritten as:

$$s = \bar{c} + (\sigma - u_i - \Delta u_{cw} + \Delta u_{dis}) \tan \bar{\phi}$$

Although the Mohr-Coulomb equation represents a great simplification of the actual strength behavior of soils, and though there can be many arguments as to just how \bar{c} and $\bar{\phi}$ should be measured and defined, this equation serves well as a basis for discussing the role of rate of loading in the several factors which determine shear strength. These factors are listed in fig. 3.7.

3.2.1 Intrinsic Properties of Soil. In this category are those properties of soil which are independent of the overall size of the soil mass or of the boundary conditions imposed upon the mass. The strength

TIME-DEPENDENT NATURE OF INTRINSIC PROPERTIES OF SOIL

$\bar{c}, \bar{\phi}$: THE STRENGTH PARAMETERS IN TERMS OF EFFECTIVE STRESS

Δu_{cw} : THE EXCESS PORE PRESSURE GENERATED DURING SHEAR AT CONSTANT WATER CONTENT

OVERALL ACTION OF MASS OF SOIL

INERTIA: MAY AFFECT THE TOTAL STRESS σ ACTING AT A POINT

CONSOLIDATION: WILL AFFECT THE EXCESS PORE PRESSURE Δu_{dis} DISSIPATED BY THE TIME OF MAXIMUM LOADING

Fig. 3.7 Factors affecting relation between strength and rate of loading

parameters \bar{c} and $\bar{\phi}$, and the excess pore pressure generated during shear at constant water content Δu_{cw} , fall in this category. Any tendencies for these factors to be functions of the rate of loading will cause shear strength to be a function of the rate of loading.

3.2.2 Overall Action of Mass of Soil. The normal stress σ acting upon a plane through a point within a soil mass, the initial pore water pressure u_i at the point, and the excess pore water pressure dissipated from the point during loading Δu_{dis} are all influenced by the dimensions and shape of the soil mass and by the way in which the soil mass is loaded. The initial pore pressure u_i does not enter into our discussion of the effect of loading rate upon strength. However, both σ and Δu_{dis} will in general change as the rate at which loads are applied to the soil mass changes, and these changes will affect the shear strength available at a given point within the mass.

Inertial effects: The behavior during a direct shear test can be

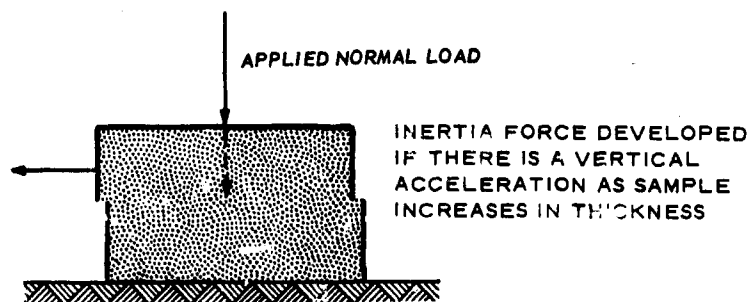
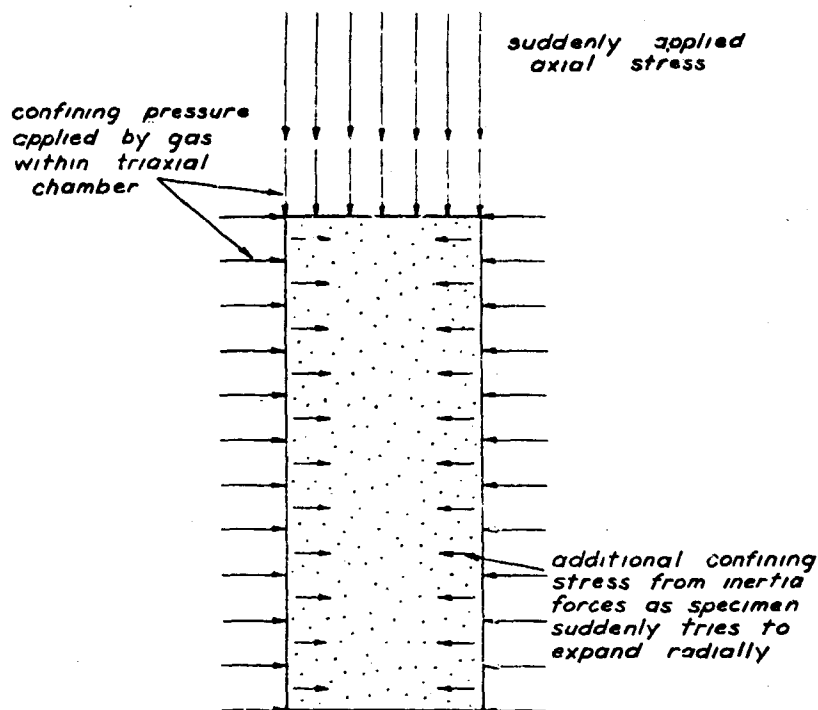


Fig. 3.8 Effect of inertia during direct shear test

used to illustrate how the normal stress σ acting at a point can be influenced by the rate of loading (see fig. 3.8). If vertical movement occurs due to soil expansion during shear, inertia

forces are generated within the specimen during a rapid loading, and the normal stress σ acting upon the failure plane may not be equal to the applied normal stress. Any change in σ with loading rate of course leads to change in strength. This effect has been neatly demonstrated by the special direct shear tests described by Schimming, Haas, and Saxe (1966). These inertia forces, whose magnitude cannot be estimated accurately, complicate the interpretation of the results of a strength test. The same effect can develop during a triaxial test (see fig. 3.9).



Consolidation:

The importance of

Fig. 3.9 Lateral inertia during triaxial test

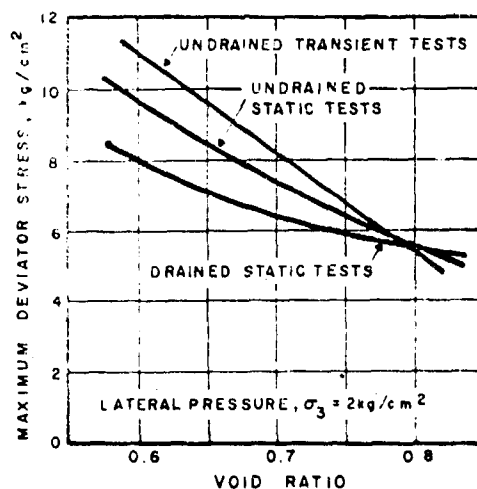


Fig. 3.10 Effect of drainage on strength of saturated sand (from Seed and Lundgren, 1954)

the hydrodynamic time lag with regard to the pore pressures existing at the end of a loading, and consequently the strength available to resist the loading, is well known and has already been discussed in section 1.3. This effect can readily be demonstrated in laboratory tests on saturated sand by performing triaxial tests with drainage permitted (see fig. 3.10). With ordinary testing speeds, full drainage occurs, and the strength is given by the curve marked "drained static."

During very rapid loadings, there is inadequate time for drainage. Excess pore pressures remain during the loading, causing a change in strength (curve marked "undrained transient"). The conditions during the transient loading can be simulated by performing tests slowly with drainage prevented (curve marked "undrained static").

Pore pressure changes can occur even during undrained shear of a dense dry sand. For example, assume that the volume of the void spaces is initially one-third of the total volume of the specimen, that the specimen expands 5% as the result of shear, and that the air in the voids is initially at atmospheric pressure (14.7 psi). Boyle's law (pressure \times volume = constant) may then be applied to find the change in pore pressure as the sand is sheared. The pore pressure is found to decrease to 12.8 psi (absolute pressure). This small change in effective stress is not enough to alter the mineral skeleton's tendency to expand. However, if the minor principal effective stress before shear were only 10 psi, the excess pore pressure would cause this confining pressure to increase by 20% during shear. Thus, the strength in the undrained test would be 20% greater than that in a drained test on the same sand, even if the friction angle remains unchanged.

The same effects show up in clay soils, except that the test must be performed very slowly if there is to be any drainage. There will be little dissipation of excess pore pressures during either rapid tests or tests at ordinary loading speeds in clay.

3.2.3 Relative Importance of Factors. The strength increases which arise from the mass action of the soil are generally more important than the strength increases which arise from the time-dependent nature of the intrinsic properties of the soil, in that they can lead to much greater strength increases. However, the mass action of the soil depends very much upon the size and shape of the soil mass and upon the way in which the mass is loaded. This mass action must be accounted for by a theoretical analysis of each problem: a dynamic analysis to account for inertia forces and a consolidation analysis to account for the hydrodynamic time lag. Hence these factors arising from the mass action of soil are not of concern in this chapter. Here we shall deal only with the effect of strain rate upon

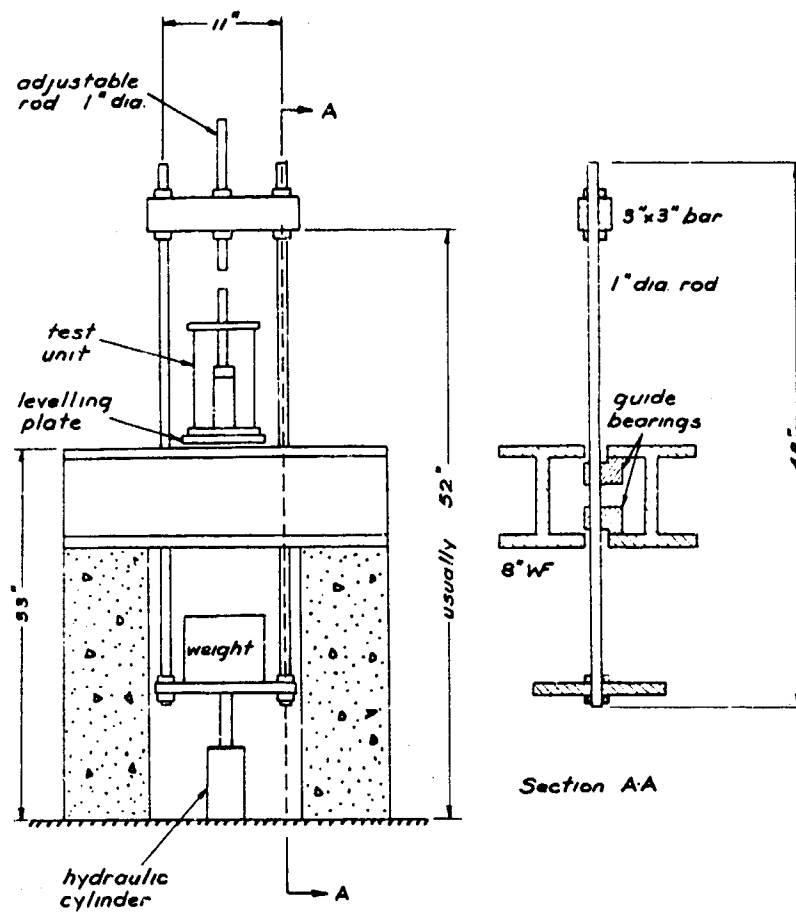
the intrinsic properties. Thus, it was decided to run tests in which inertia effects were not present and to prevent any drainage from occurring at all strain rates.

3.3 TESTING EQUIPMENT AND PROCEDURES

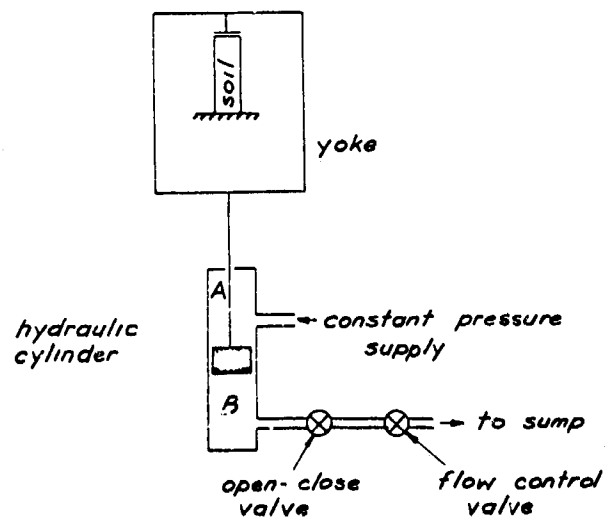
3.3.1 Loading Systems. Fig. 3.11 shows the simple rapid loading system which was developed under the present contract (see Report 2). A hydraulic system controls the movement of the loading yoke, and the basic elements of this system are shown in part b of the figure. The loading yoke is attached at its lower end to the piston rod of a hydraulic cylinder. The chamber of the hydraulic cylinder below the piston head, chamber B of the figure, exhausts through two valves. The first of these valves is a control valve and is either in a shut or open position. The second is a flow control valve designed to provide a fixed rate of fluid flow regardless of the pressure drop across the valve.

Initially the control valve is in the shut position so that the hydraulic fluid is trapped in chamber B, with the loading yoke so positioned that a gap of approximately 1 in. exists between the yoke and the plunger of the test cell. Immediately after the control valve is opened, there is a short period during which the loading yoke accelerates, but the yoke rapidly achieves a terminal velocity determined by the setting of the flow control valve. After the loading yoke has achieved its terminal velocity and has moved through the gap that separates it from the plunger of the test cell, it contacts the plunger and strains the soil sample. If the weight of the loading yoke and the fluid pressure in chamber A are of sufficient magnitude, the yoke will continue to fall at its terminal velocity even though it is doing work in failing the sample. Loading velocities between approximately 0.01 and 20 in. per sec can be achieved with this apparatus. For specimens which are 3.5 in. in length, this means strain rates between approximately 0.01 and 200% strain per sec. If the strain at failure is 5%, this means times to failure of approximately 50 sec to 25 msec.

Various other loading devices have been used to obtain the results described in this chapter. Recently a direct shear device that is a cross



a. Loading yoke and frame



b. Hydraulic control system

Fig. 3.11 MIT apparatus for rapidly loaded triaxial tests

between a controlled-stress and a controlled-strain test has been used at Notre Dame (Schimming, Haas, and Saxe, 1966).

3.3.2 Triaxial Cells. For the majority of the triaxial tests which have been conducted, specimens have been approximately 1.5 in. in diameter and 3 to 4 in. long. For the recent tests at MIT, standard triaxial cells have been modified as shown in fig.

3.12 to permit insertion of a force transducer through the baseplate. Gas was used to provide the chamber pressure, and this pressure remained substantially constant throughout each test although the gas volume within the cell decreased slightly as the plunger was pushed into the cell.

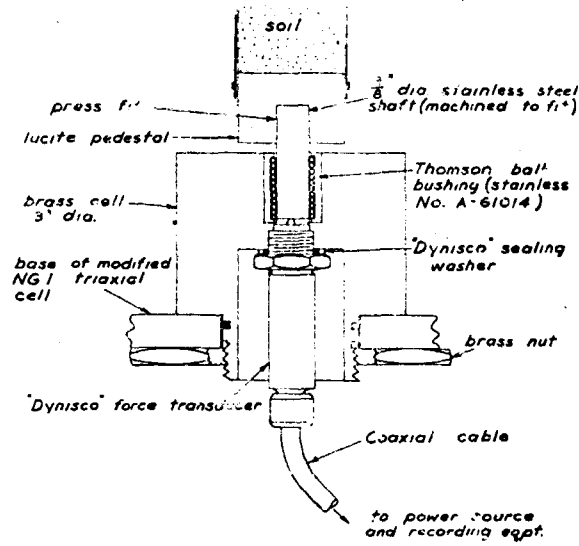


Fig. 3.12 Force transducer for recent tests at MIT

3.3.3 Force Measurement. During rapid loadings, the axial force being applied to the triaxial specimen should be measured by a force transducer located inside the triaxial cell, because the friction between the plunger and its bushing may be significantly large. Fig. 3.12 shows the arrangement used for this purpose during the recent tests at MIT. Since the ball bushing used for this arrangement does not have to seal against leakage, essentially frictionless operation is possible. The force transducer is inserted after any consolidation of the specimen has been completed and just before the shear test is conducted, and hence the transducer need not be tied up during long periods of consolidation. Report 16 provides further details concerning the operation of this force transducer.

3.3.4 Pore Pressure Measurements. Whenever possible, pore pressures have been measured during the tests at MIT so as to learn whether the strain rate affects the strength parameters \bar{c} and $\bar{\phi}$ or the excess pore pressure Δu_{cw} , or both. Early experience indicated that it seldom is satisfactory to measure the pore pressure at the ends of the specimen,

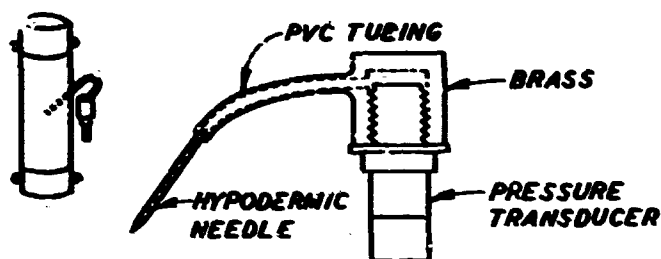


Fig. 3.13 Pore pressure measuring system

since during rapid loadings the excess pore pressures will not be uniform throughout the specimen (see Reports 15 and 16). Consequently, needles inserted into the central portions of specimens were employed, together with electrical pressure transducers of very low compliance. Fig. 3.13 shows the measuring systems finally evolved at MIT (see Reports 15 and 16 for further details).

The response time of a pore pressure measuring system depends upon the permeability and compressibility of the soil as well as upon the compliance (the quantity of water which must flow to the device to make it respond) of the system itself. Measuring systems are sensitive to changes in total stress as well as to changes in pore pressure, and it is quite difficult to know just what one is measuring when the applied loads are changing rapidly. (See Whitman, Richardson, and Healy, 1961, for a discussion of the theory of pore pressure measuring devices.) Moreover, it is difficult to devise a test which can be used to determine the time lag required before a system is really measuring the pore pressure. Report 15 describes the procedures developed at MIT for this purpose. Very rapid response times have been quoted for other measuring systems (for example: Peters, 1963), but it is not certain that these systems have been adequately evaluated.

The following maximum time lags have been achieved with the MIT system:

Coarse sand: 0.1 msec

Fine silty sand: 1 msec

Clayey silt (permeability $\approx 10^{-7}$ cm/sec): 3 sec

3.3.5 Permissible Loading Rates. If specimens are loaded too rapidly, stress and strain will not be uniform along the length of the specimen: rather there will be wave fronts within the specimen. Moreover, a triaxial specimen must expand laterally before it can fail, and during a

very rapid loading, the lateral inertia may severely inhibit development of a failure. The problem of lateral inertia is especially troublesome, since this inertia can make soil behave as though it has time-dependent properties. This problem, and the dangers stemming from a false interpretation of data obtained during very rapid loadings, have been thoroughly discussed in an appendix to Report 9.

As discussed in section 3.2.3, it is desirable to avoid all inertia effects during laboratory tests, by avoiding very short times to failure. Approximate criteria can be developed by considering the time required for compressive waves to pass back and forth along the length of the specimen and for shear waves to pass back and forth across the diameter of the specimen (see Report 9 and NUCLEAR GEOPLOSICS). For tests with specimens about 4 in. long and 1.5 in. in diameter, the time to failure should be 5 msec or greater.

3.4 BEHAVIOR OF DRY SANDS

Numerous rapid loading tests have been made on dry sands: at Harvard (Casagrande and Shannon, 1948), at Notre Dame (Schimming et al., 1966), and at MIT during both the earlier and present contracts. All of these tests have indicated that the strain-rate effect in dry sands is small; that is, that there is less than 10 to 15% increase in friction angle between times to failure of about 5 min and 5 msec. However, even only a 10% increase in friction angle can lead to a very large change in bearing capacity (see Chapter 2). Hence it would be desirable to know the strain-rate effect in dry sands more precisely. Unfortunately, the available test results do not permit a closer answer, owing to the many uncertainties and errors which can creep into the testing of dry sands.

Fig. 3.14 shows the composite average result of testing three sands during the earlier MIT tests. These sands were standard Ottawa

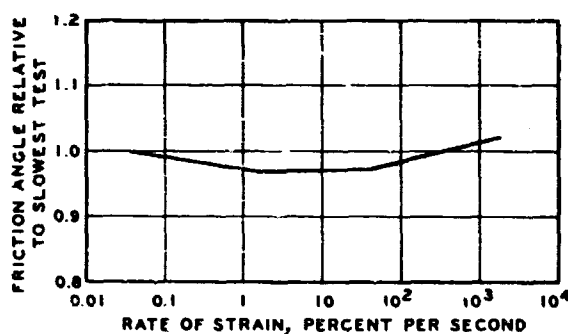


Fig. 3.14 Composite average result for three dry sands; early tests at MIT

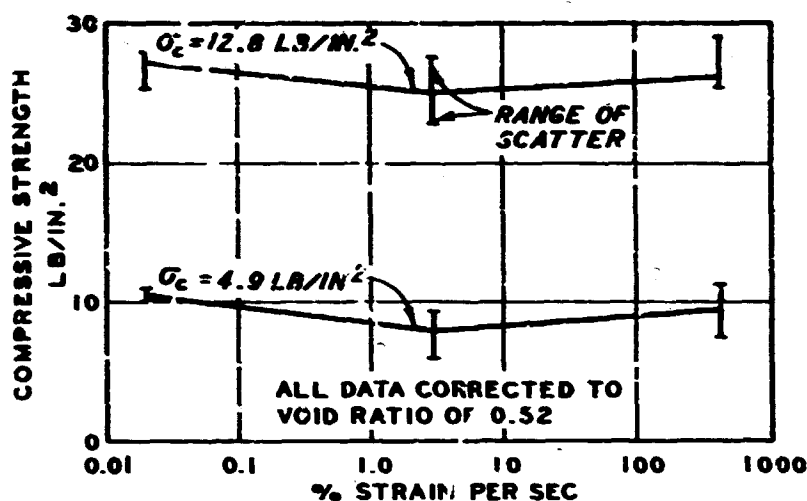


Fig. 3.15 Strain-rate effect for dry Ottawa sand

sand (a uniform sand of medium grain size), a fine well-graded river sand, and desert alluvium from Nevada. Fig. 3.15 gives results obtained under the present contract (Report 3). Both of these sets of results show a similar trend. The friction

angle first decreases as the strain rate increases beyond that required for a time to failure of 5 min. Eventually the trend reverses, and there is a slight increase in strength (and hence friction angle) with increasing strain rate.

There are some reasons for believing that these trends are simply the result of systematic errors, and hence should be ignored. The tests were vacuum triaxial tests in which partial vacuums were used to control stresses. As discussed earlier, unmeasured pore pressure changes could have occurred in the tests, especially those conducted at low confining pressures. These reasons have been discussed in Whitman and Healy (1963). There is also some additional evidence to suggest that the trends may be indeed correct. Barnes (1965) has found that the strength of sand during a slow, steady loading is decreased slightly (4 to 6%) if small vibrations are applied simultaneously (see fig. 3.16). The bearing capacity tests by Vesic et al. (1965) show first a decrease and then an increase with increasing rate of loading. Penetration tests involving steel pellets (Colp, 1965) have shown a decreased resistance as the penetration speed was increased from slow to moderately rapid. Other bearing capacity tests (see Whitman and Luscher, 1965) have shown a large increase in ultimate bearing capacity between slow and very rapid loading rates.

It is possible to suggest hypotheses to explain the trends shown in

figs. 3.14 and 3.15. The decrease of friction angle with increasing strain rate can be explained by the increased tendency for kinetic friction rather than static friction to govern the behavior, as the coefficient of kinetic friction is generally less than the coefficient of static friction. The increase of friction angle at very rapid strain rates can be explained on the basis that interlocking between particles becomes more effective when the particles are not given sufficient time to find the easiest path past one another. Tests by Healy (Report 13) have shown that sands expand more during a rapid shear than during a slow shear, thus confirming the increased importance of interlocking.

However, these hypotheses are still only speculative. Very careful work will be required to learn just how much and just why the friction angle of dry sands is affected by strain rate. Any future tests of this type should attempt to measure or eliminate pore pressure in the air voids.

3.5 BEHAVIOR OF SATURATED SANDS

There can be a strain-rate effect (as much as a factor of 2 or 3) in a

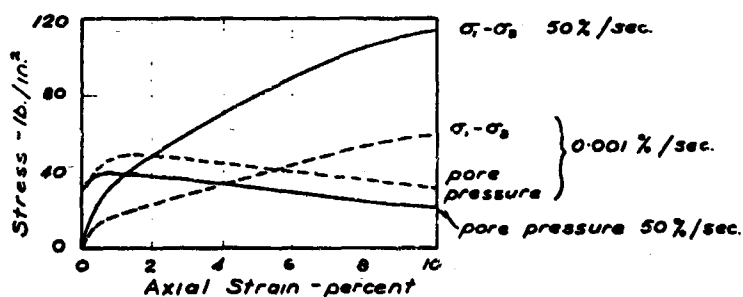


Fig. 3.17 Stress-strain curves for a loose, saturated fine sand

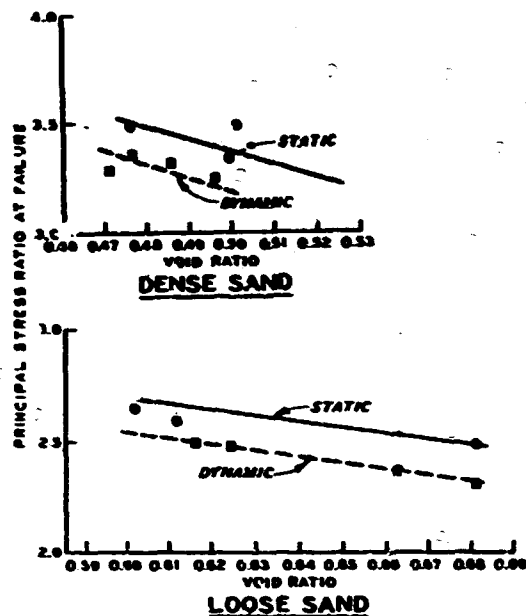


Fig. 3.16 Comparison of strength during slow loading with and without vibrations (from Barnes, 1965)

saturated sand because of differences in the excess pore pressures generated at different strain rates. This is shown in figs. 3.17 and 3.18.

This type of effect develops when a saturated sand is straining at more

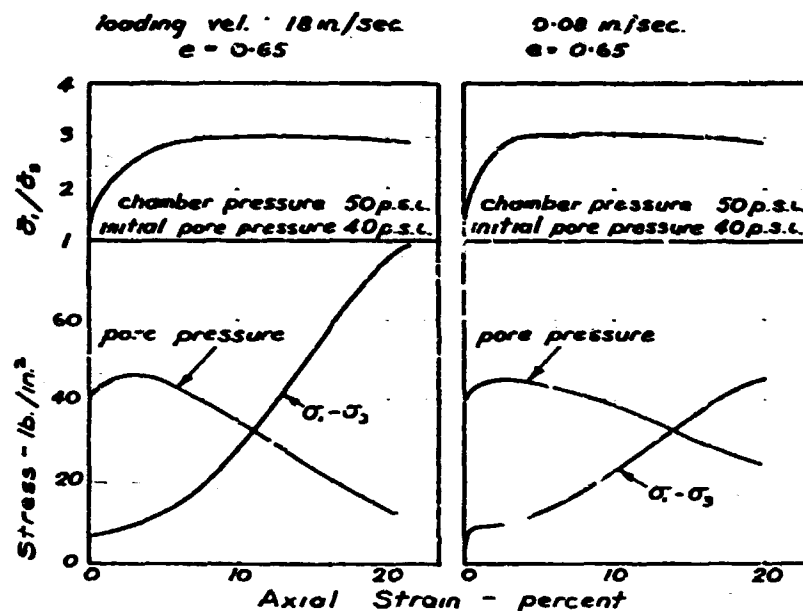


Fig. 3.18 Stress-strain curves for loose, saturated Ottawa sand

or less the critical void ratio for the particular level of effective stress; i.e. at large strains with loose specimens under low to moderate effective stresses (Reports 9 and 11). It seems likely that the same effects will appear at moderate strains when large effective stresses are present.

This effect is caused by the phenomenon noted in section 3.4. With increasing strain rate, the sand has a greater tendency to increase in volume (see Report 13). In order to maintain the constant volume condition involved in undrained shear of a saturated soil, this tendency must be counteracted by an increased effective stress; i.e. by a decreased pore pressure. Any possible changes in the friction angle with strain rate are of small consequence.

Dense specimens under low effective stress will simply cavitate, and so will cease to be sheared at constant volume (fig. 3.19). The effect of strain rate on peak strength is then small, just as in the case of dry sands.

These results have played an important role in the understanding of the effects of strain rate on strength in the case of saturated soils.

However, these results are themselves not very important in practical problems because uncertainty as to the degree of consolidation of sands during rapid loadings will mask the strain-rate effect discussed here.

3.6 BEHAVIOR OF COHESIVE SOILS

Typical results from tests on saturated remolded specimens of a clayey silt have already been shown in fig. 3.2.

Fig. 3.20 gives results from unconfined compression and consolidated

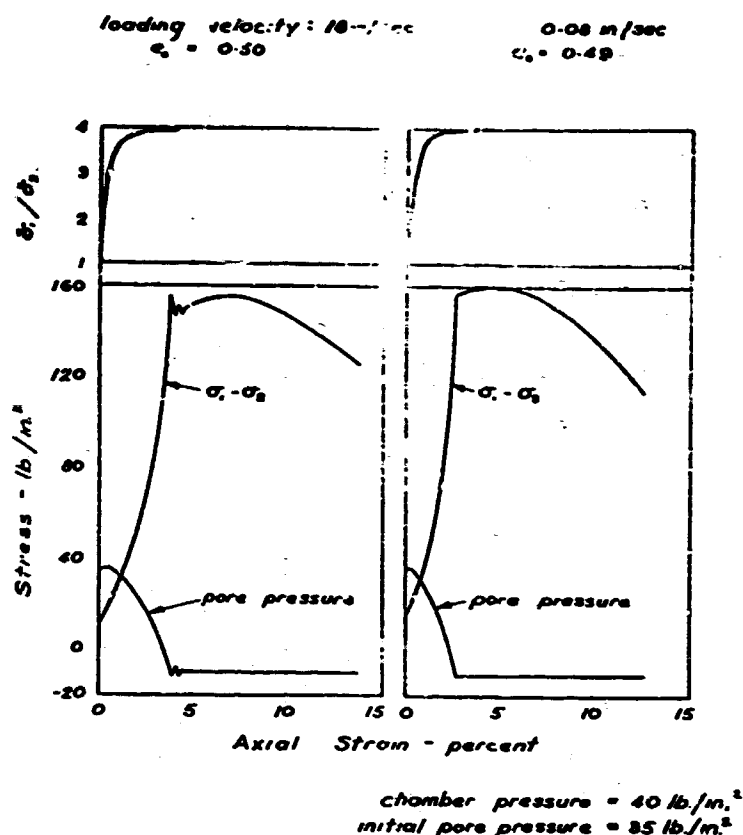


Fig. 3.19 Stress-strain curves for dense, saturated Ottawa sand

BOSTON CLAY PLASTICITY INDEX = 14-28%, PLASTIC LIMIT = 20-24%, WATER CONTENT = 30-41%

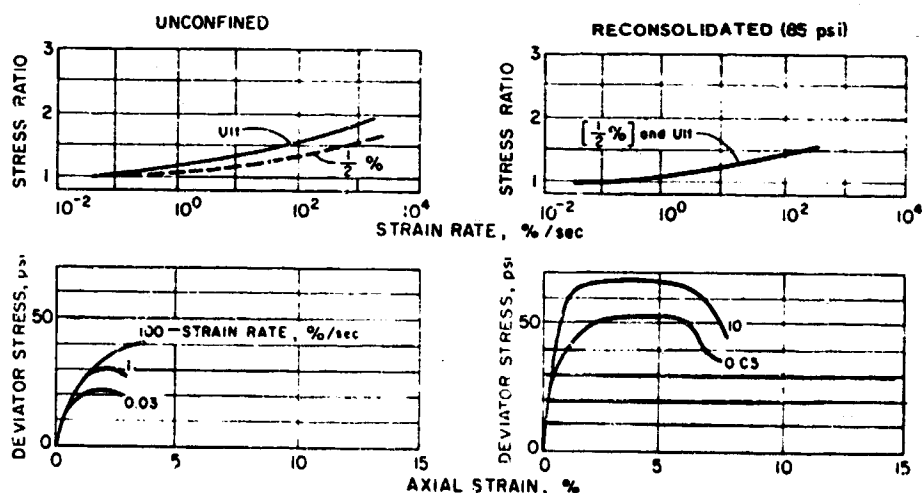


Fig. 3.20 Effect of strain rate on behavior of a saturated clay with and without confining pressure

undrained tests on undisturbed specimens of clay. All available results (except the results from Notre Dame: Schimming et al., 1966) are summarized in table 3.1.

In order that an engineer may intelligently apply these data to his particular problem, or may intelligently select the test conditions which should be employed for laboratory tests upon his particular soil, it would be desirable to understand the causes for the strain-rate effect in cohesive soils and the reasons for the differences between the various cohesive soils. Unfortunately, no complete understanding of these effects exists today.

Pore pressure has played a key role in soil mechanics with regard to the general understanding of shear strength phenomena. Furthermore, measurement of pore pressures permitted an understanding of the strain-rate effect on the strength of saturated sands. Hence, it is natural to inquire into the effect of strain rate upon the pore pressures within cohesive soils. As yet, it has not proved possible to measure satisfactorily the pore pressures induced in clay during very rapid shear. However, there are data for moderate rates of shear, together with some basis for inferring what must happen during more rapid tests.

3.6.1 Situations in Which Pore Pressures Are Positive. In every case where pore pressure measurements have been obtained, the change in excess pore pressure Δu_{cw} with changing strain rate has almost fully accounted for the effect of strain rate upon strength. This result has already been noted for the case of saturated sands, which have permitted measurement of excess pore pressures during very rapid tests. Reports 15 and 16, respectively, give data for a silty clay tested at slow to moderately rapid speeds and for a fat clay at very slow to slow speeds. It seems likely that the same trends will continue to more rapid strain rates.

In general, pore pressures are positive during tests only if these tests are conducted with confining stresses. Fig. 3.20 shows a typical set of results for such a situation. The stress-strain curves from both slow and rapid tests have a broad peak and both are similar in shape. The stress-strain curve for the rapid tests can be obtained simply by multiplying the ordinates of the "slow" stress-strain curve by a constant factor.

Table 3.1

Summary of Transient-Loading Triaxial Tests on Cohesive Soils

Soil	PI %	PL %	w %	Chamber Pressure psi	Static Compressive Strength psi	Strain-Rate Effect*	
						At Low Stress (1/2 to 4%)	At Peak Stress
Medium-soft, slightly sensitive clay, undisturbed	24	26	27	0	10	2.0	4.0
Compacted silty sand	17	11	12	0	25	1.8	2.7
Normally consolidated, sensitive ocean sediment, undisturbed	63	49	92	0	0.3	2.0	2.4
Tough compacted fill	41	21	26	42	35	2.0	2.0
Slightly organic silty clay; undisturbed, saturated	21	22	35	0	22	1.6	1.9
Compacted silty sand	17	11	16	0	35	1.7	1.7
Elastic clay, remolded	27	38	44	0	10	1.7	1.7
Plastic clay, remolded	27	38	48	0	15	1.6	1.8
Plastic clay, remolded, saturated	38	24	30	60	7	1.6	1.8
Stiff dry clay, undisturbed	23	30	20	0	36	1.6	1.6
				30	250	1.4	1.6
					330	1.4	1.4
Slightly organic silty clay; undisturbed, saturated							1.6
Compacted silty clay (also sedimented specimens of same soil)			20	0	30		1.3
			20	15	40		1.2
Compacted plastic clay	38	24	25	0	25		1.4
				15	40		1.5
Compacted clay loam	23	22	21	0	13	1.5	2.5
				30	15	1.5	1.7

* Ratio of resistance at 1000%/sec to resistance at 0.03%/sec.

3.6.2 Situations in Which Pore Pressures Are Negative. Whenever specimens of soil are under small or zero confining stress, as in unconfined compression tests, the soil has strength largely because there are capillary tensions (negative pore water pressures) which in turn cause increased effective stresses. In general, these capillary tensions become increasingly important as the water content decreases, although in very dry soils they cease to be important with regard to strength. As the confining pressure on the specimens of soil increases, the pore pressures become less negative and eventually become zero or positive.

The factors which control the magnitude of the negative pore water pressures within unconfined specimens are poorly understood. This is especially true in partially saturated soils. The negative pressures must be quite sensitive to the way in which the soil particles are arranged and how the particles move relative to one another during shear. In turn, the strength of an unconfined specimen must be rather sensitive to the magnitude of the negative pore pressure which the weakest portion of the soil can sustain.

It seems reasonable to guess that larger capillary tensions can be sustained during a rapid shear than during a slow shear and that these larger capillary tensions can be sustained to larger strains. This supposition has led to the hypothesis that the strain-rate effect upon strength will be greatest when negative pore pressures contribute most importantly to strength. This hypothesis is spelled out in fig. 3.21. The following evidence can be offered in support of this hypothesis.

- (a) Fig. 3.20 gives a typical set of stress-strain curves from a series of unconfined compression tests at different strain rates. Compared with curves from consolidated undrained tests, the stress-strain curves from these tests all have sharper peaks, and the sharper peaks are especially pronounced for the slower unconfined compression tests. As the strain rate increased, the strain at failure in the unconfined compression tests increased. The ratio of stresses in the fast and slow tests was less at low strains, such as 1/2%, than was the ratio of stresses at failure.

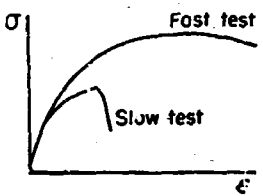
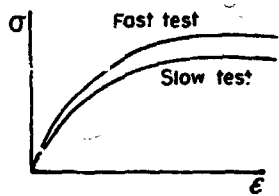
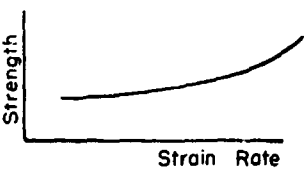
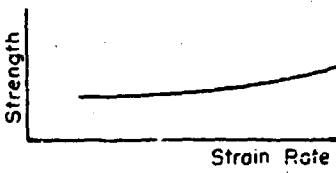
BRITTLE FAILURE	PLASTIC FAILURE
FAILURE BY SPLITTING OR PRONOUNCED FAILURE PLANES	FAILURE BY BULGING
Occurs where there are large negative pore pressures in unconfined compression tests: (1) Soils compacted dry of optimum water content. (2) Stiff saturated soils.	Occurs in triaxial tests with large chamber pressures, or where there are small negative pore pressures in unconfined compression tests: (1) Soils compacted wet of optimum water content. (2) Soft saturated soils.
STRAIN AT FAILURE AFFECTED BY STRAIN RATE 	STRAIN AT FAILURE INDEPENDENT OF STRAIN RATE 
LARGE STRAIN-RATE EFFECT 	MODERATE STRAIN-RATE EFFECT 

Fig. 3.21 Hypothesis for difference in strain-rate effect in different soils

Similar patterns have also been observed with other soils (see table 3.1).

- (b) Fig. 3.22 shows the general nature of the results from tests by Schimming et al. (1966). The strain-rate effect upon strength clearly decreases with increased confining pressure; i.e., with decreased importance of negative pore water pressures.
- (c) Fig. 3.23 shows the magnitude of the strain-rate effect upon apparent cohesion (the strength in the unconfined state) as a function of water content. This effect tends to increase as the

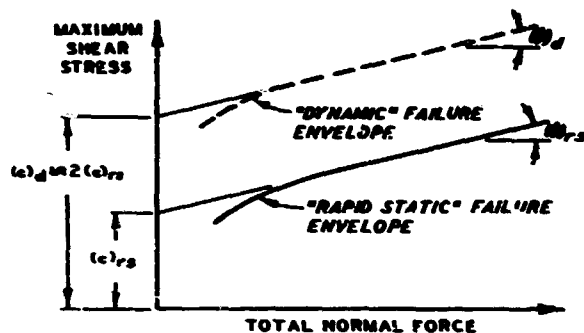


Fig. 3.22 Typical consolidated-undrained failure envelopes for a partially saturated soil (from Schimming, Haas, and Saxe, 1966)

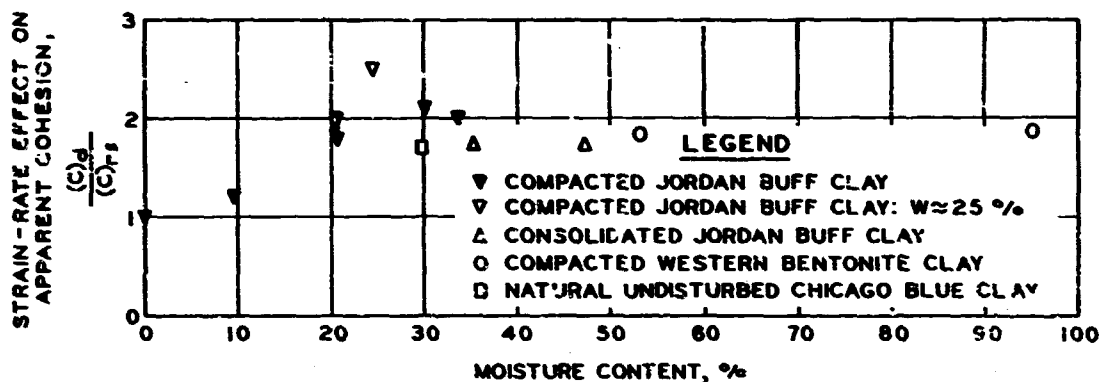


Fig. 3.23 Strain-rate effect upon apparent cohesion (from Schimming, Haas, and Saxe, 1966)

water content decreases, but falls off again for very dry soils in which capillary tensions are relatively unimportant. Thus, again the strain rate is most important when negative pore pressures are most important.

Clearly the hypothesis of fig. 3.21 is still quite speculative, but it does serve to indicate the importance of the test conditions. In particular, soils should be tested under low confining pressure only if they will actually exist under low confining pressure in the actual problem.

3.6.3 Other Effects. It should not be inferred from the foregoing that the author does not believe in the existence of a structural viscosity effect in soils. Indeed, the evidence is clear that such an effect is present for relatively small strains (Report 16; Richardson and Whitman, 1963). Furthermore, the rate-process approach developed by Mitchell (1964) is quite impressive. However, the bonds developed during consolidation tend to be destroyed during the early portion of a shearing process and so

are less important when the peak shearing resistance is being mobilized.

Actually, the author does believe that structural viscosity has some effect upon peak strength at very rapid strain rates, but he further believes that changes in the excess pore pressures are of prime importance. Incidentally, these arguments suggest that time-dependent bonding will have its greatest effect when failure takes place at very small strains, i.e. in sensitive soils. In table 3.1, it can be noted that the largest recorded value of strain-rate effect is for a sensitive natural clay.

The tests at Notre Dame also provide another valuable result: the dynamic strength was found to be the same whether the normal stress was applied in advance of or concurrently with the shear force. This confirms an earlier tentative finding by Seed and McNeill (1957).

3.7 SUMMARY AND RECOMMENDATIONS

3.7.1 Summary. Results. The following working conclusions can be drawn on the basis of present knowledge:

- (a) For fully or nearly saturated cohesive soils, which behave as though $\phi = 0$ for the unconsolidated undrained (UU) condition, the strain-rate effect upon total strength falls between 1.5 and 2.0, with 1.75 a good average value.
- (b) For partially saturated soils with a water content at or just above the plastic limit, the strain-rate effect upon total strength will decrease with increasing confining pressure (for the UU condition) perhaps being greater than 2 at zero confining pressure and perhaps less than 1.5 for confining pressures of 50 psi and greater.
- (c) Soils drier than the plastic limit will have a strain-rate effect less than 1.5 even at low confining pressures.

It should be noted that the test results contain one bit of evidence to the effect that clays of moderate sensitivity may possess a strain-rate effect as great as 4.

All of these results emphasize the need to evaluate the strain-rate effect upon strength for the particular conditions to be expected in the problem of interest.

3.7.2 Present Status of Work. A great amount of work has been done on the subject of shear strength during a single transient load, and, although inevitably there are still a few loose ends, much is now known concerning this subject. The most glaring gap is lack of facts as to the causes for the increase of strength during very rapid shearing of clay soils.

3.7.3 Suggestions for Future Research. The author does not wish to discourage the elimination of the loose ends, but only one of these loose ends seems to deserve high priority: the aforementioned cause of the strain-rate effect in clay soils. To achieve this goal, it will be necessary to develop and validate means for measuring the excess pore pressures within clays during very rapid loadings.

The writer has not attempted to assess the state of knowledge concerning the dynamic strength of rocks. It may well be that much more research is needed in this area.

Overall, the most pressing need is to show that the results developed in this chapter can be applied to practical problems. Since field tests are restricted, this will mean applying these results to the prediction of behavior during tests in the laboratory on footings and buried structures, and comparing prediction with observation.

CHAPTER 4 ONE-DIMENSIONAL COMPRESSIBILITY

4.1 INTRODUCTION

The test used to evaluate one-dimensional compressibility (also called uniaxial strain) is shown in schematic form in fig. 1.2. The key feature of the test is that lateral (horizontal) strains are prevented by a rigid container surrounding a cylindrical specimen of soil. Compressibility is evaluated as the ratio of axial (vertical) strain to change in axial stress. The result of such a test may also be expressed in terms of constrained modulus: the ratio of change in axial stress to corresponding axial strain. The apparatus used for the test is variously referred to as an oedometer or consolidometer.

This test has been used widely as a basis for estimating ground motions caused by static surface loadings: for example, settlements of buildings. The primary reason for such usage is the great simplicity of the test--simplicity both in the apparatus itself and in the testing procedures. The main justification for such usage is that the resulting estimates of settlements have proved to be reasonably satisfactory for many practical problems. However, the stress and strain conditions within an oedometer may be quite different from those within the soil beneath an actual loading (Lambe, 1964). Hence, estimates of settlements based on the results of oedometer tests can only be approximate and in some problems may be unacceptably in error.

With this background of wide usage with conventional soil engineering problems, it is natural that this same form of test has been used as a basis for estimating ground motions caused by dynamic surface loadings; i.e. airblast-induced ground motions. Once again the main reason for such usage is the simplicity of the test, and the primary justification is that predictions based upon results of such tests are in reasonable agreement with the very limited field experience. Chapter 2 has presented arguments that the stress and strain conditions during airblast-induced ground motion are quite similar to those in an oedometer test, but these arguments are not entirely convincing. However, it can be said that the oedometer test

simulates actual field conditions better than any other single, common soil test.

Section 4.2 discusses the adaptation of the oedometer test to dynamic loading conditions. Fortunately, it has not been found necessary to duplicate exactly the very rapid rise times (about 1 msec) experienced at shallow depth below an advancing airblast front. Rise times of 10 msec or even longer have proved to be satisfactory. Some special precautions are necessary to ensure that no water escapes from the soil during loading, so that the undrained conditions existing under the actual loading are maintained in the laboratory test. The greatest problem has been that the soils of interest in protective construction are generally far stiffer than the soils which are usually tested in connection with conventional soil engineering problems. In conventional (static) problems, usually there is little concern about settlements unless the modulus (with drainage permitted) is less than 5000 psi. On the other hand, sites generally will not be adequate for hardened protective construction unless the average modulus within the upper 500 ft exceeds 50,000 psi, because large explosions cause high pressures over a huge area of the surface of the earth. The emphasis upon testing stiff soils has required very rigid test devices and special test procedures.

When dealing with problems involving wave propagation, details of stress-strain behavior become important which are of little consequence to static problems; for example, energy loss during a cycle of loading. Thus, testing soil for weapons effects and protective construction problems has led to a more detailed study of stress-strain behavior than had previously been made. Section 4.3 discusses the important general features of stress-strain behavior during one-dimensional compression, as learned from this intensive study.

As discussed in Chapter 2, for most ground motion predictions it suffices to characterize the stiffness (or compressibility) of soil by a single parameter such as a modulus. However, as the discussion in section 4.3 makes clear, there is no such thing as the modulus of soil. Rather, modulus is a function of stress level, prior loading history, etc.

Section 4.4 discusses the selection of a modulus suitable for typical actual practical situations.

For some advanced prediction methods and for purposes of research, it is necessary to know typical values for other parameters such as relaxation time, recovery ratio, etc. Some ranges of typical values of such parameters are given in section 4.5.

4.2 TEST EQUIPMENT AND PROCEDURES

4.2.1 The MIT Tester. Fig. 4.1 shows the essentials of the test device developed at MIT for dynamic one-dimensional compression tests. It has the following key features:

- (a) A uniform axial stress is applied over the surface of the soil by fluid pressure acting against a rubber membrane.
- (b) Axial shortening is measured over the central portion of the

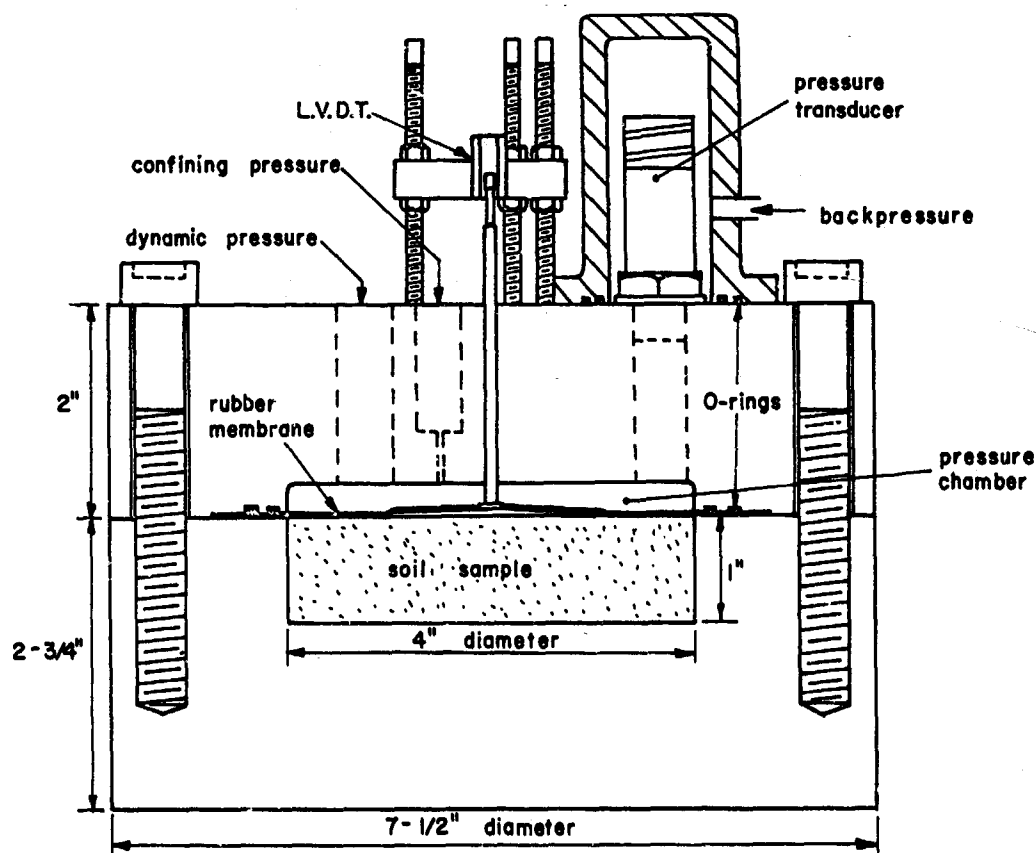


Fig. 4.1 MIT one-dimensional compression device

cross-sectional area by monitoring the motion of an aluminum disk. Thus the strains are determined in that part of the soil which is stressed and strained uniformly and is free from the unknown effects of side friction.

- (c) There is provision for an initial static stress, to simulate the effect of natural overburden and to seat the specimen against its base and the aluminum disk against the specimen.
- (d) Load increments can be applied with a rise time of about 10 to 15 msec.
- (e) The cell is extremely stiff and contains other special design features as well, so as to minimize errors caused by deformation of the cell itself.
- (f) The specimens are sealed so that there can be no drainage of pore water during the loading.

The test technique involves still another special feature: the use of repeated loadings so as to minimize the effects of disturbance during sampling.

These various features are discussed in more detail in the following paragraphs (also, see Reports 17 and 21).

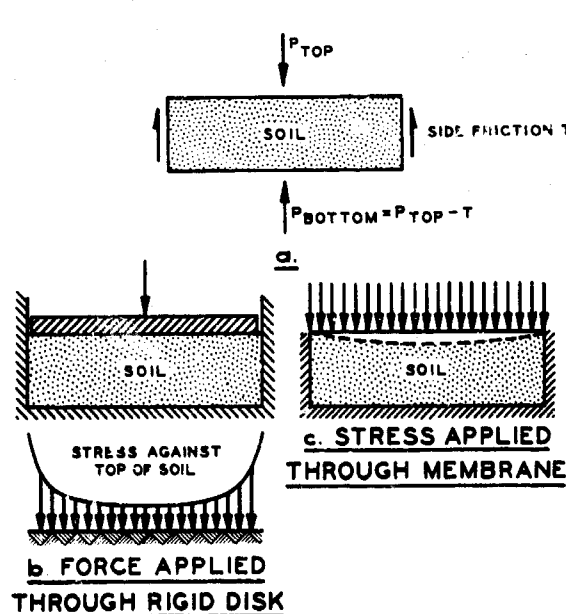


Fig. 4.2 Effects of side friction

Uniformity of stress and strain: In the ideal oedometer test there would be no shear stress between the soil and the rigid container. In actual tests such shear stresses do occur (fig. 4.2a) and are referred to as side friction. Because of side friction, stresses and strains are not uniform throughout the specimen and in particular the average axial stress decreases from the top to the bottom of the specimen. In conventional static testing, the axial stress is applied through a rigid

disk covering the entire specimen (fig. 4.2b). Since side friction acts to stiffen the soil near the wall, the stress between the disk and the soil is larger near the wall than at the center line. All of these effects complicate greatly the interpretation of the test results. In order to minimize the uncertainties associated with these effects, the diameter of a specimen should be several times the thickness. A ratio of 4 to 1 is often used. Attempts have been made to use lubricants between the soil and the wall (for example, see Aldrich, 1951) but the practical difficulties in their use generally overshadow their beneficial effects.

In the MIT tester, the uncertain effects of side friction have been minimized by applying stress through a flexible membrane and by measuring strain in the central portion of the specimen where the strains are relatively uninfluenced by side friction. With this loading arrangement, the top surface of the specimen deflects nonuniformly (fig. 4.2c). However, over some central section the deflection is uniform. Introducing a rigid disk in this central section will hence not affect the stress or strains. The proper diameter for this disk was determined by progressively decreasing the diameter until an increment of decrease had no effect upon the measured strains (fig. 4.3). A disk whose diameter is about one-half the diameter of the specimen is apparently the optimum size.

The movement of the disk is detected by a sensitive linear variable differential transformer (LVDT). The rod from the disk to the LVDT passes loosely through a hole in the upper block of the oedometer. It is important that there be no drag force on the rod at this point. The disk

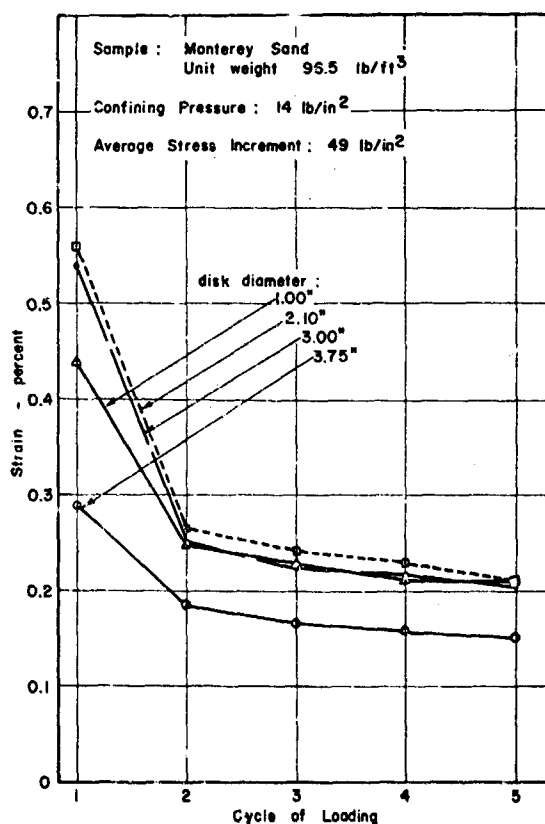


Fig. 4.3 Influence of disk size on measured strain

should be as light as possible and hence is made of aluminum.

Stiffness: If an axial stress of 100 psi is applied to a specimen with a thickness of 1 in. and a modulus of 10,000 psi, the resultant change in thickness is 0.010 in. If the modulus of the soil were 100,000 psi, the thickness change would be only 0.001 in. Obviously it is necessary that the apparatus used to house the specimen be very stiff so that the deflection of the apparatus is much less than the thickness changes which are to be measured.

By direct measurement, the relative movement between the center of the lower part of the test device and the attachment point of the LVDT was found to be about 0.00004 in. for a change of 100 psi in the pressure applied inside the test device. For a specimen of soil with a thickness of 1 in., this is equivalent to a modulus of 2,400,000 psi. Thus, measurement of modulus values up to 200,000 psi can be made without being significantly affected by lack of complete rigidity in the apparatus.

One of the keys to achieving adequate rigidity is having direct metal-to-metal contact between the upper and lower halves of the apparatus. All earlier devices in which the membrane extended entirely across the interface between the two halves had insufficient rigidity. By exercising proper care in the assembly of the device shown in fig. 4.1, leakage of air pressure past the membrane can be held to a level which is insignificant during a test of 1-hr duration.

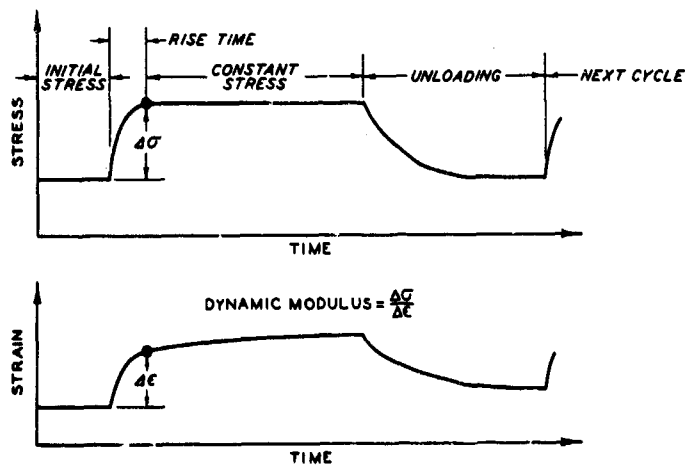


Fig. 4.4 Typical loading sequence

Loading system: In most of the tests which have been performed with the MIT tester, the loading sequence for each specimen involved (see fig. 4.4):

- (a) Application of an initial stress. This initial stress simulates the effect of overburden and

also serves to give good seating between the specimen and the bottom of the container and between the specimen and the disk for sensing strains.

- (b) A rapidly applied dynamic stress increment. The dynamic modulus is defined by the ratio of change in stress to change in strain at the end of this increment.
- (c) An interval of constant stress, during which creep is observed.
- (d) Removal of the dynamic stress increment, during which strain recovery is observed.
- (e) Several repetitions of the dynamic stress increment. Response during the second and next several cycles is often found to be more representative of in situ response than the response during the first cycle, since seating errors are removed by the first cycle.

The elements of the loading system developed for these tests are shown in fig. 4.5. The space immediately above the membrane is filled with water.

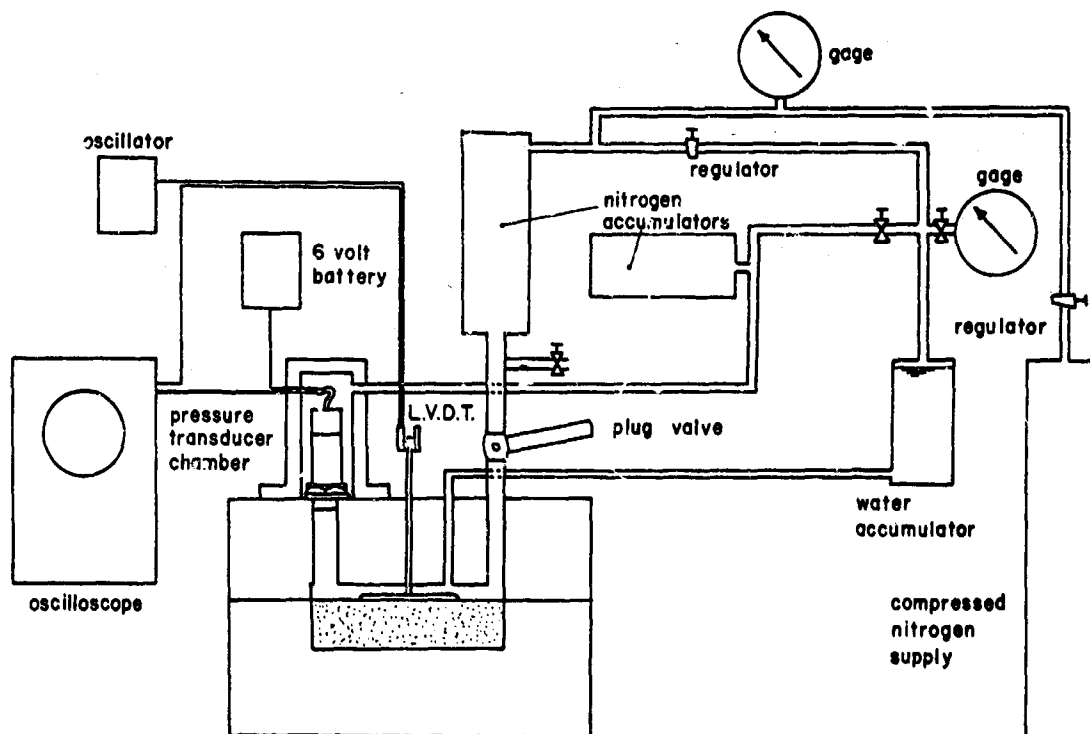


Fig. 4.5 Sketch of layout for one-dimensional compression tests

Initial confining stress is supplied through the water accumulator. Dynamic stress increments are applied by rapidly opening the plug valve leading to the nitrogen accumulator. Since the space between the plug valve and the membrane is filled with water, only a small volume of air must flow through the plug valve in order to develop pressure against the soil, and rise times of 10 to 30 msec can be readily obtained. A rubber disk (not shown) over the port to the water accumulator serves as a check valve to prevent the dynamic stress from feeding back into the confining stress system. Unloading is accomplished by merely closing the plug valve and allowing the pressure to dissipate through the leak around the rod to the LVDT. The resulting unloading time varies up to 50 sec.

Various other loading schemes were used at one time or another to provide rise times as short as 1 to 2 msec (see Report 17). However, the dynamic moduli obtained with these short rise times differed only slightly from values obtained using 10- to 30-msec rise times. Rise times less than 1 msec should not be used, since then time for a wave to propagate through the specimen approaches the rise time and hence the strains become non-uniform over the thickness of the specimen.

In some tests a rapid loading and unloading were desired. This was accomplished by means of a plunger inserted through a bushing screwed into the dynamic pressure inlet. The pressure was applied by hitting the plunger sharply. The entire cycle of loading and unloading was completed in about 30 msec.

Testing undisturbed samples: Samples taken in tight-fitting metal tubes are best tested by using the metal tubes to provide the lateral con-

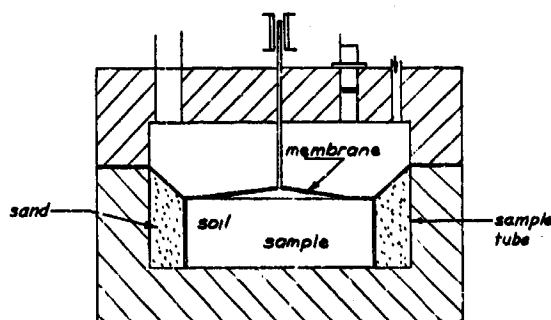


Fig. 4.6 Arrangement for testing undisturbed samples

finement, as shown in fig. 4.6. The space surrounding the metal ring is packed with sand, primarily to provide support for the membrane. The top and bottom surfaces of the specimen must be as plane as possible, and a file has been found to be very useful for preparing specimens of stiff soils. With this arrangement,

it is difficult to prevent some loss of water from the specimen, although grease placed around the bottom of the metal ring is of some help. Tests on a variety of undisturbed samples are reported in Report 17. .

4.2.2 Later Versions of the MIT Tester. Schindler (1967) has described several evolutions of the MIT tester. One of the most important advances has been placement of the transducer for measuring strain inside the pressure cell, so as to eliminate the conflicting requirements upon the bushing where the rod to the transducer passed through the top of the cell. Fig. 4.7 shows details of the arrangement developed at Stanford Research Institute (Seaman, 1966), and fig. 4.8 shows the compression device developed by the U. S. Army Engineer Waterways Experiment Station. The latter device permits testing of larger specimens, thus reducing still further errors associated with side friction and seating, and can be used in conjunction with a special loading apparatus for applying controlled-load time histories.

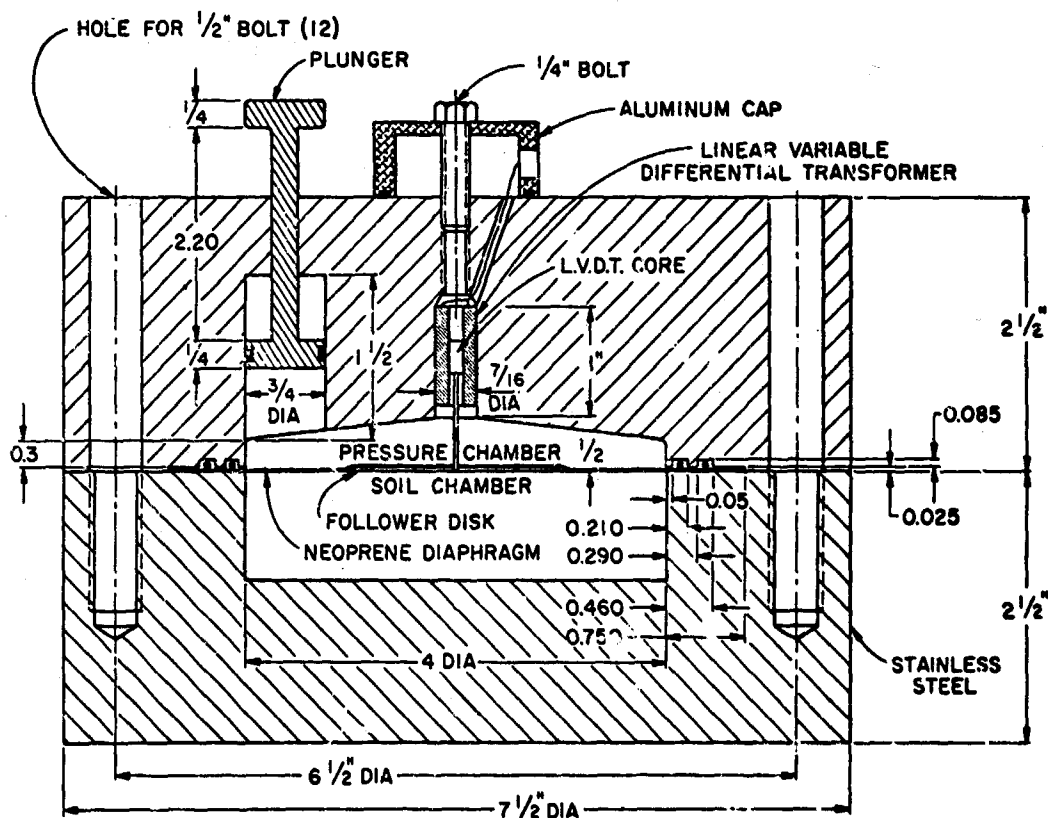


Fig. 4.7 SRI version of MIT Tester (from Seaman, 1966)

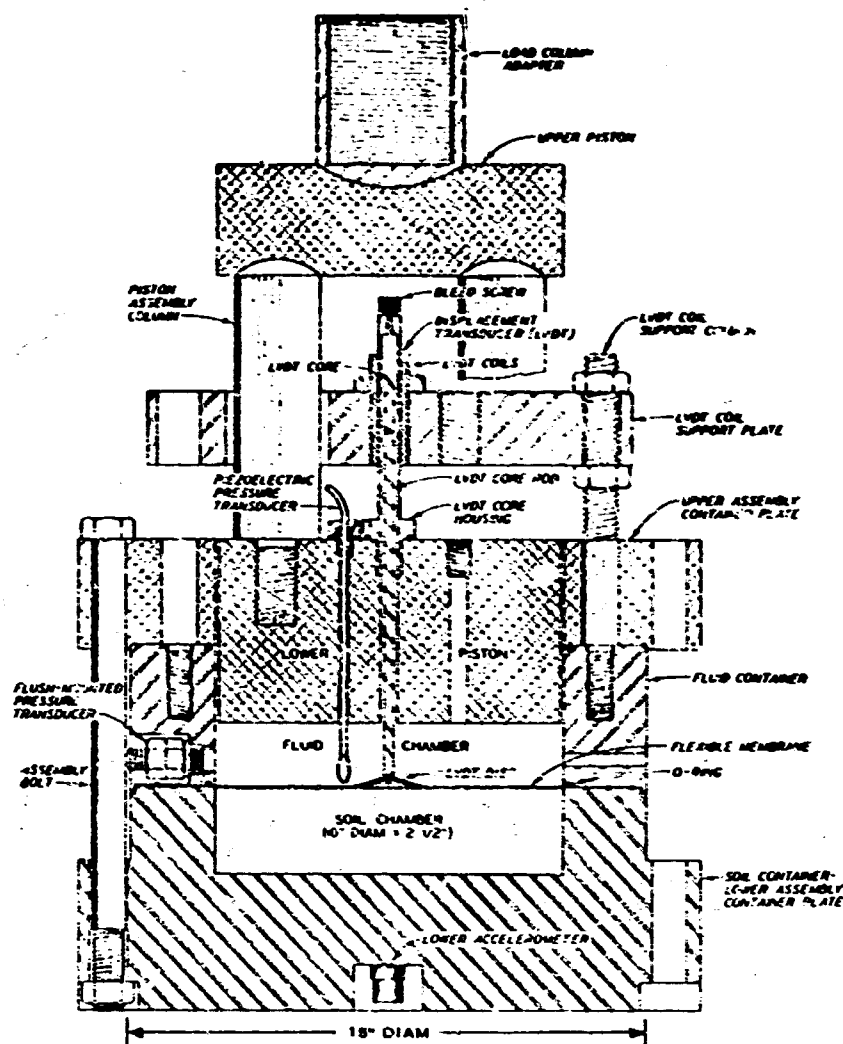


Fig. 4.8 WES version of MIT tester
(from Schindler, 1967)

4.2.3 Other Test Devices. Test devices employing a rigid piston in contact with the soil, as in the usual consolidometer, have been developed for dynamic testing.

In the system developed at the University of Illinois (Kane et al., 1964), the sample is held within a thick ring and dynamic loading is applied axially by a special loading apparatus. A strain gage placed on the thick ring is used to sense lateral stress. This device can be used with axial stresses of thousands of psi. Fig. 4.9 shows a somewhat different version of this device developed for static tests. The soil is contained

within a metal ring 6.8 in. in diameter. Circumferential strains within this ring are detected by strain gages, and the oil pressure against the outside of the ring is adjusted as necessary to maintain zero lateral stress. This arrangement comes the closest of all tests to giving a true one-dimensional compression condition, although some side friction is still present and there are other experimental difficulties.

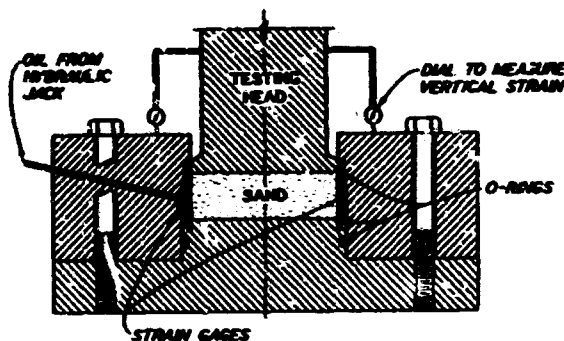


Fig. 4.9 Apparatus for accurate measurement of lateral stress during one-dimensional compression (from Hendron, 1963)

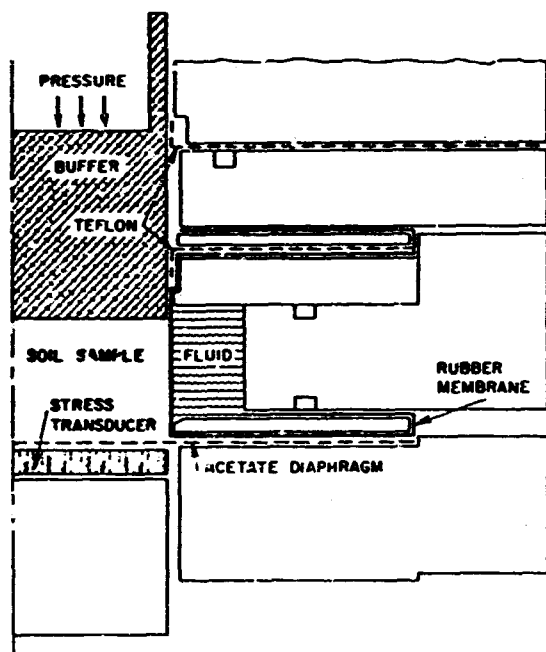


Fig. 4.10 One-dimensional compression device with fluid boundary (courtesy United Research Services)

Fig. 4.10 shows an arrangement developed by URS (Zaccor and Wallace, 1963). Loading is applied through a piston (buffer), and the specimen is contained on the sides by a closed fluid system. A rubber membrane separates the fluid and the soil. This arrangement largely eliminates the side-friction problem. However, some lateral strain actually occurs and there is no guarantee that the lateral strain is uniform along the length of the specimen. URS also has employed a series of stacked rings to provide lateral confinement in a manner similar to that shown in fig. 4.11. This system worked only with dry sands.

More recent developments in testing systems have been described by Jackson (1968).

The device shown in fig. 4.10 has also been used for wave propagation tests on long specimens; that is, tests in which the rise time is short

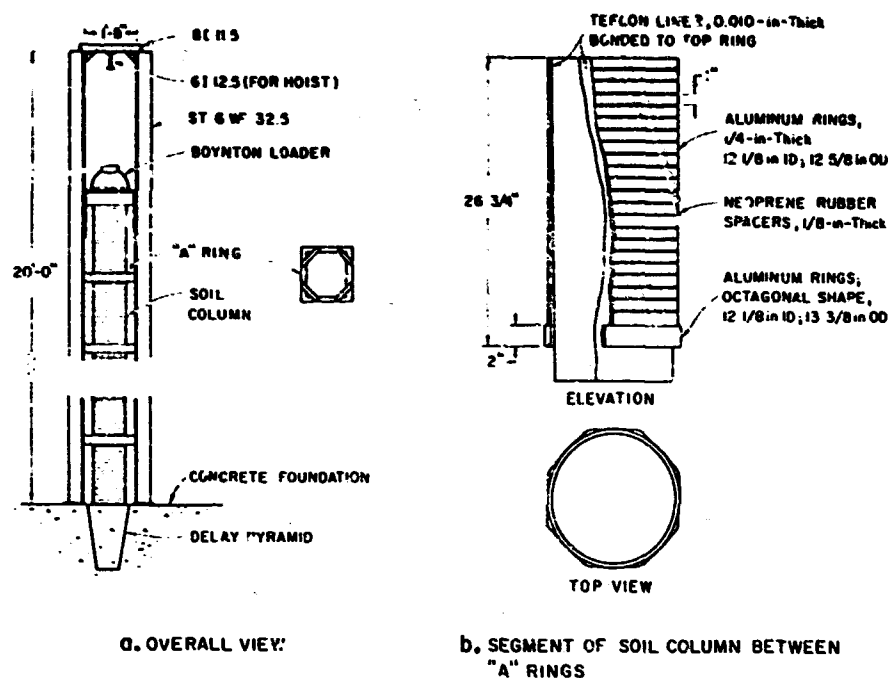


Fig. 4.11 Articulated lateral boundary for one-dimensional wave propagation tests (courtesy Stanford Research Institute)

compared to the time for the wave to propagate through the specimen. Other special systems for wave propagation tests have been developed at Stanford Research Institute (Seaman, 1966), at IIT Research Institute (Selig, 1964), at Columbia University (Stoll and Ebeido, 1965), and at the U. S. Army Engineer Waterways Experiment Station. The SRI system is shown in fig. 4.11. Lateral confinement is provided by rings separated by rubber. The rubber separators act to minimize the effects of side friction. Tests with these devices have played an important role in studying the applicability of one-dimensional compressibility to the analysis of wave propagation.

4.3 GENERAL ASPECTS OF BEHAVIOR

4.3.1 Ideal Packings of Perfect Spheres. Considerable insight into the stress-strain behavior of soil is gained from the theory for the behavior of perfectly packed, ideal elastic spheres. The general formulation of this theory is described by Deresiewicz (1958). Hendron has applied this theory to one-dimensional compression of a three-dimensional array of

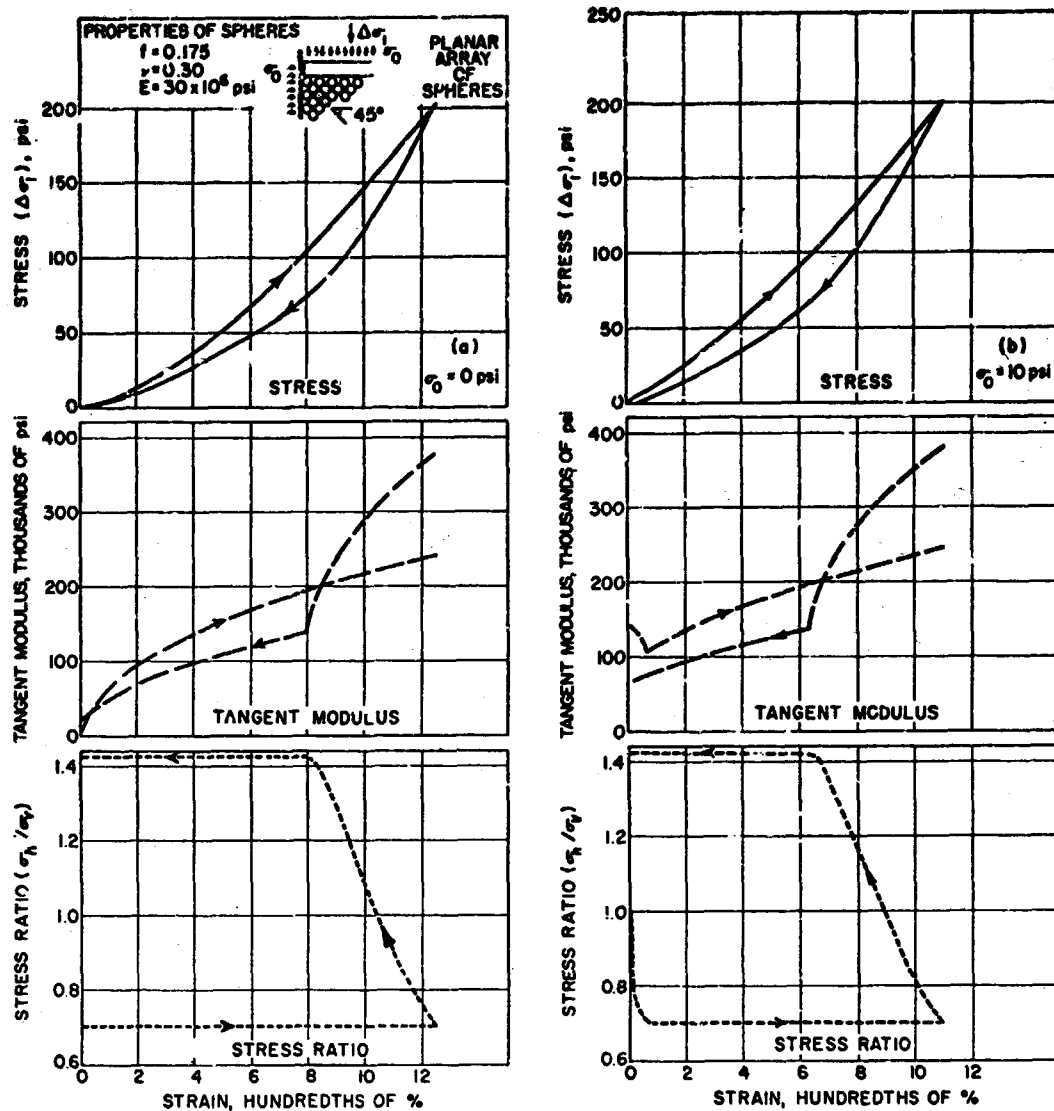


Fig. 4.12 Stress-strain curves for hypothetical one-dimensional compression tests on planar array of spheres

spheres. Report 19, from which fig. 4.12 is taken, gives results calculated for a planar array of spheres.

During one-dimensional compression of such an array, the centers of all spheres move only in the direction of the compression. There is, of course, elastic distortion of the spheres as the result of the forces between the spheres. However, compatibility requires that there also be sliding between spheres at the contacts. Thus shear forces, whose

magnitudes are determined by the coefficient of friction, develop at the contacts. Because of these shear forces, the lateral (horizontal) stress necessary to preserve the one-dimensional condition is different than the axial (vertical) stress applied.

When the loading begins with the initial stress $\sigma_0 = 0$ (fig. 4.12a), sliding between spheres begins immediately. The resulting shear forces are such that the lateral stress σ_h is less than the vertical stress σ_v during the loading. As the loading progresses, it becomes progressively more difficult to distort the spheres and hence to cause sliding between spheres, and thus the array becomes progressively stiffer--as shown by the increasing tangent modulus. During unloading, the spheres begin to regain their original shape and compatibility requires that there be reversed sliding. Thus the shear forces at the contacts reverse in direction, and the lateral stress becomes greater than the axial stress. When the stress is entirely removed, the array returns to its original condition; i.e. there is no permanent strain. However, the loading and unloading have resulted in a hysteresis loop, and hence energy has been lost during the cycle of loading.

When the loading starts with $\sigma_0 > 0$ (fig. 4.12b), there is an initial transition phase during which the frictional resistance provided by the initial stress is gradually overcome and sliding between spheres develops. During this initial phase the tangent modulus decreases. Once sliding between spheres is fully developed, the behavior is similar to that described in the previous paragraph except that a permanent strain remains after the stresses are returned to the initial stress σ_0 . A closed hysteresis loop will develop during a second cycle of loading.

4.3.2 Dry Granular Soils. Dry soils experience the same phenomena as ideally packed elastic spheres, plus one additional phenomenon: progressive rearrangement of particles into tighter packings. Thus strains within actual granular systems during loading are greater than those within the ideal system, and the permanent strains after unloading are also greater. This difference of course arises because the irregular shape and unequal size of the particles within an actual soil preclude ideal packings of the

particles. The irregularly shaped particles are also more susceptible to breakage than perfect spheres.

Virgin loading: Fig. 4.13 shows observed stress-strain curves for a uniform rounded sand.

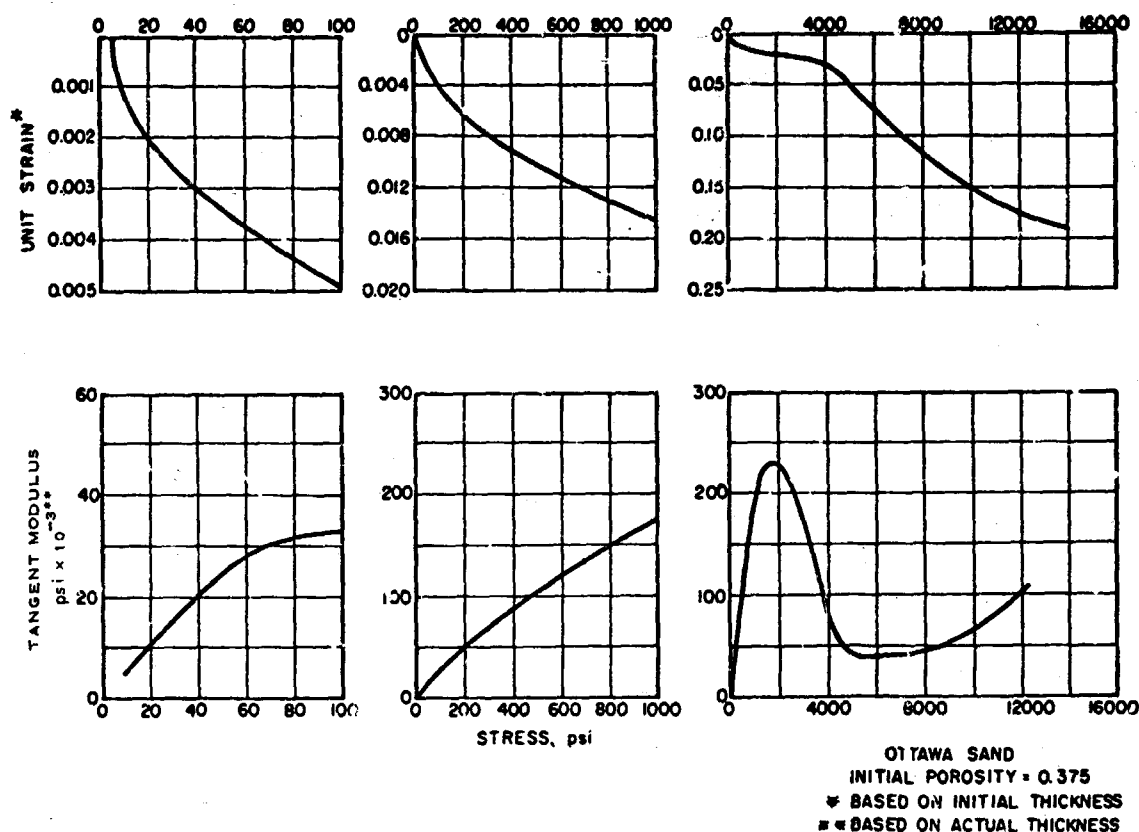


Fig. 4.13 Behavior of Ottawa sand during initial loading in one-dimensional compression

Below a stress of about 2000 psi, the stress-strain curve shows an upward concavity (stiffening behavior), and the tangent modulus increases steadily with increasing stress. The major cause of strain presumably is rearrangement of particles due to gross sliding at contact points. As the stress level increases, the effect of every rearrangement is to produce a more stable packing of particles which is more resistant to further deformation.

At a stress level of about 2000 psi, there begins a decrease in the tangent modulus. Individual grains break down, permitting a still denser

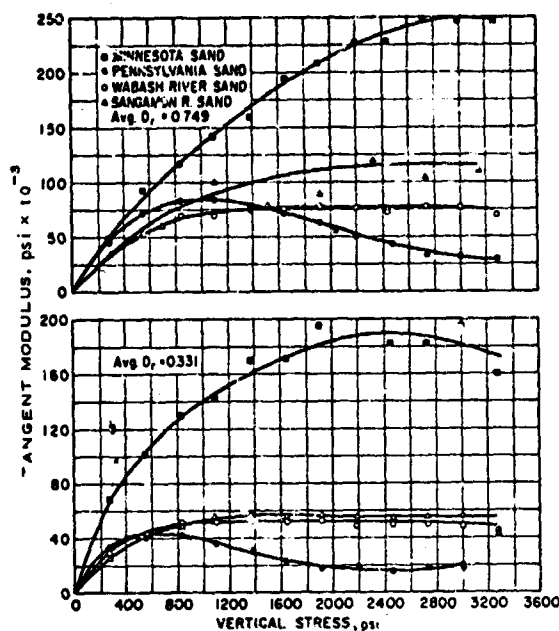


Fig. 4.14 Behavior of several sands during one-dimensional compression (from Hendron, 1963)

arrangement of the mineral matter, and eventually the modulus once again rises with increasing stress.

The general pattern shown in fig. 4.13 is exhibited by all sands. Fig. 4.14 gives curves of tangent modulus versus stress for four different sands placed initially at two different relative densities. When a sand is in a loose condition, there are fewer points of contact than when the sand is in a dense condition. Hence for a given overall stress the contact stresses are greater in the loose condition, and crushing begins at a smaller overall stress. The crushing effect is minimized when the sand is well graded, for then there are many contacts and hence relatively small contact stresses. Crushing begins at lower stresses when the sand is composed of angular particles.

The curves in figs. 4.13 and 4.14 do not define clearly the stress-strain behavior for very small stress increments such as 1 to 5 psi. The behavior with such small stress increments is studied in detail in Report 21, and a typical pattern is shown in fig. 4.15. Initially there is a yielding type of stress-strain curve as sliding at contacts develops gradually. Thus initially the modulus decreases and only after this initial transition stage does the stress-strain curve become concave to the stress axis. The extent of this initial yielding zone depends upon the initial stress, increasing as the initial stress increases. For very compact

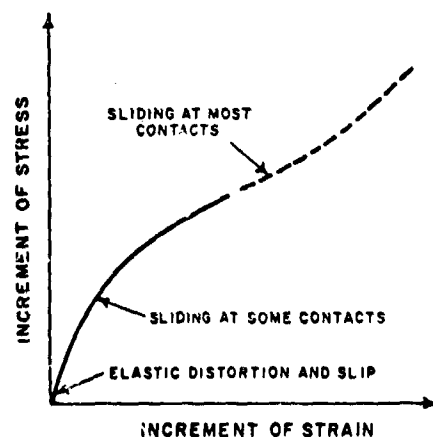


Fig. 4.15 One-dimensional stress-strain curve for small stress increments

natural sands (especially if some cementing has occurred), this initial yielding range may be quite appreciable. Yielding behavior of the type shown in fig. 4.15 also may be observed whenever a loading is resumed after the stress has been held constant at some level for a period of time.

Unloading and reloading: Fig. 4.16 illustrates the expansion and re-compression of sand as the result of removing the applied stress when it reaches some level, and then once again increasing the stress beyond this level. There are three salient facts: (a) the unloading and reloading branches are considerably steeper than the virgin loading branch; (b) a hysteresis effect is present; and (c) a net compressive strain develops as the result of unloading and reloading. The greatest part of the strain recovery during unload-

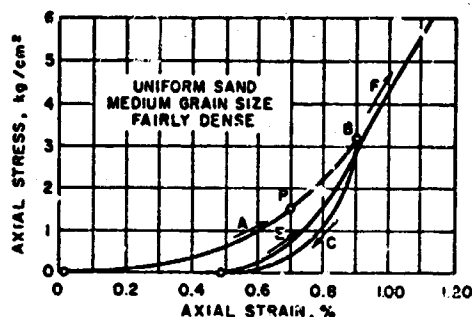


Fig. 4.16 One-dimensional stress-strain behavior during unloading and reloading (from Taylor, 1948)

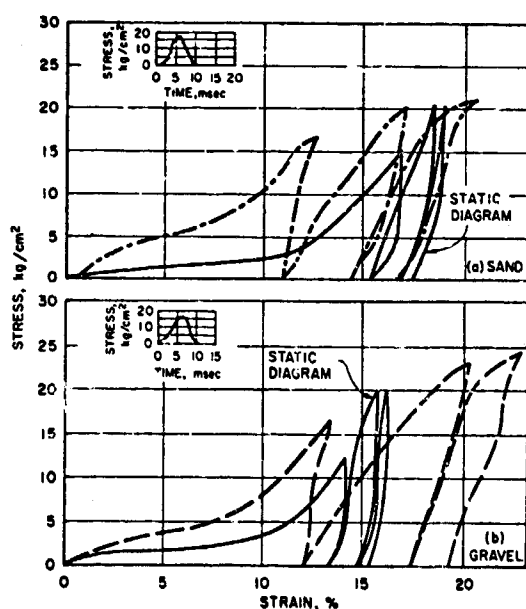


Fig. 4.17 One-dimensional stress-strain curves for very loose sand and gravel (from Heierli, 1962)

ing occurs only after the stress level falls close to zero total stress. When loading is continued beyond the level from which the unloading occurred, the stress-strain curves follow much the same path as would have been found for a continuous virgin loading.

The curves in fig. 4.16 imply that energy loss occurs during a cycle of loading and unloading. The energy loss* during a virgin cycle of loading and unloading will vary greatly with the initial density of the sand. Fig. 4.17 shows stress-strain curves for a sand and a

* Here energy loss is defined as the ratio of the area enclosed by the loading-unloading curve to the area under the loading curve.

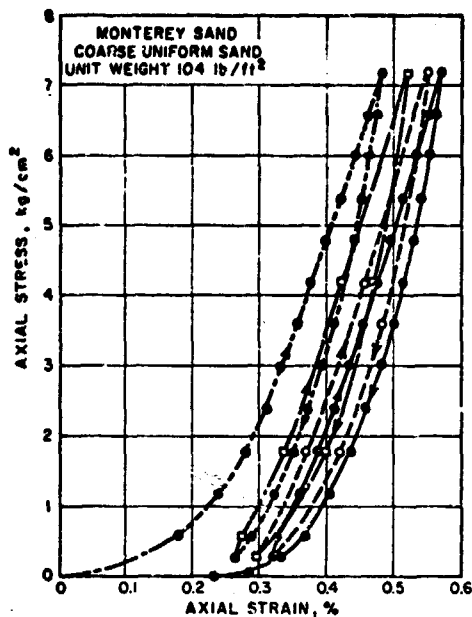


Fig. 4.18 Effect of unloading and reloading during repeated one-dimensional compression

energy loss per cycle decreases somewhat with additional cycles, and the loops gradually become steeper. However, these changes are very gradual after the first two or three cycles. Fig. 4.19 shows the gradual increase in the average slope of the stress-strain curve as the repeated loading progresses. After about 10 cycles, it becomes difficult to detect whether or not there is a net accumulation of strain per cycle; that is, it appears that the hysteresis loops have become stabilized, as shown in fig. 4.20 (see Report 17). However, it has been observed that strains still continue to increase even after 10^6 cycles.

Time effects: Creep occurs in a dry sand following a very rapid application of stress, as illustrated in fig. 4.21. The rise time in these

gravel, both in an extremely loose state, and indicates that the energy loss approaches 100% for such cases. For a dense sand, the energy loss during virgin loading and unloading is more like 50%.

Repeated loading: Fig. 4.18 illustrates the stress-strain behavior when the stress is cycled several times. The hysteresis loop for the second cycle of loading and unloading shows less net strain than does the first cycle. The

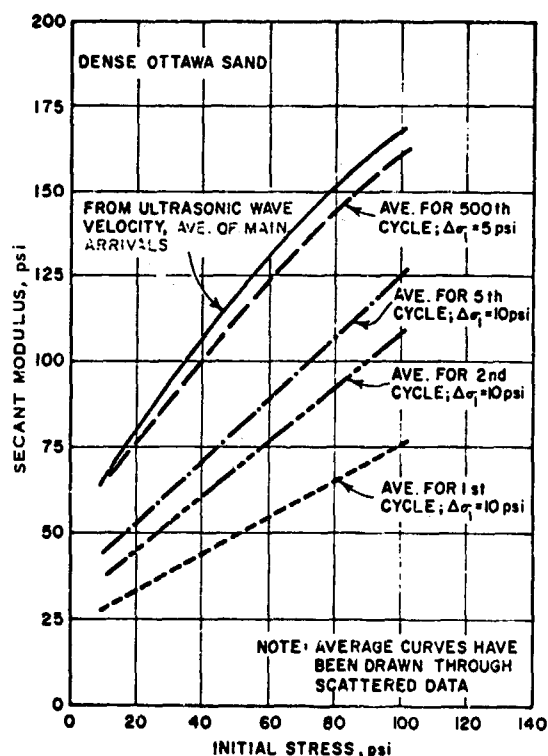


Fig. 4.19 Secant modulus versus number of repeated loadings

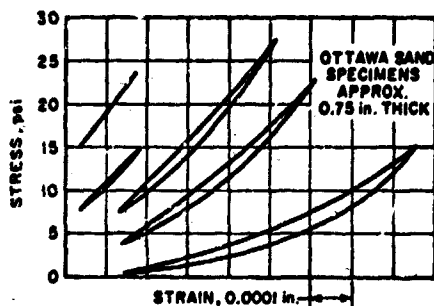


Fig. 4.20 Hysteresis loops after about 500 cycles in one-dimensional compression

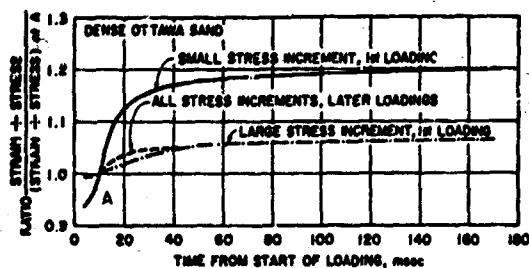


Fig. 4.21 Creep during rapid one-dimensional compression tests

tests was about 10 msec, and though creep continued at a slow rate for several minutes, most of the creep occurred within 50 to 100 msec. The same time effect shown by creep tests appears as a time lag between peak stress and peak strain during cyclic loading (Seaman, 1966). Results indicate that time effects are most pronounced when the stress increment is small; i.e. when the increment is of the same order of magnitude as that required to develop the yielding effect shown in fig. 4.15; see fig. 4.22.

Such time-dependent effects can be examined from two viewpoints: (a) the effect of rise time on modulus, where modulus is defined as the ratio of stress to strain during and at the very end of the loading, and (b) the need for, and suitable numerical values for the constants of, viscous elements in a rheological model of soil.

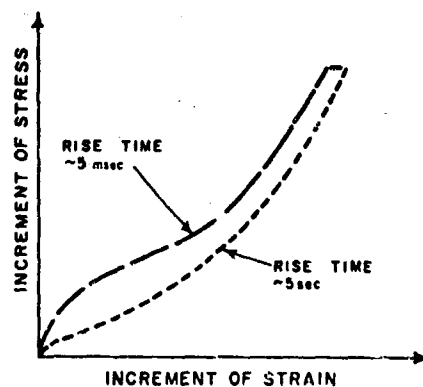


Fig. 4.22 Loading rate versus one-dimensional stress-strain behavior

The secant modulus of dry sand during a rapid loading (say 10-msec rise time) is distinctly greater than that for a slow loading (several minutes rise time). Report 21 suggests that the increase might typically be about 40%. Examination of fig. 4.21 indicates that rise times in the range of 10 to 50 msec would give values of modulus differing by only about 5%, except for small stress increments during the first loading. Such a small difference is insignificant for practical purposes. It should be

noted that the ratio of dynamic to static moduli of sand cannot be determined from tests with a rapid stress increase followed by creep during constant stress, since the strain in such tests at the termination of creep has been found to be less than the strain at the end of a slow loading to the same stress (see Report 21).

Fitting rheological models to observed results is discussed in Report 17 and in Seaman (1966). A useful model is illustrated in fig. 2.41.

Lateral stresses: Hendron (1963) has obtained excellent data concerning the relation between lateral and axial stresses. Fig. 4.23a shows a

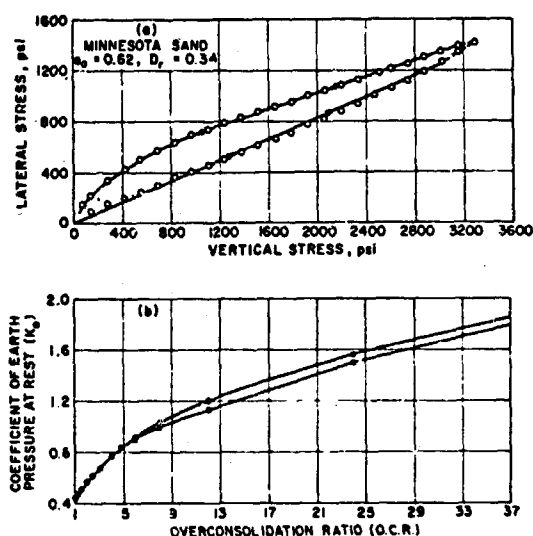


Fig. 4.23 Lateral stress during one-dimensional compression

typical set of data. During loading, the ratio of these stresses is almost constant. During unloading, however, the ratio progressively increases and near the end of unloading this ratio exceeds unity. Values of this ratio during unloading are plotted in fig. 4.23b, where overconsolidation ratio denotes the ratio of the maximum previous vertical stress to the present vertical stress.

Summary: Dry granular soils exhibit yielding in one-dimensional compression for very small stress increments, stiffening behavior for

large stress increments, relatively low recovery of strain during unloading, and hysteresis loops during repeated loadings. These features, plus that of the ratio of lateral to axial stress, can be understood qualitatively from the theoretical behavior of ideally packed spheres. Quantitatively, the behavior is influenced greatly by the size, shape, and gradation of the particles composing the actual soil.

4.3.3 Other Soils. Natural soils and soft rocks exhibit the same general stress-strain features as do dry granular soils. The influence of pore water and of fine-grained soil particles is discussed in the following paragraphs.

Fully saturated soil: In a dry soil, the resistance of the mineral skeleton to compression is much greater than the resistance of the pore air to compression. Thus, when a dry soil is compressed the air in the pore spaces offers negligible resistance to compression.

However, if the pore spaces are completely filled with water, just the reverse situation prevails: the compressive resistance of the water now exceeds the compressive resistance of the mineral skeleton (not to be confused with the compressive resistance of the minerals composing the mineral skeleton). Neglecting the very small compressibility of the mineral particles (the compressibility is much less than that of water), the compressibility of a fully saturated soil is:

$$\text{Unit compressibility} = n/B^W$$

where

n = porosity

B^W = bulk modulus of water

With $n = 0.4$ and $B^W = 300,000$ psi, the unit compressibility is 1.4×10^{-6} per psi. Thus for stress changes up to several hundred psi, the compression of fully saturated soil is very small and difficult to measure with great accuracy.

The foregoing discussion presumes that there is no movement of pore water out of the soil during compression; that is, that the loading is undrained (see Chapter 1). The undrained condition generally exists during a blast loading. During a loading so slow as to permit full drainage, a fully saturated soil may be very compressible--just as a dry soil.

Partially saturated soil: When the pore space is filled partly with gas and partly with water, the behavior during compression is more complicated. For small stress changes, the stress-strain relation is governed primarily by the resistance of the mineral skeleton. However, under very large stress changes the gas will become first highly compressed and then dissolved in the pore water so that the soil becomes fully saturated. Thus a partially saturated soil may be quite compressible for small stress changes and then rather suddenly change to a highly resistant material.

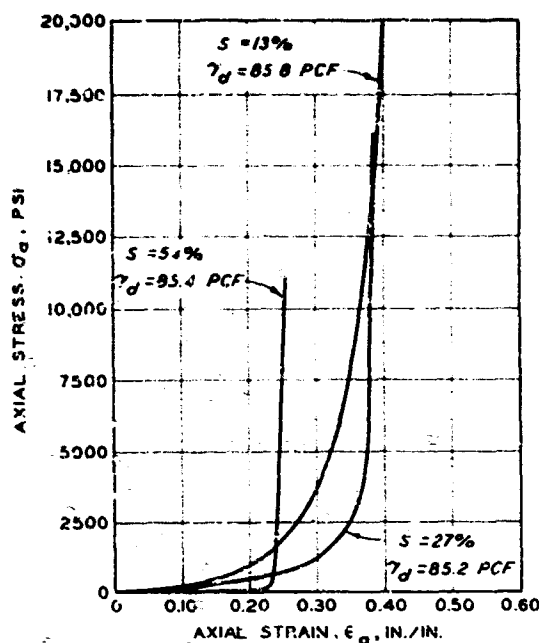


Fig. 4.24 Dynamic one-dimensional stress-strain curves for compacted silty clay (from Hendron, Davisson, and Parola, 1969)

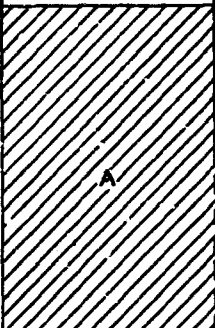



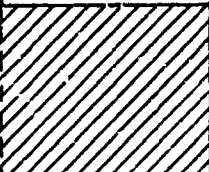

This pattern of behavior is illustrated in fig. 4.24. As the initial degree of saturation increases, the strain required to bring the soil to full saturation decreases and the transition from a compressible to a compression-resistant material becomes more abrupt.

It is possible to write approximately correct equations relating applied stress to the amount by which the pore gas compresses and dissolves (see Chapter 5 and NUCLEAR GEOPLOSICS), and these equations can be used to study the transition from partial to full saturation. The results of calculations based on these equations are useful for identifying

the range of the variables for which the resistance of both the mineral skeleton and the pore phase is important. A typical set of results is given in fig. 4.25; results for other initial pore pressures have a similar pattern with the boundary between zones A and B shifting. If the conditions of interest to any particular problem fall within zone B, it is especially important to duplicate closely the initial in situ conditions (initial pore water pressure, initial effective stress, degree of saturation) if a laboratory test is to give an accurate stress-strain curve. By the same token, values of modulus measured for conditions corresponding to zone B must be regarded with some skepticism until the validity of such measurements is confirmed by field experience.

Unfortunately, it is difficult by conventional soil mechanics tests to establish the initial in situ degree of saturation with great accuracy. It is not uncommon for a laboratory following the very best of practice to report 98% (or 102%) saturation when the actual saturation is essentially 100%. Accurate measurement of undrained modulus provides a sensitive test

Fig. 4.25 Pattern of behavior for undrained loading of partially saturated soil

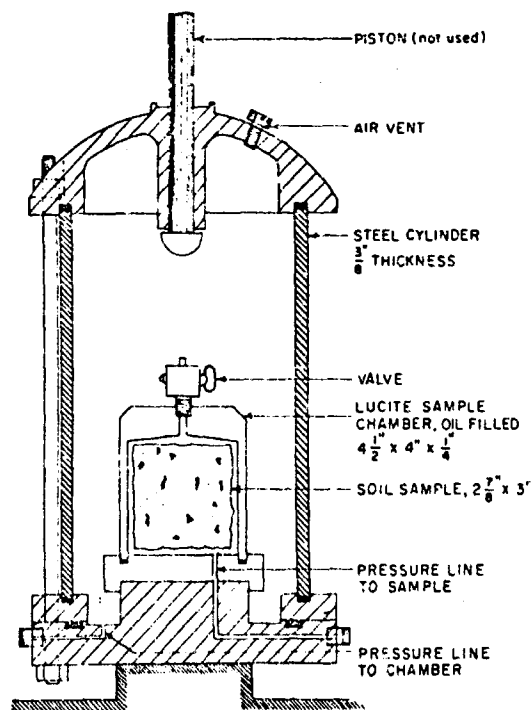
DEGREE OF SATU- RATION, %	CHANGE IN APPLIED STRESS			
	10 PSI	100 PSI	1000 PSI	
99.5	 A	B	 C	
99				
98				
95				
90				
80				

ZONE A: RESISTANCE OF PORE PHASE UNIMPORTANT, AND SOIL DOES NOT BECOME FULLY SATURATED DURING LOADING. SECANT MODULUS FOR UNDRAINED LOADING ESSENTIALLY THAT OF MINERAL SKELETON.

ZONE B: RESISTANCE OF PORE PHASE IMPORTANT AND SOIL BECOMES FULLY SATURATED DURING LOADING. SECANT MODULUS FOR UNDRAINED LOADING INTERMEDIATE BETWEEN THAT FOR FULLY SATURATED SOIL AND FOR MINERAL SKELETON.

ZONE C: SECANT MODULUS FOR UNDRAINED LOADING NEARLY EQUAL TO THAT OF FULLY SATURATED SOIL.

APPLIES FOR SECANT MODULUS OF MINERAL SKELETON = 30,000 PSI AND INITIAL PORE PRESSURE = 130 PSIA.



for full saturation; if the measured secant modulus of a soil is 200,000 psi or greater during a stress change of several hundred psi, the degree of saturation is essentially 100%. Fig. 4.26 shows a hydrostatic compression apparatus devised for special tests to determine whether undisturbed samples of natural soils are essentially fully saturated.* The chamber surrounding the soil is filled with oil,

Fig. 4.26 Triaxial cell for bulk modulus measurements (courtesy of MIT)

* Unpublished reports by the writer.

which will not penetrate into saturated soil. The change in volume of the soil can thus be determined by monitoring the volume of oil which flows into the inner chamber when pressure is applied. The inner container is subjected to the same pressure on both sides; hence this chamber experiences only very small dimensional changes as the applied pressure changes and the associated corrections for these dimensional changes are very small. Since the sample need not be trimmed or seated and since no transducing element need have contact with the soil, the major sources of error in modulus measurements are eliminated. Since no membrane need be placed around the sample, there is no danger of trapping air adjacent to the surface of the sample as jacketing is applied.

Shape of stress-strain curves: As illustrated by the curves in fig. 4.24, for very large stress changes the stress-strain curves of natural soils are concave to the stress axis (stiffening behavior). However,

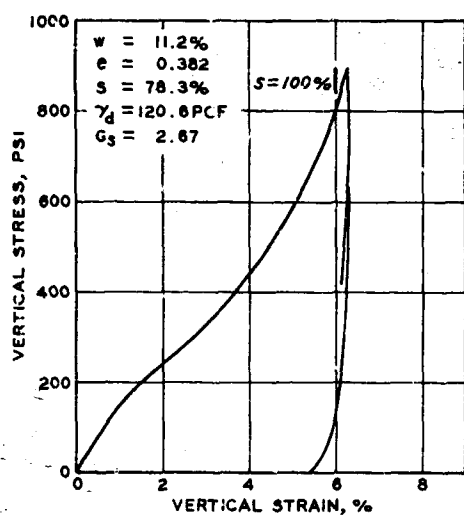


Fig. 4.27 Dynamic one-dimensional stress-strain curve for undisturbed sample of till (from Jackson, 1968)

for smaller stress changes natural soils generally exhibit yielding behavior during one-dimensional compression (fig. 4.27) to a much greater degree than for dry granular soils. Figs. 4.28-4.30 present a typical set of curves for compacted, partially saturated silt, showing that even for quite large stress changes the tangent and secant moduli generally are considerably less than the initial tangent modulus. The more pronounced initial yielding behavior in natural soils as compared with granular soils results partially from weak cementation formed within natural soils and partially because soils with fine-grained particles have a greater

"remembrance" of past loadings.

Time effects: Creep and other time-dependent effects are generally somewhat more important in natural soils than in dry granular soils. However, the difference in behavior is not great. Fig. 4.31 compares curves

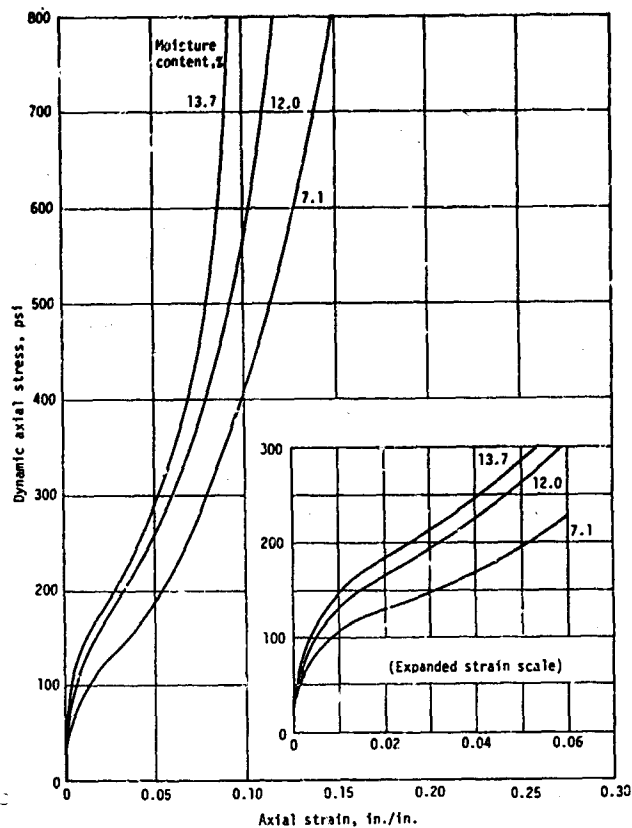


Fig. 4.28 Dynamic stress-strain curves, one-dimensional compression, 100-psi surcharge (from Calhoun and Kraft, 1966)

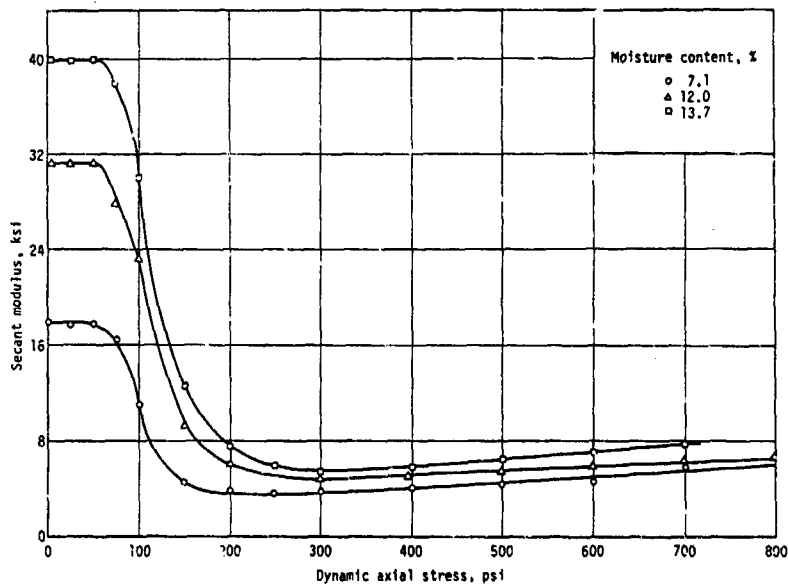


Fig. 4.29 Secant modulus versus dynamic axial stress, 100-psi surcharge (from Calhoun and Kraft, 1966)

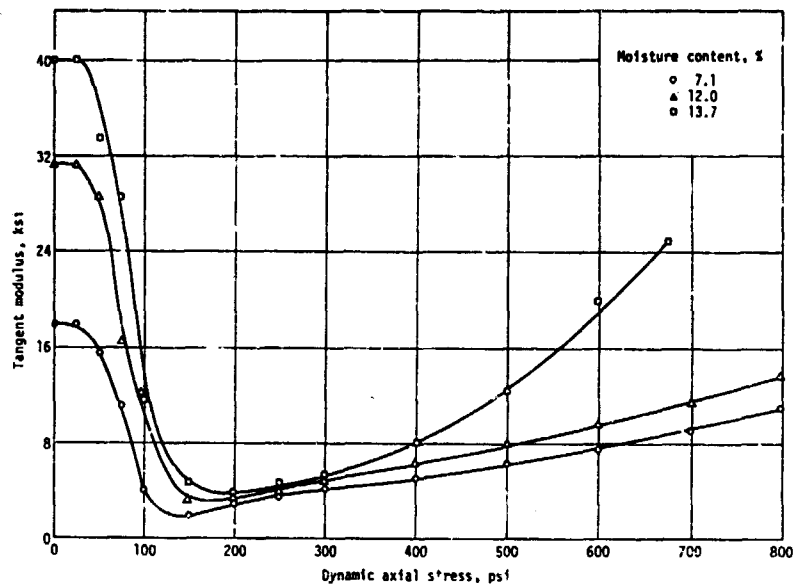


Fig. 4.30 Tangent modulus versus dynamic axial stress, 100-psi surcharge (from Calhoun and Kraft, 1966)

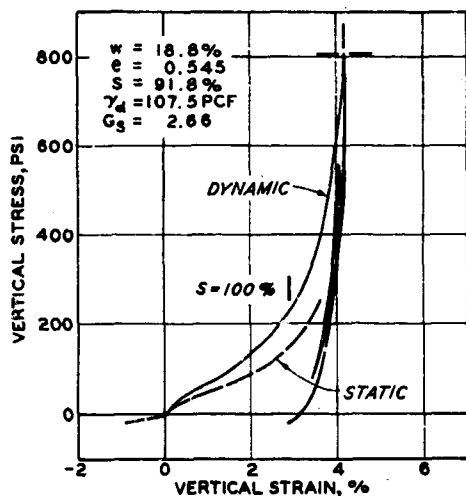


Fig. 4.31 Static and dynamic one-dimensional stress-strain curves for undisturbed sample of till (from Jackson, 1968)

effects may be observed if results from a rapid (and hence undrained) loading are compared with results from a slow loading during which drainage occurs.

from a static undrained loading test and a test with a rise time of about 10 msec. At a given stress, the strains during rapid loading are from 20 to 50% smaller than those achieved by a slow undrained loading. Fig. 4.32 illustrates creep in natural soils following a rapid loading (compare with fig. 4.21).

Of course very large time-dependent

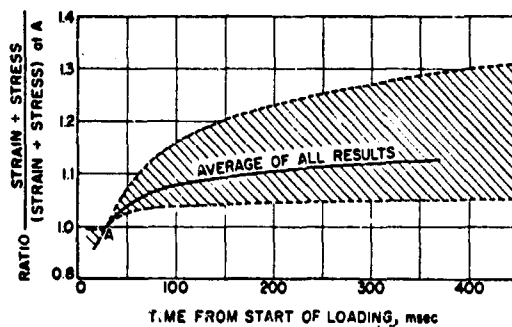


Fig. 4.32 Creep during one-dimensional compression of natural soils (from Report 17)

Other effects: Other phenomena observed in dry granular soils and discussed in section 4.3.2 are also found to similar degree in natural soils: behavior during unloading and reloading, energy loss during repeated loadings, lateral stresses, etc. Hendron and Davisson (1964) show that the ratio of lateral to axial stress increases significantly as the degree of saturation approaches 100%.

4.4 EVALUATION OF CONSTRAINED MODULUS

As discussed in Chapter 2 and as noted in the introduction to this chapter, the single most important stress-strain parameter for ground motion predictions is constrained modulus. Unless a reasonably accurate estimate can be made for the ratio of peak stress to peak strain, no method of ground motion prediction--however sophisticated--can give accurate predictions.

At the present time, the most practical and versatile tool for evaluating constrained modulus for blast loading conditions is the oedometer test as described in this chapter. However, the discussion in section 4.3 has shown that modulus, in addition to being a function of both initial stress and stress change, is also affected by many other details of the test procedure. Moreover, the applicability of modulus as measured in the laboratory is seriously affected by the quality of the sample. Hence, it generally is best to supplement such results with those from other types of tests. In situ measurements of dilatational wave velocity and resonant column tests on undisturbed samples are useful for establishing an upper bound for the stiffness of the soil. Plate bearing tests may also be useful. In short, the engineer should use every means at his disposal to obtain quantitative measures of the stiffness of the soil, and then must apply his judgment in selecting the most suitable value.

There is, of course, considerable experience in the selection of a suitable value of constrained modulus for use in prediction of settlements under static loads.* For the more compressible soils, where average strains under static loading exceed 1%, there has been reasonably good success in

* The use and abuse of constrained modulus (or compressibility) with regard to settlement estimates are discussed in Lambe and Whitman (1968).

the prediction of settlement on the basis of a modulus (or compressibility) from oedometer tests on undisturbed samples, provided of course that good sampling and testing techniques were employed. Based on an analysis of some 20 cases in which a comparison of predicted and observed settlements has been made, the average expected error is about 20% and an overestimate is as likely as an underestimate. For less compressible soils, where average strains fall between 0.1 and 1.0%, there has been less success. The average expected error would appear to be 30% or greater, and there is a consistent tendency to overestimate the settlement. For the very stiff soils, predictions of settlement based on laboratory oedometer tests generally are much greater--usually several times or even an order of magnitude greater--than observed settlements. In all cases, even those involving rock, observed settlements exceeded those predicted using a modulus derived from in situ seismic level dilatational velocity. For the stiffer materials, modulus derived from the second or later cycle of a repeated-loading plate bearing test has often been found to lead to reasonably accurate settlement predictions.

From this experience with static settlement predictions, it should be expected that no one single rule can be used for selecting constrained modulus for use in blast loading problems.

4.4.1 Recommended Procedures in Case of Compressible Soils. Three types of modulus determinations should be made: (a) in situ measurement of seismic level dilatational wave velocity; (b) measurement of wave velocity (in resonant column tests or by pulse techniques) in the laboratory using good undisturbed samples reconsolidated to the in situ effective stress; and (c) oedometer tests on good undisturbed samples, using apparatus and techniques which minimize seating and testing errors. Tests (a) and (b) are both aimed at establishing modulus for the case in which the stress increment is smaller than the initial effective stress. Young's modulus as computed from a rod velocity must be corrected into a corresponding constrained modulus using either an assumed value of Poisson's ratio or a value of Poisson's ratio deduced by comparing shear and rod wave velocities as measured in laboratory tests or shear and dilatational velocities as measured in situ. Test (c) provides values of secant modulus, evaluated

starting from an initial consolidation stress, generally determined from the initial loading. The program of oedometer tests must include stress increments spanning the range of stress increments expected in the actual problem. If the soil deposit is uniform, samples may come from only one depth, but various samples must then be consolidated under various effective stresses typical of the depths of interest. Alternatively, samples may be taken from various depths and then placed under the total stress existing at that depth.

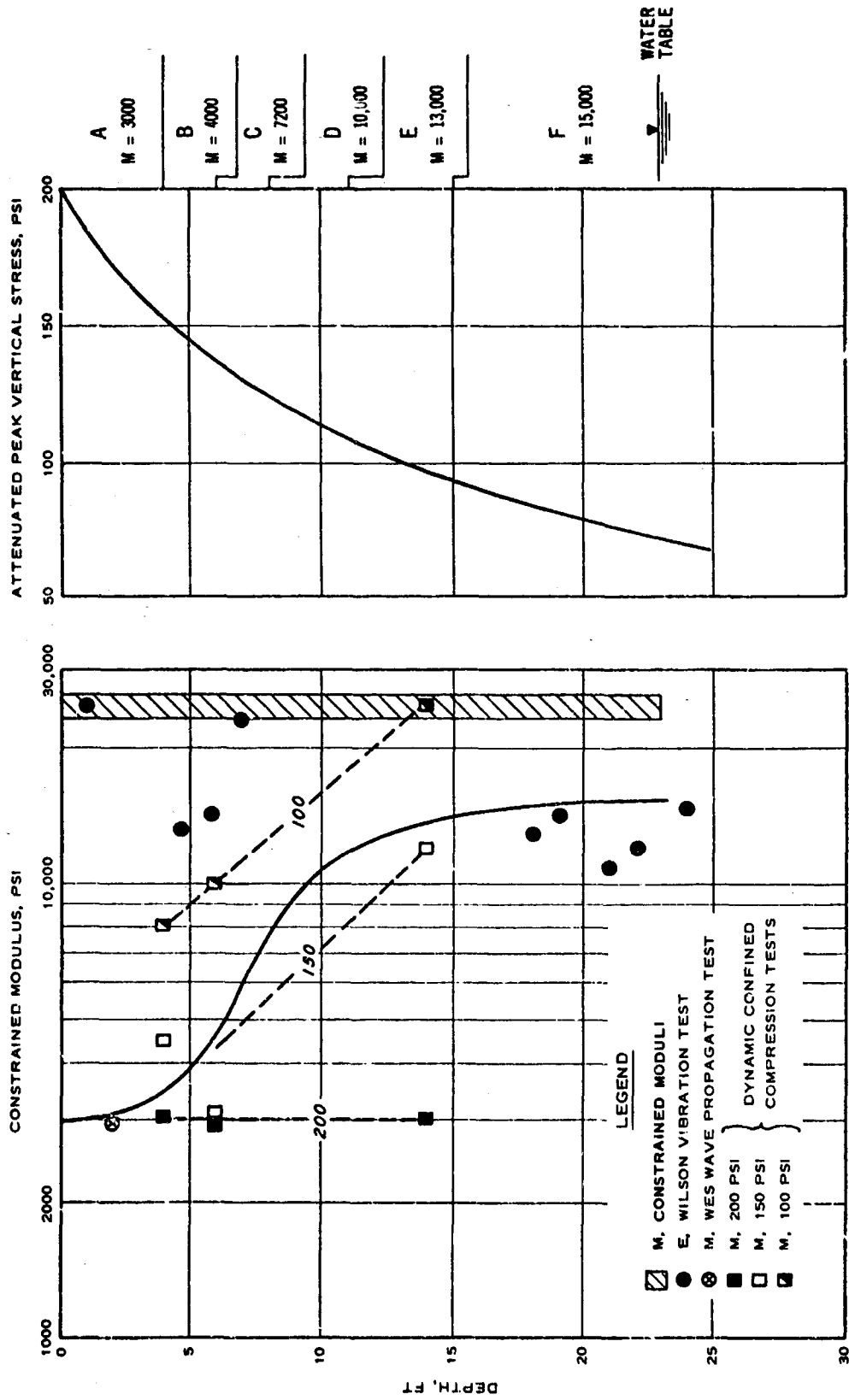
Fig. 4.33a shows a set of results from such a program of tests. The constrained moduli as deduced from the in situ dilatational and laboratory rod velocities do not agree exactly, either because of difference in the magnitude of the dynamic stress or because of testing, measurement, and disturbance errors in one or both procedures. Below the 15-ft depth, the secant constrained modulus as measured in oedometer tests with a stress increment of 100 psi is similar to the constrained modulus for small stress increments. At shallower depth and for larger stress increments, modulus from the oedometer tests is definitely less than that measured using small stress increments.

To use such results, it is necessary to estimate the peak vertical stress as a function of depth. A typical curve applying for a problem involving a large HE detonation is shown in fig. 4.33b. The solid curve in fig. 4.33a shows the estimated variation of effective modulus with depth (Hendron, 1965). This approach generally follows that suggested earlier by Wilson and Sibley (1962).

4.4.2 Experimental Verification of Procedure for Selecting Modulus.

The validity of modulus values selected according to these procedures is best checked by comparing peak vertical stress with peak vertical particle velocity, using Equation 2.4. This comparison is best made right at the loaded surface of a soil deposit or column of soil, because the peak stress is known with greatest certainty at the surface. The comparison may be made at depth provided that there are satisfactory measurements of the stress increment at depth.

Laboratory tests: Table 4.1 summarizes comparisons between particle velocities observed at the top of the soil column shown in fig. 4.11, using



(a)

(b)

Fig. 4.33 Constrained moduli-peak attenuated vertical stress-depth relations, WES 250-ft station, Operation Snowball

Table 4.1
Comparison of Predicted and Observed Particle
Velocities in Laboratory Tests

Soil*	w %	Peak	Effective	$(\dot{w})_{\max}$, cm/sec		Ratio of Observed to Predicted (\dot{w})
		σ_v psi	C_D m/sec	Predicted	Observed	
1. Kaolinite	32	37	80	181	130	0.72
2. Kaolinite	19	75	230	133	116	0.87
3. Vicksburg clay	27	84	270	126	110	0.87
4. Vicksburg clay	24	162	330	182	140	0.77
5. Sand	0	67	360	79	40	0.51
6. Sand	0	127	370	145	175	1.21

* Data for soils 1 through 5 from Seaman (1966); data for soil 6 from Seaman and Whitman (1964). Data for all except soil 5 were obtained about 15 cm below the surface; data for soil 5 were obtained about 60 cm below the surface.

a falling weight to apply dynamic loads, with particle velocities predicted using constrained moduli evaluated in the device shown in fig. 4.7. The modulus used for the predictions was the secant modulus to the peak stress, for a sample initially under the static stress at the depth of the measuring gage. The best and most complete data are for soil 3, for which the error between predicted and observed values is 13%. Larger errors, with the observed value generally being less than the predicted value, occurred for the other soils. There were a number of experimental difficulties in these tests, including the measurement of both stress and particle velocity, and some of these difficulties would tend to make the measured velocity systematically less than the predicted velocity. However, the results justify the conclusion that the peak particle velocity can be predicted within about 30%.

Field observations: Table 4.2 presents results applicable to the playa silt at the Frenchman Flat, Nevada, test site of the Atomic Energy Commission. The first line of values in the table gives the modulus determined principally from measurements of peak vertical particle velocity a

Table 4.2
Constrained Modulus for Frenchman Flat Silt

	Constrained	
	Modulus, $\text{psi} \times 10^{-3}$	
	Depth, 0-60 ft	Depth, >60 ft
Deduced from observed ground motions	14	80
Calculated from seismic velocity	35	150
Measured by dynamic one-dimensional compression tests	10	20 (initial loading)
Calculated from modulus measured in triaxial tests*	8	15 (initial loading)
	40	65 (reloading)
Calculated from resonant column test*	40	110
Calculated from plate bearing tests*	8	-- (initial loading)

* Using Poisson's ratio of 0.3.

few feet below the surface. The remaining lines give values of modulus as deduced from various field and laboratory tests. The moduli determined from in situ and laboratory wave propagation measurements at small strains are definitely greater than the secant in situ modulus under blast loading conditions. For the shallow, more compressible layers, the moduli found from the initial loading in oedometer tests, triaxial tests, and plate bearing tests were not far different from the actual secant modulus. However, these same tests badly underestimated the compression resistance of the deep, less compressible silt. For this deeper silt, the reloading modulus is in reasonably good agreement with the observed in situ behavior. Subsequent tests on the deeper silt, using improved sampling and testing, have indicated that there really is better agreement between the modulus during the initial loading in an oedometer test and the in situ modulus (Hendron and Davisson, 1964). Wilson and Sibley (1962) have also discussed motion predictions for this site.

A second comparison between particle velocities as predicted using results from oedometer tests and particle velocities observed in field

tests is described by Zaccor (1967). In this case the soil was a desert alluvium and the peak surface stress, resulting from explosion of an array of primacord, was about 300 psi. The upper 8 ft of the soil was quite compressible, with a secant modulus of about 3000 psi. Below this depth the secant modulus increased to over 7000 psi. The ratio of observed to predicted peak surface vertical particle velocity, using the secant modulus for the upper 8 ft of soil, was from 0.55 to 0.61. The effect of reflections from the interface at the 8-ft depth was not taken into account when computing the theoretical particle velocity. These reflections would tend to decrease the particle velocity, and the ratio of observed to true predicted velocity is probably more like 0.7.

A third comparison is provided by measurements of particle velocity during Operation Snowball at the Suffield Experimental Station in Canada (Murrell, 1967). The soil is a lacustrine deposit consisting of fairly uniform beds of clays and silts with occasional sand lenses. Data concerning the compressibility of the soil have already been given in fig. 4.33. The airblast loading, caused by a large chemical explosion, was from 200 to 300 psi at the location of the measuring gages. Vertical particle velocities were measured at a depth of 5 ft where the peak stress was about 40% of the peak overpressure at the surface. At this depth, the predicted and observed particle velocities agreed almost exactly, and the predicted and observed peak vertical displacements agreed within 10% (Hendron, 1965).

Summary: While it is clear from these examples that the evaluation of the effective modulus or effective wave velocity is far from an exact science, it also is clear that the suggested procedures based on oedometer tests provide reasonable estimates for many engineering purposes--at least for the more compressible soils. It appears possible to estimate the effective wave velocity to within about 30% and the effective modulus to within about a factor of 2, assuming of course that good sampling and testing techniques are employed.

4.4.3 Recommended Procedures in Case of Stiff Soil. As of this writing, there is little or no direct experience with blast loadings directly over stiffer soils. However, experience with static loadings makes it clear that sampling disturbance makes unlikely accurate evaluation

of modulus in soils having an effective modulus greater than 25,000 psi. There is some reason to believe that, because of compensating errors, the modulus determined during reloading cycles in a laboratory oedometer test may be approximately the same as the in situ modulus. Table 4.3 illustrates the differences which may be expected between modulus as deduced from seismic level wave velocity and as measured in the laboratory.

The following examples illustrate the thought processes involved in choosing the most suitable value for use in calculations concerning blast-induced ground motions. The first two examples arose in 1959, at a time when neither concepts nor testing techniques were as well developed as they are today. The final example is more recent (1962).

A deep silt-clay deposit: This example involves a more or less uniform deposit of silty-clayey material which extends to depths greater than 1000 ft. All of the top 1000 ft of the material is above the water table. This material was laid down in a series of shallow lakes which existed over a period of many, many years. There never has been more overburden than there is at the present time.

The following quantitative information was gathered concerning the material between the 60- and 200-ft depths.

Standard penetration resistance: 50 blows/ft

Shear strength (from unconsolidated-undrained tests with chamber pressure equal to overburden pressure): 2 to 3 tsf

Constrained modulus (slow initial loading): 10,000 to 40,000 psi

Young's modulus from resonant column test: 50,000 psi

Modulus from seismic dilatational velocity: 160,000 psi

The one-dimensional compression tests were relatively crude, and some juggling of the results was necessary to come up with a value for constrained modulus. The range of values above indicates the spread of the results obtained by applying different corrections to the data. If Poisson's ratio is taken to be 0.35, the Young's modulus from the vibration tests would correspond to a constrained modulus of 80,000 psi. Incidentally laboratory determinations indicated that the soil was nearly saturated, and possibly

Table 4.3

Results from One-Dimensional Compression Tests on Partially Saturated Soils

Description of Soil	Dry Unit Weight pcf	Degree of Satura- tion, %	Initial Stress psi	Stress Increment psi	Secant Modulus (psi $\times 10^{-3}$)				From Velocity
					1st Loading "Fast"	"Slow"	5th Loading "Fast"	"Slow"	
Boulder clay, unweathered	113	82	75	125	25	15	80	50	1200
Boulder clay, weathered	110	94	10	100,200	10	8	20	14	450
Weakly cemented sand									
Unweathered	122	72	135	50,165	120	60	135	95	650
Slightly weathered	106	71	40	100,260	45	21	55	32	220
Weathered	107	83	10	100,290	20	12	25	15	150
Weakly cemented clayey silt	80	94	30	30,100,270	15	11	30	25	220

Note: Fast modulus = stress + strain at end of rapid pressure rise.
 Slow modulus = stress + strain after 3 min.

fully saturated. At that time, the hydrostatic compression test had not yet been developed as a means for testing for complete saturation, and it was necessary to make the conservative assumption that saturation was not complete.

The question, then, was whether the constrained modulus under blast loading conditions would be more like the 10,000 to 40,000 psi indicated by laboratory compression tests, or the 80,000 to 160,000 psi suggested by the measurements involving small stress increments. The standard penetration results and the shear strength values were suggestive of a soil-like material. Moreover, in all of the rather extensive literature concerning this deposit, geologists described the material as uncemented, poorly consolidated, etc. Boreholes, if uncased, suffered from sloughing or squeezing.

These various observations suggested that this earth material would tend to compress significantly under the large stresses imposed by blast loadings. Hence a constrained modulus of 40,000 psi was selected for this material.

Site involving sandstones and shales: These materials were formed by outwash from nearby mountains, and there never had been more overburden than there is at the present. However, the geologists' reports spoke of these materials as being cemented and well consolidated. The following data were obtained for the material at the 100-ft depth.

Standard penetration resistance: 200 blows/ft

Shear strength (unconfined and unconsolidated-undrained tests):
10 to 40 tsf

Constrained modulus (slow initial loading): 30,000 to 200,000 psi

Modulus from seismic dilatational velocity: 1,000,000 psi

Again the one-dimensional compression tests were crude, and the results subject to interpretation.

There was every reason to feel that the appropriate constrained modulus for this material would be much higher than that of the clayey-silty material described in the preceding example, and would indeed approach 1,000,000 psi. A modulus of 300,000 psi was actually selected. This value

was probably conservative, but nonetheless led to predicted ground motions which could be tolerated economically. Subsequent experience has indicated that the constrained modulus of the material is at least 400,000 psi.

Weakly cemented sandstone: This material, which would readily crumble in one's hand, was likewise formed as an outwash deposit and has never been preloaded by since-eroded material. Careful one-dimensional compression tests, using very rapid loadings, were performed. The data obtained are as follows.

Constrained modulus (rapid initial loading): 83,000 psi

Constrained modulus (rapid reloading): 93,000 psi

Constrained modulus (slow reloading): 65,000 psi

Modulus from seismic dilatational velocity: 640,000 psi

The writer recommended a value of 80,000 psi for this material, but now believes that 100,000 psi would be a more realistic value.

4.5 EVALUATION OF OTHER PARAMETERS

For some calculations, especially for purposes of research into the attenuation of stress with depth, it is necessary to make quantitative estimates for the ratio of elastic to total strain in an irreversible model for soil or of time constants in a viscoelastic model of soil. An initial discussion of methods for evaluating such parameters appears in Report 17 and in Whitman (1963), and a more detailed discussion has been given by Seaman (1966). Some typical values of various parameters are:

Ratio of modulus for unloading to modulus for loading: 1.3 to 3

Ratio of imaginary to real parts of complex modulus: 0.1 to 0.4

Ratio of M_0 to M_1 in standard three-element viscoelastic model (see fig. 2.41): 1 to 4

Time constant $1/\mu M_0$ in standard three-element viscoelastic model:
10 to 30 msec up to $1/4$ or $1/2$ sec, depending on the rise time of interest

Results such as these are satisfactory for calculations aimed at

establishing the general importance of irreversible or time-dependent effects, but clearly much more research is needed concerning the magnitude of these parameters. Some additional data are provided by Kondner and Ho (1964).

4.6 SUMMARY AND RECOMMENDATIONS

4.6.1 Summary of Results.

- (a) Reasonably simple test apparatus and procedures have been developed for studying one-dimensional compressibility during blast loading conditions.
- (b) The many factors affecting the one-dimensional compressibility of soil have been identified.
- (c) In one-dimensional compression, soil has an S-shaped stress-strain curve, with yielding behavior at small stress increments and stiffening behavior for large stress increments. For stress increments in the range of 100 to 500 psi, the secant modulus generally is less than the modulus corresponding to seismic level dilatational wave velocity.
- (d) Only a portion of the strain which occurs during loading is recovered upon unloading, and hence energy is lost during a cycle of loading and unloading.
- (e) Stress-strain properties are somewhat time-dependent. A loading with approximately the correct rise time must be used when measuring effective modulus.
- (f) For soils with a modulus below 10,000 or possibly 20,000 psi, the effective modulus under blast loading conditions can be measured in oedometer tests on undisturbed samples.
- (g) For stiffer soils, laboratory measurement of modulus is more difficult and considerable care must be taken to minimize sample disturbance. Such disturbance generally leads to moduli that are too low, and considerable judgment must be exercised in choosing a value of modulus for use in calculations. The modulus from the second or third cycle of loading is a particularly useful guide.

4.6.2 Present Status of Work. A great deal is now known concerning

wave propagation through soil. In sands, inelastic effects are quite important, but time-dependent effects can be largely ignored provided that the stress-strain relation is obtained from a test in which loading and unloading take place in 30 msec or less. In cohesive soils, time-dependent effects may be important during loadings with durations less than 30 msec. A really satisfactory description of the time effects in cohesive soils is still lacking.

For the more compressible soils, it appears that a laboratory dynamic compression test using repeated loadings provides a satisfactory measure of in situ dynamic compressibility. However, for the stiffer earth materials (those approaching the consistency of soft rocks) there are no field data concerning in situ compressibility and hence no basis for judging the reliability of the results of laboratory tests.

4.6.3 Suggestions for Future Research. The most pressing need is for field tests to evaluate in situ dynamic compressibility. Indeed, additional laboratory research will tend to be meaningless unless such field tests are performed.

On the basic research front, there is need for more adequate study of time-dependent effects during one-dimensional compression, using stress changes as large as several hundred psi.

CHAPTER 5 PROPAGATION VELOCITY FOR STRESS WAVES OF LOW INTENSITY

5.1 INTRODUCTION

Measurement of in situ wave velocities at seismic stress intensities (low) offers the easiest and most economical method for investigating the characteristics of a large construction site. By observing the variation of seismic velocity with depth, these measurements can be used to establish qualitative features of a site, such as the depth to the water table or the depth to rock. To the extent that the magnitude of the measured velocity can be related to the stiffness of the soil at the stress level of interest, such measurements can be used quantitatively as a basis for predicting the settlement of structures or the response of structures to dynamic loadings.

The methods which are commonly used for measuring wave velocities in situ usually involve stress waves of low intensity. That is, once away from the immediate source of the wave, the stresses caused by passage of the wave are 1 psi or less--usually much less. Since soil is a very non-linear material, the velocity of a low-intensity wave will directly indicate only the stiffness of the soil for small stress changes from the initial in situ state of stress. This velocity will tend to overestimate the stiffness for larger stress changes, as has been discussed in Chapter 4. The velocity of low-intensity waves may have direct quantitative use for problems such as foundation vibrations and the ground motions caused by earthquakes. However, the velocity of low-intensity waves can only be of indirect value for problems such as the propagation of blast waves and ordinary static settlements.

This chapter discusses the various factors which influence the magnitude of wave velocities through soil, and describes the laboratory procedures and devices which have been used to investigate the influence of these factors. The laboratory techniques have some practical value as well. The methods for measuring shear wave velocity in situ are still expensive and not entirely foolproof, so that sometimes it may be more convenient to make laboratory measurements of shear wave velocity. Check tests in the field generally will be desirable, however.

5.1.1 Relation Between Wave Velocity and Modulus. Elastic theory provides the following relation between modulus and the velocity of wave propagation:

$$C = \sqrt{\frac{M}{\rho}} \quad (5.1)$$

where

C is the wave velocity, in units such as feet per second

M is the modulus, the ratio of stress to strain for the particular type of deformation involved in the wave, in units such as pounds per square foot

ρ is the mass density equal to the unit weight divided by the acceleration of gravity, in units such as pound-seconds²/feet⁴

For many soils, ρ has a value of about 3.5 lb-sec²/ft⁴. Thus a modulus of 25,000 psi (3,600,000 psf or 1800 tsf) corresponds to a wave velocity of about 1000 fps. This is a useful relation to remember, since other combinations of velocity and modulus can readily be obtained by recalling that velocity varies as the square root of the modulus.

5.1.2 Types of Waves. There are a number of different types of waves, each corresponding to a different type of motion or deformation and each having its own wave velocity. Fig. 5.1 shows the waves which will be

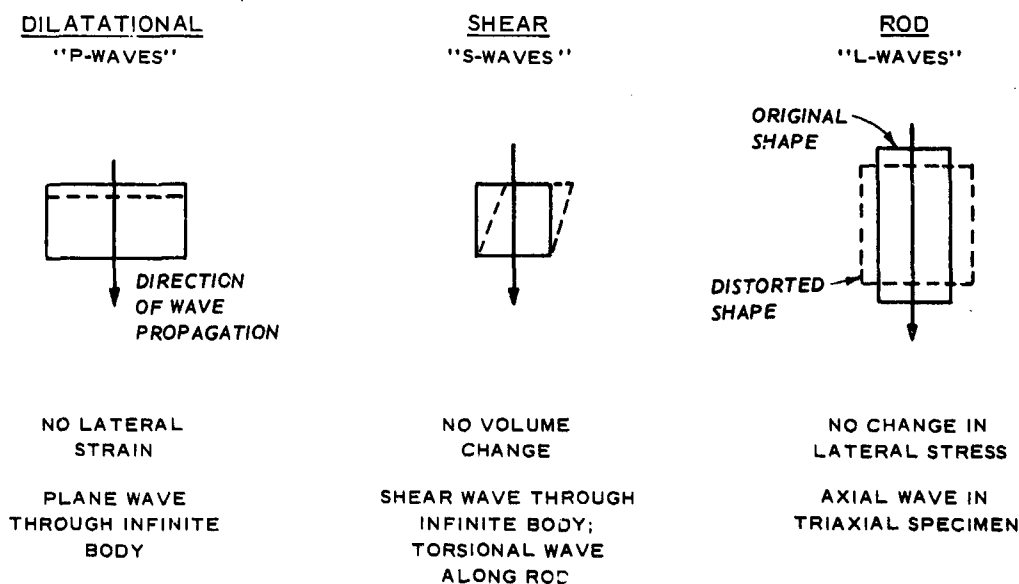


Fig. 5.1 One-dimensional waves

of the greatest concern in this chapter.

Dilatational and shear waves appear in the classical theory of elasticity. Both of these wave forms occur at a plane wave front moving through an infinite elastic body. A dilatational wave involves motions perpendicular to the wave front, while a shear wave involves motions parallel to the wave front. The strain conditions associated with the dilatational wave also occur at the very front of a wave spreading out from a point within an infinite medium (i.e. a spherical wave front), but behind the wave front the strain conditions are more complicated than those of the classical dilatational wave.

A rod wave is a special form of compression wave which appears only for a particular boundary condition. Unlike a dilatational wave, a rod wave does involve strains in the direction transverse to the wave front. A rod wave appears only in laboratory tests which are the dynamic counterpart of static triaxial tests with constant confining stress.

There are special types of wave motion associated with any boundary of an elastic body. For example, the free top surface of an elastic half-space gives rise to several types of surface waves: waves which run along this surface and which cause motions of the material down to certain depths below the surface. Of these, the most important is the Rayleigh wave. This wave, which involves simultaneous vertical and horizontal motions in a vertical plane normal to the wave front, is formed by dilatational and shear waves interacting with a free surface.

These various types of waves will develop in any type of material. In an elastic material, there are definite relations between the propagation velocities of the four waves.

The propagation velocities of dilatational, shear, and rod waves can be obtained using Equation 5.1 together with the modulus appropriate to the type of deformation involved in the wave:

Constrained modulus for dilatational wave velocity C_D

Shear modulus for shear wave velocity C_S

Young's modulus for rod wave velocity C_L

Each of these velocities can be expressed in terms of either the shear modulus G or Young's modulus E , together with Poisson's ratio μ . These various equations are given in fig. 5.2.

SHEAR VELOCITY:

$$C_s = \sqrt{\frac{G}{\rho}} = \sqrt{\frac{E}{\rho 2(1+\mu)}}$$

ROD VELOCITY:

$$C_L = \sqrt{\frac{G}{\rho} 2(1+\mu)} = \sqrt{\frac{E}{\rho}}$$

DILATATIONAL VELOCITY:

$$C_D = \sqrt{\frac{G}{\rho} \frac{2(1-\mu)}{1-2\mu}} = \sqrt{\frac{E}{\rho} \frac{(1-\mu)}{(1-2\mu)(1+\mu)}}$$

Fig. 5.2 Equations for elastic wave velocities

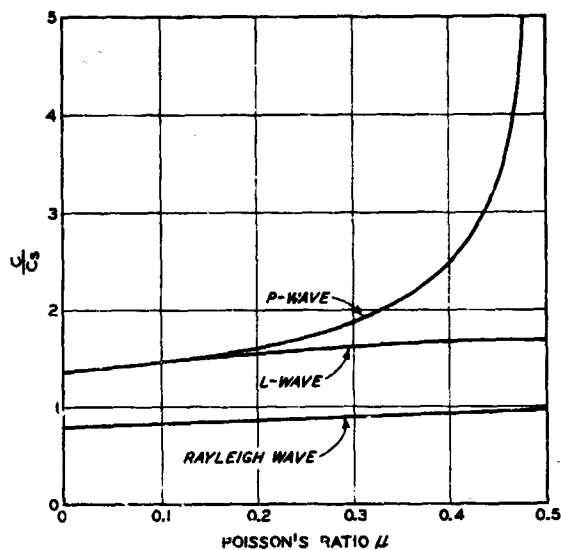


Fig. 5.3 Relation between elastic wave velocities

There is no simple equation for the velocity of Rayleigh waves; the velocity of these waves comes from the solution of a transcendental equation.

Fig. 5.3 gives values of the dilatational, rod, and Rayleigh wave velocities in ratio to the shear wave velocity, for the full range of values of Poisson's ratio applicable to an elastic material. Note that the difference between the shear and Rayleigh wave velocities is quite small, especially for $\mu \geq 0.25$.

Note also that the ratio of dilatational to shear wave velocities becomes infinitely large as μ approaches 0.5.

5.2 TESTS FOR MEASURING WAVE VELOCITIES IN THE LABORATORY

5.2.1 Resonant Column Test. The oldest and most common technique for measuring wave velocities through soil in the laboratory is to vary the frequency with which forces are applied to a cylindrical specimen of soil until a resonance condition is obtained. The desired velocity is then calculated from a relation between velocity, length of the specimen, and frequency at resonance. The theory used to interpret the results of such tests has been described by Lee (1963) and by Hardin (1965). This method

has been used by Wilson and Dietrich (1960), Hardin and Richart (1963), and Stevens (1966a). Drnevich et al. (1966) describe a version of the test using hollow cylindrical specimens; this version is useful for studying the effect of strain upon the observed results.

The method is very versatile. By applying longitudinal forces to the cylindrical specimen, the rod velocity can be measured. Shear wave velocities can be measured by applying torsional moments. The effects of confining stress and amplitude of motion on wave velocity can be studied. By exciting a series of higher order resonances, the relation between wave velocity and frequency can be established. This test also permits study of the damping properties of soils.

5.2.2 Pulse Technique. An alternate technique for measuring wave velocity through soil has been developed at MIT as part of the present contract. This technique is based on a method which the writer first observed at the Shell Research and Development Laboratories in Houston, Texas.

Measurement of dilatational wave velocity: Figs. 5.4 and 5.5 show the essential features of the apparatus as initially developed at MIT (see Reports 8 and 14).

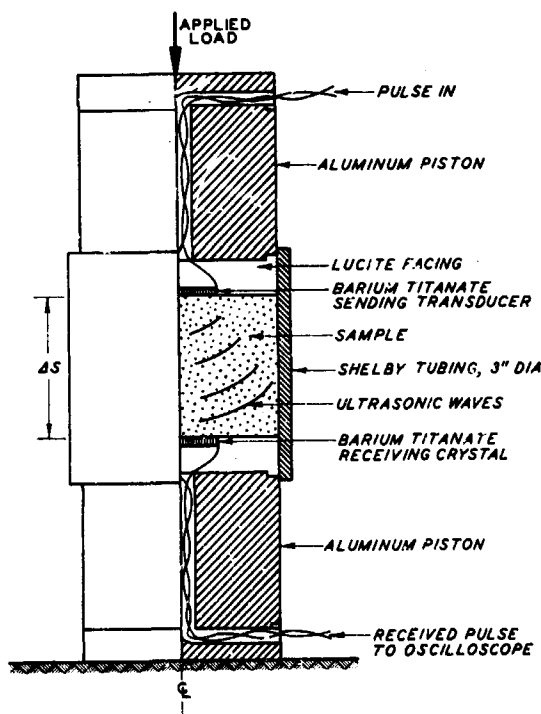


Fig. 5.4 Soil container and crystals for pulse test

An electric pulse is sent to a piezoelectric crystal placed at one end of a specimen of soil. This electric pulse causes the crystal to suddenly change in thickness, thus generating a mechanical wave within the soil. This wave passes through the soil until it encounters a second crystal placed on the other end of the specimen. The arriving wave causes stresses within this second crystal, and thus a new electric signal is generated. The wave velocity is determined by measuring the time lapse (travel time) between

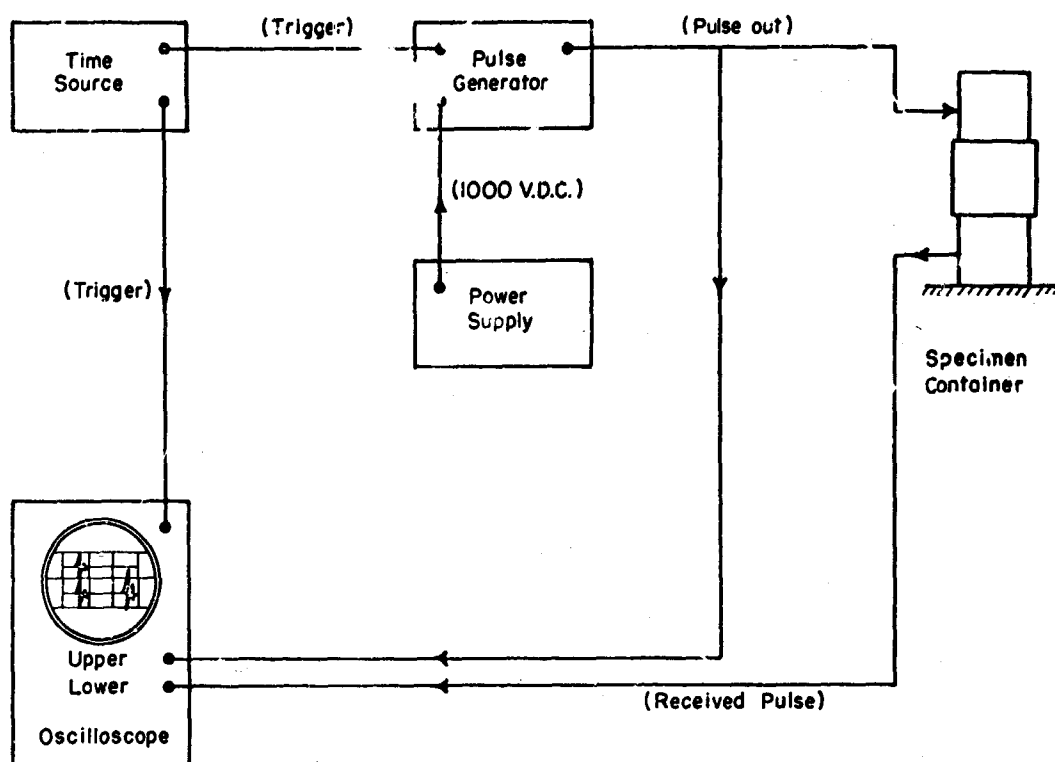


Fig. 5.5 Circuit diagram for pulse test apparatus

the start of the original and received electric signals, and dividing this time lapse into the thickness of the specimen.

The input electrical signal involves two or three cycles of voltage with a frequency of about 1 megacycle. The wave resulting from the electric signal passes back and forth through the specimen and dies out within about 1 or 2 msec. The input electric signal is repeated 50 times per second; i.e. every 20 msec. Thus there really is a succession of waves, each an independent event. By displaying the received signal on the screen of an oscilloscope, a standing wave form is obtained from which the travel time can be measured. Fig. 5.6 shows a typical result.

In the original version of the MIT device, the soil was confined by a metal jacket. When undisturbed samples were being tested, the soil was simply left in the sampling tube. Axial stresses were applied by means of a hydraulic jack so as to simulate the effects of overburden. More recently (see Report 24) the specimen has been placed within a triaxial cell, using a pedestal and top cap containing the piezoelectric crystals.

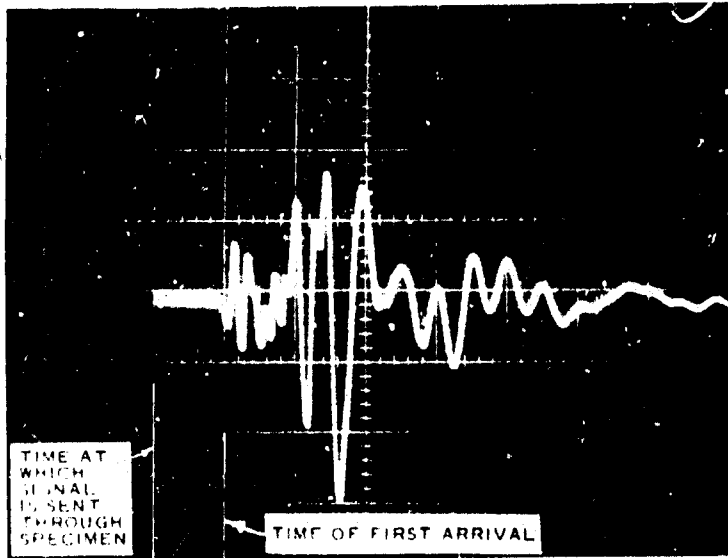


Fig. 5.6 Photograph of oscilloscope screen showing arrival of dilatational wave. This photograph shows output of receiving crystal versus time. The trace sweeps from left to right

electric signal. The twelve sending crystals are all simultaneously subjected to such a signal and thus impart a twist to the specimen. The reverse procedure causes the twelve receiving crystals to generate an electric signal when the mechanical wave through the soil reaches them. Fig. 5.9 shows a typical received signal. Report 23 describes the development of this apparatus.

This type of test is carried out within a triaxial cell similar to that shown in fig. 5.7.

Fig. 5.7 Triaxial cell for velocity measurements by pulse technique

Fig. 5.7 shows this arrangement; the tube appearing in the photograph contains the electrical leads to the top cap.

Measurement of shear wave velocity: In order to measure shear wave velocity, twelve piezoelectric crystals are placed at each end of a specimen as shown in fig. 5.8. These crystals have been manufactured in such a way that they will undergo a shear distortion when subjected to a sudden

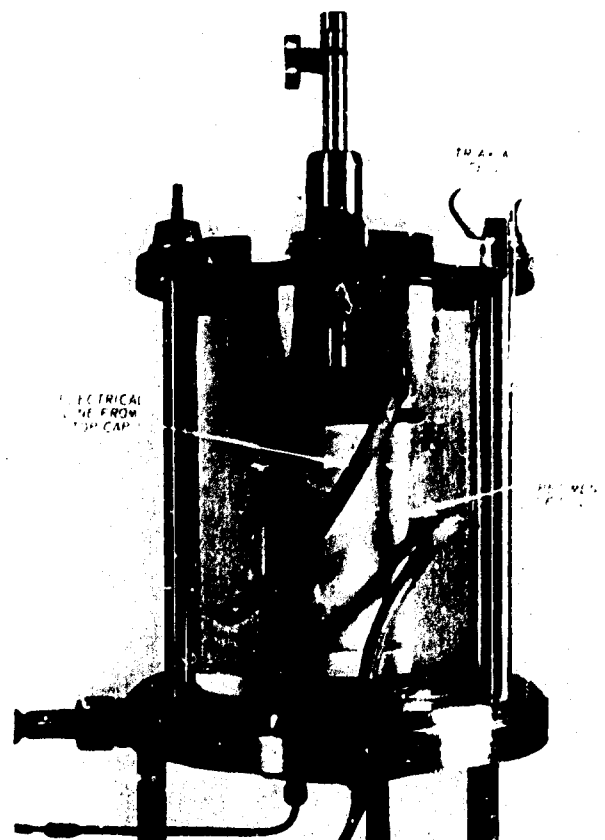




Fig. 5.8 End cap with radial crystals for sending and receiving shear wave

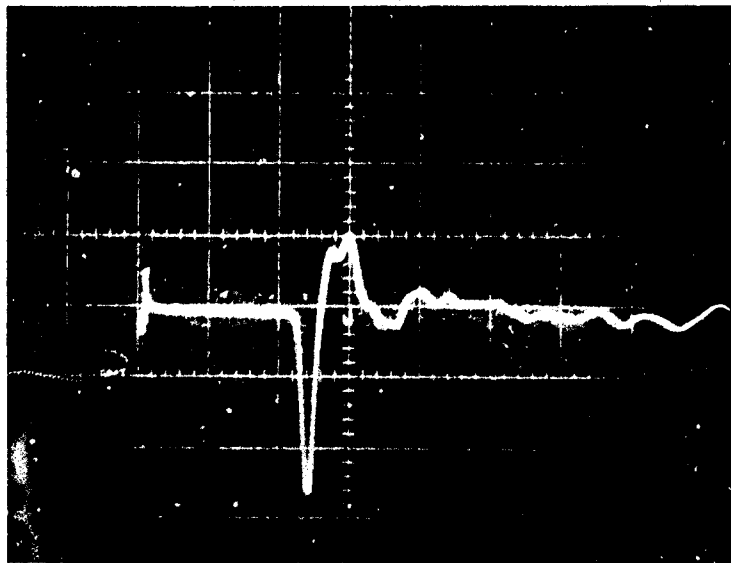


Fig. 5.9 Photograph of oscilloscope screen showing arrival of shear wave

Interpretation of received signal: There are two main difficulties in the interpretation of the results of a pulse test.

First, the wave patterns within the soil specimen are very complex. The wave spreads out from the sending crystal, and reflects off the sides of the specimen as well as the far end of the specimen. Some energy may reach the receiving crystal by traveling through a metal jacket if such a jacket is used to confine the specimen. It is necessary to establish test conditions such that the first detectable arrival at the receiving crystal will be a wave running directly along the axis of the specimen.

Second, there is always some ambiguity as to the time of the first arrival of energy at the receiving crystals. The received wave form seldom has a sharp front, and often there is an arrival of small amplitude prior to the first obviously noticeable arrival.

These difficulties have an important bearing on the permissible size of test specimens and on the way in which the specimens should be confined.

There are two reasons why the specimen must not be too long. (a) The energy in the initial dilatational wave front decreases with distance, and if the sample is too long this first arrival may cease to be detectable. (b) If the specimen is too long, a wave traveling at a higher velocity but through a roundabout path (as through a metal jacket) may arrive at the receiving crystal before the wave passing only through the soil.

There are also two reasons why the specimen must not be too short. (a) The time of the first arrival at the receiving crystal can seldom be pinpointed precisely. If the specimen is very short so that the travel time is very small, the potential error in measuring the travel time will be a large fraction of the travel time. The potential percentage error decreases as the specimen thickness increases. (b) Because soil is composed of many individual particles, a high-frequency wave is dispersed as it travels through soil. This dispersion causes certain difficulties in the interpretation of the received signal and in selecting a meaningful arrival time. These difficulties, which are discussed in detail in Report 25, decrease in importance as the thickness of the specimen increases. For granular soils, the thickness should be at least 200 times the diameter of the most typical particle.

For tests in which confinement is provided by a metal cylinder (fig. 5.4), the optimum specimen length has proved to be 2 in. For tests conducted within a triaxial cell (fig. 5.7), lengths up to 4 in. have been used successfully provided that gas and not liquid is used for the chamber fluid. (Stress waves propagating through a liquid surrounding a long specimen may reach the receiving crystal first.)

These procedures will still leave some ambiguity as to the exact time of the first arrival at the receiving crystal. At the present time, the experimental error arising from these problems can be held to $\pm 5\%$.

Advantages and disadvantages of the pulse technique: Aside from the standard electronic units (oscillator and oscilloscopes), the apparatus needed for the pulse test consists only of the two end caps containing piezoelectric crystals. Tests can be conducted within ordinary triaxial cells after only a minimum of modification. The pulse test is the one laboratory test that gives directly the dilatational wave velocity, which is the type of velocity most commonly measured in situ.

The pulse test is not adaptable for study of the influence of stress increment and frequency on wave velocity, and is not suitable for studying the type of damping which is usually of interest to civil engineers. Further work is necessary to improve the operational reliability of the test apparatus.

5.2.3 Other Tests. Whereas the tests described in section 5.2.1 employed forced vibrations, Zeevaert (1967) and others have determined shear wave velocity in the laboratory using free vibrations.

A large mass is placed on a cylindrical specimen of soil. This creates a single-degree-of-freedom system, with the stiffness provided by the soil and the inertia provided by the mass. The mass is given an initial rotation and released. The shear modulus (and thence velocity) of the soil is computed from the observed period of the resulting free vibrations, using the formula for the natural period of a single-degree-of-freedom system. The mass is supported in part by a counterweight, so that the mass does not induce large static stresses in the soil. The specimen can be placed within a triaxial cell.

This is the simplest of all the tests that can be used to determine

shear wave velocity, but the results obtained with it still appear to be somewhat crude.

5.3 WAVE VELOCITIES THROUGH DRY GRANULAR SOILS

With dry soils, the three types of waves found in laboratory tests (dilatational, rod, and shear) are all transmitted via the same basic mechanism and all are affected

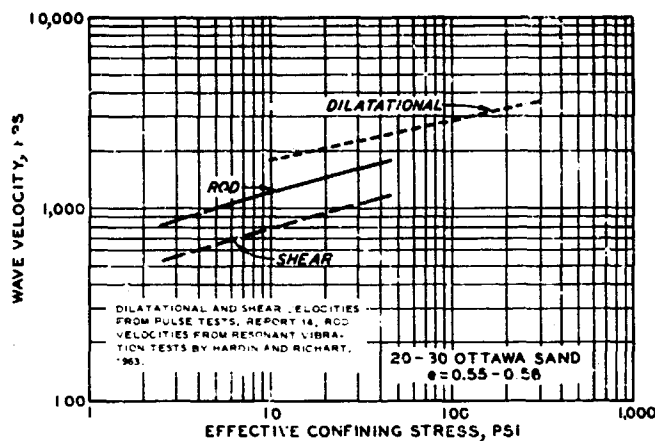


Fig. 5.10 Comparison of dilatational, rod, and shear wave velocities in a dry sand

similarly by the many factors which influence the magnitude of velocity. A typical comparison is shown in fig. 5.10. Note that the relative magnitudes follow the trend predicted by elastic theory:

$C_D > C_L > C_S$. More will be said about the relative magnitudes in the section dealing with Poisson's ratio.

The following sections

discuss the various factors which influence the magnitude of velocity. Since the same trends appear for all velocities, the best available data will be selected to illustrate these trends.

5.3.1 Effect of Confining Stress. Fig. 5.11 shows a typical set of data. When plotted on log-log paper, the relation between velocity and confining stress is almost a straight line, but tends to be somewhat concave downward. If this relation were straight, it would mean that velocity varies as σ^m . Typically, for many different granular

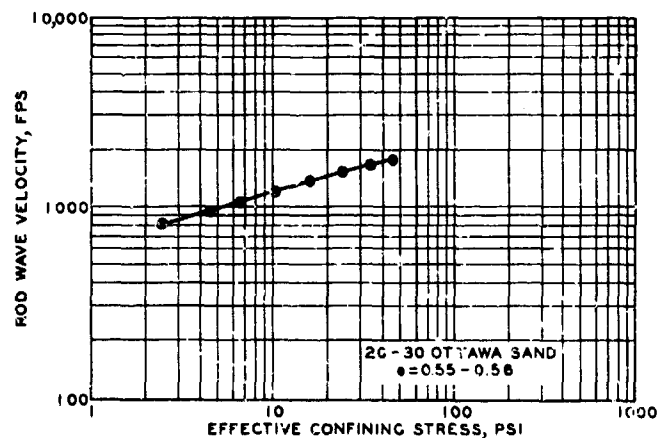


Fig. 5.11 Rod wave velocity through dry sand as a function of confining stress (from Hardin and Richart, 1963)

soils, the exponent m is close to 0.25, ranging from about 0.2 to about 0.5. The smallest exponents occur for the densest soils and higher confining stresses.

There are two explanations for the effect of confining stress. The first explanation concerns the way in which deformations occur within a given arrangement of particles. The second explanation involves the way in which particle arrangements are changed by increasing confining stress.

Behavior of a fixed arrangement: Within a given arrangement of particles, a small increment of stress causes distortion of the particles near their contact points with other particles. The theory for the interaction between elastic spheres can be used to examine this behavior: see Deresiewicz (1958).

Fig. 5.12 shows the effect of a normal force between spheres. The increment of force dN resulting from an increment of movement $d\alpha$ is found to be proportional to $\sqrt[3]{N}$. Thus as N increases, the stiffness $dN/d\alpha$ increases. The normal contact force N can be related to the all-around confining stress σ_0 , and the movement α can be related to

strain. In this way, it is found that the ratio of stress to strain during a small increment of stress, i.e. the tangent modulus, should vary as $\sqrt[3]{\sigma_0}$. Assuming that the wavelength is very great compared with the size of individual particles, and using Equation 5.1, this leads to the prediction that velocity should vary as $\sigma_0^{0.167}$.

The complete equation relating velocity and confining stress also involves the elastic properties of the individual spheres and the way in which the spheres are packed together. However, the velocity is predicted to be independent of particle size. For an accurate analysis, it also is

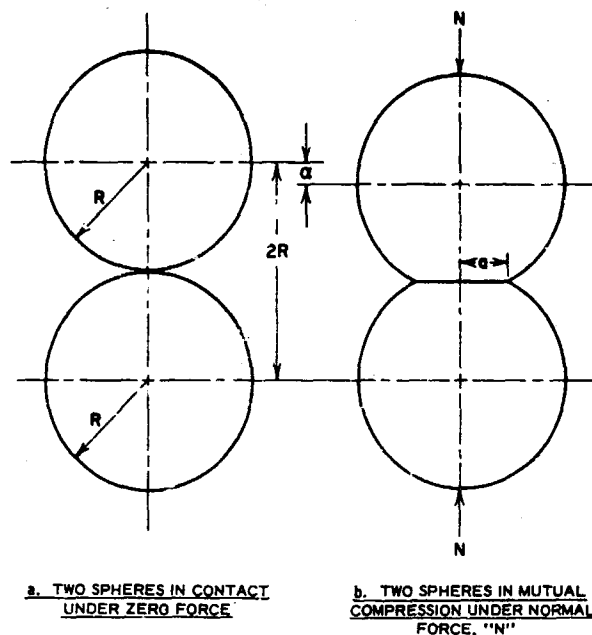


Fig. 5.12 Deformation of elastic spheres by contact forces

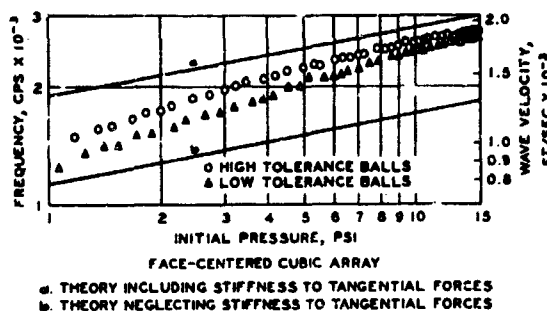


Fig. 5.13 Predicted and actual rod velocities through dense array of steel balls (from Duffy and Mindlin, 1957)

necessary to consider the tangential forces which occur at contact points. Fig. 5.13 shows the predicted rod velocity through densely packed steel spheres. These velocities are much less than the wave velocity through solid steel. The time for a wave to travel across a particle is much less than the time needed to develop the distortions near the contact point.

Relative movement between particles: The foregoing analysis presumes an ideal arrangement of perfectly spherical particles, with each particle in contact with each of its neighbors and with exactly the same force at each contact. Of course these conditions do not exist within actual soils, and cannot even be realized in packings of steel balls.

The data in fig. 5.13 show that the velocity increases more rapidly than $\sigma^{0.167}$, especially for small confining stresses. Even with balls made to strict tolerance requirements, the initial packing cannot be perfect. The forces are not the same at all contacts, and perhaps contact is not actually made between some neighboring spheres. As σ increases, the spheres are brought into better and more uniform contact, and the experimental results come into better agreement with the theory. The disagreement with theory is increased when balls made to less strict tolerance are used, and the disagreement naturally becomes more severe for soils. Nonetheless, the theory gives remarkably good estimates for the approximate magnitude of the velocities of low-intensity stress waves measured in soils for confining stresses of 100 to 200 psi: see NUCLEAR GEOPLOSICS.

Wave velocity as a function of depth: Because of increased confining stress with depth, the wave velocity through homogeneous natural ground should increase with depth, approximately as:

$$\text{velocity} \approx (\text{depth})^{0.25} \quad (5.2)$$

It is possible to predict the actual variation with depth from the results of laboratory tests at various confining stresses.

The foregoing results were obtained using a confining stress which was the same in all directions; i.e. the three principal stresses σ_1 , σ_2 , and σ_3 were equal. In natural ground, however, the principal stresses seldom are equal. The vertical stress σ_v at any depth may be from one-half to twice the horizontal stresses, depending upon past geologic processes. Thus conditions may range from $\sigma_v = \sigma_1 = 3\sigma_o/2$ to $\sigma_v = \sigma_3 = 3\sigma_o/5$, where σ_o is the average principal stress; i.e.

$$\sigma_o = \frac{\sigma_1 + \sigma_2 + \sigma_3}{3} \quad (5.3)$$

Report 23 has investigated the magnitude of shear wave velocity during triaxial compression tests with $\sigma_1 > \sigma_2 = \sigma_3$. It was found that velocity was related to σ_o at least so long as the shear stresses were less than those at failure (see fig. 5.14). The same conclusion has been reached by

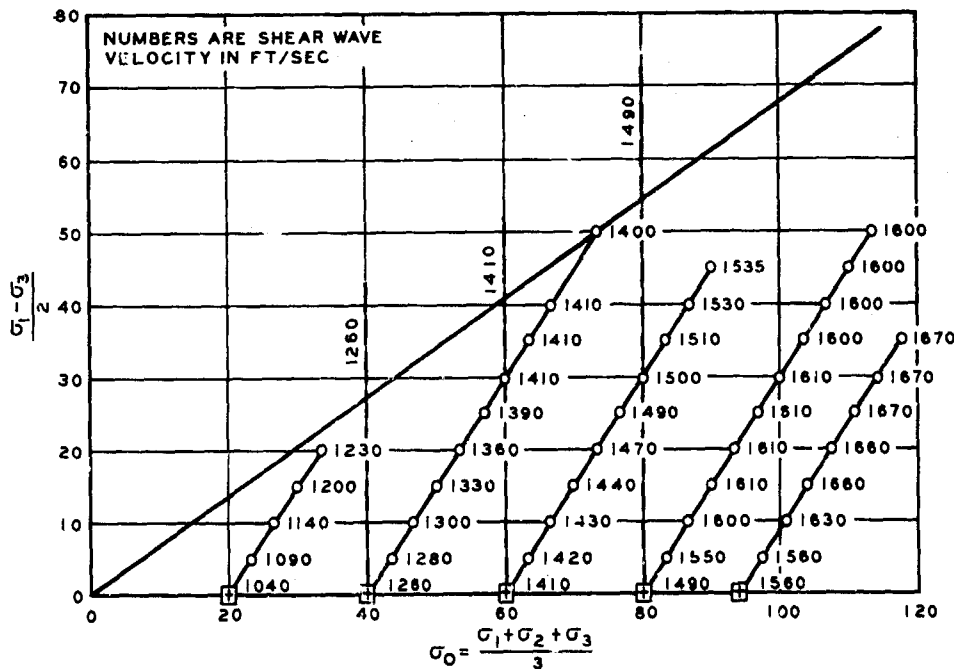


Fig. 5.14 Influence of shear stress on shear wave velocity in Ottawa sand (from Report 23). For example, compare velocities at same σ_o for: (a) test which started at 40 psi; and (b) initial point of test starting at 60 psi

Hardin and Black (1966). Stevens (1966a) and Barnes (1965) give still more data which appear to confirm this conclusion. Earlier data by Shannon, Yamane, and Dietrich (1960) suggested that velocity was dependent only on σ_1 , but the more recent data just cited are more convincing. Actually, it makes relatively little difference which rule is used to relate σ_v to velocity, since the ratio $(\sigma_v/\sigma_o)^{0.25}$ varies only from 1.11 to 0.88.

5.3.2 Effect of Amplitude of Dynamic Stress. Because soil is such a nonlinear material, the amplitude of the dynamic stress or strain in a wave

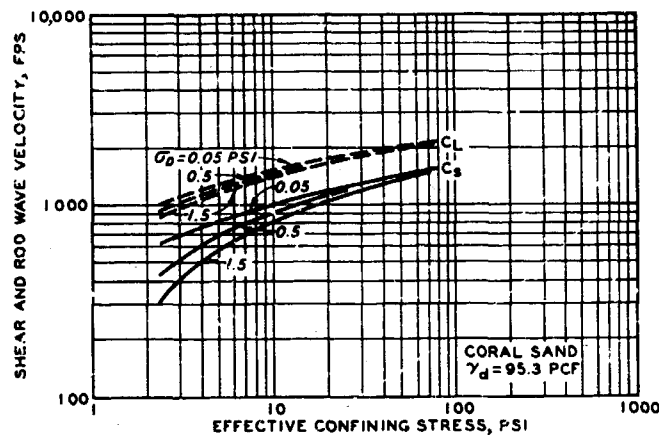


Fig. 5.15 Effect of amplitude of dynamic stress on velocity

has an influence on the wave velocity, even for stresses or strains which can be considered as "very small."

This is shown in fig. 5.15. The curves are labeled with the maximum shear stress within the specimen, computed from the measured motions using elastic theory. The deviation between the several curves of course is greatest

for small confining stresses, where the dynamic stresses become a significant fraction of the confining stresses.

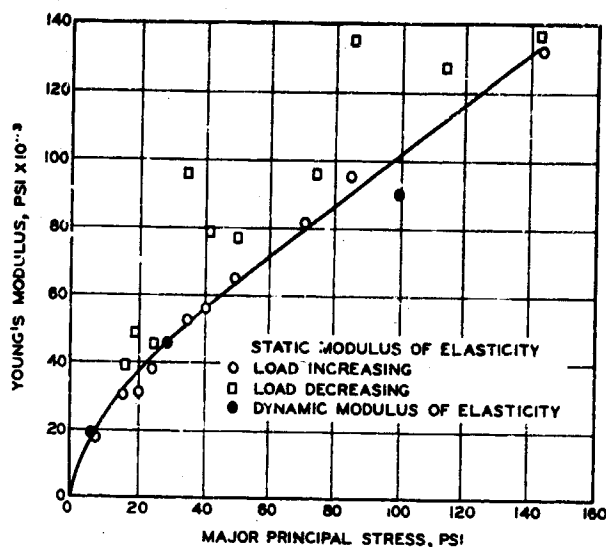
The effect of amplitude has also been investigated by Hall and Richart (1963).

5.3.3 Effect of Frequency. By exciting higher order resonances during resonant vibration tests, it is possible to investigate the effect of frequency on wave velocity. Both Hardin (1965) and Stevens (1966b) have found that velocity is independent of frequency for the range from 25 to 800 cps.

There is good evidence that the velocity through sands can be predicted using Equation 5.1 together with a modulus measured during static repeated-loading tests involving small changes in stress. Some of this evidence is given in fig. 5.16. See also Report 21 and NUCLEAR GEOPLOSICS.

5.3.4 Effect of Void Ratio. The effect of void ratio on velocity is

Fig. 5.16 Young's modulus versus confining stress for quartz sand by various methods (from Shannon, Yamane, and Dietrich, 1960)



illustrated in fig. 5.17. Increasing the void ratio has two effects: (a) the density decreases, which should tend to increase the velocity; and (b) the modulus decreases, which will tend to decrease velocity. The data show that the decrease in modulus outweighs the decrease in density.

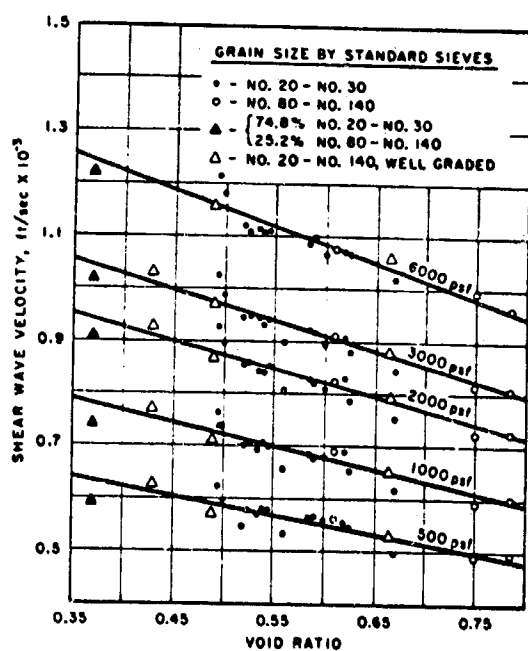


Fig. 5.17 Shear wave velocity versus void ratio for Ottawa sand (from resonant vibration tests by Hardin and Richart, 1963)

For a given sand at a given confining pressure, the change in velocity between the densest and loosest state is usually only 25% of the velocity for medium density.

5.3.5 Effect of Particle Size, Shape, and Gradation. According to the data in fig. 5.17, the velocity for a given void ratio and confining stress appears to be independent of these factors. These factors, of course, influence the void ratio which a granular soil will achieve.

Results similar to those in fig. 5.17 have also been obtained for sands with very angular particles. The two sets of results are superimposed in fig. 5.18. As a first

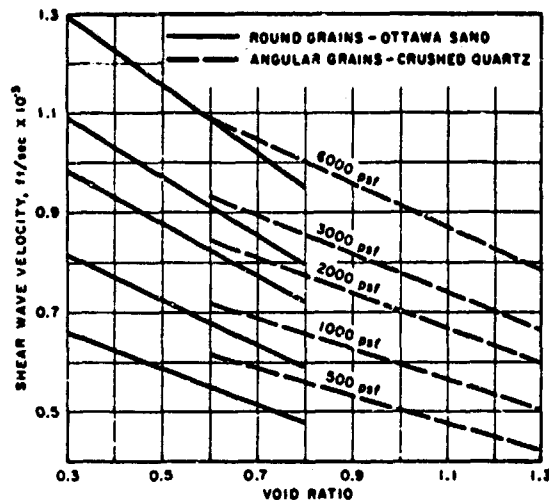


Fig. 5.18 Shear wave velocity versus void ratio for quartz sand (from resonant vibration tests by Hardin and Richart, 1963)

approximation, it appears that particle size, shape, and gradation affect velocity only through their effect upon void ratio. Fig. 5.18 can be used to estimate the shear wave velocity for a wide range of granular soils.

5.3.6 Poisson's Ratio. By comparing the several wave velocities at a given confining stress and void ratio, and assuming that the equations from elastic theory apply (fig. 5.2), values of Poisson's ratio μ can be determined. However, relatively small changes in the measured values of velocity can lead to large changes in μ . Very erratic and misleading values of μ can be obtained from tests in which the dynamic stresses are a significant fraction of the confining stress. Resonant vibration tests with large confining stresses also often give values of μ which are difficult to believe.

In the majority of cases, values of μ between 0.3 and 0.4 have been obtained by this procedure, and 0.35 is recommended for use with granular soils. Thus rod and dilatational velocities will be about 1.65 and 2.1, respectively, times the shear velocity.

5.3.7 Behavior with Small Porosity. Wyllie et al. (1958) have suggested the following rule for the dilatational velocity C_D through porous rock

$$\frac{1}{C_D} = \frac{n}{C^v} + \frac{1-n}{C_D^m} \quad (5.4)$$

where

n = porosity

C^V = dilatational velocity through pore fluid, in this case air (for air, $C^V = C^a$)

C_D^m = dilatational velocity through mineral

This rule is based on the concept that a wave passes straight through porous rock, partly through solid mineral, and partly through void space, and that behavior at contact points between minerals is of no consequence. Alternatively, this equation might be based on the concept that the wave travels at dilatational velocity along a tortuous path whose length depends on the porosity. Since the actual travel distance is thus greater than the apparent distance, the apparent velocity is less than the dilatational velocity through solid mineral. Wyllie et al. found good agreement between velocities measured in porous rocks using a pulse technique and velocities predicted by this rule, provided that very large confining stresses (on the order of 10,000 psi) were used.

This same rule might be expected to apply to granular soils of low porosity (say $n < 0.2$); i.e. to very well graded soils, especially those with a large content of cobbles and boulders. Dobry (1962) found that the in situ dilatational velocity of the surface gravels near Santiago, Chile, is very much influenced by the presence of large particles. Typical velocities above the water table were 2600 to 3000 fps, but occasionally values went as high as 4000 to 4500 fps.

For conditions where this mechanism of propagation is valid, there will not necessarily be any simple relation between shear and dilatational velocities. Brandt (1955) and Viksne et al. (1961) have also made studies of sands with very small porosity and cemented sands.

5.4 SHEAR AND ROD VELOCITIES THROUGH SOILS WITH WATER

When the degree of saturation exceeds about 50%, there starts to be a great difference in the mechanisms by which shear and dilatational waves are transmitted through soil. Dilatational waves result from volume changes, and pore water resists volume change. On the other hand, pore water does not provide any resistance to shear distortions. Since shear

stresses are always present with rod waves, the behavior of rod and shear waves is essentially the same.

This section will consider shear and rod waves through saturated and partially saturated soils. Dilatational waves through soils containing water will be discussed in subsequent sections.

5.4.1 Role of Total and Effective Stress. Pulse tests at the Shell Research and Development Laboratory have demonstrated that the shear wave velocity through a sand depends only upon the effective confining stress. If the total stress acting on a saturated specimen is changed but the specimen is not permitted to drain, the shear wave velocity remains unchanged. Report 23 reports identical results in the case of clays. Presumably the same is true regarding rod wave velocity.

5.4.2 Effective Mass of Pore Fluid. Suppose that two specimens, one dry and the other fully saturated, have exactly the same shear modulus and dry unit weight. If the pore fluid moves as a shear wave passes through a specimen, the saturated specimen should have a smaller wave velocity than the dry specimen. That is, the value of ρ in Equation 5.1 will be increased by the presence of pore water.

For example, if the void ratio of a soil is 0.7 and the specific gravity is 2.7, the saturated total unit weight is 1.26 times the dry unit weight. The wave velocity through the saturated soil should be 0.89 of that through the dry soil.

It is not obvious that all of the pore fluid will be able to move with the mineral skeleton. That is, only part of the pore fluid may be "effective" in slowing down the wave. Thus the effective mass density of a saturated soil might be expressed as:

$$\rho = \rho^S + \beta n \rho^W = \rho^W [(1 - n)G + \beta n] \quad (5.5)$$

where

ρ^S = density of skeleton, proportional to the dry unit weight

β = a factor between 0 and 1

n = porosity

ρ^W = mass density of water

G = specific gravity of mineral

The choice of a suitable value for β is of some minor concern when converting from modulus to wave velocity and vice versa.

Theory for effective mass: There are two interactions between the mineral skeleton and pore water.

First, owing to the viscosity of water, shear stresses will develop at mineral-water interfaces. A simplified version of this situation is shown in fig. 5.19a. If the water-filled tube is accelerated, viscous boundary layer forces will tend to drag the water with the tube. With very small accelerations, the viscous forces will be sufficient to make the water move almost as though it were rigidly joined to the tube. Hence the water is strongly coupled to the tube, and all of the mass of the water is effective

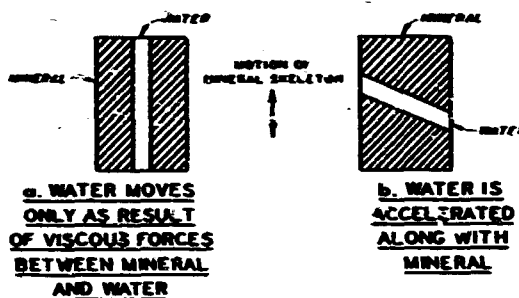


Fig. 5.19 Factors which influence magnitude of effective mass

in resisting acceleration of the tube. As the magnitude of the acceleration increases, the viscous forces no longer are able to make all of the water move with the tube. The water near the walls will still move with the tube, but the water near the center line will lag. Thus β decreases. With very rapid accelerations, the water will remain stationary as the tube moves past it, and $\beta = 0$.

The second interaction arises because individual flow channels within the mineral skeleton generally are not aligned with the direction of motion of the skeleton (fig. 5.19b). In such a case, the water must move when the skeleton moves, even though viscous stresses are absent. If the mineral skeleton is given a very large acceleration, the water within the flow channel will accelerate with it and thus will add to the inertia of the system. The amount of inertia added by the water is a function of the degree of misalignment. Normal stresses at the mineral-water interfaces will give the pressure gradients necessary to accomplish the acceleration. With smaller accelerations, the water will, in the absence of viscous

shear, tend to escape from the tube. Thus β will tend to decrease with decreasing acceleration.

The viscous effect thus predominates at low frequencies, and tends to make $\beta = 1$. The misalignment effect predominates at high frequencies, and tends to make β less than unity. Thus, β decreases (and hence the velocity increases for a given modulus) with increasing frequency. Whether a frequency is "high" or "low" depends primarily upon the viscosity of the pore fluid and the size of the flow channels. Presumably viscous effects strongly predominate in clay, but are of small importance for a coarse sand.

Biot (1956) has developed a theory which takes these two effects into account for the case of a porous-elastic material. Hall (1962) has applied this theory to saturated sands. Although the theory gives great insight into the interactions between the mineral and pore phases, the numerical results are not in particularly good agreement with actual experimental results.

30-30 OTTAWA SAND - $e = 0.54$

$$\sigma_v = 14.4 \text{ PSI}$$

CONDITION	SHEAR VELOCITY, FPS	
	PREDICTED	OBSERVED
DRY		860
MOIST ($w \approx 2\%$)	850	840
SATURATED ($w = 20\%$)	785	810

Fig. 5.20 Effect of mass of pore water on shear wave velocity through sand (data from resonant vibration tests by Hardin and Richart, 1963)

Data regarding effective

mass: Fig. 5.20 summarizes data concerning the effect of pore water on the wave velocity through a coarse sand. If it is assumed that the shear modulus remains unchanged as water is added to the specimen, the wave velocities for the moist and saturated conditions can be predicted from the velocity when dry. The

observed change in velocity as a result of saturating the soil was distinctly less than the predicted value, indicating that only a part of the pore water contributed to the effective density of the soil. From a study of such data, Hall (1962) concluded that in sands β is approximately $1/3$.

It is more difficult to determine experimentally the effective mass in the case of silt or clay, since it is difficult to be sure that the

shear modulus is really the same for two specimens having different degrees of saturation. Fig. 5.21 shows results for compacted clay-sand mixtures.

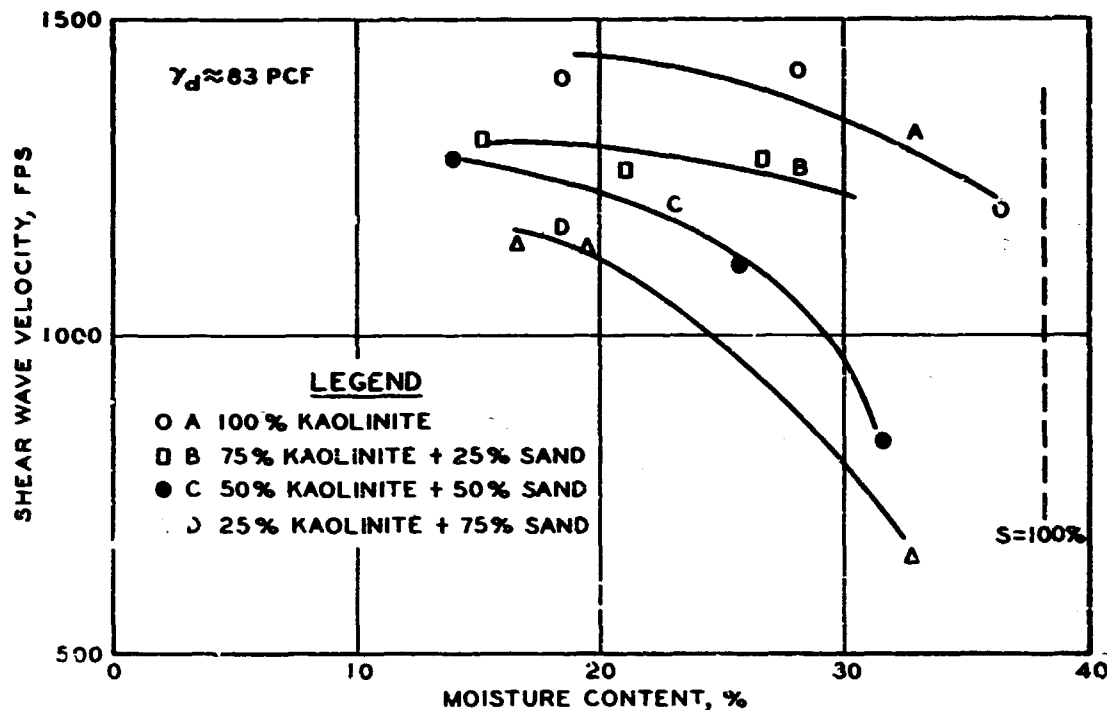


Fig. 5.21 Shear wave velocity for different degrees of saturation (from pulse tests described in Report 24)

All specimens were at the same dry density and were tested with the same total confining stress. However, the effective stresses were unknown and possibly varied with the degree of saturation. The soil fabric (i.e. the arrangement of particles) also may have varied with the degree of saturation. But perhaps it is more than coincidence that the decreasing velocity with increasing saturation can be explained almost exactly by assuming that modulus stays constant while the total density increases.

The following recommendations are made concerning the value of β to be used for saturated soils in connection with Equation 5.1:

Soil Type	β
Sand	1/3
Coarse and medium silt	2/3
Fine silt and clay	1

For partially saturated soils, ρ is obtained by using $\rho^S + \beta \rho^W$ or $\rho^S + S \rho^W$, whichever is smaller.

5.4.3 Effects of Confining Stress and Void Ratio. Except for the correction stemming from the mass of the pore water, the influence of effective confining stress and void ratio on velocity through sand is the same whether the sand is dry or saturated.

Until very recently, little has been known quantitatively concerning the influence of effective confining stress and void ratio on rod and shear velocities through silts and clays. In many tests, the effective stresses were not known because capillary tensions were present in the pore water to an unknown degree.

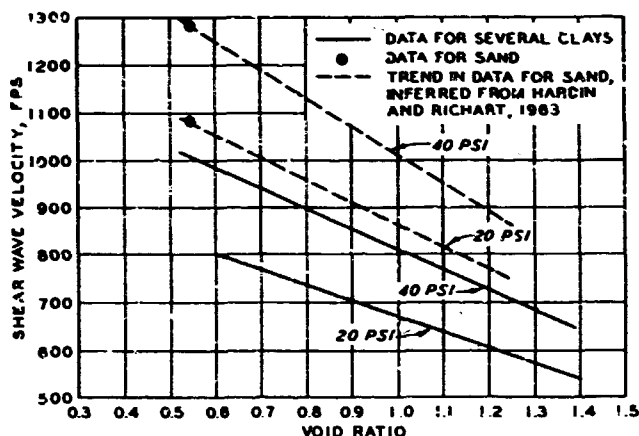


Fig. 5.22 Shear wave velocities through saturated clays and sands (from pulse tests described in Report 23)

Fig. 5.22 gives data from early tests on several saturated clays. Data points for sand are also shown, and the trend for sand has been sketched based on the data in fig. 5.18. (Since pulse tests give somewhat higher velocities than resonant vibration tests, the lines for fig. 5.18 were adjusted upward to pass through the data points in fig. 5.22.) Taking into ac-

count the difference in the effective mass of the pore water, it appears that clays have only slightly smaller velocities than sands for the same effective confining stress and void ratio. Consider for example the data for $e = 0.54$ and $\sigma_o = 40$ psi. Using $\beta = 1/3$ for sand and $\beta = 1$ for clay, the velocity through clay should be 94% of that through sand if the modulus is the same for both sand and clay. The observed relation is 79%.

Recently, results for clays have been published by Hardin and Black (1968) and Humphries and Wahls (1968). The results confirm that, except for very plastic soils, the relation between shear velocity, effective confining stress, and void ratio is much the same for clays as for sands.

The relation for clays is affected by the phenomenon of secondary consolidation.

5.4.4 Effect of Amplitude of Dynamic Stress. The effect of amplitude is essentially the same whether the soil is dry or wet.

5.4.5 Effect of Frequency. On the basis of tests by Stevens (1966b), there appears to be little if any effect of frequency on shear and rod velocities through saturated sands, although some minor effect might be expected on theoretical grounds (see section 5.4.2).

As yet, relatively little is known concerning the effect of frequency on the wave velocity through clays. The scant evidence suggests that frequency has an effect which may be important in some cases. Table 5.1 compares Young's modulus as measured during static repeated-load tests with this modulus as calculated using Equation 5.1 and measured rod velocity.

Table 5.1
Rod and Shear Modulus Data for Saturated Clays
(from Wilson and Dietrich, 1960)

Clay	Modulus, psi $\times 10^{-3}$			Poisson's Ratio
	E_s^*	E_d^{**}	G_d^{**}	
Duwamish silt	5.5	5.7	1.86	0.53
Birch Bay clay (five samples with different properties)	8.35	12.3	3.82	0.61
	11.9	10.8		
	11.0	15.2	4.91	0.54
	13.7	16.5		
	18.2	23.6	8.10	0.46
Whidbey Island clay (four samples with different properties)	2.88	2.91	0.90	0.62
	5.10	5.73	1.82	0.57
	9.50	8.70	2.88	0.50
	14.65	16.9	5.45	0.42

* From static repeated loading.

** From resonant vibration.

5.4.6 Poisson's Ratio. Theoretically μ should be very nearly 0.5 for a saturated soil, since the pore water makes the resistance to volume change much greater than the resistance to shear. Thus the rod velocity should be 1.73 times the shear velocity.

In the case of saturated clays, values of μ calculated from rod and shear velocities usually scatter about 0.5 (see table 5.1). With sands, however, μ has been found to be much the same whether the sand is dry or saturated. It may well be that local volume changes can occur within saturated sand, owing to a high permeability, even during tests with high frequencies.

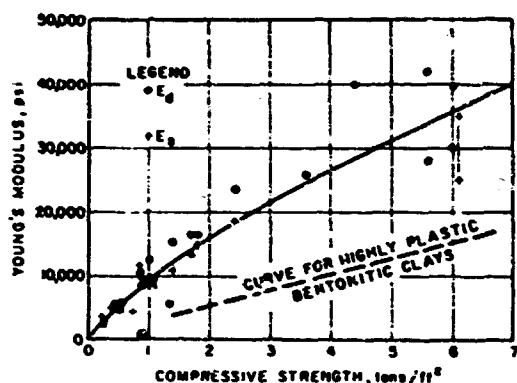


Fig. 5.23 Relation of rod modulus to undrained compressive strength in clays (from Wilson and Dietrich, 1960)

5.4.7 Velocity and Strength.

For a saturated soil, both velocity and undrained strength are related to the effective confining stress and void ratio before loading. Hence, it might be expected that there would be a relation between velocity and undrained strength. Fig. 5.23 presents some data. Many different soils do fall along a common relation, but as fig. 5.23 shows, there is at least one major class of exceptions, i.e. highly plastic bentonitic clays.

5.5 DILATATIONAL VELOCITY THROUGH SATURATED SOILS

Dilatational stress waves can propagate through water as well as through the mineral skeleton. Moreover, the compressibility of water is very small compared to the compressibility of the mineral skeleton of typical soils. To be specific, the bulk modulus of water B^W (which varies somewhat with the content of dissolved impurities, especially dissolved gases) is about 300,000 psi. This modulus corresponds to a wave velocity of

$$C^W = \sqrt{\frac{B^W}{\rho^W}} = 4720 \text{ fps} \quad (5.6)$$

where ρ^W is the mass density of water. This velocity is much greater than the dilatational velocities through dry mineral skeletons. Thus it would be expected that the presence of water will have a profound effect

on the dilatational wave velocity through soils.

As usual, the following treatments assume that the wavelengths are long compared to the size of individual particles, so that reflections and refractions at the myriad mineral-water interfaces can be ignored.

5.5.1 Suspension of Soil in Water. As mineral particles are added to water so as to form a suspension or slurry, two effects develop:

- (a) The overall mass density of the system increases, since mineral particles are heavier than the water they displace. The overall mass density is given by Equation 5.5 with $\beta = 1$.
- (b) The overall compressibility is decreased, since mineral particles are much less compressible than the water they displace. In fact, since the bulk modulus for quartz is about 50 times that of water, the mineral particles can be considered as incompressible. Thus the effective compression of a suspension per unit of volume is:

$$\Delta \epsilon = \frac{n}{B^W} \Delta u \quad (5.7)$$

where Δu is the change of pressure in the suspension.

Applying the elastic formula for dilatational velocity to this suspension then gives

$$C_D = C^W \sqrt{\frac{1}{n[(1-n)G + n]}} \quad (5.8)$$

The ratio of C_D/C^W is plotted in fig. 5.24 versus $(1-n)$, the portion of the total volume which is occupied by mineral matter. As soil particles are first added, the velocity through the suspension drops below that through pure water, since the increased mass is more important than the decreased compressibility.

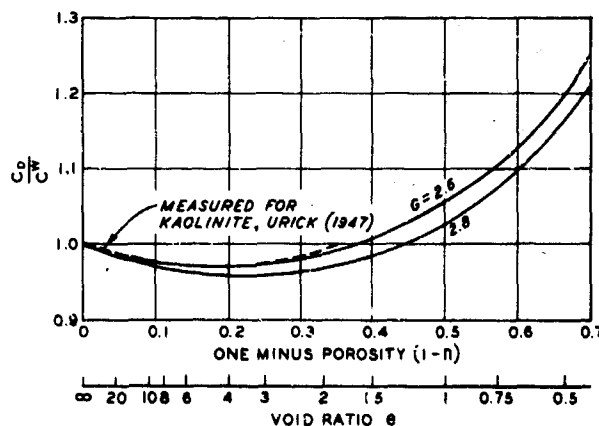


Fig. 5.24 Wave velocity through soil assuming no stress is carried by mineral skeleton

As more soil particles are added, however, the decreased compressibility becomes more important and the velocity through the suspension rises above that of pure water. Results obtained using artificially prepared kaolin slurries (Urick, 1947) are shown in fig. 5.24. Equation 5.8 has been used to good advantage to study wave velocities through ocean bottom sediments; for example, see Report 4.

5.5.2 Effect of Mineral Skeleton. When the void ratio becomes less than 3, the mineral particles will be in contact with each other so as to form a mineral skeleton which can transmit stress.

The total stress involved in the wave will be carried jointly by the pore water and mineral skeleton. If D^s is the constrained modulus of the skeleton, $\Delta\bar{\sigma}/D^s$ is the strain in the mineral skeleton where $\Delta\bar{\sigma}$ is increment of effective stress. The strain in the pore water is $\Delta u/B^w$ where Δu is the increment of pore pressure. These two strains must be equal:

$$\Delta\epsilon = \frac{\Delta\bar{\sigma}}{D^s} = \Delta u \frac{n}{B^w} \quad (5.9)$$

The increment of total stress is $\Delta\sigma = \Delta\bar{\sigma} + \Delta u$. From this

$$\frac{\Delta u}{\Delta\sigma} = \frac{B^w}{B^w + nD^s} \quad (5.10)$$

The strain can thus be expressed as:

$$\Delta\epsilon = \frac{n}{B^w} \frac{B^w}{B^w + nD^s} \Delta\sigma = \frac{n}{B^w + nD^s} \Delta\sigma \quad (5.11)$$

And the effective constrained modulus is:

$$D = \frac{\Delta\sigma}{\Delta\epsilon} = \frac{B^w}{n} + D^s \quad (5.12)$$

Combining this modulus with the effective density (equation 5.5) leads finally to an equation for the effective wave velocity:*

* $\beta = 1$ for the first term in Equation 5.13, but not necessarily in the second term. Some of these assumptions concerning the effective mass density can certainly be disputed.

$$C_D = C^W \sqrt{\frac{1}{n[(1-n)G + n]} + \left(\frac{C_D^S}{C^W}\right)^2 \frac{1}{1 + \frac{\beta n}{(1-n)G}}} \quad (5.13)$$

where C_D^S = dilatational wave velocity through dry mineral skeleton, equal to $\sqrt{D^S/\rho^S}$. Equation 5.13 is plotted in fig. 5.25 for a particular value of porosity (void ratio) and an assumed relation between C_D^S and effective confining stress. The horizontal lines show the velocity through water alone, and the velocity as given by Equation 5.8. The mineral skeleton influences the effective wave velocity only for the higher effective confining stresses for which C_D^S begins to approach and then exceed C^W .

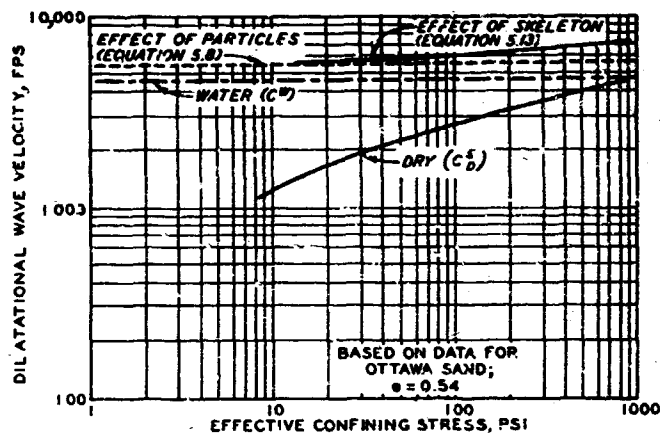


Fig. 5.25 Calculated dilatational wave velocity through saturated soil

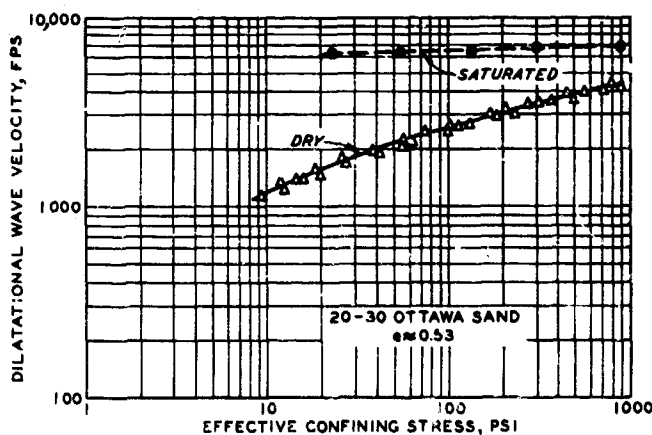


Fig. 5.26 Measured dilatational velocity through dry and saturated sands (data obtained by Shell Research and Development Laboratory using pulse technique)

Fig. 5.26 shows actual data for the dilatational velocity through a saturated sand. The actual result is very similar to that calculated in the previous figure.

5.5.3 Effect of Various Parameters. There has been little study of the influence of factors such as frequency and void ratio on the dilatational velocity through saturated soils. The main point

of course is that this velocity is related only slightly to the characteristics of the mineral skeleton. If a soil is saturated, measurement of

dilatational velocity in situ is of limited use as a means for assessing the compressibility of the mineral skeleton. Laughton (1957) and Shumway (1958, 1960) have used dilatational velocities to study certain aspects of the properties of ocean bottom sediments.

For very large effective stresses and for very small porosities, C_D^S will exceed C^W . Then the effective wave velocity will be controlled primarily by the magnitude of C_D^S . Equation 5.4 (with $C^V = C^W$ and $C_D^m = C_D^S$) applies to such situations.

5.6 DILATATIONAL VELOCITY THROUGH PARTIALLY SATURATED SOILS

The compressibility of the pore phase of a soil changes radically as the degree of saturation changes. With complete saturation, the pore phase is much less compressible than the mineral skeleton. Since $C^V = C^W > C_D^S$, dilatational waves propagate primarily through the pore phase. For low degrees of saturation, on the other hand, the pore phase is much more compressible than the mineral skeleton. Now $C^V = C^a < C_D^S$, and dilatational waves propagate primarily through the mineral skeleton.

In the latter case ($S \ll 1$), the dilatational wave velocity is indicative of the stiffness of the mineral skeleton. However, when $S \approx 1$, the dilatational wave velocity gives a relatively poor indication of the stiffness of the mineral skeleton. Thus, if dilatational wave velocities are to give useful information concerning the stiffness of the mineral skeleton, the degree of saturation must be less than some value. It is of considerable practical interest to determine this threshold value; possible means are discussed in the following section.

5.6.1 A Possible Mathematical Model. A possible, approximate expression for the compressive strain in the pore phase is:

$$\Delta\epsilon = n \left(\frac{S}{B^W} + \frac{1-S}{u_i} \right) \Delta u \quad (5.14)$$

where u_i = the initial pressure in the gaseous phase. The second term in parentheses comes from Boyle's law, assuming that the change in pressure is small compared to u_i .

Combining the above expression with that for the strain in the

mineral skeleton (section 5.5.2) leads to:

$$\frac{\Delta u}{\Delta \sigma} = \frac{1}{1 + \frac{D^s n S}{B^w} + \frac{D^s n}{u_i} (1 - S)} \quad (5.15)$$

Combining the two previous expressions gives the effective modulus

$$D = \frac{1}{n \left(\frac{S}{B^w} + \frac{1 - S}{u_i} \right)} + D^s \quad (5.16)$$

Finally we obtain an expression for the effective wave velocity:*

$$C_D = \sqrt{\frac{\frac{B^w}{n} \frac{u_i}{u_i S + B^w (1 - S)} + D^s}{\rho^w [(1 - n)G + S n]}} \quad (5.17)$$

If $u_i \ll B^w$ and $S < 0.999$, this simplifies to:

$$C_D = \sqrt{\frac{\frac{u_i}{n(1 - S)} + D^s}{\rho^w [(1 - n)G + S n]}} \quad (5.18)$$

Equation 5.18 is plotted in fig. 5.27 for a particular set of conditions. Until the degree of saturation is very close to 100%, the pore phase remains much more compressible than the mineral skeleton. The effective wave velocity is essentially that through dry soil, but decreases slightly with increasing S because of the increased mass. As S approaches 100%, the effective velocity suddenly shoots up to that for saturated soil.

On the basis of this model, the threshold value of S is essentially unity. For

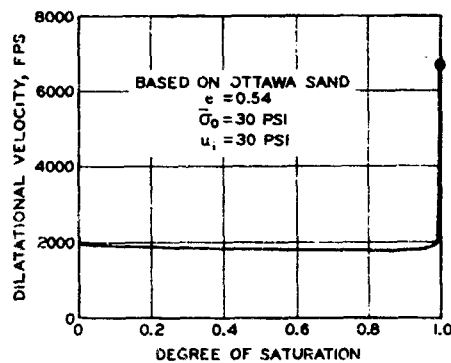


Fig. 5.27 Calculated relation between dilatational velocity and degree of saturation

* In Equation 5.17, it is presumed that $\beta = S$.

any S measurably less than unity, the dilatational velocity is controlled by the stiffness of the mineral skeleton, but is influenced somewhat by the mass of the pore fluid.

5.6.2 Data. Most geophysicists appear to believe that the situation shown in fig. 5.27 is actually indicative of field conditions; i.e. that there is an abrupt change in dilatational wave velocity as the degree of saturation changes from 99 to 100%. Such a situation must exist if geophysical exploration using wave velocities is to detect accurately the location of the water table. However, there seems to be little or no direct, published evidence to substantiate this belief.

Fig. 5.28 shows results obtained in the laboratory using the pulse technique. Four different sand-clay mixtures were involved in these tests. Despite the fact that the shear wave velocities through the various mixtures were quite different (fig. 5.21), the dilatational velocities at a given degree of saturation and confining stress were the same for all

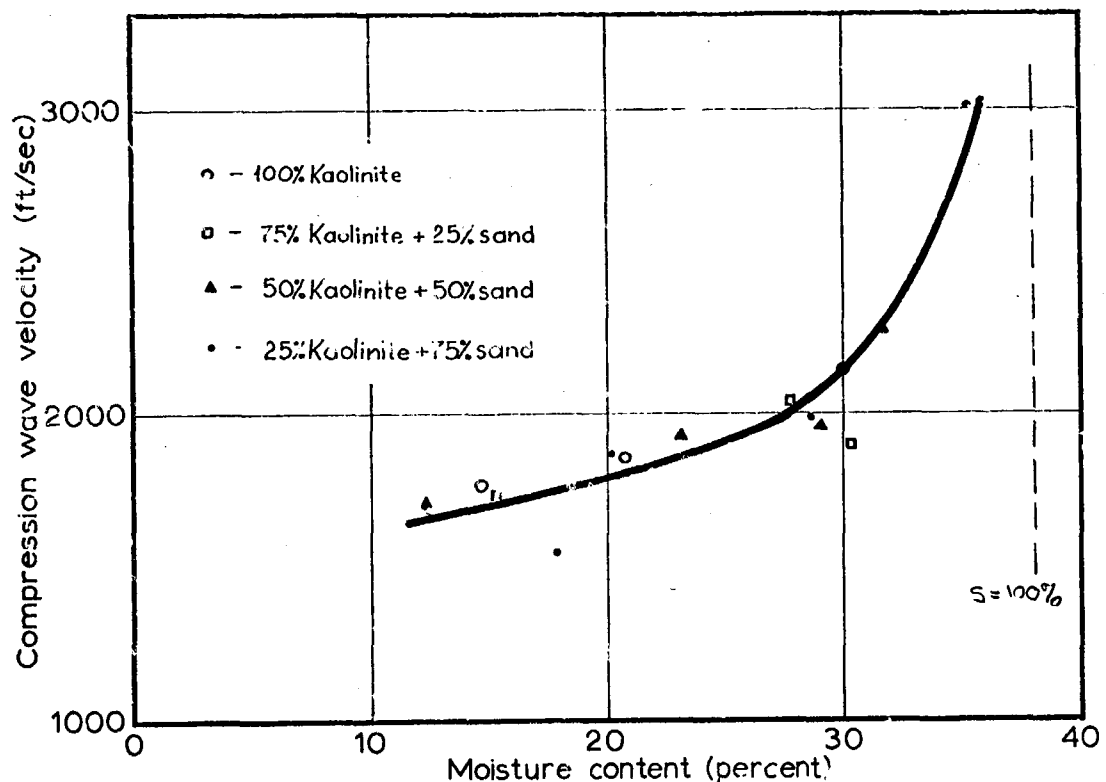


Fig. 5.28 Dilatational velocity for various degrees of saturation (from pulse tests described in Report 23)

mixtures. Thus, the dilatational velocity appeared to bear little relation to the stiffness of the mineral skeleton. The dilatational velocity increased rapidly for degrees of saturation above 75%. However, the transition was much more gradual than indicated by the theory in section 5.6.1.

It may well be that the pulse test using thin specimens does not give results representative of field conditions. With very high frequencies and thin specimens, it is conceivable that a wave simply travels through water and mineral in a tortuous path around the air bubbles without actually compressing the bubbles. As the degree of saturation increases, the travel path becomes less tortuous; hence the travel time across a given thickness decreases and the apparent velocity increases. Thus laboratory tests might give the gradual transition shown in fig. 5.28 even though 5.27 were actually the true condition.

However, the available evidence indicates that the laboratory pulse technique gives an accurate measurement of the in situ dilatational velocity (Report 17). Fig. 5.29 shows one of the results. When the undisturbed specimen was placed under a confining stress equal to the in situ overburden stress, the laboratory test gave a velocity identical to that which had been logged in the field.

The increase in velocity with increasing confining stress results from both increasing effective stress and increasing degree of saturation. During the second loading, the specimen apparently was compressed to almost full saturation. The velocity reached a level typical of a fully saturated sample. This velocity was almost constant with further increase in confining stress, suggesting that with full saturation the change in confining stress was producing no change in effective stress.

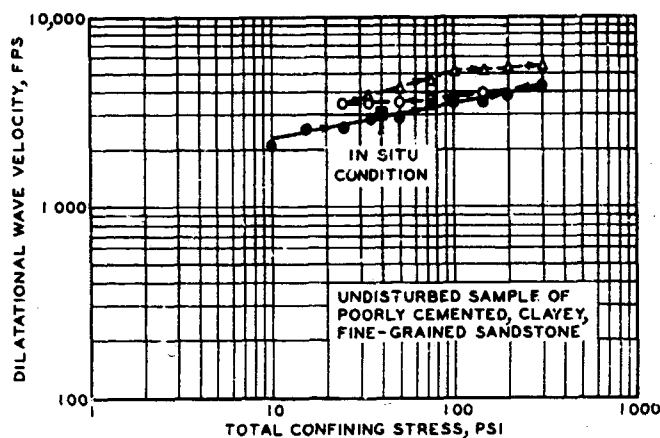


Fig. 5.29 Dilatational velocity through partially saturated undisturbed sample. (Data from files of writer. The laboratory data points were obtained using the pulse technique)

These results hardly have served to clarify the relation between degree of saturation and dilatational velocity. The situation still is confused, and much more study is necessary.

5.7 SUMMARY AND RECOMMENDATIONS

5.7.1 Summary of Results. The following working conclusions can be drawn on the basis of present knowledge:

- (a) The wave velocity through a dry soil depends upon the effective confining stress $\bar{\sigma}_0$ and the void ratio. The effect of factors such as particle shape, size, and gradation enters primarily through the effect of these factors upon void ratio. Wave velocity is more or less independent of frequency.
- (b) The shear and rod wave velocities through soils containing water depend in addition to the void ratio upon the mass of pore water which moves with the mineral skeleton. For coarse saturated sands, only about 1/3 of the pore water contributes to the effective mass. In clays, all of the pore water contributes to the effective mass. For comparable void ratios and effective stresses, the product ρC_s^2 (or ρC_L^2) is very similar for both sands and clays.
- (c) For fully saturated soils, the dilatational velocity is primarily the result of propagation through the pore phase and the magnitude of this velocity is not a good indicator of the stiffness of the mineral skeleton.
- (d) For degrees of saturation between 50 and 100%, the mechanisms by which dilatational waves propagate through soil are still poorly understood. Only for $S < 50\%$ can the magnitude of the dilatational velocity be used to indicate the stiffness of the mineral skeleton.

5.7.2 Present Status of Work. Much is now known concerning shear and dilatational wave velocities through dry and saturated sands, and of the relation between these velocities and one-dimensional compressibility. However, knowledge is very incomplete with regard to cohesive soils, especially partially saturated cohesive soils.

5.7.3 Suggestions for Future Research. Two fundamental avenues of investigation deserve high priorities:

- (a) Further tests to establish the relation between shear velocity, void ratio, and effective stress for a variety of soils, including partially saturated soils.
- (b) Further study of the relation between degree of saturation and dilatational wave velocity.

Ultrasonic pulse apparatus is needed for the second of these investigations, and can be used for the first. This apparatus should be modified to permit better control and measurement of drainage and volume changes and to permit measurement of pore water pressure.

Every opportunity should be taken to compare these laboratory measurements of velocity with in situ measurements, and with measurements of dynamic compressibility.

LITERATURE CITED

Ablow, C. M. and Sauer, F. M., Jan 1967: "Computation by the Method of Characteristics of Disturbance in an Elastic Half-Space Caused by a Blast-like Surface Loading," AFWL-TR-66-113, Air Force Weapons Laboratory, Kirtland Air Force Base, N. Mex.

Agbabian-Jacobsen Associates, June 1966: "Study of Shock Isolation for Hardened Structures," Contract Report No. AJA-6424, Los Angeles, Calif.

Air Force, 1962: "Air Force Design Manual; Principles and Practices for Design of Hardened Structures," Technical Documentary Report No. TDR-62-138, Air Force Special Weapons Center, Kirtland Air Force Base, N. Mex.

Aldrich, H. P., 1951: Analysis of Foundation Stresses and Settlements at the Hayden Library, Sc. D. thesis, Massachusetts Institute of Technology, Cambridge, Mass.

Allgood, J. R. et al., Apr 1963: "Blast Loading of Small Buried Arches," Technical Report R-216, Type C, Final Report, U. S. Navy Civil Engineering Laboratory, Port Hueneme, Calif.

American Society of Civil Engineers, 1961: "Design of Structures to Resist Nuclear Weapons Effects," Manuals of Engineering Practice No. 42, New York, N. Y.

Ang, A. and Ranier, J. H., Apr 1964: "Model for Wave Motions in Axi-Symmetric Solids," Journal, Engineering Mechanics Division, American Society of Civil Engineers, Vol 90, No. EM2, pp 195-223.

Ang, A. and Ranier, J. H., Nov 1965: "Digital Calculation of Axi-Symmetric Elastic-Plastic Ground Motions from Nuclear Bursts," AFWL-TR-65-115, Air Force Weapons Laboratory, Kirtland Air Force Base, N. Mex.

Barnes, G. W., 1965: An Investigation of the Effects of Dynamic Loads on the Shear Strength of Soils, M.S. thesis, Department of Civil Engineering, Arizona State University, Tempe, Ariz.

Baron, M. L., Bleich, H. H., and Weidlinger, P., Oct 1960: "Theoretical Studies on Ground Shock Phenomena," SR-19, Mitre Corporation, Bedford, Mass.

Baron, M. L. and Parnes, R., 1961: "Diffraction of a Pressure Wave by an Elastically Lined Cylindrical Cavity in an Elastic Medium," SR-44, Mitre Corporation, Bedford, Mass.

Biot, M. A., 1956: "Theory of Propagation of Elastic Waves in a Fluid-Saturated Porous Solid," Journal of Acoustical Society of America, Vol 28, pp 168-178.

Bleich, H. H., Matthews, A., and White, J. P., Sept 1965: "Step Load Moving with Superseismic Velocity on the Surface of a Half-Space of Granular Material," AFWL-TR-65-59, Air Force Weapons Laboratory, Kirtland Air Force Base, N. Mex.

Brandt, H., 1955: "A Study of the Speed of Sound in Porous Granular Media," Journal of Applied Mechanics, Vol 22, pp 479-486.

Brode, H. L., May 1964: "A Review of Nuclear Explosion Phenomena Pertinent to Protective Construction," Report R-425-PR, RAND Corporation, Santa Monica, Calif.

Brode, H. L. and Bjork, R. L., June 1960: "Cratering from a Megaton Surface Burst," Research Memo RM-2600, RAND Corporation, Santa Monica, Calif.

Bultmann, E. H., McDonough, G. F., and Sinnamon, G. K., 1959: "Loading on Simulated Buried Structures at High Incident Overpressures," Report WT-1406, U. S. Atomic Energy Commission, Oak Ridge, Tenn.

Bustamante, J. I., Jan 1965: "Dynamic Behavior of Noncohesive Embankment Models," Proceedings, Third World Conference on Earthquake Engineering, Wellington, N. Z., Vol III, pp IV-596 - IV-612.

Calhoun, D. E. and Kraft, D. C., May 1966: "An Investigation of the Dynamic Behavior of a Partially Saturated Silt with Applications to Shock Wave Propagation," AFWL-TR-65-176, Air Force Weapons Laboratory, Kirtland Air Force Base, N. Mex.

Casagrande, A. and Shannon, W. L., 1948: "Research on Stress-Deformation and Strength Characteristics of Soils and Soft Rocks Under Transient Loading," Soil Mechanics Series No. 31, Harvard University, Cambridge, Mass.

Casagrande, A. and Wilson, S. D., June 1951: "Effect of Rate of Loading on Strength of Clays and Shales at Constant Water Content," Geotechnique, Vol 2, pp 251-263.

Cauthen, L. H., Jr., 1964: "The Effects of Seismic Waves on Structures and Other Facilities," Proceedings, Third Plowshare Symposium on Engineering with Nuclear Explosives, U. S. Atomic Energy Commission, pp 207-228.

Chabai, A. J. and Hankins, D. M., Dec 1960: "Gravity Scaling Laws for Explosion Craters," SC-4541(RR), Sandia Corporation, Albuquerque, N. Mex.

Chelapati, C. V., 1964: "Arching in Soil Due to the Deflection of a Rigid Horizontal Strip," TN N-591, U. S. Naval Civil Engineering Laboratory, Port Hueneme, Calif.

Colp. J. L., 1965: "An Experimental Investigation of the Continuous Penetration of a Blunt Body into a Simulated Cohesionless Soil," Report SC-RR-65-260, Sandia Corporation, Albuquerque, N. Mex.

Constantino, C. H., 1966: "Automated Design of Advanced Hardened Facilities Study," BSD TR-66-256, Air Force Ballistic Systems Division, Air Force Systems Command, Norton Air Force Base, Calif.

Deresiewicz, H., 1958: "Mechanics of Granular Matter," Advances in Applied Mechanics, Vol V, Academic Press, Inc., New York, pp 233-306.

Dobry, R., 1962: Determinacion del Ripio de Santiago par el Metodo Sismico de Refraccion (Exploration of Santiago Gravel by the Seismic Refraction Method), thesis, Physical Sciences and Mathematics, University of Chile.

Dorris, A. F., July 1965: "Response of Horizontally Oriented Buried Cylinders to Static and Dynamic Loading," Technical Report No. 1-682, U. S. Army Engineer Waterways Experiment Station, CE, Vicksburg, Miss.

Drnevich, V. P., Hall, J. R., Jr., and Richart, F. E., Jr., Oct 1966: "Large Amplitude Vibration Effects on the Shear Modulus of Sand," Contract Report No. 3-161, U. S. Army Engineer Waterways Experiment Station, CE, Vicksburg, Miss.

Duffy, J. and Mindlin, R. D., Dec 1957: "Stress-Strain Relations and Vibrations of a Granular Medium," Journal of Applied Mechanics, Vol 24, No. 4, pp 585-593.

Finn, W. D. L., Sept 1963: "Boundary Value Problems of Soil Mechanics," Journal, Soil Mechanics and Foundations Division, American Society of Civil Engineers, Vol 89, No. SM5, pp 39-72.

Gans, R. F. and Brooks, J. A., Dec 1965: "Theoretical Ground Shock Effects; Ground Motion in Elastic Half-Spaces Induced by Air Blast," Vol I, SCR-275, United Aircraft Corporate Systems Center, El Segundo, Calif.

Gill, H. L. and Allgood, J. R., Jan 1964: "Static Loading on Small Buried Arches," Technical Report R-278, U. S. Navy Civil Engineering Laboratory, Port Hueneme, Calif.

Glasstone, S., ed., Apr 1962: "The Effects of Nuclear Weapons," U. S. Government Printing Office, Washington, D. C.

Graves, E., Jr., Oct 1964: "Nuclear Excavation of a Sea-Level Isthmian Canal," Civil Engineering, Vol 23, No. 10, pp 48-55.

Hall, J. R., Jr., 1962: Effect of Amplitude on Damping and Wave Propagation in Granular Materials, Ph. D. dissertation, Department of Civil Engineering, University of Florida, Gainesville, Fla.

Hall, J. R., Jr., and Richart, F. E., Jr., 1963: "Effect of Vibration Amplitude on Wave Velocities in Granular Materials," Proceedings, Second Panamerican Conference on Soil Mechanics and Foundation Engineering, Vol 1, pp 145-162.

Hankins, D. M., 1964: "Seismic Amplitudes at an Intermediate Range from Explosions," Proceedings, Third Flowshare Symposium on Engineering with Nuclear Explosives, U. S. Atomic Energy Commission, pp 195-206.

Hardin, B. O., Jan 1965: "The Nature of Damping in Sands," Journal, Soil Mechanics and Foundations Division, American Society of Civil Engineers, Vol 91, No. SML, pp 63-97.

Hardin, B. O., 1965: "Dynamic Versus Static Shear Modulus for Dry Sand," Materials Research and Standards, American Society for Testing and Materials, Vol 5, pp 232-235.

Hardin, B. O. and Black, W. L., Mar 1966: "Sand Stiffness Under Various Triaxial Stresses," Journal, Soil Mechanics and Foundations Division, American Society of Civil Engineers, Vol 92, No. SM2, pp 27-42.

Hardin, B. O. and Black, W. L., Mar 1968: "Vibration Modulus of Normally Consolidated Clay," Journal, Soil Mechanics and Foundations Division, American Society of Civil Engineers, Vol 94, No. SM2, pp 371-389.

Hardin, B. O. and Richart, F. E., Jr., Jan 1963: "Elastic Wave Velocities in Granular Soils," Journal, Soil Mechanics and Foundations Division, American Society of Civil Engineers, Vol 89, No. SML, pp 33-65.

Heierli, W., 1962: "Inelastic Wave Propagation in Soil Columns," Journal, Soil Mechanics and Foundations Division, American Society of Civil Engineers, Vol 88, No. SM6, pp 33-63.

Heller, L. W., 1965: "Motion of Subsurface Soil Inclusions Subjected to Surface Blast Loading," Technical Report R-372, U. S. Navy Civil Engineering Laboratory, Port Hueneme, Calif.

Hendron, A. J., Jr., 1963: The Behavior of Sand in One-Dimensional Compression, Ph. D. dissertation, Department of Civil Engineering, University of Illinois, Urbana, Ill.

Hendron, A. J., Jr., Oct 1965: "Correlation of Operation SNOWBALL Ground Motions with Dynamic Properties of Test Site Soils," Miscellaneous Paper No. 1-745, U. S. Army Engineer Waterways Experiment Station, CE, Vicksburg, Miss.

Hendron, A. J., Jr., and Davisson, M. T., Sept 1964: "Static and Dynamic Constrained Moduli of Frenchman Flat Soils," Proceedings, Symposium on Soil-Structure Interaction, University of Arizona, pp 73-97.

Hendron, A. J., Jr., Davisson, M. T., and Parola, J. F., Apr 1969: "Effect of Degree of Saturation on Compressibility of Suffield Experimental Station Soils," Contract Report S-69-3, U. S. Army Engineer Waterways Experiment Station, CE, Vicksburg, Miss.

Hess, W. N. and Nordyke, M. D., Oct 1961: "Throwout Calculations for Explosion Craters," Journal of Geophysical Research, Vol 66, No. 10, pp 3405-3412.

Höeg, K., Apr 1966: "Pressure Distribution on Underground Structural Cylinders," Technical Report No. AFWL-TR-65-98, Air Force Weapons Laboratory, Kirtland Air Force Base, N. Mex.

Humphries, W. K. and Wahls, H. E., Mar 1968: "Stress History Effects on Dynamic Shear Modulus of Clay," Journal, Soil Mechanics and Foundations Division, American Society of Civil Engineers, Vol 94, No. SM2, pp 353-369.

Jackson, J. G., Jr., July 1968: "Factors That Influence the Development of Soil Constitutive Relations," Miscellaneous Paper No. 4-980, U. S. Army Engineer Waterways Experiment Station, CE, Vicksburg, Miss.

Kane, H. et al., June 1964: "A Study of the Behavior of a Clay Under Rapid and Dynamic Loading in the One-Dimensional and Triaxial Tests," Technical Documentary Report No. RTD-TDR-63-3116, Air Force Weapons Laboratory, Kirtland Air Force Base, N. Mex.

Knox, J. B. and Terhune, R. W., 1964: "Calculation of Explosion Produced Craters," Proceedings, Third Plowshare Symposium on Engineering with Nuclear Explosives, U. S. Atomic Energy Commission, pp 75-98.

Kondner, R. L. and Ho, M. M. K., June 1964: "A Rheologic Investigation of the Dynamic Response Spectra of Soils; Energy Dissipative Response of a Cohesive Soil," Contract Report No. 3-62, Report 3, U. S. Army Engineer Waterways Experiment Station, CE, Vicksburg, Miss.

Lambe, T. W., July 1963: "An Earth Dam for Storage of Fuel Oil," Proceedings, Second Panamerican Conference on Soil Mechanics and Foundation Engineering, Brazil, Vol 2, pp 257-308.

Lambe, T. W., Sept 1964: "Methods of Estimating Settlement," Journal, Soil Mechanics and Foundations Division, American Society of Civil Engineers, Vol 90, No. SM5, pp 43-67.

Lambe, T. W. and Whitman, R. V., 1968: Soil Mechanics, Wiley, New York.

Laughton, A. S., 1957: "Sound Propagation and Compacted Ocean Sediments," Geophysics, Vol 22, p 233.

Lee, T. M., May 1963: "Method of Determining Dynamic Properties of Viscoelastic Solids Employing Forced Vibration," Journal of Applied Physics, Vol 34, No. 5, pp 1524-1529.

Luscher, U., 1963: "Static and Dynamic Tests on 4-Inch Tubes," Internal Report, University of New Mexico, Shock Tube Facility, Albuquerque, N. Mex.

Luscher, U., Sept 1965: "Behavior of Flexible Underground Cylinders," Technical Report No. AFWL-TR-65-99, Air Force Weapons Laboratory, Kirtland Air Force Base, N. Mex.

Luscher, U. and Höeg, K., 1965: "The Action of Soil Around Buried Tubes," Proceedings, Sixth International Conference on Soil Mechanics and Foundation Engineering, Montreal, Canada, Vol II, pp 396-400.

Mason, H. G. et al., Dec 1963: "A Study of the Dynamic Soil-Structure Interaction Characteristics of Real Soil Media," Technical Documentary Report No. TDR-63-3075, Air Force Weapons Laboratory, Kirtland Air Force Base, N. Mex.

McCormick, J. M. and Baron, M. L., Dec 1966: "Report on Task No. 2, Investigation of Air Induced Ground Shock Effects on an Elastic Half-Space," memorandum by Paul Weidlinger, Consulting Engineer, New York, N. Y.

Merritt, J. L. and Newmark, N. M., 1964: "Effects on Underground Structures and Equipment," Nuclear Geoplosics, DASA-1285(V), Part V, Defense Atomic Support Agency, Washington, D. C.

Mickey, W. V., 1964: "Seismic Wave Propagation," Proceedings, Third Flow-share Symposium on Engineering with Nuclear Explosives, U. S. Atomic Energy Commission, pp 181-194.

Mitchell, J. K., Jan 1964: "Shearing Resistance of Soils as a Rate Process," Journal, Soil Mechanics and Foundations Division, American Society of Civil Engineers, Vol 90, No. SMI, pp 29-61.

Murrell, D. W., Mar 1967: "Operation SNOWBALL, Project 3.6--Earth Motion Measurements," Technical Report No. 1-759, U. S. Army Engineer Waterways Experiment Station, CE, Vicksburg, Miss.

Neidhardt, G. L. and Harkin, J. B., 1962: "Theoretical Study of Energy Distribution in a Half-Space Under Dynamic Loads," Technical Documentary Report No. TDR-62-43, Air Force Special Weapons Center, Kirtland Air Force Base, N. Mex.

Newmark, N. M., 1965: "State-of-the-Art in Dynamic Analysis and Techniques for the Design of Underground Protective Construction," Symposium on Protective Structures for Civilian Populations, National Academy of Sciences - National Research Council, pp 166-179.

Newmark, N. M. and Halmiwanger, J. D., 1962: "Air Force Design Manual; Principles and Practices for Design of Hardened Structures," Technical Documentary Report No. TDR-62-138, Air Force Special Weapons Center, Kirtland Air Force Base, N. Mex.

Nielsen, F. D., 1967: "Soil Structure Arching Analysis of Buried Flexural Structures," presented at 46th Annual Meeting of the Highway Research Board, Washington, D. C.

Nordyke, M. D., Aug 1961a: "On Cratering: A Brief History, Analysis and Theory of Cratering," UCRL-6578, Lawrence Radiation Laboratory, University of California, Livermore, Calif.

Nordyke, M. D., Oct 1961b: "Nuclear Craters and Preliminary Theory of Mechanics of Explosive Crater Formation," Journal of Geophysical Research, Vol 66, No. 10, pp 3439-3459.

Nordyke, M. D., 1964: "Cratering Experience with Chemical and Nuclear Explosives," Proceedings, Third Flowshare Symposium on Engineering with Nuclear Explosives, U. S. Atomic Energy Commission, pp 51-74.

Nordyke, M. D. et al., 1963: "Nuclear Excavation," Highway Research Record No. 50, Highway Research Board.

Peters, J., 1963: A Cage for Measuring Pore Pressures in Soils Under Dynamic Loads, Sc. D. dissertation, Department of Civil Engineering, University of Illinois, Urbana, Ill.

Rajapaksee, Y. D. S. et al., 1960: "Theoretical Study of Ground Motion Induced in Nonhomogeneous Media by Nuclear Explosions," Technical Report No. AFSWC-TR-61-6, Vol II, Air Force Special Weapons Center, Kirtland Air Force Base, N. Mex.

Richardson, A. M. Jr., and Whitman, R. W., 1963: "Effect of Strain-Rate upon Undrained Shear Resistance of a Saturated Remolded Fat Clay," Geotechnique, Vol 13, pp 310-324.

Rogers, G. L. and Palmer, D. M., July 1962: "Numerical Studies of Moving Pressure Pulses Over an Elastic Halfspace," Contract Report No. 2-58, U. S. Army Engineer Waterways Experiment Station, CE, Vicksburg, Miss.

Rooke, A. D., Jr., and Chew, T. D., Dec 1965: "Operation SHOW BALL, Project 3.1, Crater Measurements and Earth Media Determinations," Miscellaneous Paper No. 1-764, Interim Report, U. S. Army Engineer Waterways Experiment Station, CE, Vicksburg, Miss.

Sager, R. A., Denzel, C. W., and Tiffany, W. B., May 1960: "Cratering from High Explosive Charges; Compendium of Crater Data," Technical Report No. 2-547, Report 1, U. S. Army Engineer Waterways Experiment Station, CE, Vicksburg, Miss.

Sauer, F. M., Clark, G. B., and Anderson, D. C., 1964: "A Sourcebook of Underground Phenomena and Effects of Nuclear Explosions; Empirical Analysis of Ground Motion and Cratering," Nuclear Geophysics, DASA-1285(V), Part IV, Defense Atomic Support Agency, Washington, D. C.

Schimming, B. B., Haas, H. J., and Saxe, H. C., Mar 1966: "A Study of Dynamic and Static Failure Envelopes," Journal, Soils Mechanics and Foundations Division, American Society of Civil Engineers, Vol 92, No. SM2, pp 105-124.

Schindler, L., Aug 1967: "An Improved Facility for Testing Soils in One-Dimensional Compression," Proceedings, International Symposium on Wave Propagation and Dynamic Properties of Earth Materials, University of New Mexico, Albuquerque, N. Mex., pp 847-860.

Seaman, L., 1964: "Propagation of Dynamic Stresses in Soil," Proceedings, Symposium on Soil-Structure Interaction, University of Arizona, pp 98-104.

Seaman, L., Feb 1966: "One-Dimensional Stress Wave Propagation in Soils," DASA 1757, Stanford Research Institute, Menlo Park, Calif.

Seaman, L. and Whitman, R. V., June 1964: "Stress Propagation in Soils," DASA 1266-4, Final Report, Part IV, Stanford Research Institute, Menlo Park, Calif.

Seed, H. B. and Chan, C. K., Mar 1966: "Clay Strength Under Earthquake Loading Conditions," Journal, Soil Mechanics and Foundations Division, American Society of Civil Engineers, Vol 92, No. SM2, pp 53-78.

Seed, H. B. and Lee, K. L., 1965: "Studies of the Liquefaction of Sands Under Cyclic Loading Conditions," Report TE-65-5, Soil Mechanics and Bituminous Materials Laboratory, Department of Civil Engineering, Institute of Transportation and Traffic Engineering, University of California, Berkeley, Calif.

Seed, H. B. and Lundgren, R., 1954: "Investigation of the Effect of Transient Loading Upon the Strength and Deformation Characteristics of Saturated Sands," Proceedings, American Society for Testing Materials, Vol 54, p 1288.

Seed, H. B. and Martin, G. R., May 1966: "The Seismic Coefficient in Earth Dam Design," Journal, Soil Mechanics and Foundations Division, American Society of Civil Engineers, Vol 92, No. SM3, pp 25-58.

Seed, H. B. and McNeill, R. L., 1957: "Soil Deformations Under Repeated Stress Applications," Special Technical Publication 232, American Society for Testing Materials, pp 177-210.

Selig, E. T., 1964: "Characteristics of Stress Wave Propagation in Soil," Symposium on Soil-Structure Interaction, University of Arizona, pp 27-61.

Shannon, W. L., Yamane, G., and Dietrich, R. J., 1960: "Dynamic Triaxial Tests on Sands," Proceedings, First Panamerican Conference on Soil Mechanics and Foundation Engineering, Mexico, Vol 1, pp 473-489.

Sherman, W. C., Jr., and Strohm, W. E., Jr., 1964: "Engineering Properties of Explosion-Produced Craters," Proceedings, Third Plowshare Symposium on Engineering with Nuclear Explosives, U. S. Atomic Energy Commission, pp 99-108.

Shumway, G., July 1958: "Sound Velocity Versus Temperature in Water-Saturated Sediments," Geophysics, Vol 23, No. 3, pp 494-505.

Shumway, G., 1960: "Sound Speed and Absorption Studies of Marine Sediments by a Resonance Method," Geophysics, Vol 25; No. 2, Part I, Apr 1960, pp 451-467; No. 3, Part II, June 1960, pp 659-682.

Spangler, M. G., 1960: Soil Engineering, 2d ed., International Textbook Co., Scranton, Pa.

Stevens, H. W., Apr 1966a: "Measurement of the Complex Moduli and Damping of Soils Under Dynamic Loads," Technical Report 173, U. S. Army Materiel Command, Cold Regions Research and Engineering Laboratory, Hanover, N. H.

Stevens, H. W., 1966b: "Laboratory Test Results for Dynamic Modulus of Soil from Kwajalein Atoll," Technical Report by U. S. Army Materiel Command, Cold Regions Research and Engineering Laboratory, Hanover, N. H.

Stoll, R. D. and Ebeido, I. A., July 1965: "Shock Waves in Granular Soil," Journal, Soil Mechanics and Foundations Division, American Society of Civil Engineers, Vol 91, No. SM4, pp 107-125.

Strange, J. N., Denzel, C. W., and McLane, T. I., June 1961: "Cratering from High Explosive Charges; Analysis of Crater Data," Technical Report No. 2-547, Report 2, U. S. Army Engineer Waterways Experiment Station, CE, Vicksburg, Miss.

Swift, L. M. and Sachs, D. C., May 1954: "Small Explosion Tests; Second Interim Report, Phase II of Project MOLE," AFSWP-289, U. S. Army Engineer District, Sacramento.

Taylor, D. W., 1948: Fundamentals of Soil Mechanics, Wiley, New York.

Urlick, R. J., 1947: "A Sound Velocity Method for Determining the Compressibility of Finely Divided Substances," Journal of Applied Physics, Vol 18, pp 983-987.

Vesić, A. S., Banks, D. C., and Woodward, J. M., 1965: "An Experimental Study of the Dynamic Bearing Capacity of Footings on Sand," Proceedings, Sixth International Conference on Soil Mechanics and Foundation Engineering, Vol 2, pp 209-213.

Vesić, A. and Barksdale, R. D., Sept 1963: "Theoretical Studies of Cratering Mechanisms Affecting the Stability of Cratered Slopes," Contract Report No. 3-75, U. S. Army Engineer Waterways Experiment Station, CE, Vicksburg, Miss.

Viksne, A., Berg, J. W., Jr., and Cook, K. L., Feb 1961: "Effect of Porosity, Grain Contacts, and Cement on Compressional Wave Velocity Through Synthetic Sandstones," Geophysics, Vol 26, No. 1, pp 77-84.

Violet, C. E., Oct 1961: "A Generalized Empirical Analysis of Cratering," Journal of Geophysical Research, Vol 66, No. 10, pp 3461-3470.

Vortman, L. J., Nov 1964: "Nuclear Excavation of a Sea-Level Isthmian Canal," Journal, Waterways and Harbors Division, American Society of Civil Engineers, Vol 90, No. WW4, pp 27-54.

Whitman, R. V., Dec 1959: "Soil Mechanics Considerations Pertinent to Predicting the Immediate and Eventual Size of Explosion Craters," SC-4405, Sandia Corporation, Albuquerque, N. Mex.

Whitman, R. V., 1963: "Effects of Viscosity and Inelasticity Upon Stress Waves Through Confined Soil," Proceedings, Thirty-Second Symposium on Shock, Vibration and Associated Environments, U. S. Department of Defense, Part II, pp 107-123.

Whitman, R. V. and Healy, K. A., 1963: "Shear Strength of Sands During Rapid Loadings," Transactions, American Society of Civil Engineers, Vol 128, Part I, pp 1553-1594.

Whitman, R. V., Healy, K. A., and Richardson, A. M., Jr., 1961: "Time Lags in Pore Pressure Measurements," Proceedings, Fifth International Conference on Soil Mechanics and Foundation Engineering, Vol 1, pp 407-411.

Whitman, R. V. and Luscher, U., 1965: "Footings for Protective Structures," Proceedings, Symposium on Protective Structures for Civilian Populations, National Academy of Sciences - National Research Council, Washington, D. C.

Whitman, R. V., Miller, E. T., and Moore, P. J., July 1964: "Yielding and Locking of Confined Sand," Journal, Soil Mechanics and Foundations Division, American Society of Civil Engineers, Vol 90, No. SM4, pp 57-84.

Whitman, R. V. and Richart, F. E., Jr., 1967: "Design Procedures for Dynamically Loaded Footings," Journal, Soil Mechanics and Foundations Division, American Society of Civil Engineers, Vol 93, No. SM6, pp 169-193.

Whitman, R. V. and Taylor, D. W., June 1954: "The Behavior of Soils Under Dynamic Loadings: Review and Preliminary Correlation of Laboratory and Field Studies," AFSWP-119, Report 4, Office, Chief of Engineers, U. S. Army.

Wilson, S. D. and Dietrich, R. J., June 1960: "Effect of Consolidation Pressure on Elastic and Strength Properties of Clay," Research Conference on Shear Strength of Cohesive Soils, American Society of Civil Engineers, pp 419-435.

Wilson, S. D. and Sibley, E. A., Dec 1962: "Ground Displacements from Air Blast Loading," Journal, Soil Mechanics and Foundations Division, American Society of Civil Engineers, Vol 88, No. SM6, pp 1-31.

Wyllie, M. R. J., Gregory, A. R., and Gardner, G. H. F., July 1958: "An Experimental Investigation of Factors Affecting Elastic Wave Velocities in Porous Media," Geophysics, Vol 23, No. 3, pp 459-493.

Zaccor, J. V., Apr 1967: "Procedures for Prediction of Ground Shock Phenomena Based on One-Dimensional Shock Propagation Considerations; Procedures and Applications," Contract Report No. 3-171, Report 1, U. S. Army Engineer Waterways Experiment Station, CE, Vicksburg, Miss.

Zaccor, J. V. and Wallace, N. R., Nov 1963: "Techniques and Equipment for Determining Dynamic Properties of Soils," DASA-1421, Final Report, United Research Services Corporation, Burlingame, Calif.

Zeevaert, L., 1967: "Free Vibration Torsion Tests to Determine the Shear Modulus of Elasticity of Soil," Proceedings, Third Panamerican Conference on Soil Mechanics and Foundation Engineering, Caracas, Vol 1, p 111.

APPENDIX A ABSTRACTS OF SOIL DYNAMICS REPORTS

Reports Issued Under First Contract with Defense Atomic Support Agency (then Armed Forces Special Weapons Project), 1951-1954

1. Hydraulic Machine for Dynamic Compression Tests

R. V. Whitman and D. W. Taylor, August 1952, AFSWP-116

This report describes and discusses the design and construction of a hydraulically actuated rapid loading machine capable of failing specimens of soil and soft rock in 5 msec or less. The loading was accomplished by means of a large pump and specially designed quick-acting valves. In hindsight, the machine was overdesigned; that is, it had far greater capability than required for the test program that finally evolved.

2. Interim Report on Wave Propagation and Strain-Rate Effect

D. W. Taylor and R. V. Whitman, July 1953, AFSWP-117

This report presents results from vacuum triaxial tests on three sands, unconfined compression tests on undisturbed samples of Boston blue clay, and additional tests on several cohesive soils. Wave propagation effects were noted in the tests on Boston blue clay, and a special apparatus, capable of rapid triaxial tests on specimens with lengths up to 32 in., was designed.

3. Final Report on Laboratory Studies

D. W. Taylor, R. V. Whitman, and six others, August 1954, AFSWP-118

This long report is divided into three parts. Part A deals with the strain-rate effect on compressive strength of soils; it presents additional test data, including results for saturated sands with pore pressure measurements, and then summarizes and discusses all of the test results. Part B, which deals with stress-strain and wave propagation studies, presents results concerning creep and relaxation behavior of sand and results from wave propagation studies, using the special apparatus described in Report 2, using this same sand. Part C presents

an analytical study, based on rigid plastic bodies, of footing motion under transient loadings and results from small-scale tests of footings subjected to such loadings.

4. Review and Preliminary Correlation of Laboratory and Field Studies

R. V. Whitman and D. W. Taylor, June 1954, AFSWP-119

This report summarizes the results from the laboratory test program, uses these results to interpret cratering and transient motion phenomena observed during field explosion tests, and discusses the validity of stress measurements made during these field tests.

Reports Issued Under Present Contract with U. S. Army
Engineer Waterways Experiment Station, 1957-1968

1. Scope of Test Program and Equipment Specifications

R. V. Whitman, November 1957

This report was written to guide design and construction of the rapid loading machine for high-speed triaxial tests. The report was of no further interest once the equipment was constructed.

2. Test Equipment for High-Speed Triaxial Tests

January 1959

This report describes the design, construction, and performance of the devices for carrying out triaxial shear tests under rapid loading conditions and for measuring the stresses and strains during such tests.

3. First Interim Report on Dynamic Soil Tests

October 1959

This report contains a general discussion of the effects of time on the shear strength and compressibility of soils, and a description of the first apparatus developed for one-dimensional compression tests. The following results are included in the report: (a) rapid triaxial strength tests on two compacted clays and on compacted samples of the

silt from Frenchman Flat; (b) conventional triaxial strength tests on saturated remolded samples of a fat clay; (c) rapid triaxial strength tests on a dry sand; and (d) one-dimensional compression tests on dry sand and on a compacted clay.

4. One-Dimensional Compression and Wave Velocity Tests

R. V. Whitman, J. E. Roberts, and S-W. Mao, August 1960

Included in this report are: (a) a general discussion of the stress-strain relation for particulate masses; (b) specifications for the preparation of fat backswamp clay samples by static compaction; (c) data concerning creep, using a load rise time of 30 msec; (d) description of a preliminary attempt to measure pore pressures during compression creep; (e) data concerning the sonic dilatational wave velocity in a core of soft clay; and (f) description of a preliminary attempt to measure the sonic dilatational wave velocity in a soft clay sample during consolidation.

5. Pore Pressure Measurements During Transient Loadings

K. A. Healy, November 1960

This report consists of a general discussion of the problems involved in pore pressure measurement during transient loadings, a description of conventional pore pressure measuring systems and their inadequacies, and a description of the design and preliminary testing of a new system for pore pressure measurement. The feasibility of employing the new pore pressure measuring system in rapid testing was demonstrated by one-dimensional compression tests on fat clay and silty loam and by triaxial tests on a saturated clay-silt and a fat clay.

6. Effects of Rate of Strain on Stress-Strain Behavior of Saturated Soils

A. M. Richardson, Jr., April 1961

This report presents results from a series of static and rapid triaxial compression tests on a saturated loess and from a series of rapid triaxial compression tests on a saturated clay. The tests performed at rapid rates were of a preliminary nature, and the conclusions

drawn were used in planning a more comprehensive test program.

7. Adaptation and Use of the Boynton Device for Rapid One-Dimensional Compression Tests, P. J. Moore, June 1961

This report presents results from a series of one-dimensional compression tests using an explosive loading system to apply dynamic loads. Considerable difficulty was experienced in the use of this loading system, and the system was abandoned following these tests.

8. Laboratory Measurement of Dilatational Wave Propagation Velocity
F. V. Lawrence, Jr., July 1961

This report describes the design and operation of laboratory devices for measuring sonic dilatational wave velocity in samples of soil. Also included are results of preliminary tests on fat clay, glacial till, and Ottawa sand. The successful results obtained during these tests provided the basis for the extensive development of this testing system.

9. Shearing Resistance of Sands During Rapid Loadings
R. V. Whitman and K. A. Healy, May 1962

This report presents experimental and theoretical results concerning the behavior of sands when sheared very rapidly. Included are: (a) a review of previously existing data regarding strain-rate effects in dry sands; (b) an analysis of the errors and uncertainties which can develop when testing dry and saturated sands in rapid triaxial compression; (c) new data concerning a saturated coarse sand; and (d) a discussion of the possible implications of the sum total of the new and old data.

10. Strength of Saturated Fat Clay

R. V. Whitman, A. M. Richardson, Jr., and N. M. Nasim, June 1962

Results are presented from two series of undrained triaxial tests on saturated remolded specimens of a fat clay, both normally consolidated and heavily overconsolidated. In the first series, the strain

rate ranged from 1% strain in 5 min to 1% strain in 1.5 msec. In the second series, 1% strain was achieved in from 1000 min to 1 min, and pore pressures were measured. Both series revealed the importance of internal moisture redistribution in heavily overconsolidated specimens when the time to 1% strain exceeds 1 min. The excess pore pressure was observed to decrease as the rate of strain was increased.

11. Triaxial Tests upon Saturated Fine Silty Sand

K. A. Healy, September 1962

Results are presented from a series of saturated undrained triaxial tests on a fine silty sand, carried out at two strain rates: 760% strain per sec and 2.6% strain per sec. Pore pressures were measured in all tests. The specimens failed at the fast strain rate showed a greater dilatant tendency, as evidenced by a lower pore pressure and a lower friction angle, than those failed at the slow strain rate.

12. Static Tests upon Thin Domes Buried in Sand

R. V. Whitman, Zvi Getzler, and K. Höeg, December 1962

Thin-walled domes were buried within a sand mass which was 5 ft in diameter. A uniform static pressure was applied to the top surface of the sand mass. Instrumentation measured the total vertical force reaching the dome, vertical movements of the dome, strains within the dome, and movements within the sand mass. Small negative arching was observed when the dome had a stiff support, but considerable positive arching did appear when the support for the dome was soft. The buried domes did not develop buckling under an average vertical pressure almost three times the pressure that buckled the dome when unburied.

13. The Dependence of Dilation in Sand on Rate of Shear Strain

K. A. Healy, February 1963

This report is a compilation of the results of all investigations into the effect of strain rate on the strength of sand, including results previously documented in Reports 9 and 11 and new results. The

new results are primarily from a test in which an annular ring of dry sand is sheared by twisting. This form of test was specially designed to measure the effect of strain rate on the ultimate void ratio. It was found that the ultimate void ratio increased slightly with increasing rate of strain. These results thus provided confirmation of the earlier observation that the pore pressure during undrained shear decreased (became less positive or more negative) as the strain rate increased.

14. Propagation Velocity of Ultrasonic Waves Through Sand

F. V. Lawrence, Jr., March 1963

This report discusses an improved version of the apparatus first described in Report 8, and presents data for the dilatational velocity through dry sand and glass beads. The results are shown to be consistent with rod and shear wave velocities measured in other laboratories.

15. Undrained Strength of Saturated Clayey Silt

K. A. Healy, March 1963

This report marked the conclusion of that phase of the soil dynamics research dealing with the effect of strain rate upon strength. With these tests, four different soils ranging from a fat clay to a clean coarse sand had been tested under undrained conditions. As with the other soils, the pore pressures generated within the clayey silt decreased as the strain rate increased, although the phenomenon was partially obscured by the pore pressure gradients which developed within the samples. The strength increase was about 75% between strain rates of 0.0013 and 760% strain per sec.

16. Effective Stress Versus Strength: Saturated Fat Clay

A. M. Richardson, Jr., April 1963

With the fat clay, it was not possible to measure excess pore pressures for times to failure shorter than several seconds. Hence a program of tests at essentially static strain rates was undertaken in

order to establish the basic effective stress versus strength behavior of this soil. Both normally consolidated and heavily overconsolidated specimens were tested, with strain rates ranging from 1% strain in 0.5 min to 1% strain in 1440 min (1 day). The trends in the results were very similar to those observed in more pervious soils at faster strain rates.

17. Stress-Strain-Time Behavior of Soil in One Dimensional Compression

R. V. Whitman, May 1963

The appendixes discuss the evolution of test devices for the one-dimensional compression test, and present some results not previously reported. The main body presents the rationale for the test program, summarizes the test data, and discusses the implication of the data with regard to propagation of high-intensity stress waves through earth. The main body is identical with the paper "Effects of Viscosity and Elasticity upon Stress Waves Through Confined Soil" presented by R. V. Whitman to the 32nd Symposium on Shock Vibration and Associated Environments, held in the spring of 1963. This report is essentially a final report upon the one-dimensional compression testing phase of the total research effort to date.

18. The Dynamic Passive Pressure Problem for Sand

W. C. Kerr, May 1963

The dynamic counterpart of the passive earth pressure problem was investigated (in a preliminary way) both experimentally and theoretically. The experiments revealed that the pattern of sand movements is quite different for static and for dynamic loadings of very short duration. With rapid loadings, a "crater" is excavated behind the wall, presumably as the result of "spalling" of the cohesionless surface.

19. Stresses and Strains in a Planar Array of Elastic Spheres

E. T. Miller, August 1963

In this study the deformational behavior of soil is simulated by

a planar array of elastic spheres. The theoretical calculations take into account both deformation of the spheres and sliding between spheres. Several of the key features of the behavior of soil in one-dimensional compression are demonstrated by use of this theoretical model: the development of an S-shaped stress-strain curve, hysteresis loops during loading and unloading, and the locking in of high lateral stresses by loading and unloading.

20. Further Study of a Rapid Response Pore Pressure Gage

E. T. Miller, November 1963

The report discusses design principles and concepts for a miniaturized pore pressure gage, using a piezoresistive transducing element, which could be embedded within a triaxial specimen of standard size. Due to failure of the transducing element, evaluation of the gage was not completed.

21. One-Dimensional Compression and Wave Propagation

P. J. Moore, October 1963

This report demonstrates, by very precise measurements in an oedometer of superior construction, the existence of an S-shaped stress-strain curve in sand. For small stress increments, the moduli as measured in the oedometer were generally the same as moduli backfigured from wave propagation velocity. The effect of varying the rate of increase of stress in the oedometer was investigated.

22. Dynamic Response of a Particulate Soil System

W. C. Kerr, March 1964

The theoretical study in this report was motivated by the problem of lateral inertia during triaxial testing. One- and two-dimensional mass-spring systems were used to approximate the response of an assemblage of particles such as in a granular soil. The laws for the deformation of elastic spheres were used to guide the selection of the spring constants of the lumped system. The effect of geometry change on the response of the two-dimensional system was considered.

Computer programs were developed to carry out the analysis of the dynamic response. The results showed the dispersion which is observed during wave propagation through granular soils, but the calculations were not carried to the point where the possible importance of lateral inertia could be clarified.

23. Ultrasonic Shear Wave Velocities in Sand and Clay

F. W. Lawrence, Jr., January 1965

This report describes the measurement of shear wave velocities using the ultrasonic technique. Tests on saturated sand yielded results very similar to those obtained in other laboratories. Tests on clays showed that velocity was related principally to effective stress and void ratio, although small structural changes during secondary compression had a significant effect. The relation between shear wave velocity, effective stress, and void ratio was quite similar for sands and clays.

24. Wave Velocities Through Partially Saturated Sand-Clay Mixtures

H. A. Balakrishna Rao, March 1966

These tests established in a preliminary way the effect of degree of saturation on dilatational and shear wave velocities. Increasing degree of saturation means increased mass and generally decreased shear modulus, and hence shear wave velocity decreases with increasing degree of saturation. On the other hand, increasing degree of saturation means increased resistance to compression, and hence increased dilatational wave velocity. These trends were confirmed experimentally.

25. Miscellaneous Studies of the Formation of Wave Fronts in Sand

R. V. Whitman, May 1966

This report contains (a) data concerning the stress-strain behavior of dry Monterey sand, as measured in confined compression and also as measured using ultrasonic waves; and (b) theory for the dispersion of a wave front passing through a system of discrete particles. These

results were utilized in a report, DASA 1266-4, by Stanford Research Institute to study the development of shock waves in sand.

APPENDIX B HISTORY OF THE MIT SOIL DYNAMICS CONTRACT

In order to appreciate the factors which determined the evolution of the research at MIT, it is necessary to first look briefly at the entire history of research concerning soil dynamics.

B.1 EVOLUTION OF SOIL DYNAMICS RESEARCH IN GENERAL

Prenuclear age: It usually is said that soil dynamics had its start in Germany during the 1930's, when engineers investigated the dynamics of machine foundations and the use of in situ wave velocities to reveal soil properties. It would be more accurate to say that these were the first systematic investigations in the area now known as soil dynamics; obviously engineers had for some time been faced with problems of ground motions caused by earthquakes and blasting.

During these early years of soil dynamics, the emphasis was on seismic wave velocity and on correlations between this velocity and engineering performance. This velocity was readily measurable, and furthermore the art of testing soil in the laboratory was in its infancy. There was little study of the fundamentals of stress-strain behavior during dynamic loadings. The laboratory tests of Iida (1936) in Japan, dealing with wave velocities and damping in soil, stand out as almost the only fundamental study during the pre-nuclear age.

The years since the dawn of the nuclear age (1945) have witnessed numerous developments which have influenced the course of soil dynamics research: tracking radars with their stringent foundation requirements, heavier traffic loads for highway and airport pavements, increased concern over the devastating effects of earthquakes, an increased capability for sophisticated laboratory and field tests, and a great upswing of interest in soil mechanics research in general. It safely can be said that the nuclear weapons effects problem has given the major impetus for much of the soil dynamics research which has taken place since 1945. However, there has been research directed at other problems as well. These several categories of research will be treated separately in the following

paragraphs; however, there have continually been important interactions between them.

Nuclear weapons effects research: At the beginning of the nuclear age, the emphasis in soil mechanics research was on shear strength, and this emphasis continued throughout the subsequent 15 years. Furthermore, the first major engineering problem posed by the advent of nuclear explosives was a problem involving shear strength: the possible instability, as the result of near misses by a large explosion, of the slopes of a sea-level Panama Canal. Thus it was that the first major, systematic soil dynamics investigation of the nuclear age (the tests at Harvard in the late 1940's) dealt with shear strength. Moreover, when nuclear weapons effects field tests began on a large scale about 1950 and MIT was asked to undertake suitable soil dynamics research, it was also natural to continue the shear strength tests begun earlier at Harvard.

This initial emphasis on shear strength naturally led to attempts to apply the resulting information to practical problems, such as cratering and footing motion. However, it was found that lack of mathematical techniques capable of handling such complex problems was a far more serious limitation than uncertainty as to the effect of strain rate on strength. At the same time, another type of problem began to grow in importance: the ground motions associated with the airblast emanating from explosions. The emphasis in the laboratory program thus began to shift from shear strength to tests giving the type of stress-strain information necessary to understand the ground motion problem.

The start of the Ballistic Missile Base program in the late 1950's gave a major new impetus to soil dynamics research. Up until this time, the work at MIT was the only major laboratory effort directed at the soil mechanics aspects of nuclear weapons effects. Now important efforts started at numerous government laboratories, research institutes, and universities. Initially some of these new efforts dealt with shear strength. More generally, however, these efforts took up the problems of stress-strain relations in compression, wave propagation tests, and studies of the interaction between soil and buried structures. Today a wide variety of tests, too numerous to mention in this brief summary, are being

conducted. The applied stresses of interest have gradually increased: from a few psi to tens of psi, then to hundreds of psi, and finally to thousands of psi and even more.

Measurements which have been made in the field during actual nuclear explosions have of course been vital to the understanding and interpretation of the laboratory results. Unfortunately, such field observations have been limited in number and generally preceded the laboratory studies rather than being specifically designed to validate certain key concepts.

Other modern developments: When concerned with nuclear weapons effects, one is concerned primarily with a single intense loading. There are many other problems which involve repeated loadings.

Traffic loadings and earthquakes produce repeated loadings of moderate intensity, in some cases sufficient to progressively weaken soil and to finally bring about a shear failure. Seed at the University of California has conducted extensive investigations into the behavior of soil subjected to such loadings.

Foundations for machinery producing periodic loads involve rapidly varying stresses of small intensity. This stress condition is also met when using explosively or mechanically produced waves to evaluate in situ ground conditions. Recently there has been much interest in vibratory pile driving, which also involves rapidly varying stresses of small intensity. The resonant column test originally developed by Iida is designed to study the behavior of soil under these conditions. This form of test was introduced into this country in the late 1940's by Wilson, then at Harvard University. Wilson refined the technique, and Richart (first at the University of Florida and now at the University of Michigan) has also made valuable contributions using this technique. This test, with various modifications, is now being used in a number of laboratories throughout the country.

B.2 HISTORY OF SOIL DYNAMICS RESEARCH AT MIT

1951-1954: As stated above, the initial emphasis concerned shear strength during dynamic loading: more precisely, the effect of strain rate on strength during a single loading. A large, multipurpose testing machine

was constructed (Report 1), and tests were run on dry and saturated sands and on a variety of cohesive soils (Reports 2 and 3). In an attempt to understand how these results might be applied to practical problems, the first small-scale tests on footings were conducted (Report 3). An attempt also was made to apply basic soil mechanics considerations to the problem of crater size (Report 4).

MIT personnel participated in the planning of the nuclear weapons effects field test programs of the early 1950's, and it soon became apparent that knowledge of stress-strain behavior and wave propagation phenomena was of more practical consequence than knowledge concerning the effect of strain rate on shear strength. Wave propagation phenomena had been detected during the triaxial strength tests with the most rapid loadings. It was decided, in 1953, to construct a very long triaxial specimen so that the wave propagation phenomena could be observed clearly. These were the first laboratory tests involving the propagation of intense stress waves through soil (Report 3).

1957-1965: Strength testing was resumed when the present contract started. A much simpler test machine was built (Reports 1 and 2 of present series) and the limitations on the rate at which loads may be applied in such a test have been studied (Report 22). Again a variety of soils were tested, especially saturated sands and clays (Reports 3, 6, 9, 10, 11, 15, and 16). Primary emphasis was given to understanding the causes for the strain-rate effect on strength, especially the role played by excess pore pressures (Reports 9, 10, 11, 13, 15, and 16). Toward this end, special devices were developed for measuring pore pressures induced by rapid loadings (Reports 5, 9, 11, 14, 15, 16, and 20).

An interest in soil behavior as it applied to wave propagation was also carried over from the earlier contract. The first tests using one-dimensional compression with rapid loadings were started in 1958, and the technique was refined during the next few years (Reports 4, 7, and 17). The technique was ready for use when the Ballistic Missile Base program required data concerning the dynamic compressibility at various sites, and laboratory tests using this technique played a key role in the design of several of the bases. The results from the studies during this period

helped to sort out the relative importance of inelastic and time-dependent effects and to indicate the degree of stress attenuation present in practical problems (Report 17). More recent research has led to an understanding of why shock waves sometimes do but more often do not form in soil (Reports 19, 21, and 25).

In 1959, investigations were started into the factors controlling the velocities of seismic level waves through soil and the relation between these velocities and other soil properties such as compressibility. Apparatus was developed for measuring these velocities in the laboratory (Reports 4 and 8). This apparatus, and the knowledge gained therewith, also played an important role in the investigation of sites for Ballistic Missile Bases. Recent research has finally begun to provide a real understanding of the relations mentioned above (Reports 14, 21, 23, and 24).

Two studies were started in order to learn how to relate stress-strain data to soil-structure interaction phenomena (Reports 12 and 18). Each study revealed the existence of previously uninvestigated phenomena, and thus provided a better orientation for further research.

B.3 SUMMARY OF CONTRIBUTIONS UNDER PRESENT CONTRACT

1. With regard to shear strength during transient loadings:
 - (a) Developed a simple form of test device and produced data for a wide variety of soils.
 - (b) Gave some unity to the mass of data which has been obtained.
 - (c) Made the first steps toward pinpointing the physical causes for the strain-rate effect.
2. With regard to dynamic compressibility:
 - (a) Stimulated early interest in the problem of intense stress waves through soil and in the use of the one-dimensional compression test to assess the pertinent soil properties.
 - (b) Developed equipment and techniques for performing accurate dynamic one-dimensional compression tests.
 - (c) Produced the first useful data concerning time-dependent effects during one-dimensional compression.
 - (d) Completed a detailed explanation of nonlinear stress-strain

behavior of sand, involving the concept of an S-shaped stress-strain curve, and of the effect of this behavior upon wave front development.

3. With regard to waves of low intensity:

- (a) Developed and used a device for measuring dilatational wave velocity in the laboratory.
- (b) Established, for dry sands, the relation between seismic wave velocity and compressibility as measured in one-dimensional compression.
- (c) Made a start toward the understanding of the relation between dilatational velocity and degree of saturation.
- (d) Obtained first data to show that the shear velocity-void ratio-effective stress relation for clays is quite similar to that for sands.

Unclassified

Security Classification

DOCUMENT CONTROL DATA - R & D		
(Security classification of title, body of abstract and indexing annotation must be entered when the overall report is classified)		
1. ORIGINATING ACTIVITY (Corporate author) Massachusetts Institute of Technology Cambridge, Mass.		2A. REPORT SECURITY CLASSIFICATION Unclassified
		2B. GROUP
3. REPORT TITLE THE RESPONSE OF SOILS TO DYNAMIC LOADINGS; Report 26, FINAL REPORT		
4. DESCRIPTIVE NOTES (Type of report and inclusive dates) Report 26 of a series		
5. AUTHOR(S) (First name, middle initial, last name) Robert V. Whitman		
6. REPORT DATE May 1970	7A. TOTAL NO. OF PAGES 236	7B. NO. OF REFS 128
8A. CONTRACT OR GRANT NO. DA-22-079-eng-224	8B. ORIGINATOR'S REPORT NUMBER(S)	
9. PROJECT NO.		
10. OTHER REPORT NO(S) (Any other numbers that may be assigned this report) U. S. Army Engineer Waterways Experiment Station Contract Report No. 3-26		
11. DISTRIBUTION STATEMENT This document has been approved for public release and sale; its distribution is unlimited.		
11. SUPPLEMENTARY NOTES Prepared under contract for U. S. Army Engineer Waterways Experiment Station, CE, Vicksburg, Miss.		12. SPONSORING MILITARY ACTIVITY Defense Atomic Support Agency Washington, D. C.
13. ABSTRACT This report, the 26th in a series of reports prepared under contract by MIT, deals with the role of soil mechanics with regard to weapons effects prediction and protective construction design. It assesses the state-of-the-art as of 1967, and summarizes all the research performed under the contract as well as contributions by other investigators. Results from field experiments and theoretical analyses are interpreted so as to show the relation between soil properties and such phenomena as crater size and shape, ground motions, and response of buried structures. Chapters deal specifically with the evaluation of dynamic uniaxial strain and dynamic shear strength, and with the relation between seismic wave velocity and soil properties. Appendix A contains abstracts of the 25 earlier reports issued under the contract. Appendix B gives a brief history of the MIT soil dynamics contract.		

DD FORM 1473

REPLACES DD FORM 1473, 1 JAN 64, WHICH IS OBSOLETE FOR ARMY USE.

Unclassified
Security Classification

Unclassified
Security Classification

14.	KEY WORDS	LINK A		LINK B		LINK C	
		ROLE	WT	ROLE	WT	ROLE	WT
	Dynamic loads						
	Ground motion						
	Seismic waves						
	Soil dynamics						
	Soil properties						
	Subsurface structures						

Unclassified
Security Classification